LAWRENCE
LIVERMORE
NATIONAL
LABORATORY

UCRL-TR-222275

Modeled Neutron and Charged-Particle Induced Nuclear Reaction Cross Sections for Radiochemistry in the Region of Yttrium, Zirconium, Niobium, and Molybdenum

R. D. Hoffman, K. Kelley, F. S. Dietrich, R. Bauer, M. G. Mustafa

June 20, 2006

This work was performed under the auspices of the U.S. Department of Energy by University of California, Lawrence Livermore National Laboratory under Contract W-7405-Eng-48.

UCRL-TR-222275

Modeled Neutron and Charged-Particle Induced Nuclear Reaction Cross Sections for Radiochemistry in the region of Yttrium, Zirconium, Niobium, and Molybdenum

R.D. Hoffman, K. Kelley, F. S. Dietrich and R. Bauer
Nuclear Theory and Modeling Group
Physics and Advanced Technologies, N-Division
Lawrence Livermore National Laboratory
Livermore, CA 94550
rdhoffman@llnl.gov

M. G. Mustafa
Nuclear and Defense Technologies, AX-Division
Lawrence Livermore National Laboratory
Livermore, CA 94550

(June 20, 2006)

ABSTRACT

We have developed a set of modeled nuclear reaction cross sections for use in radiochemical diagnostics. Systematics for the input parameters required by the Hauser-Feshbach statistical model were developed and used to calculate neutron, proton, and deuteron induced nuclear reaction cross sections for targets ranging from strontium ($Z = 38$) to rhodium ($Z = 45$).

Subject headings: Nuclear cross sections, Radiochemistry, Nuclear Physics

1. Introduction

1.1. Radiochemistry

Various aspects of nuclear explosive device performance can be determined through the use of radiochemistry. During the UGT (Under Ground Test) Program, select naturally occurring elements were often loaded into a device prior to a test and their activation products subsequently retrieved for counting. The products are measured as isotopic ratios (such as $^{87}Y/^{88}Y$ produced from a stable isotope of the naturally occurring element). From the measured activity and prior knowledge of the amount of loaded detector material, performance aspects could be inferred by comparing the measured isotope ratios with those calculated using particle fluences from one of the design codes and group-averaged cross section sets that have been prepared for this purpose.

This paper continues the collaborative effort between AX-Division (DNT) and N-Division (PAT) to update and improve the existing RADCHEM cross section detector sets. Previous papers treated the regions of bromine and krypton (Hoffman *et al.* 2004a), iodine and xenon (Hoffman *et al.* 2004b), samarium, europium, and gadolinium (Hoffman *et al.* 2004c), scandium, titanium, vanadium, chromium, manganese, and iron (Kelley *et al.* 2005), arsenic (Kelley *et al.* 2006a), and nickel, copper, and zinc (Kelley *et al.* 2006b). Here we focus on reactions proceeding on targets of yttrium, zirconium, niobium, and molybdenum.

Contents

List of Figures

List of Tables

1.2. Current Detector Sets

Over the last 40 years a number of detector sets have been developed at LLNL and LANL. Twenty-three neutron threshold detector sets and five charged particle sets are currently available. The sets of interest in this modeling effort are as follows:

- Yttrium neutron-induced set (YT0585), used to calculate the production of ^{87}Y ($t_{1/2}$ = 3.317 d), ^{87m}Y ($t_{1/2}$ = 13.37 h), and ^{88}Y ($t_{1/2}$ = 106.7 d) from stable ^{89}Y.
- Yttrium charged-particle set (YT0488), used in conjunction with sets YT0585 and Zr0982 to calculate the production of zirconium isotopes from stable ^{89}Y.
- Zirconium neutron-induced set (Zr0982), used to calculate the production of ^{87}Zr ($t_{1/2}$ = 1.68 h), ^{88}Zr ($t_{1/2}$ = 82.6 d), and ^{89g}Zr ($t_{1/2}$ = 3.268 d) from stable zirconium.
- Niobium neutron-induced set (Nb0179), used to calculate the production of ^{92m}Nb ($t_{1/2}$ = 10.15 d) from stable ^{93}Nb.
- Molybdenum neutron-induced set (Mo1278), used to calculate the production of ^{88}Zr ($t_{1/2}$ = 82.6 d), ^{89g}Zr ($t_{1/2}$ = 3.268 d), and ^{93m}Nb ($t_{1/2}$ = 16.13 y) from stable molybdenum.

The cross sections available in these detector sets, as listed in (Nethaway 1998) are summarized in table 5 in appendix A.1. Most of the cross sections are taken from calculations performed at LLNL and LANL between 1972 and 1988. The charged-particle reactions on ^{89g}Y are taken from measurement. Several other cross sections (primarily (n,2n) reactions on stable targets) have been scaled to match measured cross section data at or around 14.1 MeV of incident energy. These sets can be accessed on the world wide web at http://nuclear.llnl.gov/CNP/nads/main.html.

1.3. Motivation for Updating the Detector Sets

Previous successes in updating other detector sets suggest that the YT0488, YT0585, Zr0982, Nb0179, and Mo1278 sets may also benefit from a new evaluation.

Many of the RADCHEM detector sets updated in our previous modeling efforts had a clear need for improvement Some of the more disturbing shortfalls of these sets included neutron capture cross sections being copied from other targets and adjusted, (n,2n) cross sections with an assumed maximum cross section and standard shape rising from a calculated threshold, and educated guesses for extrapolating cross sections to higher or lower energies. In each of these cases it is preferable to model the cross section using all available input data and then scale the cross section to match a measured data point if necessary (i.e. scale a cross section with a calculated shape).

The detector sets considered in the present work do not suffer from such deficiencies. Every cross section included was either measured or calculated. However, we sometimes find that only a few neutron-induced reactions of interest for a given target were calculated explicitly. The remaining reaction channels (in Y) were lumped together as a so-called (n,X) "destruction" cross section. In several instances, the (n,X) cross section is significantly larger than the channels explicitly calculated. In these cases, it is desirable to know which reactions dominate at a given incident energy. Furthermore those reactions should be explicitly included in the network so that the largest nuclear flows can be properly accounted for. The detector sets of interest in this work also have several instances where a dominant reaction channel (neutron capture for ^{92}Nb, for example) was grouped in with an (n,X) destruction cross section.

Another motivation is drawn from the general improvement in cross section modeling capabilities. In the nearly two decades since these sets were developed, many new cross section measurements have been performed, and the amount of nuclear structure data used to constrain model parameters has increased. Additionally, several efforts have been made to develop consistent approaches to modeling nuclear reaction cross sections (Belgya *et al.* 2005), and there are more accurate methods of calculating and estimating cross sections for which we have no data.

Thirdly, our proposed new evaluation of these cross sections will include an in-depth investigation into the sensitivity of the modeled cross sections to variations in the various statistical model inputs. In doing so we are able to determine which parameters are the most important for a given reaction. This also allows us to estimate how much a calculated cross section will change if new experimental measurements place more constraints on

the model inputs.

1.4. Proposed Detector Sets

We consider as targets each of the isotopes listed in Table 6 of Appendix A.2. For each of these targets, we model the reaction channels indicated in the table. In cases where the residual nucleus has a long-lived isomer (which we define as $t_{1/2} > 1$ μs), we model individual cross sections leading to the ground and isomeric states, as well as an "activation" cross section, defined as the total cross section producing a given isotope. This modeling effort includes all of the reactions previously available in the RADCHEM detector sets, but also includes many additional targets and reaction channels. These additional reactions are included primarily to provide further comparisons to measured cross section data and bolster our confidence in the accuracy of cross sections modeled for unstable targets. These reactions also account for the various possible destruction reactions that are significant in this mass range.

Our goal is to develop a consistent set that reproduces, as closely as possible, measured cross sections on targets in the *local region of interest*. To do this we develop *local systematics* for the many input quantities used in the theoretical reaction modeling calculations. These systematics are based on experimental data that are often only available for compound nuclear systems formed from a stable target plus a neutron. Of course, we use experimental data whenever it is available, but reactions proceeding through unstable systems are unavoidable in radiochemistry. Short of developing new experimental techniques to measure cross sections on unstable targets, our only hope of reproducing measured activity from UGT shots, and addressing the uncertainty associated with the nuclear cross sections, is to develop cross section sets that reproduce well the measured cross sections in the local region of interest.

In §2 we describe the theoretical techniques used in the modeling effort. §3 describes the input parameters. §4 gives results. We conclude with §5.

2. Nuclear Reaction Theory

2.1. Reaction Mechanisms

Conceptually, we consider nuclear reaction mechanisms to be of two general types: direct processes and compound processes. Direct processes can be pictured as simple interactions of the incident particle with the nuclear potential of the target nucleus. They proceed on a rapid time scale (of order $\sim 10^{-22}$ s), and the reaction products are often highly peaked in the incident particle direction. Direct reactions are generally quite small over the energy range of interest in this study, and have not been included in our calculations.

Compound processes are pictured as complicated interactions proceeding over a much longer timescale ($10^{-15} - 10^{-18}$ s) in which the reaction is mediated by the formation of a "compound nucleus", with the excitation energy of the incident particle being statistically "shared" with the ensemble of nucleons in the target over all energetically allowed degrees of freedom. The reaction products are largely isotropic.

Other intermediate reaction mechanisms exist between these two extremes. We refer to these as "pre-equilibrium" nuclear processes, where a particle may be emitted from the target+projectile compound system prior to equilibration. Over the energy range of interest to this project (a few keV to 20 MeV) we will consider pre-equilibrium and compound nuclear processes, with the pre-equilibrium processes operating principally above 10 MeV of incident particle energy.

2.2. Hauser-Feshbach Statistical Model

A traditional theoretical approach to compound nuclear reactions is the statistical or Hauser-Feshbach model (Hauser & Feshbach 1952). This model is valid for high level densities in the compound nucleus, allowing one to use energy averaged transmission coefficients T, which describe absorption via an imaginary part in the (optical) nucleon-nucleus potential (Mahaux & Weidenmüller 1979). For the reaction I (in state μ) $+j \rightarrow k +$ L (in state ν), with $\mathrm{I}^{\nu} + j$ interacting with center-of-mass energy E_j^{μ} (in MeV), the average cross section is given by

$$\sigma_{jk}^{\mu\nu}(E_j^{\mu}) = \frac{\pi\lambda_j^2}{g_I^{\mu} g_j} \sum_{J,\pi} g_J \frac{T_j^{\mu}(J^{\pi}) T_k^{\nu}(J^{\pi})}{T_{tot}(J^{\pi})} W(J^{\pi}) \tag{1}$$

where the summation extends over all compound nuclear spins and parities J^{π}, μ and ν are states in the target and product (=0 for the ground state, 1 for the 1^{st} excited state, etc.). The cross section has units of area, described by $\pi\lambda_j^2 = 0.6566(\hat{A}_j E_j^{\mu})^{-1}$ barns, with $\hat{A}_j = (A_I A_j)/(A_I + A_j)$ being the reduced mass in atomic mass units and E_j^{μ} is the center of mass energy in units of

MeV. $\lambda\!\!\!^{-}_j$ is the wavelength related to the wave number k_j in the target plus incident particle channel by $\lambda\!\!\!^{-}_j = 1/k_j$ The statistical weights are given by $g^x_y = (2J^x_y + 1)$. Items without superscripts refer to the compound nucleus.

The transmission coefficients in the numerator are given by $T^\mu_j(J^\pi)$ = the total transmission coefficient for forming the state J^π in the compound nucleus $I^\mu + j$ at energy E^μ_j. Likewise, $T^\nu_k(J^\pi)$ is the same as $T^\mu_j(J^\pi)$ but for the pair $L^\nu + k$ at energy E^ν_k. Implicit in these definitions is a sum over all possible $l-$waves and channel spins, i.e.

$$T^\mu_j(J^\pi) = \sum_{l,s} T^\mu_j(J^\pi, l, s) \qquad (2)$$

where l is any partial wave number (orbital angular momentum) that can couple the state μ to the compound nuclear state having spin and parity J^π subject to quantum mechanical selection rules and s is the vector sum of the spins J^μ_I and J_j. Hence s takes on all integer (or half-integer) numbers from $|J^\mu_I - J_j|$ to $J^\mu_I + J_j$.

T_{tot} represents the sum of transmission coefficients over all possible decay channels (i.e. for all particles and photons). The cross section for the formation of species L, regardless of its state ν, is obtained by summing Eq. [1] over all bound states ν of L for which the reaction is energetically allowed.

When evaluating these sums, if energies become of interest which exceed the highest discrete excited state for which energy, spin, and parity are explicitly known, a nuclear level density formula must be employed. Specifically, the definitions for the transmission coefficients $T_j(J^\pi)$, $T_k(J^\pi)$, and $T_{tot}(J^\pi)$ must be modified:

$$T_k(J^\pi) = \sum_{\nu=0}^{\omega} T^\nu_k(J^\pi) + \sum_{J^\nu \pi^\nu} \int_{\xi^\omega_L}^{\xi^{max}_L} T^\nu_k(\xi^\nu_L, J^\pi)\rho(\xi^\nu_L, J^\nu, \pi^\nu) d\xi^\nu_L d\pi^\nu dJ^\nu \qquad (3)$$

where for the nucleus L, ξ^ω_L is the energy of the highest excited state, ω, of known energy, spin, and parity; $\xi^{max}_L = E^0_k = E^0_j + Q_{jk}$ is the maximum excitation energy available, and $\rho(\xi^\nu_L, J^\nu, \pi^\nu)$ is the density of states per unit energy of spin and parity J^ν and π^ν at the excitation energy ξ^ν_L. The above integral approximates a sum and is subject to the same quantum mechanical restrictions implied in the definition of the transmission function.

2.3. Width Fluctuations

In addition to the ingredients required for Eq. [1], we apply width fluctuation corrections ($W(J^\pi)$, hereafter WFC), which define correlation factors with which all partial channels of incoming particle j and outgoing particle k, passing through excited state (E, J, π), should be multiplied. The major effect is to enhance the elastic channel and accordingly decrease the other open channels. They are most often observed at or near channel opening energies, for example when a (p,γ) and a (p,n) channel compete and the weaker (p,γ) channel is enhanced. Above a few MeV of excitation energy, when many competing channels are open, WFC's can be neglected.

A reasonably complete treatment for the WFC, obtained with the Gaussian orthogonal ensemble (GOE) approach, requires the evaluation of a triple integral and to date has been considered much to costly to apply in nuclear cross section calculations. Several approximations have been developed, the most popular ones are the Moldauer model (Moldauer 1976), and the HRTW model (Hofmann *et al.* 1975). We use the Moldauer model approximation in this study. For a detailed description of the full (GOE) treatment and a comparison with the Moldauer and HRTW approximation models mentioned above, see (Hilaire Lagrange & Koning 2003).

2.4. Pre-Equilibrium Processes

For excitation energies starting around 10 MeV, pre-equilibrium processes become important. The pre-equilibrium cross section is subtracted from the total reaction cross section leading to the first compound nucleus, and is usually unimportant for subsequent compound nuclei. Here we describe equilibration of the compound nuclear system in terms of the exciton model (Cline & Blann 1971) including alpha particle emission (Milazzo-Colli & Braga-Marcazzan 1973). We adopt an initial 2-particle 1-hole configuration. Average rates for internal transitions, corrected for the Pauli principle by Cline (1972), are related by the formulas of Williams (1970) to the absolute square of the average effective matrix element $|M|$ of the residual interactions as per Eq. [7] of (Uhl & Strohmaier 1976). The dependence of $|M|^2$ on mass number and excitation energy is

$$|M|^2 = \langle FM \rangle A^{-3} E^{-1} \qquad (4)$$

The description of alpha particle emission in the

pre-equilibrium model is a straightforward extension of nucleon emission, assuming nucleons preform alpha clusters. In making such an extension, one introduces a parameter ϕ which represents the probability that the incoming particle will strike a pre-formed alpha cluster.

In the pre-equilibrium stage of the reaction, particle emission is assumed to be the only decay mode. For the equilibration, the WFC corrected Hauser Feshbach formula (Eq. [1]) is applied. All subsequent processes are treated as sequential evaporation steps.

2.5. The STAPRE Hauser-Feshbach Reaction Code

We model our cross sections using the statistical model code STAPRE (Uhl & Strohmaier 1976), which embodies all of the physical models discussed above. The version of the code we use is STAPRE-H95 (Avrigeanu & Avrigeanu 1976), available from the NEA web site. We have made several modifications, primarily to the level density routines. Prior versions of the code were used to develop parts of the existing RADCHEM data sets (Vonach 1982).

In the following we discuss the important ingredients of statistical model calculations, and the methods utilized to estimate them. These are the requisite nuclear structure data, such as the binding energies of all nuclei included (which define the separation and reaction threshold energies and Q-values of the various reaction channels considered), as well as the energies, spins, and parities of the ground states and all known excited states of these nuclei, and the detailed branching ratios for the gamma-ray cascade from excited to low-lying states. Also needed are parameters controlling the width fluctuation corrections and the pre-equilibrium model, the particle and γ-transmission coefficients, and the nuclear level densities of all nuclei involved in a given reaction. The reliability with which these ingredients can be calculated determines the accuracy (or reliability) of a given cross section calculation.

2.6. Breakup of Incident Deuterons

Due to its relatively weak binding, an incident deuteron may be separated into its constituent nucleons in the presence of the Coulomb barrier. The now separate nucleons are then free to interact with the target nucleus by either scattering (elastically or inelastically) or fusing to the target. The STAPRE code does not address these so-called "deuteron breakup" processes. We must first calculate the breakup and breakup-fusion cross sections using the methods of (Udagawa & Tamura 1986) and express the resulting total breakup/breakup-fusion cross section as a fraction of the reaction cross section. The reaction cross section in the STAPRE code can then be reduced by the appropriate amount.

A more thorough treatment of deuteron breakup would allow the excited target (in the case of an inelastically scattered nucleon) or compound nucleus (in the case of breakup-fusion) to decay via the usual statistical models. However, this capability has not yet been incorporated into our suite of reaction codes.

2.7. Determination of Destruction Reactions

Reaction channels other than those listed explicitly in Appendix A.2 may comprise a significant portion of the total reaction cross section. Rather than attempt to calculate all kinematically allowed channels explicitly, we supply a "destruction" cross section to account for additional depletion of a given target. The destruction cross section is determined by subtracting from the reaction cross section the sum of the compound elastic and all other explicitly calculated channels. The remaining cross section is designated (n,X), (p,X), or (d,X) depending on the incident particle. Since we have explicitly calculated most of the important neutron induced channels, our (n,X) cross sections are expected to be quite small.

The greatest obstacle faced in calculating destruction cross sections is the numerical precision at which cross sections are stored in the computer memory or files. To eliminate numerical "noise" that arises from these precision issues, we apply a sequence of filters to our "raw" calculated destruction cross sections. First, since we have included all open channels up to about 3 MeV of incident energy for each incident particle considered in this study, we set any resulting destruction cross section below 3 MeV to zero (actually to 1 nanobarn, which is in practice equal to zero for network calculations). Any point in the energy grid where the cross section is non-zero but the cross section at the grid point to both sides is zero (i.e. "spikes" that show up in the cross section) are also set to zero. A two step Savitsky-Golay smoothing filter (linear over a short range and quadratic over a larger range) is then applied. Any cross section lower than 1 millibarn or 0.1% of the reaction

cross section (whichever is greater) is then set to zero, and the smoothing filter applied again. This is followed by one last search for "spikes". A comparison of the raw destruction cross section and the filtered one indicates that the filtering process does not significantly alter the "real" destruction cross section (i.e. the destruction cross section due to unaccounted reaction channels, as opposed to that arising from precision error).

This concludes our discussion of the methods and models used in our calculations. we now proceed to describe the various quantities used as input in these models.

3. Inputs for the Reaction Models

3.1. Nuclear Structure Data

3.1.1. Ground State Masses and J^π Assignments

We adopt for nuclear masses the experimental mass excess values of (Wapstra *et al.* 2003; Audi *et al.* 2003). In the event that an experimental mass excess is not available, we adopt the values from the finite range droplet model (FRDM) (Möller *et al.* 1995). Spin and parity assignments are from (Tuli 2000). In appendix B.1 we present the binding energies (in MeV, calculated from the adopted masses) and the separation energies for neutrons, protons, α-particles, and deuterons for each of the nuclei included in this study. Ground state spin and parity assignments are given in Table 6 (Appendix A.2). In Appendix B.2, we provide reaction Q-values for the cross sections modeled in this study.

3.1.2. Nuclear Level Schemes

The nuclear structure data needed to model the gamma-ray cascade was adopted from (Belgya *et al.* 2005). We include all levels up to the energy where spins, parities, and γ-ray branching ratios have been unambiguously assigned. For several isotopes, including $^{76-83}$Br, $^{77-84}$Kr, ^{78}Rb, $^{83-89}$Sr, $^{84-91}$Y, and $^{86-91}$Zr, additional evaluations were performed by R. Bauer (Bauer 2003). The modified nuclear level schemes for the bromine, krypton, and rubidium isotopes can be found in (Hoffman *et al.* 2004a). The remaining modified schemes, including level energies, spin and parity assignments, and γ-ray branching ratios, may be found in appendix B.3.

Occasionally we encounter a situation where, due to missing spin/parity assignments or branching ratios, an isomer is not included in the level scheme. In most of these cases, the only missing data was branching ratios. In order to include the isomers in our calculations, we have estimated the missing branching ratios as follows:

- ^{94}Y: First excited state decays to the ground state (only possible γ-ray decay).
- ^{90}Zr: Branching ratios were removed from the first and second excited states (0+ at 1.761 MeV, 2+ at 2.186 MeV). Even though these states have very short lifetimes (61.3 ns and 88.4 fs, respectively), they were treated as isomers in the RADCHEM Zr0982 detector set. We have also considered these states as isomers to maintain consistency with the RADCHEM set.
- ^{91}Nb: In order to include the 17/2- isomer at 2.034 MeV, we assume that the second excited state (7/2- at 1.040 MeV) decays by an E1 transition to the 9/2+ ground state. We also assume that the 9/2+ level at 1.885 MeV decays 67% of the time by E1 to the 7/2- state at 1.040 MeV and 33% of the time by M1 to the 7/2+ state at 1.581 MeV. Since the first isomer lies below these states (1/2- at 0.104 MeV), these assumed branching ratios will have an effect on our modeled cross sections, particularly those that have ^{91}Nb as a residual.
- ^{90}Mo: Filled in several branching ratios for levels between the 0+ ground state and the 8- isomer at 2.875 MeV. Since any population of these levels will eventually decay to the ground state, the choice of branching ratios will not affect our modeled cross sections.
- ^{93}Tc: For the 7/2- level at 1.555 MeV, we assume an E1 transition to the ground state. This branching ratio was needed in order to include the 17/2- isomer at 2.185 MeV. This choice of branching could affect the amount of cross section going to the ground state and first isomer at 0.392 MeV.
- ^{98}Tc: Assumed that the third excited state (3- at 0.073 MeV) decays via E1 to the second excited state. This is done in order to include the 2- isomer at 0.091 MeV in our level scheme. There are no isomers between this state and the ground state, so this assumed branching ratio will not affect our modeled cross sections.

Each of these modified level schemes are also included in appendix B.3. For ^{100}Rh the number of missing levels, spins, and/or parities prevented the inclusion of the isomer in our calculations.

A few of the nuclei included in this study have a first excited state that is nearly degenerate in energy with the ground state. Since having two levels with the same energy cannot be handled by our Hauser-Feshbach code, we have increased the energy of the first excited state for these nuclei to 10 eV. The isotopes affected are ^{96}Y, ^{98}Y, ^{87}Nb, ^{88}Nb, ^{89}Nb, ^{91}Ru, ^{94}Rh, and ^{98}Rh.

In some cases a visual inspection of the cumulative number of levels as a function of energy suggests that levels are missing from the discrete level scheme. In such cases, we reduce the number of discrete levels used in our calculations (see section 3.3.3). In cases where no discrete level data is available we only include a ground state in our calculations.

3.2. Transmission Coefficients

Energy-averaged transmission coefficients are needed for each particle considered as a possible exit channel in the Hauser-Feshbach denominator. In our modeling effort, we include outgoing neutrons, protons, α-particles, deuterons, and photons. We do not include other light particles (such as tritons and ^{3}He).

3.2.1. The Neutron and Proton Optical Potential

For the calculation of the neutron and proton particle transmission coefficients, we adopt the optical model of (Koning & Delaroche 2003). Although they have tuned their parameters to fit data for many different species (see their Tables 6 and 7), we use the global nucleon-nucleon optical model potential (OMP), as it gives a very satisfactory fit to measured total neutron cross section data and measured total proton reaction cross section data in the range of interest to us. Specifically, we adopt the potential depth parameters and Fermi energies for the neutron and proton global OMP defined in their Section 5.2, tables 14 and 15. The particle transmission coefficients were generated by the optical model code ECIS-96 (Raynal 1996). Although designed for coupled channel calculations, we used the code in a spherical optical model mode.

We present in Figure (1) results of the Koning & Delaroche optical model compared to measured total neutron cross sections for select targets in our region of interest. For nuclei with $A < 96$, the optical model prediction (solid black line) closely replicates the measured total neutron cross sections above ∼500 keV. At lower energies, the measured cross sections generally exhibit structure due to individual resonances. This structure cannot be reproduced by an optical model, which only predicts average cross sections.

We have performed additional comparisons for total neutron cross sections on targets of strontium, technetium, and rhodium, with similar results. This optical potential has also produced favorable comparisons to measured total neutron cross sections in other regions of the periodic chart (Hoffman *et al.* 2004a; Hoffman *et al.* 2004b; Hoffman *et al.* 2004c; Kelley *et al.* 2005; Kelley *et al.* 2006). Further evaluations are provided in (Koning & Delaroche 2003).

For nuclei with $A \geq 96$, the optical model over predicts the measured total neutron cross section by roughly 50% between ∼80-500 keV. One possible cause is that we have neglected nuclear deformations. The heavier nuclei in our region of interest are somewhat deformed, and the collectivity of the even-even nuclei (defined as the ratio of the energies of the first $J^\pi = 4^+$ to $J^\pi = 2^+$ levels) above $A = 96$ have values ranging between 2.0 and 2.6, indicating that the nuclei may be better treated as deformed vibrators. However, the loaded detector elements considered in this study (stable yttrium, zirconium, niobium, and molybdenum) almost all lie below $A = 96$. All of the reactions that will significantly affect the production of the radioactive species of interest lie at or below $A = 92$. Thus, we may adopt the simpler spherical model without introducing significant errors into the modeled cross sections.

Further information regarding the quality of the neutron optical potential may be obtained by comparing the s- and p-wave strength functions and mean scattering radii predicted by the model to measured values. We make such a comparison in Figure 2. Each of these plots show the ratio of the quantity predicted by the optical potential to the measured value, plotted against the mass of the compound (target plus neutron) system. The error bars reflect this same ratio using the upper and lower errors in the measured values. Hence, if the error bars cross unity, the optical model prediction is within the errors of the measured value. For the s-wave strength functions (S_0), we see that many of the optical model predictions lie within the errors of the measured values. In all cases, the modeled/measured ratio is with a factor of two (in-

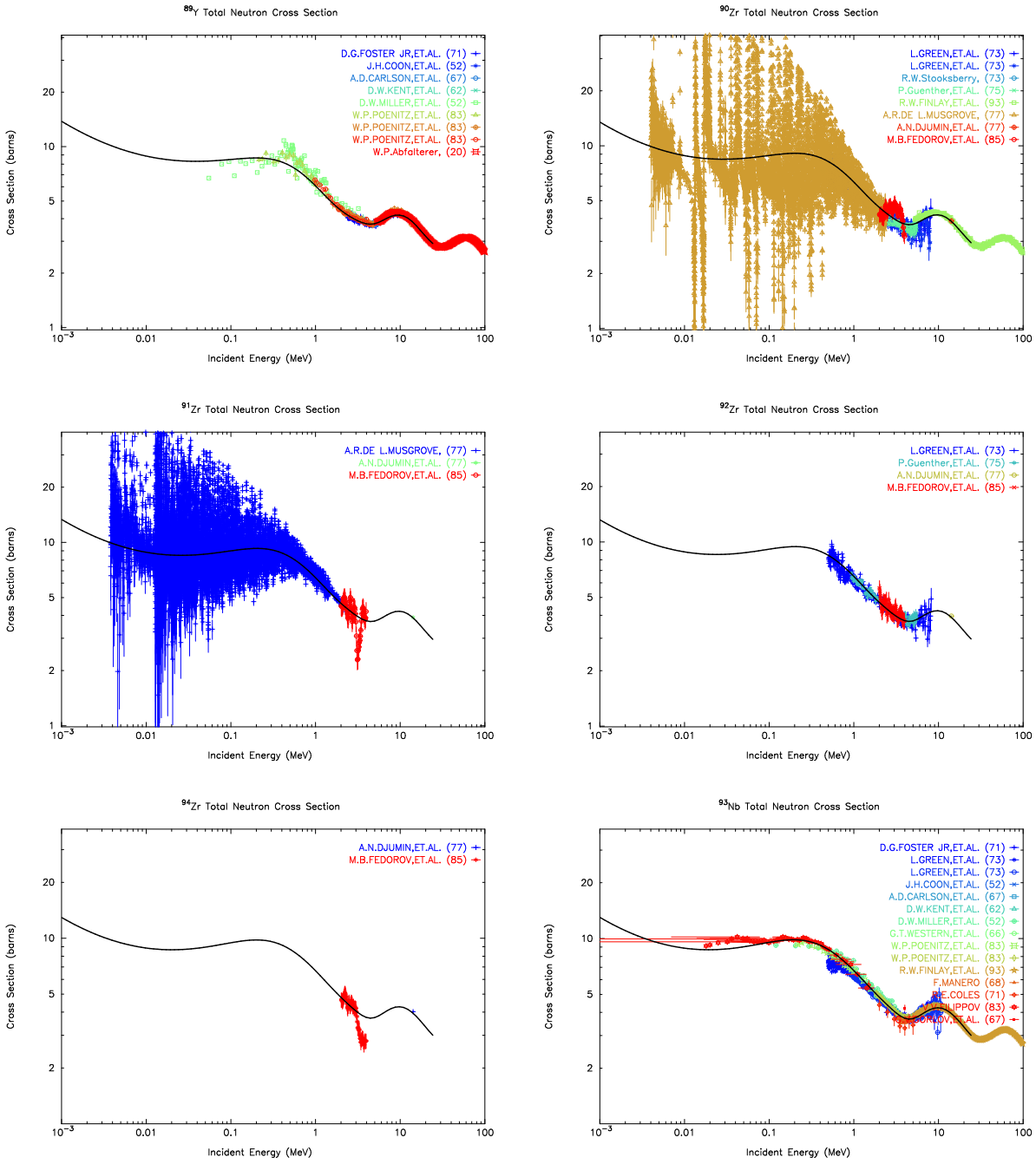

Fig. 1.— Total measured neutron cross sections vs those predicted by the optical model of Koning-Delaroche for select targets in the range $38 \leq Z \leq 45$. Measured values were obtained from (EXFOR 2006). The optical model prediction is indicated by the solid black line.

dicated by the two outer dotted lines). Similarly, the predicted p-wave strength functions (S_1), also fall within a factor of two of the measured values. The mean scattering radii predicted by the optical potential (R'), are slightly higher than the measurements.

There is some evidence that the proton transmission coefficients derived from this optical potential may be too large for lighter nuclei (Kelley *et al.* 2005). To gauge whether or not the proton transmission function is also too large for nuclei in the current region of interest

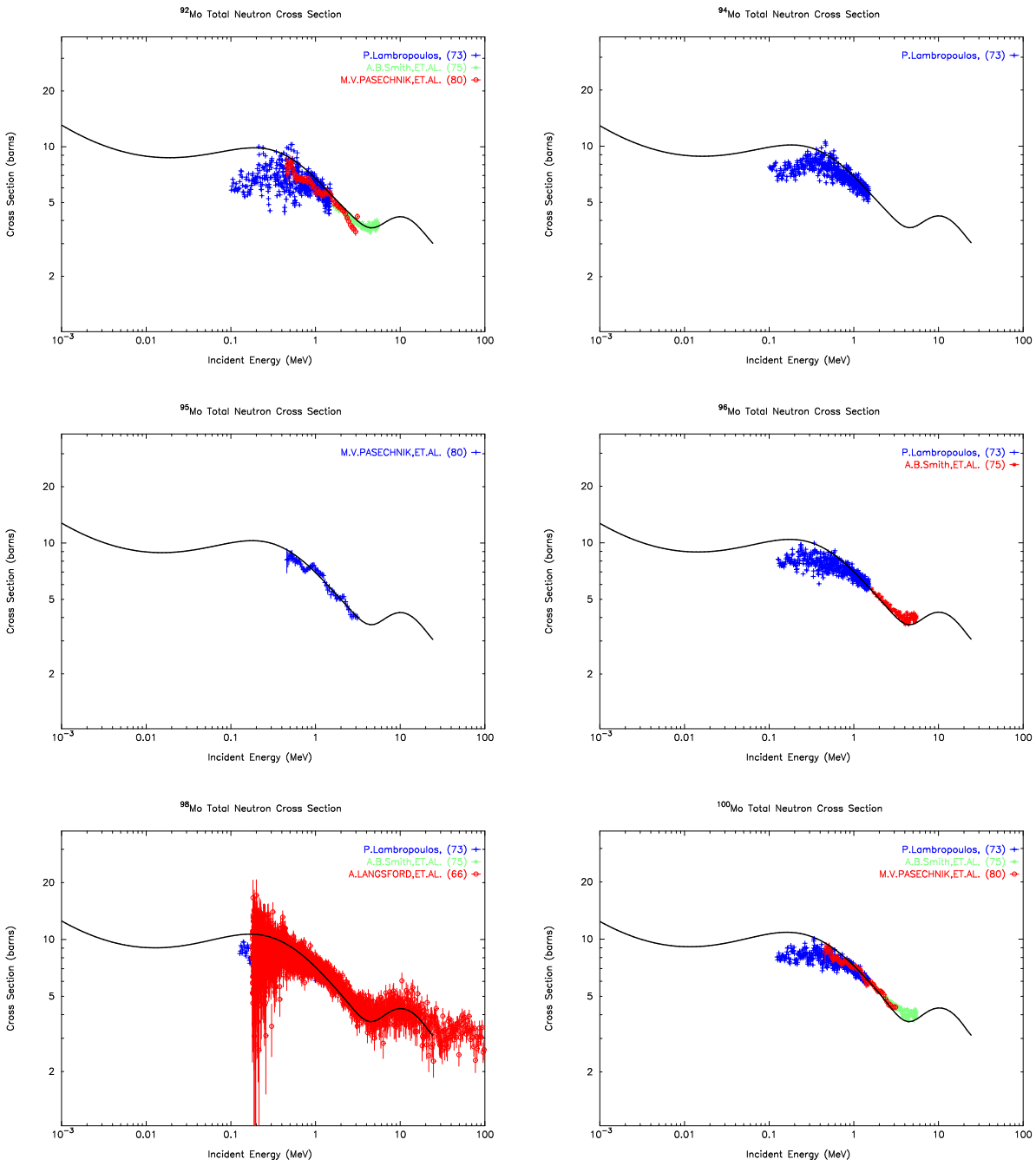

Fig. 1.— (continued)

$(38 \leq Z \leq 45)$, we compare the total proton reaction cross section predicted by the optical model to measured values in Figure 3. In this figure, the black line represents the optical model calculation and the red data represents measurements taken from (EXFOR 2006). These comparisons indicate that the proton transmission coefficients for the Koning and Delaroche optical potential may be somewhat high for the lighter targets considered in this study, though only by 10-15% at most at 14.5 MeV. A large proton transmission coefficient should only appreciably affect the calculated (p,n), (p,2n), (n,p), and (n,np) cross sections.

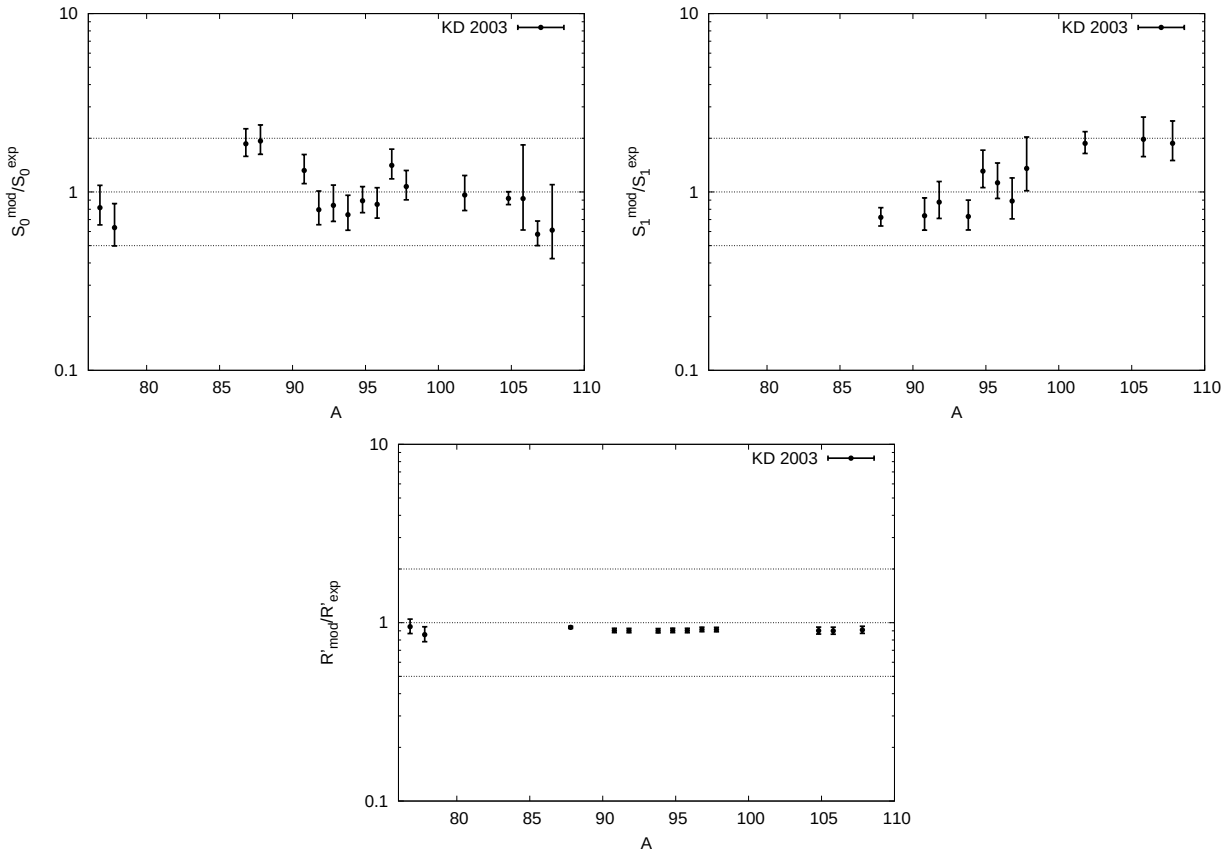

Fig. 2.— Measured s- and p-wave strength functions and mean scattering radii compared to the predictions of the Koning and Delaroche optical potential. The measured values for the s- and p-wave strength functions (S_0 and S_1) are taken from (Belgya *et al.* 2005). Measured scattering radii are taken from (Mughabghab *et al.* 1981). Plotted are the ratios of the modeled quantities to their measured counterparts. The dotted lines indicate unity and factor of two deviations.

3.2.2. The Alpha and Deuteron Optical Potentials

We have included possible alpha and deuteron exit channels (and appropriate transmission coefficients) in this modeling effort. For these particles we use the well-established spherical optical potentials of (Avrigeanu *et al.* 1994) and (Lohr & Haeberli 1974), respectively.

We do not include a quality analysis of these potentials in this report. This is primarily due to the lack of total cross section (and total reaction cross section) data in the local region at energies of interest in this study. For the majority of the reaction channels critical to the the radiochemical diagnostics, the deuteron and alpha particle exit channels are quite small when compared to the dominant exit channel, and hence errors introduced through the deuteron and alpha particle optical models should be insignificant. The only exceptions are the (n,α) and (n,nα) reactions producing zirconium from stable molybdenum in the detector set Mo1278. Nonetheless, the degree to which our modeling effort is able to reproduce measured (n,α) and (n,nα) cross sections up to 15 MeV in the region of interest gives us some confidence in the alpha particle optical potential (see Appendices C.8 and C.9).

The deuteron exit channels are always very small compared to the dominant channel, and were not included in the previous RADCHEM detector sets. Incident deuteron reactions, particularly (d,2n) and (d,3n), are of importance in radiochemical diagnostics, though. The deuteron induced reactions of greatest importance have been measured, and will be used in lieu of modeled cross sections in the UGT analysis.

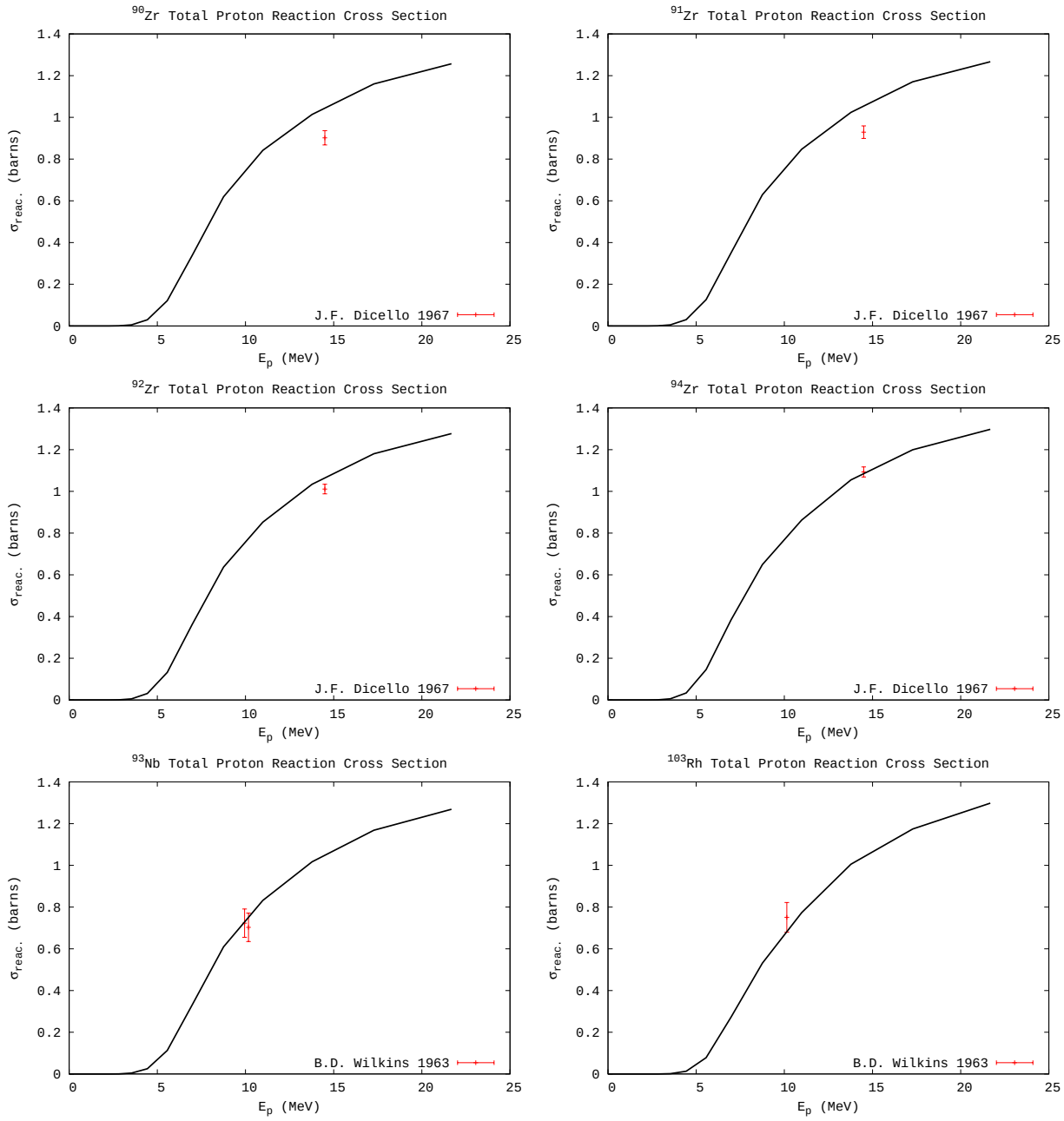

Fig. 3.— Total measured proton reaction cross sections vs those predicted by the optical model of Koning-Delaroche for select targets in the range $38 \leq Z \leq 45$. Measured values were obtained from (EXFOR 2006). The optical model prediction is indicated by the solid black line.

3.2.3. Transmission Coefficients for Photons

Gamma ray transmission coefficients were calculated using a simple model which depends only on the multi-pole type (XL) and the transition energy (ϵ). They are related to the gamma ray strength function $f^{\gamma}_{XL}(\epsilon)$ by

$$T^{\gamma}_{XL}(\epsilon) = 2\pi\epsilon^{2L+1} f^{\gamma}_{XL}(\epsilon) \qquad (5)$$

The energy dependence of the strength function was determined using the GDR model with enhanced generalized Lorentzian (EGLO) line shapes (Kopecky *et al.* 1993). In particular, the E1 strength function is given by

$$f^{\gamma}_{E1}(\epsilon) \quad = \quad \mathcal{N}\frac{4}{3\pi}\frac{e^2}{\hbar c}\frac{1}{M_p c^2} \times$$

$$\left[\frac{\epsilon\Gamma_{GDR}(\epsilon,T_f)}{(\epsilon^2-E_{GDR}^2)^2+(\Gamma_{GDR}(\epsilon,T_f)\epsilon)^2}+0.7\frac{\Gamma_{GDR}(0,T_f)}{\epsilon^3}\right] \quad (6)$$

where M_p is the proton mass. The energy dependent width $\Gamma_{GDR}(\epsilon,T_f)$ is given by

$$\Gamma_{GDR}(\epsilon,T_f) = \left[\kappa+(1-\kappa)\frac{\epsilon-\epsilon}{E_{GDR}-\epsilon}\right]\times \frac{\Gamma_{GDR}}{E_{GDR}^2}\left[\epsilon^2+(2\pi T_f)^2\right] \quad (7)$$

with $\epsilon = 4.5$ MeV. For nuclei with $A < 148$, the factor κ is unity. For heavier nuclei, $\kappa = 1 + 0.009(A-148)^2\exp[-0.18(A-148)]$. The T_f that appears in Equations 6 and 7 is the temperature of the final state, determined from the level density parameters. For a backshifted transition energy $U = S_n - \epsilon - \Delta$ one first determines the energy dependent level density parameter a (see Section 3.3.2). Provided U is positive, the temperature is given by

$$T_f = \frac{a}{2}\left[1+\sqrt{1+4aU}\right] \quad (8)$$

Otherwise, $T_f = 1/a$.

The parameters E_{GDR}, Γ_{GDR}, and σ_{GDR} (the energy, width, and peak cross section of the GDR resonance) have been measured for several nuclei (Belgya *et al.* 2005). Based on these measurements, we have adopted a systematic description of these parameters for other targets. Using only measured GDR parameters from the local region of interest, we fit systematic values of the form $E_{GDR} \propto A^{-1/6}$, $\Gamma_{GDR} \propto A^{-1/3}$, and $\sigma_{GDR} \propto A$. As suggested in (Woosley *et al.* 1976), the GDR width of nuclei on or near closed shells will generally be lower than those predicted by such systematics. To account for these "shell effects", we divide the measured GDR widths of closed shell nuclei by a factor of 0.6 and those one nuclei away from a closed shell by a factor of 0.8 prior to fitting the systematics. The resulting systematic GDR widths for closed shell and near-closed shell nuclei are then multiplied by factors of 0.6 and 0.8, respectively. Measured GDR parameters are used in preference to systematics where they are available. The resulting systematic fits are presented in Figures (4-6), and are given by

$$E_{GDR} = \frac{34.3506 \text{ MeV}}{A^{1/6}}$$

$$\Gamma_{GDR} = \frac{26.7114 \text{ MeV}}{A^{1/3}}$$

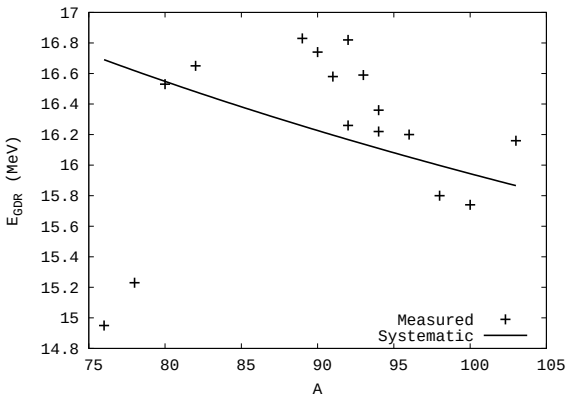

Fig. 4.— Systematics for the GDR energy. The measured data in the local region of interest are taken from (Belgya *et al.* 2005).

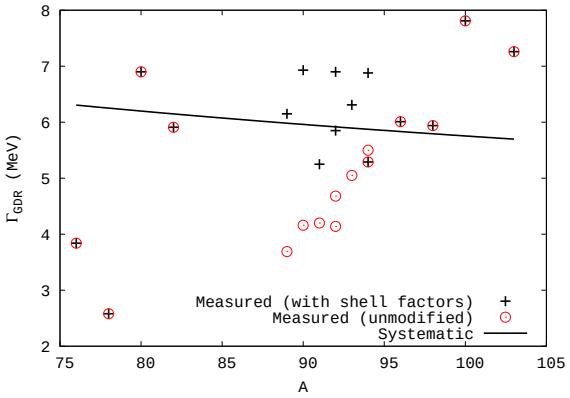

Fig. 5.— Systematics for the GDR width. The unmodified measured data in the local region of interest, indicated by the red circles, are taken from (Belgya *et al.* 2005). The modified data to which the systematic was fit, as described in the text, is indicated by the solid black markers.

$$\sigma_{GDR} = A \times 1.81357 \text{ mb} \quad (9)$$

where A is the mass number of the compound nucleus. We consider only a single E1 resonance.

We also include M1, E2, M2, E3, and M3 transitions in our modeling. For the M1 strength function, we adopt a Simple Lorentzian (SLO) model

$$f_{M1}^{\gamma}(\epsilon) = \mathcal{N}_{M1}\frac{4}{3\pi}\frac{e^2}{\hbar c}\frac{1}{M_p c^2}\times \frac{\epsilon\Gamma_{GDR}}{(\epsilon^2-E_{GDR}^2)^2+(\Gamma_{GDR}\epsilon)^2} \quad (10)$$

with the global set of GDR parameters given in (Belgya *et al.* 2005):

$$E_{GDR} = \frac{41}{A^{1/3}}$$

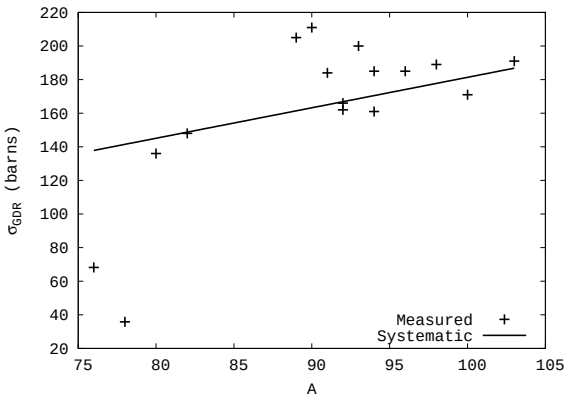

Fig. 6.— Systematics for the GDR peak cross section. The measured data in the local region of interest are taken from (Belgya *et al.* 2005).

$$\Gamma_{GDR} \quad = \quad 4 \tag{11}$$

The overall normalization for the M1 strength function ($\mathcal{N}_{M1}$) is determined such that

$$\frac{f_{E1}(S_n)}{f_{M1}(S_n)} = 0.0588 \cdot A^{0.878} \tag{12}$$

where S_n is the neutron separation energy.

The remaining transmission coefficients are simply proportional to ϵ^{2L+1}, i.e. their strength functions are constants. In particular,

$$\begin{aligned} f^{\gamma}_{E2}(\epsilon) &= 7.2 \times 10^{-7} A_C^{2/3} f^{\gamma}_{E1}(S_n) \\ f^{\gamma}_{M2}(\epsilon) &= 2.2 \times 10^{-7} f^{\gamma}_{E1}(S_n) \\ f^{\gamma}_{E3}(\epsilon) &= 3.4 \times 10^{-13} A_C^{4/3} f^{\gamma}_{E1}(S_n) \\ f^{\gamma}_{M3}(\epsilon) &= 1.1 \times 10^{-13} A_C^{2/3} f^{\gamma}_{E1}(S_n) \end{aligned} \tag{13}$$

The factor $\mathcal{N}$ appearing in equation 6 is an overall normalization constant, determined by fitting the average total s-wave radiation width at the neutron binding energy,

$$\begin{aligned} \langle \Gamma_\gamma \rangle_0 &= \frac{J+1}{2J+1} \left\langle \Gamma_\gamma \left(B_n, J + \frac{1}{2} \right) \right\rangle \\ &+ \frac{J}{2J+1} \left\langle \Gamma_\gamma \left(B_n, J - \frac{1}{2} \right) \right\rangle \end{aligned} \tag{14}$$

$$\Gamma_\gamma \left(E, J \right) = \frac{T_\gamma(E,J)}{2\pi\rho(E,J)} \text{ (meV)}$$

(Uhl & Strohmaier 1976). Here, J is the spin of the target nucleus. The gamma-ray transmission coefficients are evaluated as in Equation 3 with the summation over multipoles instead of spins and parities.

Since the total s-wave radiation width is generally measured only for stable isotopes plus a neutron, we have developed a systematic approach for estimating this value for the many unstable nuclei in our region of interest. Systematic descriptions of the average total s-wave radiation width generally exhibit a dependence on the mass and s-wave resonance spacing (D_0) of the nucleus (Gardner 1975). We find that the measured radiation widths from (Belgya *et al.* 2005) are generally well fit by a plane in the (A, $\log_{10} D_0$) coordinate space:

$$\begin{aligned} \langle \Gamma_\gamma \rangle_0^{\text{sys}} &= (251.536\ A - 14590.7) \\ &\times (\log_{10} D_0 - 8.10272) \end{aligned} \tag{15}$$

This systematic is shown in Figure (7). Whenever they are available, we use measured radiation widths instead of systematics.

3.3. Nuclear Level Densities

3.3.1. Level Density Models

Another important input to the statistical model code is the nuclear level density. For this project, we have adopted a standardized, semi-empirical approach which is numerically efficient, can be tied to experimental data, and is fairly accurate. The level density is described by two functions. Both are energy dependent, and the second factor contains the spin dependence. This is the "Back-shifted Fermi Gas" formulation of the nuclear level density:

$$\rho\left(U, J\right) = \rho\left(U\right) f\left(U, J\right) \tag{16}$$

where $\rho(U)$ is the state density, with $U = E - \Delta$ the back-shifted energy. Δ is the so called "back-shift", and J is the spin of the compound nucleus. It is assumed that the parity distribution of nuclear states is equal, i.e. for a given parity Π $\rho(U, J, \Pi) = \frac{1}{2}\rho(U, J)$. We will further treat each of these in two ways, depending on the excitation energy of interest. The demarcation point will be roughly between the energy range of the known excited levels of a given compound nucleus (the low energy domain), and near (and above) the neutron binding energy (the high energy domain).

For the high energy domain, we describe the level density assuming a Fermi gas formula,

$$\rho\left(U\right) = \frac{\sqrt{\pi}}{12} \frac{\exp\left(2\sqrt{aU}\right)}{a^{1/4}U^{5/4}} \frac{1}{\sqrt{2\pi}\sigma} \tag{17}$$

$$f\left(U, J\right) = \frac{2J+1}{2\sigma^2} \exp\left[\frac{-\left(J+\frac{1}{2}\right)^2}{2\sigma^2}\right] \tag{18}$$

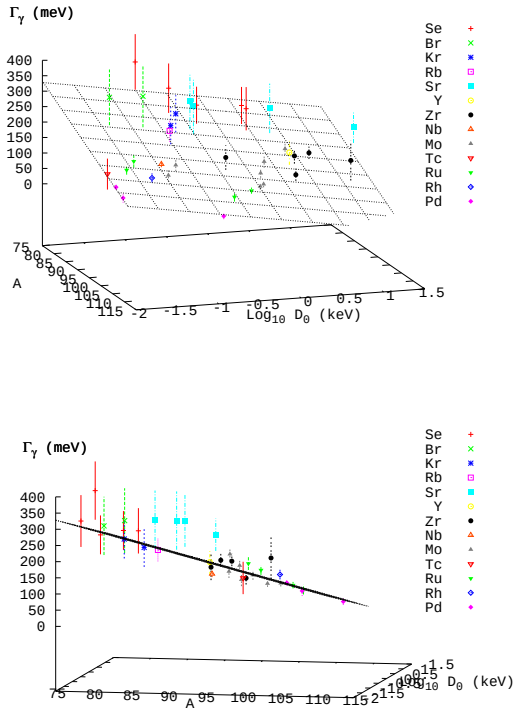

Fig. 7.— Systematics for average total s-wave radiation widths. The systematic is presented from two perspectives. The upper pane shows the relative mass and resonance spacing of the nuclei with measured radiation widths. The lower pane show the same systematic, only looking directly down the systematic plane to illustrate deviations of the systematic from measured values.

where $a(E)$ is the level density parameter (in MeV^{-1}). The spin cutoff parameter σ^2 is defined as

$$\sigma^2 = 0.01496\ \lambda A^{5/3}\sqrt{\frac{U}{a}} \qquad (19)$$

The level density assumes an equal distribution of parity states. Note that at low excitation energy (for a positive back-shift), Eq. (17) diverges. At low energies, the nuclear level density is better described by a constant temperature formula:

$$\rho(E) \propto \exp\frac{E - E_0}{T} \qquad (20)$$

The level density parameters can be calculated using experimental data. For the Fermi-gas state density (Eq. 17), the level density parameter, $a(E)$, can be related to the average level spacing (D_0) near the neutron binding energy. The backshift Δ is calculated as a difference in binding energies of adjacent nuclei (Bohr & Mottelson). The constant temperature parameters E_0 and T are fixed by the choice of a matching energy E_x (chosen such that the state density that goes through the low lying spectroscopic levels) and the condition that the two state densities match tangentially at E_x. We describe below how we determined these parameters for all of the nuclei considered in this study.

3.3.2. Fermi-Gas Level Densities

Our goal is to fit the level density parameter a in Eq. (17) to experimental data where available. We adopt an energy dependent form, $a(U, Z, N)$, and begin by fixing the spin cutoff parameter and the pairing energies.

The Spin Cutoff Parameter

The spin cutoff parameter σ^2, Eq. (19), characterizes the spin distribution of the Fermi gas level density. It depends on the parameters a, the level density parameter, and λ, which determines the effective moment of inertia for the nucleus in question. In principle it could be determined by experiment, for example, by comparing ratios of cross sections leading to different isomers of the product nucleus (Keisch 1963). Because data like this is often sparse, especially in the limited regions of the periodic chart we are interested in, and because we are often interested in reactions that proceed on or through radioactive species where no such data exists, we must resort to models. In our analysis, we fix $\lambda = 1$ in Eq. (19), corresponding to the moment of inertia of a rigid sphere.

Pairing Energies

In determining the backshift Δ, also known as the pairing energy, we use the method of (Rauscher *et al.* 1997). The total pairing energy is equal to the sum of the proton and neutron pairing energies

$$\begin{aligned} \Delta(Z,N) &= \frac{1}{2}\left(\Delta_p + \Delta_n\right) \qquad (21)\\ \Delta_p\left(Z,N\right) &= E^G\left(Z,N\right) \\ &- \frac{1}{2}E^G\left(Z-1,N\right) \\ &- \frac{1}{2}E^G\left(Z+1,N\right) \\ \Delta_n\left(Z,N\right) &= E^G\left(Z,N\right) \end{aligned}$$

$$- \quad \frac{1}{2} E^G (Z, N-1)$$
$$- \quad \frac{1}{2} E^G (Z, N+1)$$

where $E^G(Z,N)$ is the binding energy of the nucleus (Z,N).

The Level Density Parameter

At high energies, the level density parameter a behaves essentially as a function of mass number only. However, it has been shown (Iljinov *et al.* 1992) that at low energies it is more appropriate to use an energy dependent form:

$$a(U,Z,N) = \tilde{a}(A)\left[1 + \delta W(Z,N)\frac{f(U)}{U}\right] \quad (22)$$

with

$$f(U) = 1 - \exp(-\gamma U) \quad (23)$$

and as usual $U = E - \Delta$.

In previous works where a more global prescription was developed [(Rauscher *et al.* 1997), (Iljinov *et al.* 1992)], one would adopt a semi-empirical shell correction, $\delta W(Z,N)$, and fit $\tilde{a}(A)$ to known experimental data. Here we choose to adopt a simple form for the mass dependent term and fit the shell correction. In our analysis, we followed the convention of (Rauscher *et al.* 1997) in choosing the parameters $\gamma = 0.04884$ and $\tilde{a} = 0.1337\ A - 0.06571\ A^{2/3}$.

Shell Corrections

Given an asymptotic value of the level density parameter, the shell corrections can be determined for select nuclei from experimental values of the average level spacings D_0 as determined by neutron resonance analysis (Belgya *et al.* 2005). For $s-$wave resonances (neutron angular momentum equal to zero), the calculated level spacing, D_{calc}, evaluated at the neutron binding energy $U = B_n - \Delta$, is related to the nuclear level density (e.g. Equations 16-18)

$$D_{calc} = \frac{2}{\rho\left(U, J = \frac{1}{2}\right)} \quad (24)$$

for nuclei with spin $s = 0$ and

$$D_{calc} = \frac{2}{\rho\left(U, J = s + \frac{1}{2}\right) + \rho\left(U, J = s - \frac{1}{2}\right)} \quad (25)$$

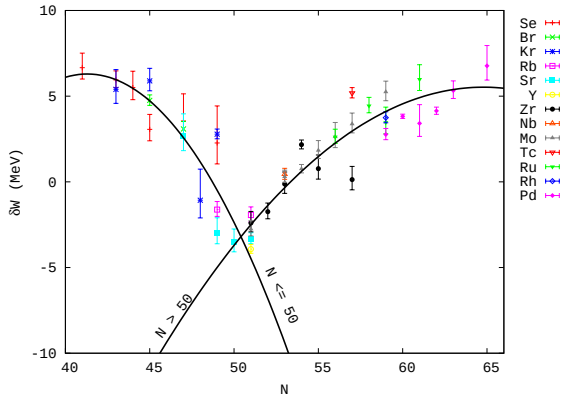

Fig. 8.— χ^2 fit to experimentally determined shell corrections, used to systematically determine unknown shell corrections.

for nuclei with $s \neq 0$. In each case, the level densities $\rho(U,J)$ were calculated using the other parameters $(\lambda, \Delta, \gamma, \tilde{a}(A))$ set as previously described. We then numerically solved for the value of δW that would minimize the quantity $D_{calc} - D_0$ using root bisection methods.

There are only a limited number of nuclei for which the average resonance spacing D_0 has been measured (i.e. for compound nuclei formed from a stable target plus a neutron). As a result, we were required to systematically predict the shell correction for the remaining nuclei in the range of interest. After plotting the "experimental" δW in our region of interest and their associated errors we noted two segments with a roughly quadratic behavior. A χ^2 fit to the data results in the systematic

$$N \leq 50 \quad : \quad \delta W = -0.114\ N^2 + 9.45\ N - 188.8$$
$$N > 50 \quad : \quad \delta W = -0.042\ N^2 + 5.46\ N - 171.3 \quad (26)$$

This systematic, along with the derived "experimental" shell corrections, is shown in Figure 8. Of course, where available, we always use an experimentally determined shell correction over a systematic one.

3.3.3. Constant Temperature Level Density

For the lower energy regions, below the neutron binding energy B_n, the nuclear level density has the same formulation as Equation (16). However, particularly at and below the pairing energy Δ, the state density in Equation (17) becomes imaginary. Unfortunately, experimental level schemes are rarely known above 2 MeV of excitation en-

ergy. In practice we are forced again to assume a model and use all available experimental data to constrain its parameters.

Of course the two prescriptions for the level density must match at some energy intermediate to where they are constrained by experiment. Henceforth we will refer to the high energy level density as ρ_1, and the low energy density as ρ_2.

Gilbert and Cameron (Gilbert & Cameron 1965) noticed that the cumulative number of observed levels (the so-called staircase plot, which increase exponentially), can be fit with straight lines in a semi-log plot. They adopted a constant temperature formula to fit these:

$$N(E) = \exp\left[\frac{E - E_0}{T}\right] \tag{27}$$

with $N(E)$ being the cumulative number of levels at excitation energy E, E_0 and T are two free parameters to be fit to the observed level structure. The observable level density is given by

$$\rho_2(E) = \frac{dN(E)}{dE} = \frac{1}{T}\exp\left[\frac{E - E_0}{T}\right] \tag{28}$$

where T now takes on the meaning of a nuclear temperature which is constant in the region of the discrete levels. We assume that Eq. (27) can be extrapolated from the region of the known discrete levels to higher energies, where the Fermi-gas level density (ρ_1) is valid. We then define the notion of a fit to the total level density over the entire range as being achieved if: (a) a good fit can be made to the low lying levels, (b) the observed level spacing at the neutron binding energy is exactly reproduced, and (c) the energy of the matching point E_x for the two prescriptions falls between $E = \Delta$ and $E = B_n$, and that they match at this point with the same slope, i.e. for $E = E_x$:

$$\rho_1(E_x) = \rho_2(E_x) \tag{29}$$

$$\frac{d\log\,\rho_1(E_x)}{dE} = \frac{d\log\,\rho_2(E_x)}{dE} \tag{30}$$

From the first of these, we can determine E_0:

$$E_0 = E_x - T\,\log\,T\rho_1\,(U_x) \tag{31}$$

where $U_x = E_x - \Delta$. The second condition can be satisfied by assuming that at E_x the constant nuclear temperature T of the low lying states is equal to the energy dependent nuclear temperature $\tau(U_x)$ of the high excited states,

$$\begin{aligned}\frac{1}{T} &= \sqrt{\frac{a}{U_x}} - \frac{3}{2U_x} \\ &+ \frac{(\tilde{a} - a)(1 + \gamma U_x) + \tilde{a}\gamma\delta W}{\sqrt{aU_x}}\end{aligned} \tag{32}$$

where a is given by Eq. (22). If there is no shell correction, the latter term in the above equation is zero. Typical values for the matching energy are $2 \leq E_x \leq 8$ MeV, and are approximated by $E_x = 2.5 + \frac{150}{A} + \Delta$ (Gilbert & Cameron 1965). However, we fit the spectroscopic levels for each nucleus manually, adjusting E_x to give the best possible fit.

Occasionally when fitting E_x to the spectroscopic discrete levels, one encounters a situation where the ideal E_x either lies below the backshift (so that the Fermi gas portion of the level density diverges) or results in a negative temperature when E_0 and T are determined by the tangential match at E_x. We prefer to avoid such unphysical level densities. Usually, these situations occur where the cumulative number of levels (i.e. the "staircase plot") is not well fit by a constant temperature formula because levels are likely missing from the scheme. In these cases, we reduce the number of levels fit until they are well described by a constant temperature formula, and adjust E_x to get the best match possible. We also make an extra effort to fit the level density to the highest known discrete level included in the level scheme, so that the effective level density used in the Hauser-Feshbach calculations will be continuous between energies where the discrete levels and level densities are used.

We present in Figure (9) a sample of constant temperature fits to low lying levels. In these figures, the blue lines represent the cumulative number of levels for which spins and parities are known. The green lines represent additional levels above the point where the level scheme is complete. Red lines represent Fermi gas level densities, and magenta lines represent constant temperature level densities. Red circles indicate the value of the matching energy E_x. The larger plot shows the the fit compared to the levels used in our Hauser-Feshbach calculation. The smaller insets show the fit compared to all available levels, including those above the point where the level scheme is considered complete.

Behavior of the Spin Cutoff Parameter Below E_x

At the matching energy E_x, the spin cutoff parameter is given by Equation (19). For energies below E_x, we assume $\sigma^2 = \sigma^2(E_x)$.

Other treatments have been suggested for the behavior of σ^2 below E_x.One may define E_{cut} as the energy of the highest known excited level for

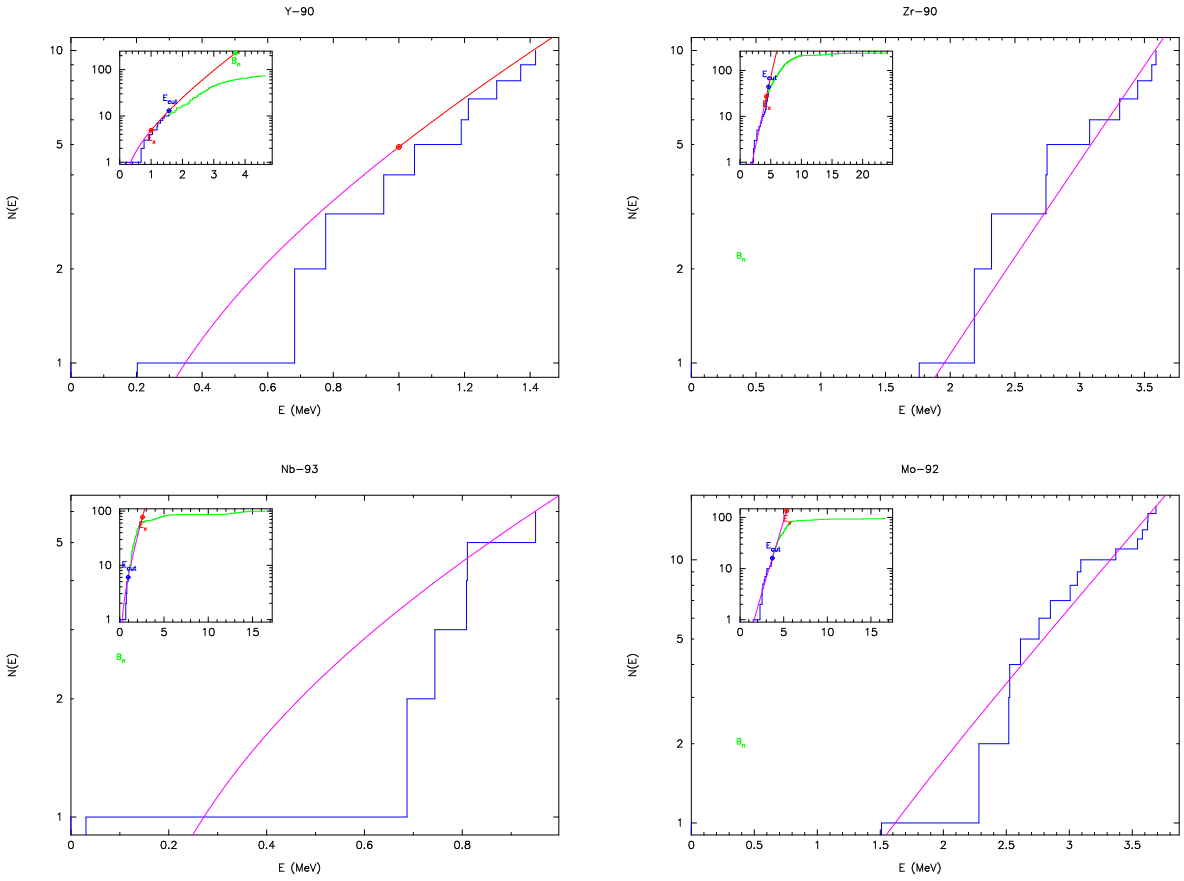

Fig. 9.— Select constant temperature level density fits to the low lying spectroscopic levels. See text for details.

which energy, spin and parity are explicitly known. Using the known spectroscopic levels, a low energy spin cutoff parameter at E_{cut} may be defined:

$$\sigma^2_{E_{cut}} = \frac{1}{2N}\sum_{i=1}^{N}(J_i + \frac{1}{2})^2 \qquad (33)$$

where N represents the number of the level with energy E_{cut}, J_i are the spins of the individual levels. The sum excludes the ground state (i=0). This value is used for energies $0 \leq E \leq E_{cut}$. For energies $E_{cut} \leq E \leq E_x$, the spin cutoff parameter is given by a linear fit between these two values (Equations (19) and (33)). Specifically,

$$\sigma^2_I = \sigma^2_{E_x} - \frac{\sigma^2_{E_x} - \sigma^2_{E_{cut}}}{E_x - E_{cut}}(E_x - E) \qquad (34)$$

This conforms to the treatment of σ^2 in the IDA reaction code system (Reffo 1978). This particular treatment works well when there are a reasonably large number of levels to fit.

Another treatment, used in the GNASH code system (Chadwick 1998), defines:

$$\begin{aligned} \sigma^2_H &= \sigma^2_{E_x} \\ U_L &= \max(E_{cut} - \Delta, 0.1) \\ \sigma^2_L &= \lambda\sqrt{aU_L}A^{2/3} \\ \sigma^2_G &= \sigma^2_L + \frac{E - \frac{1}{2}E_{cut}}{E_x - \frac{1}{2}E_{cut}}(\sigma^2_H - \sigma^2_L) \end{aligned} \qquad (35)$$

The form σ^2_G is then used between $\frac{1}{2}E_{cut}$ and E_x.

The behavior of σ^2 below E_x will only affect the level density used in Hauser-Feshbach calculations between E_{cut} and E_x, since the discrete levels are accounted for individually. The changes that arise in the level density between E_{cut} and E_x due to the choice of how σ is treated in this range are generally small.

The fitted parameters for the total level density are presented in Appendix B.4. The symbols in the legend are the same as described above. In column five, an "x" indicates the shell correction

δW was derived from an experimentally known level spacing D_0, an "s" indicates the shell correction was derived from the systematic shown in Figure 8. The last column indicates the number of excited states included in the fit.

3.4. Pre-Equilibrium Model Parameters

The exciton model described in section 2.4 has two free parameters which can be tuned to best reproduce measured cross sections in conjunction with the other statistical model inputs. The first is the constant $\langle FM \rangle$ which scales the average effective matrix element of the residual interactions. Increasing this parameter enhances the particle emission rates and, subsequently, the fraction of the reaction cross section involved in pre-equilibrium processes. We have found that a value of $\langle FM \rangle = 250$ MeV is optimal for reproducing measured (n,2n), (n,p), and (p,n) cross sections in this region. Radiative neutron capture reactions, being very small at incident energies where pre-equilibrium processes are important, exhibit no sensitivity to this parameter.

The other tunable parameter, ϕ, describes the probability of alpha cluster preformation. It follows that an increase in this variable will lead to an enhancement of alpha particle emission during the pre-equilibrium phase. However, since alpha emission is small compared to nucleon emission, modifying ϕ will have negligible effects on cross sections that do not involve alpha particles in the exit channel. We may thus use the (n,α) reaction to tune this parameter, for which we find a value of $\phi = 0.20$ to give satisfactory results. Previous works suggest that for compound nuclei of various masses this parameter will generally fall in the range $0.1 \leq \phi \leq 0.8$ (Milazzo-Colli & Braga-Marcazzan 1973).

We assume an initial two-particle one-hole configuration for the exciton model. In calculating emission rates we use the nuclear level densities developed in section 3.3.

4. Modeled Cross Sections

4.1. Comparison to Measured Cross Sections

Having developed the various input quantities based on available experimental data in the previous section, we now turn to the results of the STAPRE-H95 model and compare to available measured cross sections in the region of interest. We restrict our attention primarily to ground state targets of ^{89}Y, ^{90}Zr, ^{93}Nb, and ^{92,94}Mo (stable loaded detector elements closest in mass to the measured radioactivities). Comparisons to other measured cross sections are provided in the appendices.

4.1.1. Comparison to experimental (n,γ) capture cross sections

In Figure 10 we present comparisons for neutron capture reactions on select targets. Shown is the activation cross section (solid black lines in all plots that follow) defined as the sum of emission (both particle emission and gamma-ray cascade) from the compound nucleus that eventually leads to the ground state of the product (final) nucleus. We also provide (where appropriate) separate cross sections that decay to the ground state (red lines), and any long lived isomer (blue and green lines, see Appendix A.2 for a list of the isomers and their respective half-lives). These cross sections are plotted against the available experimental data, taken from the Experimental Nuclear Reaction Data File (EXFOR 2006). Cross sections for the total, ground, and isomeric states are colored in a similar manner to the modeled cross sections (gray is activation, orange is to ground, and light blue and green to an isomer, respectively), with different symbols distinguishing results from various experiments.

Our results are in excellent agreement with the wealth of measured data for ^{89}Y(n,γ)^{90}Y and ^{93}Nb(n,γ)^{94}Nb. The only general exception is around 14 MeV incident energy, where direct capture mechanisms (not included in our calculations) begin to become significant. Since the neutron capture cross section is usually two or three orders of magnitude smaller than the dominant neutron induced reactions at these energies, neglecting direct capture will introduce negligible errors into any network calculations. For ^{90}Zr(n,γ)^{91}Zr, our calculation is high by roughly a factor of 1.5 between ~5-50 keV. Below 5 keV, the effects of individual resonances (which cannot be reproduced with the statistical model) are present. For ^{94}Mo(n,γ)^{95}Mo our calculation is in excellent agreement with the single measured data point.

Additional comparisons for neutron capture cross sections are presented in Appendix C.1. A similar degree of agreement between our calculations and experiment is found in these comparisons (though our calculation appears to be high for ^{87}Sr(n,γ)^{88}Sr and ^{99}Tc(n,γ)^{100}Tc, and a bit low for ^{96}Ru(n,γ)^{97}Ru). Such results are con-

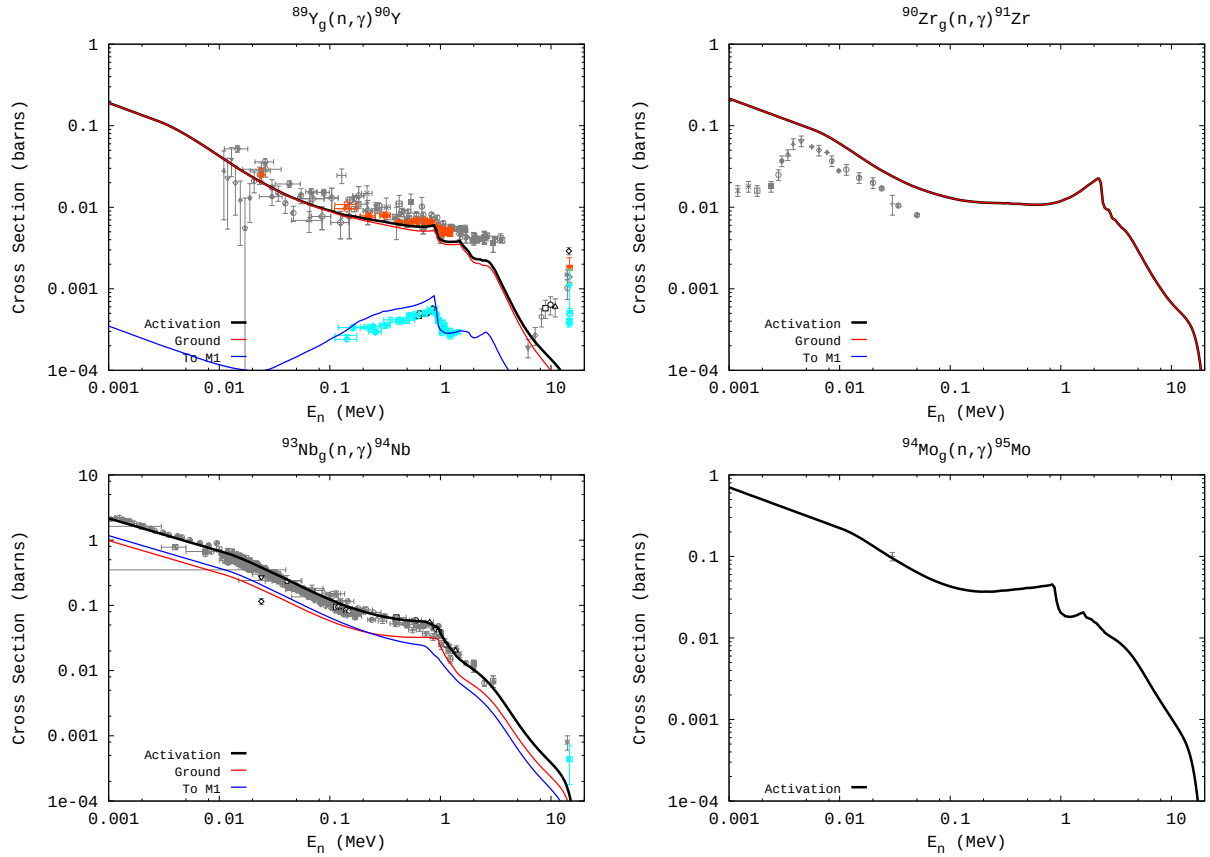

Fig. 10.— Calculated vs. measured (n,γ) cross sections on select stable isotopes in the region of interest. The data is taken from (EXFOR 2006). The black, red, and blue solid lines represent our modeled cross sections (total, leading to the ground state, and leading to the first isomer, respectively). The Gery, orange, and light blue data points are measured cross section data (total, ground state, and first isomer).

sidered good for (n,γ) activation cross sections. Using global systematics, (n,γ) cross sections can typically be modeled within a factor of two, often to within 30% (Hoffman *et al.* 1999).

A quantitative comparison of our calculated cross sections to the experimental data shown in Figures 10 and 25 is given in Table 1. For (n,γ) reactions we restrict our analysis to data with incident neutron energies of 30±2 keV. For each target listed in column (1), the subsequent column entries identify: (2) Res., the state of the residual (product) nucleus (activation, ground state, isomer); (3) N, the number of experimental data points falling within the incident energy range; (4) $\bar{\sigma}$, the weighted average of the measured data (in barns), with weights corresponding to the inverse geometric mean of the errors in cross section and energy (i.e. $w_i = (dE^2 + d\sigma^2)^{-1/2}$); (5) Dev., the standard deviation from the mean (also in barns), which gives an indication of the spread in the experimental data; (6) $\sigma_{mod.}$, our modeled capture cross section (in barns); and (7) $\bar{\sigma}/\sigma_{mod.}$, the ratio of the weighted average of the data to our modeled value, which may be used as a scaling factor to be applied to a given cross section to bring it into conformity with its respective average experimental value. Also provided at the bottom of the table is an average absolute percent error (defined as $\%E = N^{-1}\sum_{i=1}^{N}\left(|\sigma_i^{mod.} - \bar{\sigma}_i|/\bar{\sigma}_i\right) \times 100\%$) for all capture cross sections and the activation cross sections only.

On average, our modeled cross sections are within 35% of the weighted mean at 30 keV. Our activation cross sections are within 30% on average.

4.1.2. Comparison to Maxwellian averaged (n,γ) capture cross sections

Yet another comparison to experimental data comes from the extensive efforts to measure and

Table 1: Comparison of our modeled (n,γ) cross sections to experimental data at 30±2 keV

^{A}Z	Res.	N	$\bar{\sigma}$	Dev.	$\sigma_{mod.}$	$\bar{\sigma}/\sigma_{mod.}$
^{84}Sr	A	1	0.470	0.000	0.426	1.103
^{86}Sr	M1	1	0.122	0.000	0.051	2.397
^{86}Sr	A	21	0.097	0.061	0.068	1.434
^{87}Sr	A	21	0.089	0.026	0.182	0.491
^{89}Y	A	6	0.024	0.008	0.017	1.360
^{90}Zr	A	1	0.011	0.000	0.024	0.459
^{91}Zr	A	2	0.064	0.006	0.061	1.043
^{92}Zr	A	1	0.034	0.000	0.039	0.871
^{94}Zr	A	3	0.021	0.003	0.025	0.838
^{96}Zr	A	2	0.022	0.014	0.016	1.366
^{93}Nb	A	18	0.281	0.030	0.319	0.882
^{94}Mo	A	1	0.100	0.000	0.095	1.052
^{95}Mo	A	1	0.440	0.000	0.276	1.596
^{96}Mo	A	2	0.103	0.002	0.093	1.108
^{97}Mo	A	1	0.330	0.000	0.330	1.000
^{98}Mo	A	7	0.108	0.125	0.078	1.380
^{100}Mo	A	4	0.099	0.034	0.095	1.043
^{99}Tc	A	7	0.860	0.207	1.454	0.591
^{96}Ru	A	1	0.312	0.000	0.162	1.931
^{101}Ru	A	10	1.294	0.078	1.255	1.031
^{102}Ru	A	11	0.214	0.051	0.133	1.603
^{104}Ru	A	12	0.169	0.030	0.215	0.789
^{103}Rh	GS	1	0.600	0.000	0.989	0.607
^{103}Rh	M1	1	0.045	0.000	0.070	0.640
^{103}Rh	A	48	0.911	0.108	1.058	0.861
					Average error:	33.2%
					Average error (activation only):	29.6%

Table 2: Comparison of our modeled Maxwellian-averaged (n,γ) cross sections (in millibarns) to recommended values at 30 keV

^{A}Z	Recommended	Modeled	%E
^{84}Sr	368±126	404.5	9.9
^{86}Sr	64±3	69.7	8.9
^{87}Sr	92±4	176.2	91.6
^{88}Sr	6.2±0.3	12.8	106.6
^{89}Sr	19±14	27.0	42.3
^{89}Y	19.0±0.6	19.0	0.2
^{90}Zr	21±2	26.2	24.9
^{91}Zr	60±8	63.1	5.1
^{92}Zr	33±4	41.9	27.1
^{93}Zr	95±10	191.2	101.2
^{94}Zr	26±1	25.8	0.6
^{95}Zr	79±12	116.7	47.8
^{96}Zr	10.7±0.5	18.1	69.2
^{93}Nb	266±5	305.7	14.9
^{94}Nb	482±92	609.5	26.4
^{95}Nb	310±65	379.9	22.6
^{92}Mo	70±10	64.5	7.9
^{94}Mo	102±20	96.7	5.2
^{95}Mo	292±12	268.1	8.2
^{96}Mo	112±8	89.8	19.8
^{97}Mo	339±14	310.9	8.3
^{98}Mo	99±7	79.6	19.6
^{99}Mo	240±40	231.8	3.4
^{100}Mo	108±14	98.1	9.2
^{99}Tc	781±50	1377.8	76.4
^{96}Ru	238±60	161.6	32.1
^{98}Ru	173±36	184.3	6.5
^{99}Ru	631±99	997.9	58.1
^{100}Ru	206±13	177.2	14.0
^{101}Ru	996±40	1186.6	19.1
^{102}Ru	186±11	136.7	26.5
^{103}Ru	343±52	502.9	46.6
^{104}Ru	161±10	213.0	32.3
^{103}Rh	811±14	972.3	19.9
		Average percent error:	29.8%

evaluate Maxwellian averaged capture cross sections for astrophysical applications (Bao *et al.* 2000). The Maxwellian-averaged neutron capture cross section is defined as the reaction rate $\langle \sigma v \rangle$ divided by the mean velocity $v_T = \sqrt{2kT/\mu}$ at a given temperature T. Here, μ is the reduced mass. For particle fluences and temperatures typical to stellar nucleosynthesis, the velocity distribution of the neutrons is well described by a Maxwell-Boltzmann distribution. In this case, the Maxwellian-averaged cross section reduces to (Beer *et al.* 1992)

$$\frac{\langle \sigma v \rangle}{v_T} = \frac{\int_0^\infty \sigma_{n\gamma} v \Phi(v) dv}{v_T} = \frac{2}{\sqrt{\pi}(kT)^2} \int_0^\infty \sigma_{n\gamma}(E) W(E, kT) dE \quad (36)$$

where $W(E, kT) = E \exp(-E/kT)$ and E is the center of mass energy.

Figure 11 compares our calculated Maxwellian-averaged capture cross sections for select targets to their evaluated counterparts (Bao *et al.* 2000). The error bars on all points are identical and represent the measured error for a given cross section at 30 keV. We used spline interpolation to determine the value of the (n,γ) cross section between points on the energy grid. For energies below our lowest grid energy, we assume an (n,γ) cross section with an $E_{lab}^{-1/2}$ dependence. For energies greater than our highest grid energy, we take the cross section to be zero.

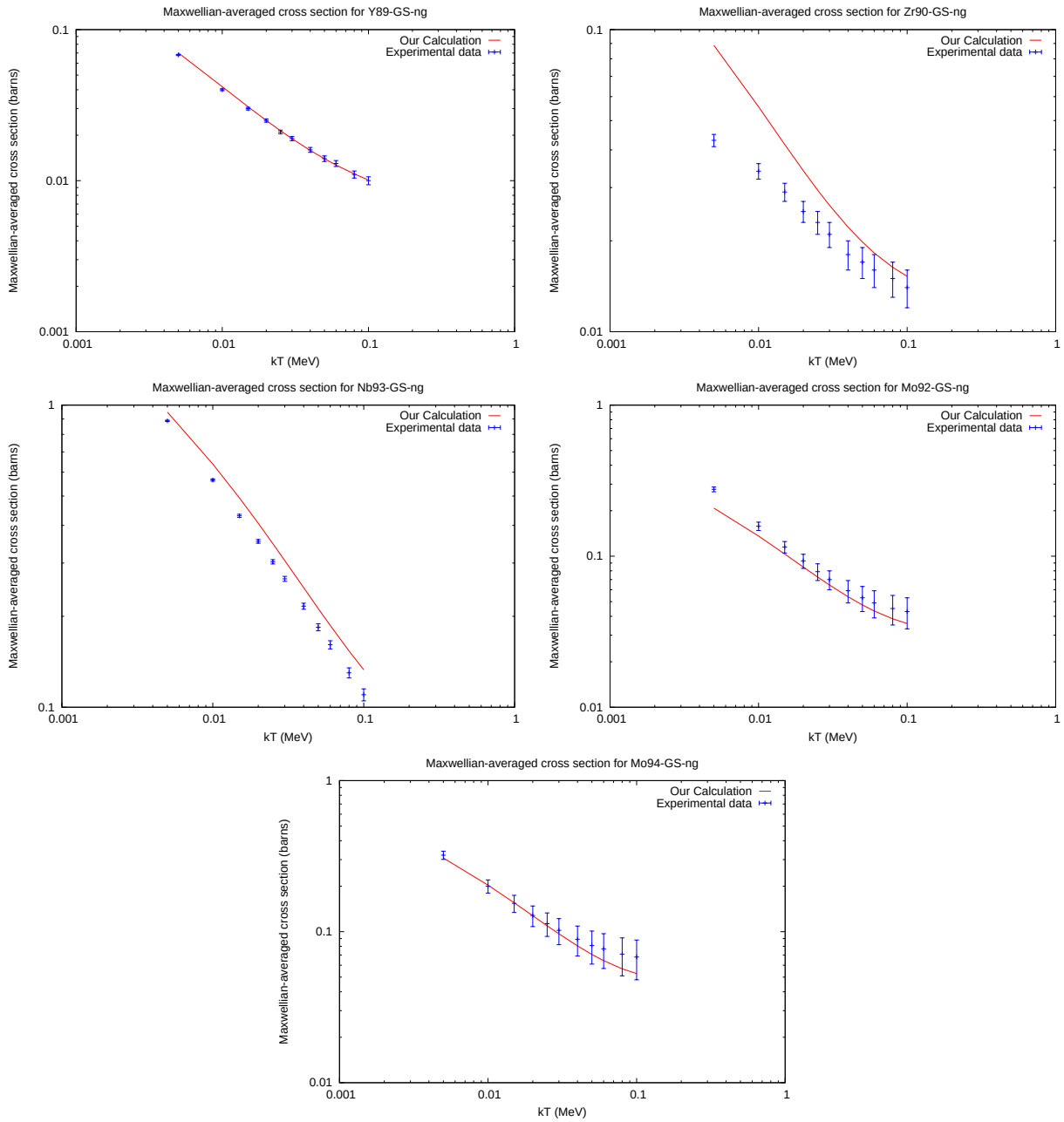

Fig. 11.— Calculated vs. recommended Maxwellian-averaged capture cross sections on select stable isotopes in the region of interest. The data is taken from (Bao *et al.* 2000). The solid line represent our modeled cross section. The data points are the recommended values, with the error bars for each energy identical to the quoted error at 30 keV.

Overall our calculated Maxwellian averaged cross sections agree with those of (Bao *et al.* 2000). Our result for ^{90}Zr is a bit high, consistent with Figure 10. Additional comparisons found in Appendix C.2 exhibit similar agreement.

It is also useful to establish a quantitative measure of how well our model calculations can replicate the recommended 30 keV Maxwellian-averaged cross sections. We define the average percent error as

$$\%E = \frac{1}{N}\sum_{i=1}^{N} \frac{\left|\frac{\langle \sigma_i^{mod} v\rangle}{v_T} - \frac{\langle \sigma_i^{rec} v\rangle}{v_T}\right|}{\frac{\langle \sigma_i^{rec} v\rangle}{v_T}} \times 100\% \quad (37)$$

The errors for each of our modeled 30 keV Maxwellian-averaged cross sections, relative to the recommended values, are listed in Table 2. Listed in the table are the target, recommended cross section (with error, in millibarns), our modeled value, and the percent error. On average, our modeled Maxwellian averaged capture cross sections are within 30% of the recommended values, consistent with our findings in Table 1.

4.1.3. Comparison to experimental (n,2n) cross sections

Our calculated (n,2n) cross sections for select targets are presented in Figure 12. We begin with ^{88}Y(n,2n)^{87}Y, a rare case where an (n,2n) cross section has been measured for a radioactive target. The amount of data is understandably limited, consisting of two measurements near 14 and 15 MeV. Our calculation is within the error bar for the point at 14.8 MeV, and only slightly below the error bar for the point at 14.2 MeV.

As one would expect, the ^{89}Y(n,2n)^{88}Y cross section has been measured in many different experiments. For the most part, the various data sets are in good agreement. We note that a few of the data sets, indicated by the open black data points at 15 MeV, are not identified as going to the final state (i.e. the data file does not specify whether the measured cross section leads to the ground state, isomer, etc...). It is likely that these measurements are cross sections leading to the first or second isomer. Overall, our calculation is in good agreement with the data. An improvement could be made by adjusting the pre-equilibrium parameters, as will be discussed in section 4.2.1.

Our calculation also exhibits good agreement against measured data for the ^{88}Zr(n,2n)^{87}Zr reaction. Again, this cross section has been measured numerous times, and the various data sets are generally consistent with each other. We can also achieve slightly better agreement with this cross section by modifying the pre-equilibrium parameters, but only in a manner which would reduce the agreement with ^{89}Y(n,2n)^{88}Y. See section 4.2.1 for details. We note that ^{88}Zr(n,2n)^{87}Zr has been measured at 14.8 MeV, and our calculation is in near perfect agreement with this measurement (see Appendix C.3).

The ^{93}Nb(n,2n)^{92}Nb calculation is in good agreement with measured activation cross section data. The relative amounts of cross section leading to the first and second isomers (blue and green lines, respectively), however, does not appear to correspond with the measurements. The source of this disagreement lies primarily in our assignment of isomers. We treat as isomers any state with a lifetime greater than 1 μs. The lifetime of the first isomer is quite long (10 days), while that of the second isomer is only 5.9μs. This second excited state, which decays via internal transition to the first isomer, would not normally be considered an isomer itself, and therefore measurements would include the population of the second excited state into the cross section leading to the first isomer. One will note that the sum of our first and second isomer cross sections would lie in near perfect agreement with the measured first isomer cross section.

Our calculation reproduces the measured ^{92}Mo(n,2n)^{91}Mo activation cross section up to about 16 MeV. The agreement with the cross section leading to the isomer is in good agreement for the entire energy range. There is a considerable amount of spread in the data for the cross section leading to the ground state, as well as the cross section leading to the isomer below 15 MeV.

The data for ^{94}Mo(n,2n)^{93}Mo is quite limited. Our cross section leading to the isomer is in excellent agreement with the data. However, our calculation is higher than the lone activation cross section data point by more than a factor of two.

Appendix C.3 presents additional comparisons between our modeled (n,2n) cross sections and experiment. We note that there is a significant disagreement between the measured activation data sets for ^{84}Sr(n,2n)^{83}Sr, and that the lowest data set may be a misidentified cross section leading to the isomer. Also, we note for ^{91}Zr(n,2n)^{90}Zr that the measured cross section leading to the first isomer is in excellent agreement with our cross section leading to the third isomer. This is due to our considering the first two excited states of ^{90}Zr, whose lifetimes are 61.3 ns and 88.4 fs, respectively, to be isomers, consistent with what was done in the previous RADCHEM data sets. Our third isomer (lifetime 809 ms) corresponds to the state identified as the first isomer in the experiments. See section 3.1.2.

As a further means of evaluating our (n,2n) cross sections, we present in Table 3 a quantified comparison of our results to the experimental data shown in Figures 12 and 27. We include all data with incident energies of 14.1±0.1 MeV. The format of the table is identical to Table 1.

The average deviation of our cross sections from the weighted means for the (n,2n) reac-

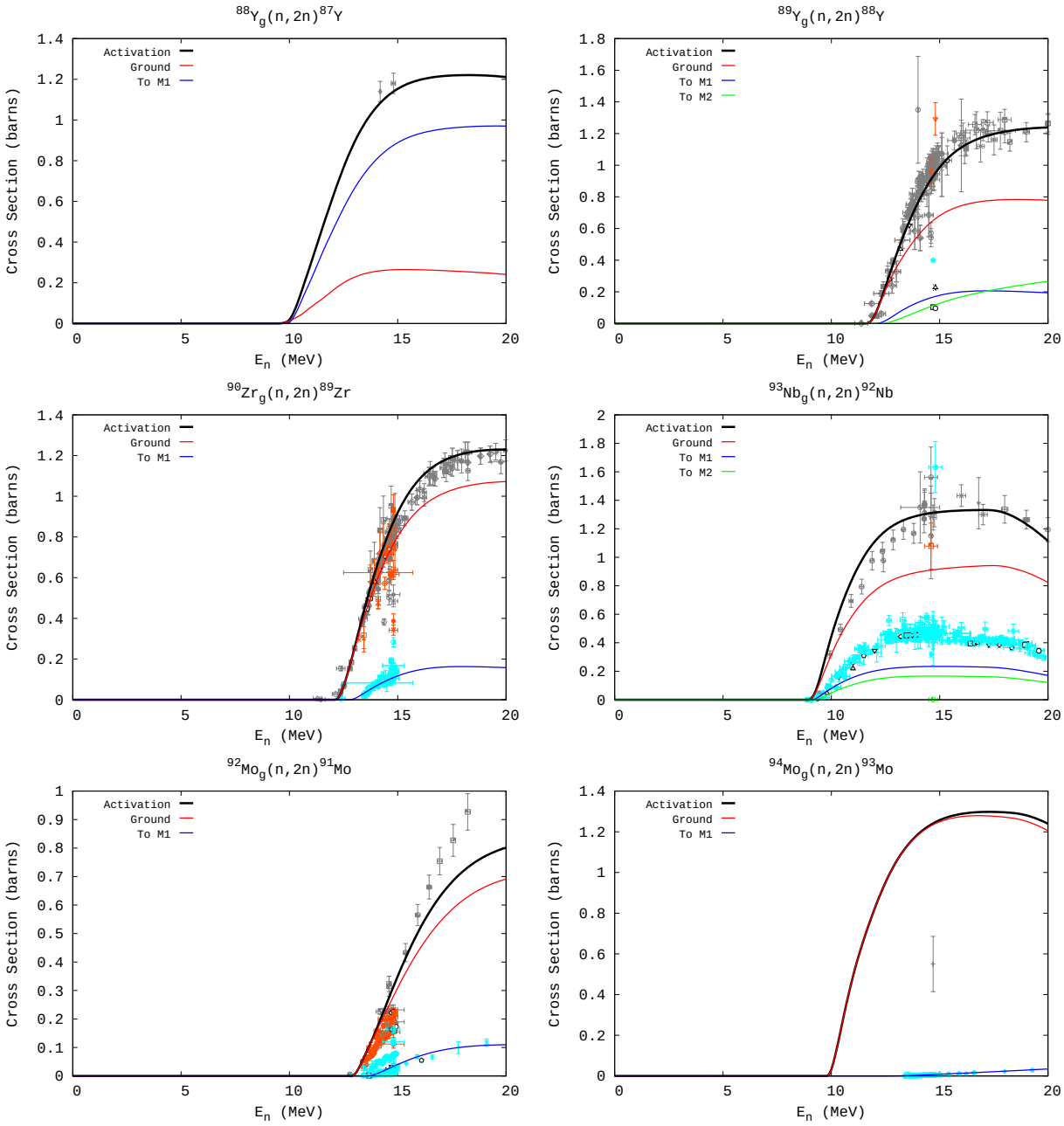

Fig. 12.— Calculated vs. measured (n,2n) cross sections on select stable isotopes in the region of interest. The data is taken from (EXFOR 2006). The black, red, and blue solid lines represent our modeled cross sections (total, leading to the ground state, and leading to the first isomer, respectively). The Gery, orange, and light blue data points are measured cross section data (total, ground state, and first isomer).

tions is 16.6% when only activation measurements are considered. For three cases (namely ^{84}Sr(n,2n)^{83}Sr, ^{92}Mo(n,2n)^{91}Mo, ^{96}Ru(n,2n)^{95}Ru, and ^{103}Rh(n,2n)^{102}Rh) there are several activation data sets that are not in agreement with each other. In each of these cases, our calculation lies close to at least one of the data sets. Excluding these three reactions, the average deviation for the (n,2n) activation cross sections is 6.4%.

Larger deviations occur for the cross sections to specific final states (ground state, isomers). When these are included in the average, the deviation is closer to 20% (12.5% when the three reactions noted above and ^{103}Rh(n,2n)^{102}Rh$_{m1}$, which ex-

Table 3: Comparison of our modeled (n,2n) cross sections to experimental data at 14.1±0.1 MeV

^{A}Z	Res.	N	$\bar{\sigma}$	Dev.	$\sigma_{mod.}$	$\bar{\sigma}/\sigma_{mod.}$
^{84}Sr	A	4	0.526	0.349	0.558	0.942
^{86}Sr	GS	1	0.547	0.000	0.639	0.856
^{86}Sr	M1	3	0.257	0.043	0.184	1.397
^{86}Sr	A	2	0.731	0.034	0.823	0.888
^{88}Sr	M1	5	0.225	0.029	0.209	1.077
^{88}Y	A	1	1.140	0.000	1.073	1.062
^{89}Y	A	22	0.853	0.147	0.791	1.078
^{90}Zr	GS	4	0.520	0.120	0.603	0.862
^{90}Zr	M1	11	0.078	0.011	0.073	1.062
^{90}Zr	A	21	0.618	0.063	0.676	0.915
^{96}Zr	A	5	1.544	0.059	1.536	1.005
^{93}Nb	M1	37	0.459	0.032	0.233	1.973
^{93}Nb	A	1	1.350	0.000	1.296	1.041
^{92}Mo	GS	8	0.123	0.032	0.170	0.726
^{92}Mo	M1	14	0.008	0.019	0.010	0.848
^{92}Mo	A	8	0.129	0.044	0.180	0.716
^{94}Mo	M1	5	0.003	0.000	0.004	0.779
^{100}Mo	A	9	1.472	0.162	1.537	0.958
^{96}Ru	A	4	0.576	0.032	0.870	0.661
^{98}Ru	A	2	1.093	0.102	1.206	0.906
^{104}Ru	A	3	1.607	0.531	1.556	1.033
^{103}Rh	GS	5	0.677	0.111	0.608	1.113
^{103}Rh	M1	5	0.494	0.093	0.762	0.648
^{103}Rh	A	4	0.846	0.113	1.369	0.618
					Average error:	20.3%
					Average error (activation only):	16.6%

hibits a similar disparity in the measured data, and ^{93}Nb(n,2n)^{92}Nb$_{m1}$, as discussed earlier, are excluded).

4.1.4. Comparison to experimental (n,p) cross sections

For most stable isotopes, the neutron capture and (n,2n) reactions are the dominant neutron induced reaction channels at low and high incident energies, respectively. However, as one moves to the proton rich side of stability, proton separation energies become small, and reaction channels involving charged particles in the exit channel, specifically (n,p) and (n,np) can become dominant.

In Figure 13 we present our modeled cross sections for select target isotopes compared to measurement. For ^{89}Y(n,p)^{89}Sr our calculation is in good agreement with the data between threshold and ∼10 MeV. At 14 MeV incident energy, our calculation lies roughly 50% higher than the bulk of the experimental data. This behavior is a common feature in our (n,p) cross sections, and is likely due to the simple treatment of pre-equilibrium. Fortunately, the (n,p) cross section is rarely dominant above ∼12 MeV (see Appendix D), so that errors in our calculation at and above 14 MeV will likely have insignificant impact in network calculations.

Our results for the other three targets in Figure 13 are in better agreement with experiment up to ∼15 MeV incident energy. We note that for the ^{92}Mo(n,p)^{92}Nb reaction the same situation arises that we saw for ^{93}Nb(n,2n)^{92}Nb (Section 4.1.3) where the sum of our cross sections leading to the first and second isomer in ^{92}Nb sum roughly to the measured cross section to the first isomer. We remind the reader that this is due to our considering the second excited state (lifetime 5.9 μs, decaying to the first isomer) as an isomer, where it would not be considered an isomer in the experiments.

Additional comparisons of our (n,p) cross sections to experiment can be found in Appendix C.6. The agreement between the calculation and measurement in comparable to that presented in Figure 13.

Due to the spread in the data in measured (n,p) cross sections and the presence of large error bars, a quantitative analysis of our calculations similar to that found in Tables 1 and 3 is difficult. For example, our calculation for ^{100}Ru(n,p)^{100}Tc is actually in good agreement with the data, but averaging the measured cross sections at 14.8 MeV would suggest our cross section is high by nearly a factor of two. There are also several instances where the activation cross section data is not consistent with the sum of the measured cross sections leading to the ground state and isomers.

4.1.5. Comparison to experimental (n,np) cross sections

On the proton rich side of stability, the (n,np) reaction can be larger than the (n,2n) reaction near 14 MeV incident energy (see Appendix D). Unfortunately, experimental data for this reaction is sparse in this region. Available measurements generally consist of only a few data points near threshold, with cross sections on the order of 10 mb or less (see Figure 31 of Appendix C.7). Only two (n,np) reactions in this region have measured data in an energy range where the cross section is greater than a few hundred millibarns. These are shown in Figure 14. For ^{88}Zr(n,np)^{87}Y, the measured activation cross section is 253±25 mb at 14.8±0.1 MeV incident en-

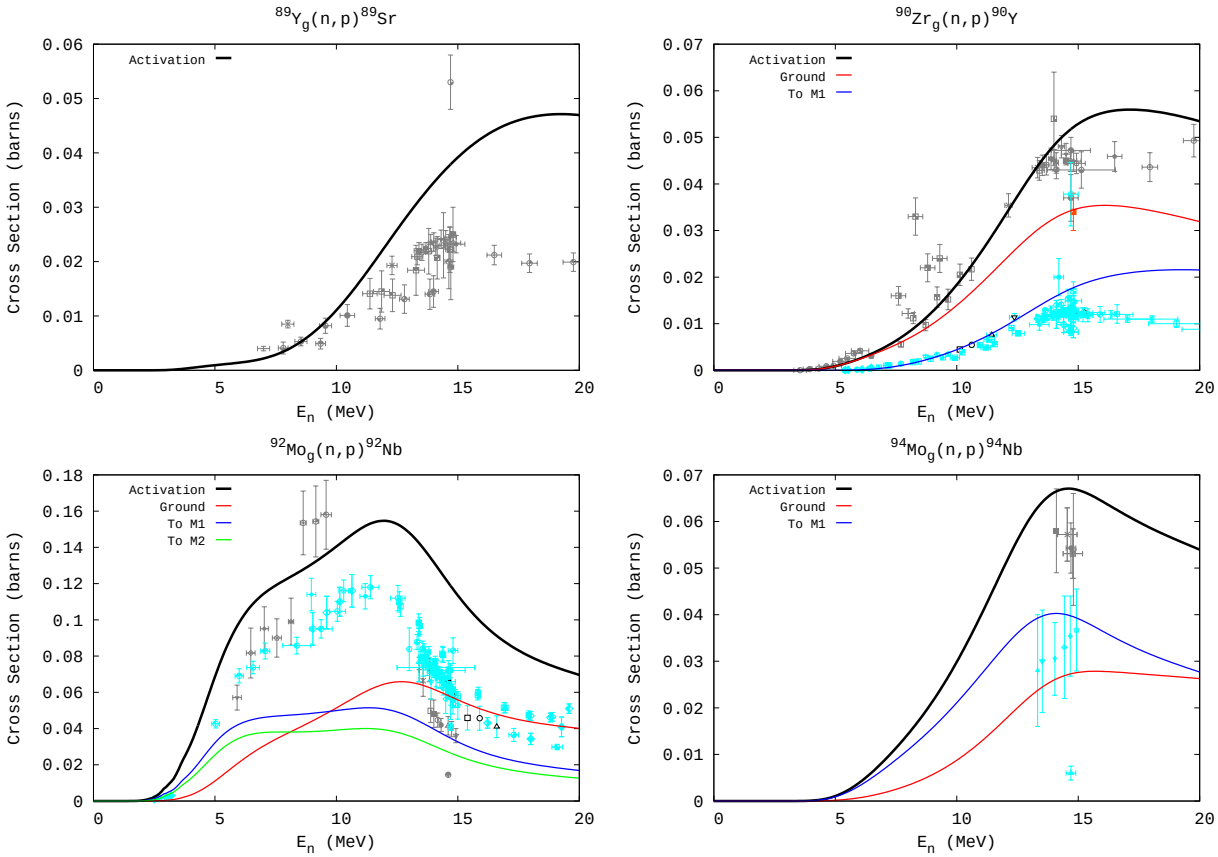

Fig. 13.— Calculated vs. measured (n,p) cross sections on select stable isotopes in the region of interest. The data is taken from (EXFOR 2006). The black, red, and blue solid lines represent our modeled cross sections (total, leading to the ground state, and leading to the first isomer, respectively). The Gery, orange, and light blue data points are measured cross section data (total, ground state, and first isomer).

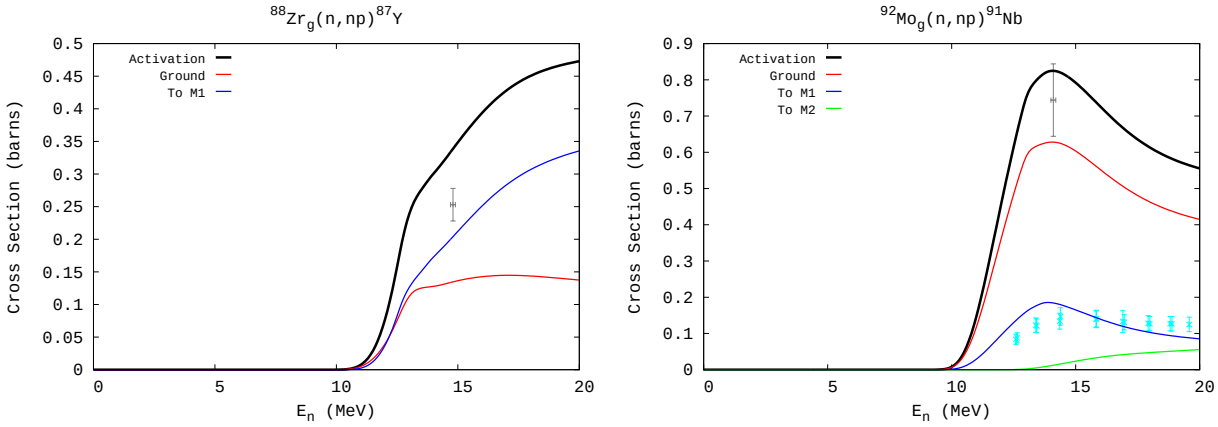

Fig. 14.— Calculated vs. measured (n,np) cross sections on select stable isotopes in the region of interest. The data is taken from (EXFOR 2006). The black, red, and blue solid lines represent our modeled cross sections (total, leading to the ground state, and leading to the first isomer, respectively). The Gery, orange, and light blue data points are measured cross section data (total, ground state, and first isomer).

ergy (Prestwood *et al.* 1984). Our calculation for this reaction yields a cross section of 338.7 mb at 14.8 MeV, which is high compared to the measurement by 34%. For ^{92}Mo(n,np)^{91}Nb, our calculated

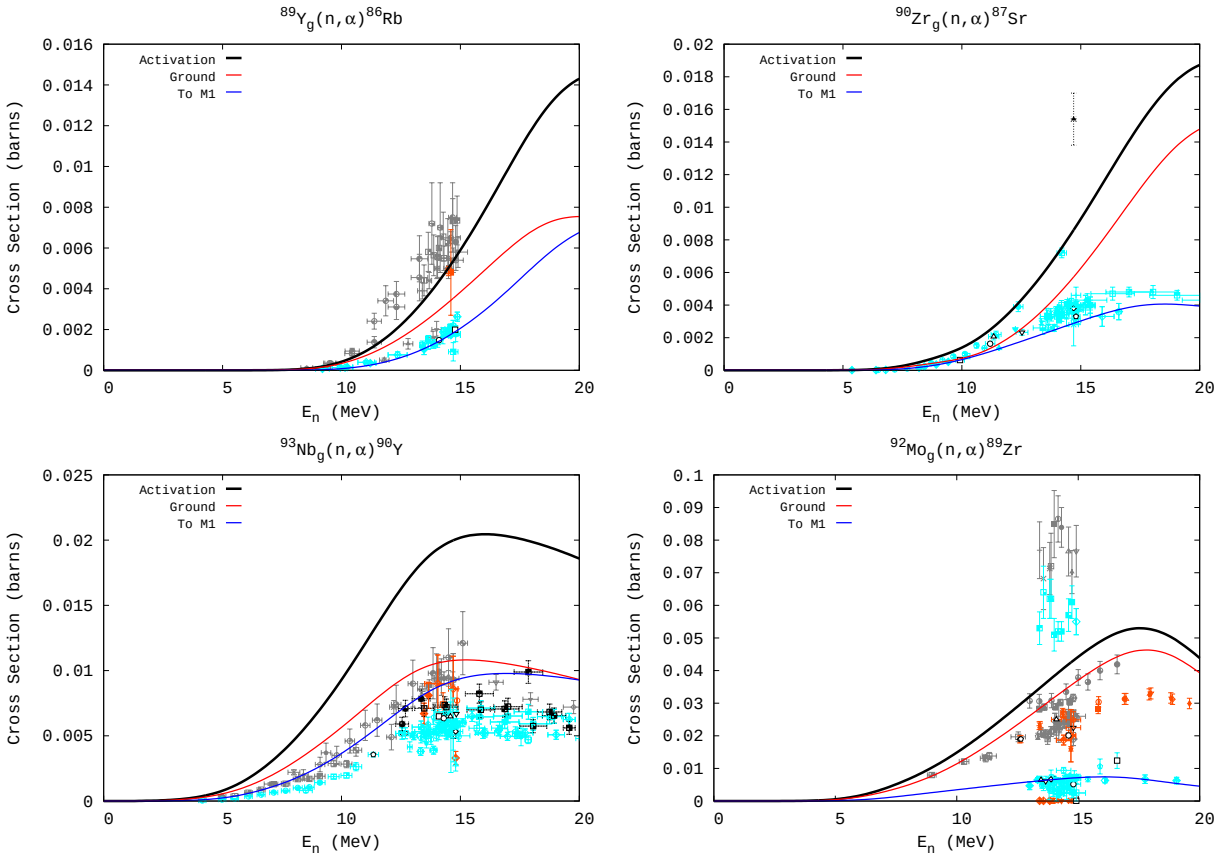

Fig. 15.— Calculated vs. measured (n,α) cross sections on select stable isotopes in the region of interest. The data is taken from (EXFOR 2006). The black, red, and blue solid lines represent our modeled cross sections (total, leading to the ground state, and leading to the first isomer, respectively). The Gery, orange, and light blue data points are measured cross section data (total, ground state, and first isomer).

activation cross section is within the errors of the measured data, and the agreement with the measured cross section leading to the isomer of ^{91}Nb is good.

The scarcity of measured (n,np) data makes it difficult to estimate the accuracy at which we can predict (n,np) cross sections.

4.1.6. Comparison to experimental (n,α) cross sections

The (n,α) channel is generally small compared to other open channels. However, due to the prominence of (n,α) cross sections in the Mo1278 detector set, we make special mention of them here.

The availability and quality of (n,α) data in this region is comparable to what is available for (n,p). There are occasions where the spread in the data is quite large, and many of the data points have rather large error bars. Again, this precludes us from making a meaningful quantitative analysis of our (n,α) calculations. However, we present in Figure 15 a sample of our results compared to data for a few select targets. Additional comparisons can be found in Appendix C.8.

For ^{89}Y(n,α)^{86}Rb, our calculation is in good agreement with experiment. For ^{90}Zr(n,α)^{87}Sr, only data for cross section leading to the isomer is available (the other data points did not unambiguously designate a final state). Our cross section is in reasonable agreement with the bulk of the measured data. Our modeled cross section for ^{93}Nb(n,α)^{90}Y is high, though we note that the activation cross section data is in conflict with the bulk of the data to the ground state and isomer, i.e. the sum of the ground state and isomer cross sections would yield an activation cross section somewhat higher than what has been measured. We note particularly that our cross section to the ground state is in reasonably fair agreement with

experiment, being high be perhaps ∼20%. Our cross section to the isomer of ^{90}Y appears to be high by about 60%. Our activation cross section would be ∼40-50% higher than the sum of the measured ground state and isomer cross sections.

The experimental data for ^{92}Mo(n,α)^{89}Zr is rather disparate. There are two distinct groups of measurements, each involving several experiments, for the activation cross section. The same is true for the cross sections leading to the ground state and first isomer. Our calculated cross section leading to the isomer is in very good agreement with the lower set of isomer data, while our ground state cross section (and consequently our activation cross section) appear to be high by ∼20-25% at 14 MeV.

Similar agreement will be found for the other comparisons in Appendix C.8. For the most part, our calculations do quite well, with a few notable exceptions, including ^{99}Tc(n,α)^{96}Nb and ^{103}Rh(n,α)^{100}Tc, for which we are high by a factor of ∼2.

4.1.7. Comparison to other experimental neutron induced cross sections

We have also made comparisons for other neutron induced reaction channels, described here briefly.

For the two (n,3n) reactions for which data is available (Appendix C.4) our calculations fare quite well. However, the thresholds for these reactions are well above 14 MeV.

Our calculations agree nicely with the measured (n,n') data (Appendix C.5). We remind the reader of the issue regarding the isomers in ^{90}Zr, as explained in section 3.1.2, which is why our (n,n') cross section for that target leaving the nucleus in the third isomer compares favorably to the data leading to the first isomer.

The (n,nα) channel is always very small compared to the dominant channel, and the data is limited (Appendix C.9). A similar statement can be made of the (n,d) cross sections (Appendix C.10).

4.1.8. Comparison to experimental (p,n) cross sections

Our calculations for (p,n) cross sections are compared to experimental data for four select targets in Figure 16. The black data on the plot for ^{89}Y(p,n)^{89}Zr represents measurements from (Mustafa *et al.* 1988), used in the Yt0488 detector set. Our calculation runs higher than the measurement by roughly 15%, with the overall shape in good agreement. The amounts going to the ground state and isomer are somewhat more uncertain. Our ground state cross section is in good agreement with one data set (solid red squares), but is significantly higher than the other larger set (red open squares). Keep in mind that the *measured* cross section will be used for radiochemical analysis in lieu of this calculation.

The agreement between our calculated activation cross section and experiment is satisfactory for ^{90}Zr(p,n)^{90}Nb. The amounts going to the various final states of ^{90}Nb are more in question. Certainly the isomer data set below the reaction threshold is not to be believed. The experimental isomer data is most likely associated with the second excited state (lifetime 18.8 seconds), which is denoted as the second isomer in our modeling effort. The first excited state (first isomer in our modeling, lifetime 63 μs) decays to the ground state, and the eighth excited state (third isomer in our calculation, lifetime 6.19 ms) decays to the second excited state (second isomer in our calculation). So, in reality the ground state data (red data points) should be compared to the sum of our ground state and first isomer calculations (red and blue lines). The comparison would be fairly good, though the data is limited. The experimental isomer data (light blue points) should be compared to the sum of our second and third isomer cross sections (green and magenta lines). It appears that our calculation would overestimate the measured isomer cross section.

Our calculated ^{93}Nb(p,n)^{93}Mo activation cross section is in excellent agreement with experiment. The cross section leading to the isomer in ^{93}Mo also does quite well up to 15 MeV incident energy. For ^{94}Mo(p,n)^{94}Tc, our cross section leading to the ground state is in fair agreement with the data, though it appears out isomer and activation cross sections may be a bit high.

Additional comparisons to measured (p,n) cross sections can be found in Appendix C.11. Overall, our calculations generally do well in reproducing the experimental data, typically to within ∼20%. We note that for ^{100}Ru(p,n)^{100}Rh our discrete level scheme for ^{100}Ru did not encompass the isomer, which prevents us from calculating isomer and ground state cross sections. We also note (yet again) that the sum of the first and second isomer cross sections of ^{92}Zr(p,n)^{92}Nb should be summed for comparison to the measured isomer data.

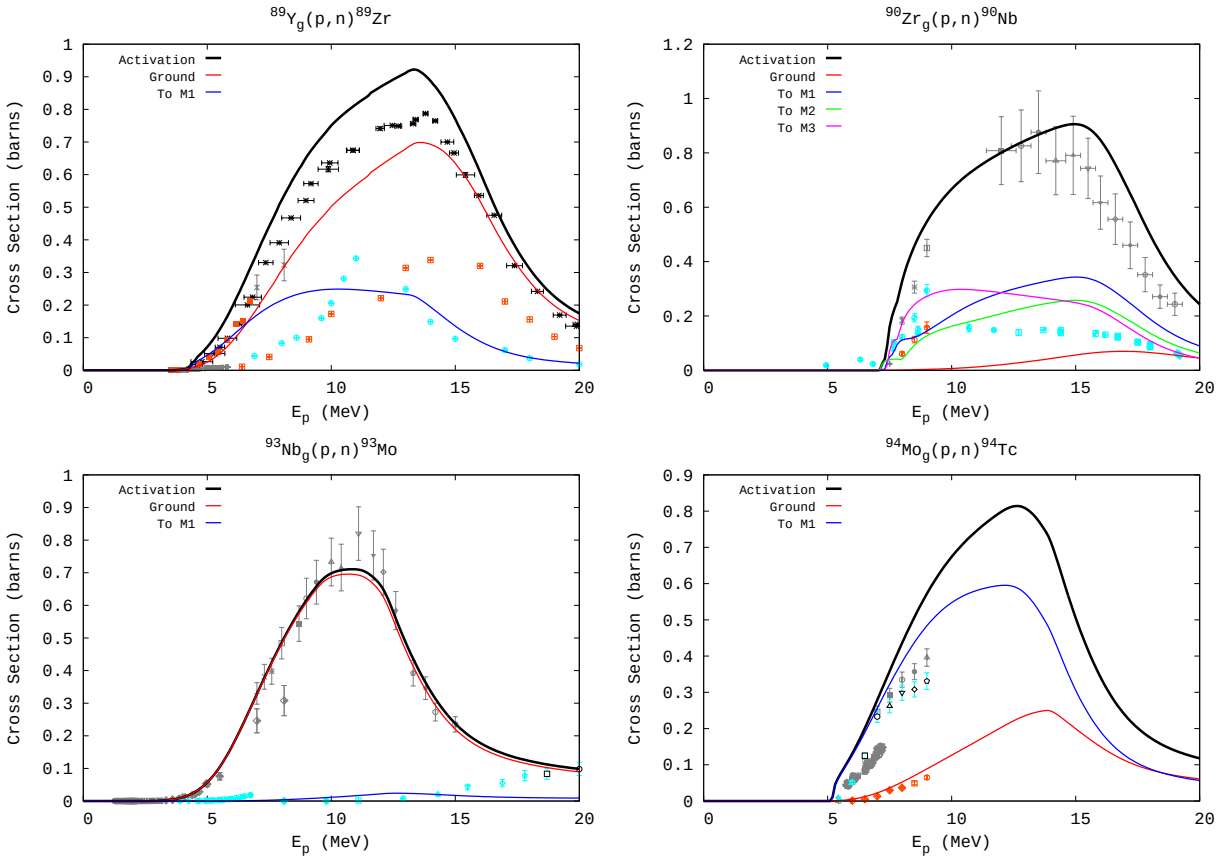

Fig. 16.— Calculated vs. measured (p,n) cross sections on select stable isotopes in the region of interest. The data is taken from (EXFOR 2006). The black, red, and blue solid lines represent our modeled cross sections (total, leading to the ground state, and leading to the first isomer, respectively). The Gery, orange, and light blue data points are measured cross section data (total, ground state, and first isomer).

4.1.9. Comparison to other experimental charged particle cross sections

In general, the available data for other charged particle reactions, including (p,2n), (p,pn), (p,p'), (d,n), (d,2n), and (d,3n), is sparse. We provide comparisons between our calculations and measurement for these reactions in Appendices C.12-C.19. Our calculations for the proton induced reactions are typically in good agreement with the data, keeping in mind that the first and second isomer cross sections for ^{93}Nb(p,np)^{92}Nb should be summed before comparing to the data (see Section 4.1.3). We also note that our calculation for ^{89}Y(p,p')^{89}Y is several orders of magnitude greater than the measurements. Whether this is a result of errors in the modeling or in reporting the data has yet to be determined.

We also may make a few general statements regarding our modeled deuteron induced cross sections. By far, the greatest difficulty in modeling these cross sections accurately lies in the breakup calculations. These calculations are in turn highly dependent on the choice of optical potential employed. Our calculated (d,n) cross sections are generally in good agreement with the data near threshold, but then tend to either over- or underestimate the peak significantly. We note that the peak of this cross section occurs usually between 5-10 MeV of incident energy, which is also where the deuteron breakup fraction (the fraction of reaction cross section used in deuteron breakup) is typically the largest. We find a somewhat better agreement between our modeled (d,2n) cross sections and the data, usually being within 20%. The available (d,3n) data is limited to a single point at 19 MeV incident energy for the ^{89}Y target.

We make note that the charged particle cross sections of greatest import in radiochemical analysis, i.e. those leading directly from the loaded detector elements to the measured radioactive

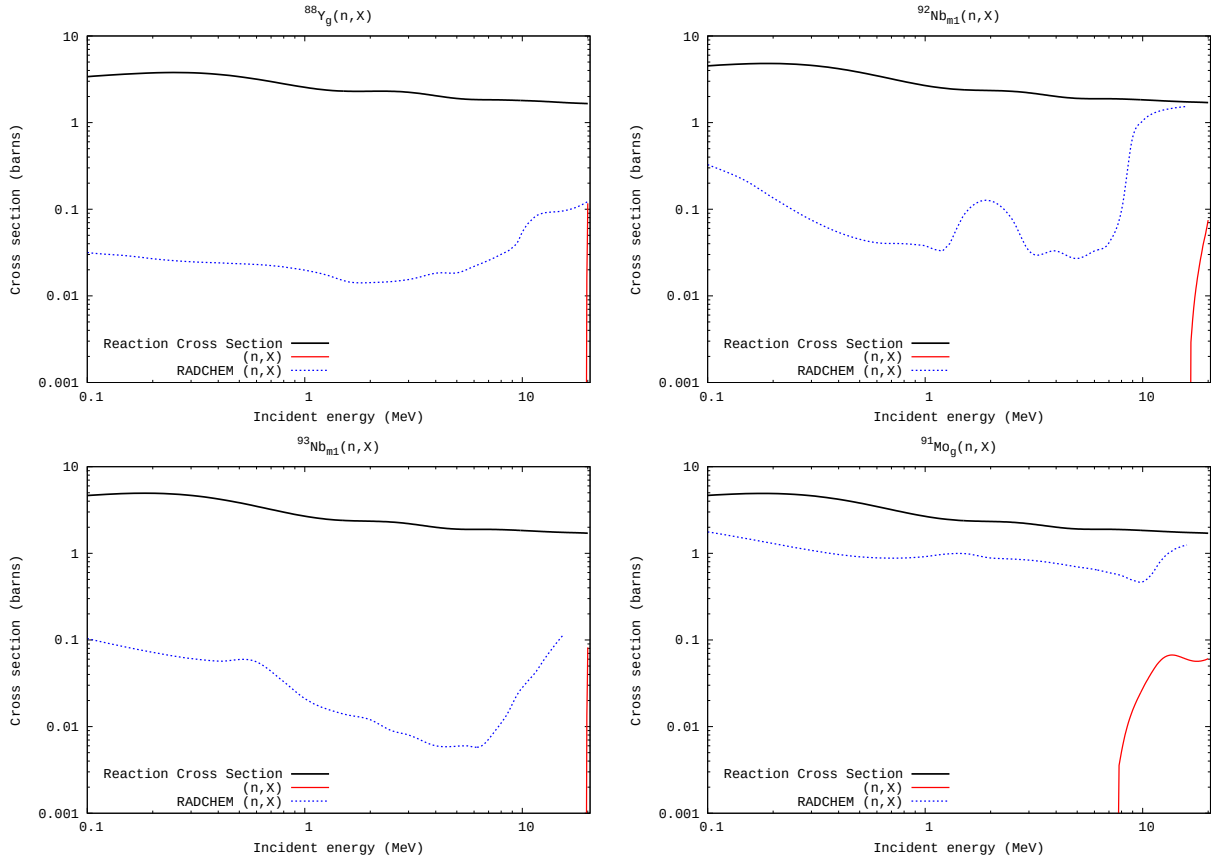

Fig. 17.— Calculated (n,X) cross sections on select targets. The reaction cross section from our calculation is represented by the black line, and our calculated (n,X) cross section by the red line. The blue line represents the (n,X) cross section from the RADCHEM database.

species, have been measured. These measured cross sections should be used in lieu of any theory calculation in UGT analysis.

4.1.10. Destruction cross sections

In Figure 17 we present select (n,X) cross sections, calculated via the method of section 2.7. Additional (n,X) cross sections can be seen on the plots in Appendix D. The targets represented in Figure 17 were chosen because (a) our calculated (n,X) cross section was greater than 1 mb, (b) an (n,X) reaction for the target had been included in the previous detector set, and (c) with the exception of ^{91}Mo, each of these targets are one of activities measured during UGT. We have included ^{91}Mo on the basis that it is among our larger (n,X) cross sections. Because we have made a special effort to include all of the most important neutron reaction channels in this study, many of our (n,X) cross sections are less than 1 mb over the entire energy range studied.

We note that three of our (n,X) cross sections are non-existent below 15 MeV of incident energy (recall that any (n,X) cross section less that 1 mb is set to zero to avoid "noise" due to precision issues). The exception here is ^{91}Mo(n,X) which is still an order of magnitude smaller than the dominant reaction channel over the entire energy range. This is representative of our (n,X) cross sections. They can, in all likelihood, be left out of any network calculations, provided that all of the other important channels are included.

On the other hand, the (n,X) cross sections in the existing RADCHEM database can be quite large, in some cases comprising upwards of 20-25% of the reaction cross section or more. For the targets shown here, we specifically note that the following important (>10 mb at some given energy) channels have been grouped in with the (n,X) cross section: the (n,p), (n,np), and (n,α) reactions on ^{88}Y$_g$; the (n,γ), (n,p), (n,np), and (n,α) reactions on ^{92}Nb$_{m1}$; the (n,γ), (n,2n), (n,p), and (n,α) re-

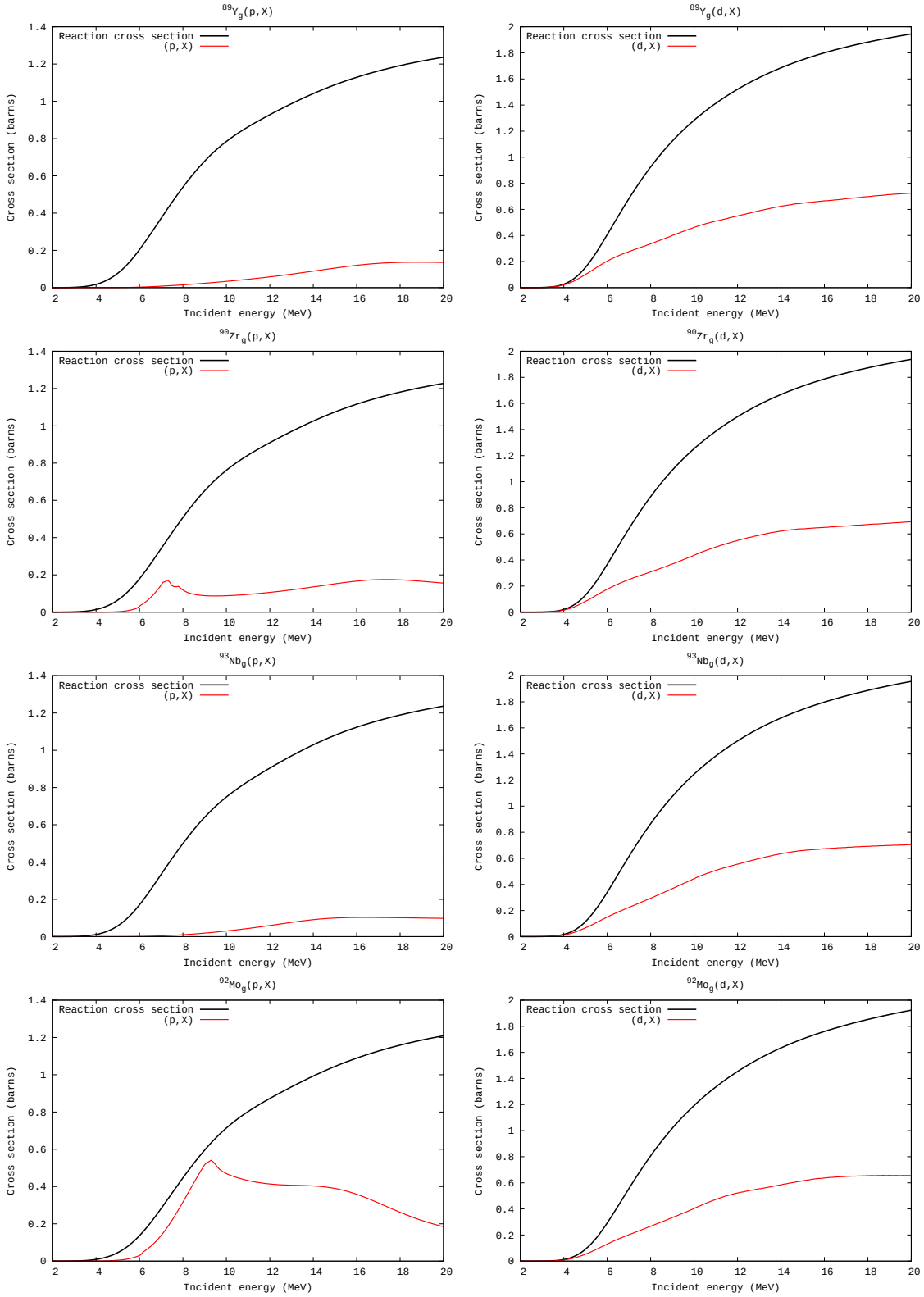

Fig. 18.— Calculated charged particle destruction cross sections on select targets. The reaction cross section from our calculation is represented by the black line, and our calculated (p,X) or (d,X) cross section by the red line.

actions on $^{93}Nb_{m1}$; the (n,γ), (n,2n), (n,p), and (n,np) reactions on $^{91}Mo_g$. Many of these omitted channels are the dominant reaction channel over part of the energy range, as shown in Appendix D.

For incident charged particles, we have not included as many outgoing channels, and hence our charged particle destruction cross sections will be larger than those for neutrons. In Figure 18 we present our (p,X) and (d,X) cross sections, along with their respective reaction cross sections, for four of the loaded detector elements. The (p,X) reactions generally account for about 20% of the reaction cross section, except for the even-Z targets at incident energies below 10 MeV, where the amount may be as large as 50-90%. The (d,X) cross sections are fairly uniform across all targets, and account for ∼40% of the reaction cross section.

4.2. Sensitivity Studies

We now illustrate the sensitivity of our modeled results to variations in the input parameters developed in §3.

4.2.1. Sensitivity to the Pre-Equilibrium Cross Section

As stated in section 3.4, the simple exciton model has two free parameters which may be tuned to replicate experimental cross sections. One of these parameters affects alpha emission only and will be studied in a later section. The other parameter, $\langle FM \rangle$, scales the average effective matrix element for residual interactions. We have determined that a value of $\langle FM \rangle = 250$ MeV optimally replicates measured cross sections in this region of interest.

The choice of $\langle FM \rangle = 250$ MeV is based primarily on (n,2n) cross sections on various isotopes of yttrium and zirconium. Initial comparisons between measured data and cross sections modeled with varying values of $\langle FM \rangle$ indicated that this parameter should be somewhere between 200 and 300 MeV. To improve the estimate, we appealed to critical (n,2n) activation cross sections found in the RADCHEM library. Specifically, we attempted to match the RADCHEM ^{89}Y(n,2n)^{88}Y and ^{90}Zr(n,2n)^{89}Zr activation cross sections at 14.1 MeV, which are 840 mb and 632 mb, respectively. The ^{89}Y(n,2n)^{88}Y was best matched with $\langle FM \rangle = 300$ MeV, yielding a value of 826 mb at 14.1 MeV (1.7% lower than the RADCHEM value, or -1.7%). Decreasing $\langle FM \rangle$ decreases this cross section, with $\langle FM \rangle = 200$ MeV giving a 14.1 MeV cross section of 748 mb (-11.0%). The second cross section, ^{90}Zr(n,2n)^{89}Zr, was best matched using $\langle FM \rangle = 200$ MeV, which gave a cross section of 644 mb (+1.9%). Using $\langle FM \rangle = 300$ MeV increased this cross section to 698 mb (+10.4%). Rather than use different $\langle FM \rangle$ for different elements (we wish to maintain consistency in the model parameters for each reaction in this detector set), we settled on a value of $\langle FM \rangle = 250$ MeV, which resulted in 14.1 MeV cross sections of 791 mb for ^{89}Y(n,2n)^{88}Y (-5.8%) and 676 mb for ^{90}Zr(n,2n)^{89}Zr (+7.0%). The cross section (in mb) obtained for other critical (n,2n) reactions at 14.1 MeV in the yttrium and zirconium detector sets, along with the RADCHEM values, can be seen in Table 4. In this table, cross sections not specifying a final state are activation cross sections, and those not included in the existing RADCHEM detector sets are indicated by dashes.

Table 4: Sensitivity of critical 14.1 MeV (n,2n) cross sections to the $\langle FM \rangle$ parameter. The second column shows the value of the cross section (in millibarns) in the current RADCHEM library. A "*" indicates a measured cross section. The other three columns show the cross section calculated using values of $\langle FM \rangle$ = 200, 250, and 300 MeV.

Reaction	Lib.	200	250	300
$^{89}Y_g$(n,2n)$^{88}Y_g$	561	541	571	596
$^{89}Y_g$(n,2n)$^{88}Y_{m1}$	142	131	139	145
$^{89}Y_g$(n,2n)$^{88}Y_{m2}$	137	76	81	85
$^{89}Y_g$(n,2n)^{88}Y	840*	748	791	826
$^{88}Y_g$(n,2n)$^{87}Y_g$	311*	246	258	267
$^{88}Y_g$(n,2n)$^{87}Y_{m1}$	801*	775	815	845
$^{88}Y_g$(n,2n)^{87}Y	1112*	1021	1073	1112
$^{87}Y_g$(n,2n)$^{87}Y_g$	—	454	487	505
$^{87}Y_g$(n,2n)$^{87}Y_{m1}$	—	44	47	49
$^{87}Y_g$(n,2n)^{87}Y	471	498	535	554
$^{87}Y_{m1}$(n,2n)$^{87}Y_g$	—	412	442	459
$^{87}Y_{m1}$(n,2n)$^{87}Y_{m1}$	—	176	190	197
$^{87}Y_{m1}$(n,2n)^{87}Y	560	588	632	657
$^{90}Zr_g$(n,2n)$^{89}Zr_g$	549	574	603	622
$^{90}Zr_g$(n,2n)$^{89}Zr_{m1}$	83	70	73	76
$^{90}Zr_g$(n,2n)^{89}Zr	632*	644	676	698
$^{89}Zr_g$(n,2n)^{88}Zr	767*	664	700	723
$^{89}Zr_{m1}$(n,2n)^{88}Zr	896	892	937	969
$^{88}Zr_g$(n,2n)$^{87}Zr_g$	—	311	324	337
$^{88}Zr_g$(n,2n)$^{87}Zr_{m1}$	—	14	15	15
$^{88}Zr_g$(n,2n)^{87}Zr	315*	325	339	352
$^{87}Zr_g$(n,2n)^{86}Zr	695	282	293	306
$^{87}Zr_{m1}$(n,2n)^{86}Zr	—	426	443	462

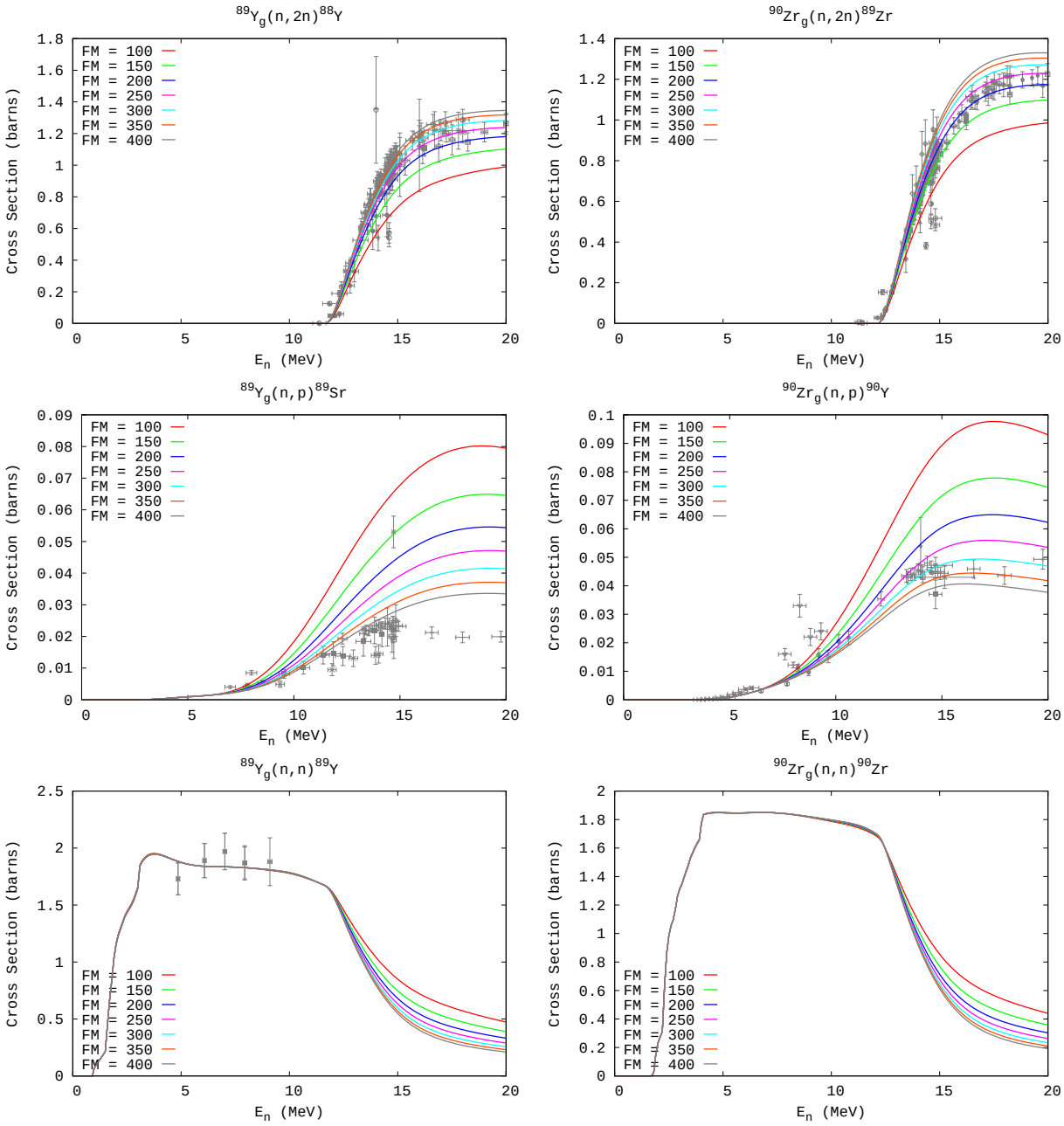

Fig. 19.— Sensitivity of select activation cross sections to the $\langle FM \rangle$ parameter. The activation cross section data (gray data points) are taken from (EXFOR 2006).

We also present in Figure 19 the sensitivity of other select neutron-induced cross sections, over the entire modeled energy range, to the $\langle FM \rangle$ parameter. As a percentage of the cross section, the sensitivity is greatest for the (n,p) reactions, followed by (n,2n) and (n,n'). However, it is worthwhile to note that the (n,p) cross section is also considerably smaller than the other two channels, so one might expect the sensitivity to be greater.

4.2.2. Sensitivity to the Alpha Preformation Parameter

The other free parameter in the exciton model which we tune to match measured cross section data describes the tendency of nucleons to preform alpha clusters in the nucleus. This parameter, ϕ, is expected to have a value somewhere between 0.1 to 0.8. In Figure 20 we present the sensitivity of select (n,α) cross sections to this parame-

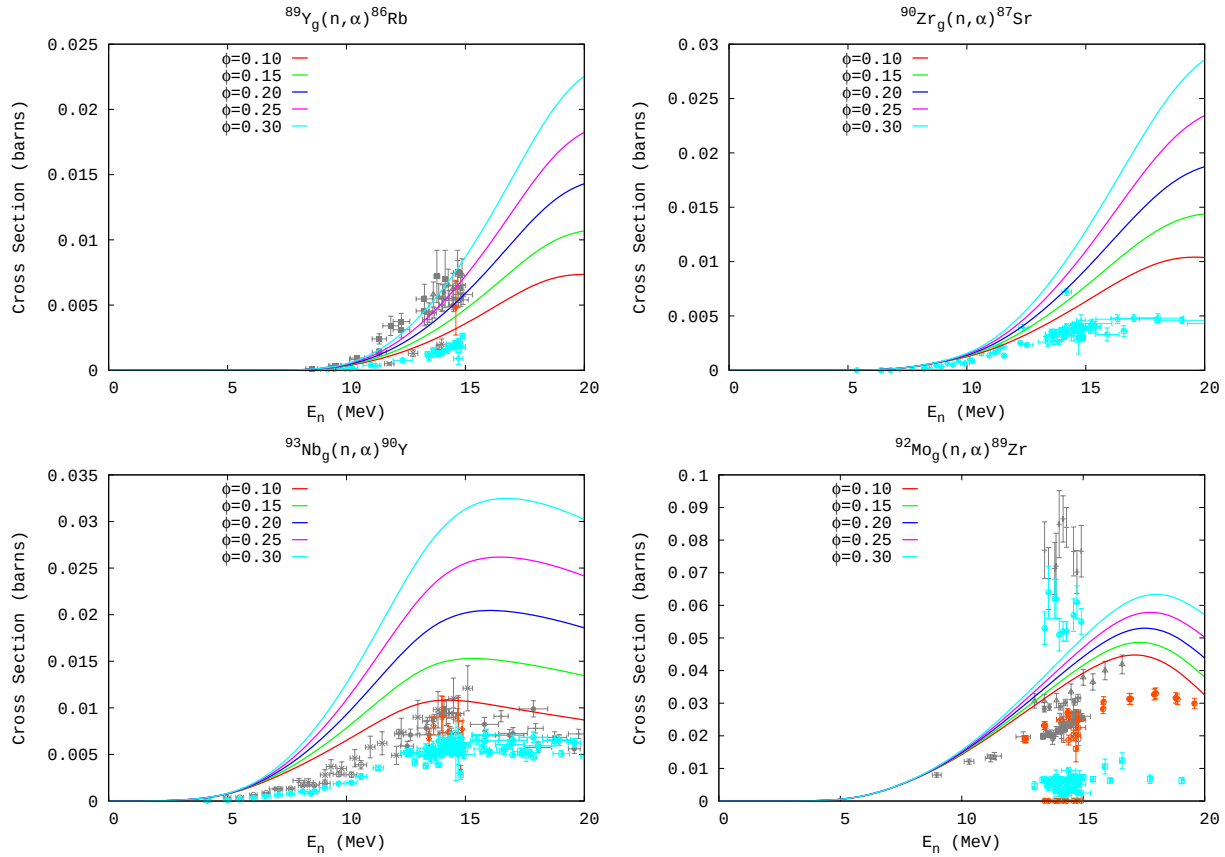

Fig. 20.— Sensitivity of select activation cross sections to the alpha preformation parameter. The cross section data (gray, orange, and cyan representing activation, ground state, and isomer data, respectively) are taken from (EXFOR 2006).

ter. All of the modeled cross sections presented in this figure are activation cross sections. The data leading to the ground state and isomers has been left on the plot, to allow a comparison with data to be made for the ^{90}Zr target. These comparisons, along with additional comparisons not shown in this report, justify a choice of $\phi = 0.2$. Because the alpha channel is small compared to other exit channels, the effect on other cross sections, such as (n,2n) and (n,p) is negligible, and the only other calculated reaction channel that will show any sensitivity to this parameter is the (n,nα) channel.

4.2.3. Sensitivity to the Level Density - Shell Correction Systematic

The systematic presented in Figure 8 represents a least squares fit to shell corrections (δW) derived from known resonance spacings, assuming a specific form for other Fermi gas level density parameters (§3.3). The error bars correspond to errors in the measured resonance spacings, obtained by deriving shell corrections from the upper and lower limits of the measurement. The average size of these error bars is 0.60 MeV, with about half of them of them being smaller than 0.5 MeV.

In Figure 21 we investigate the effect of varying the shell corrections up or down by 1 MeV. In each case, the matching energy E_x was refit to the spectroscopic data. The cross section obtained using our preferred shell correction is shown in red, and the cross section calculated using the ±1 MeV variations are shown in black. The activation cross section data is obtained from (EXFOR 2006).

The changes are most significant in the capture cross sections, with the variations at low incident energies being as large as ∼35%. These changes are due primarily to the corresponding adjustments in the normalization of the photon transmission functions (see Section 3.2.3). On the other hand, the (n,2n) cross sections exhibit almost no sensitivity to changes in the shell correction. The (n,p) cross sections also exhibit very

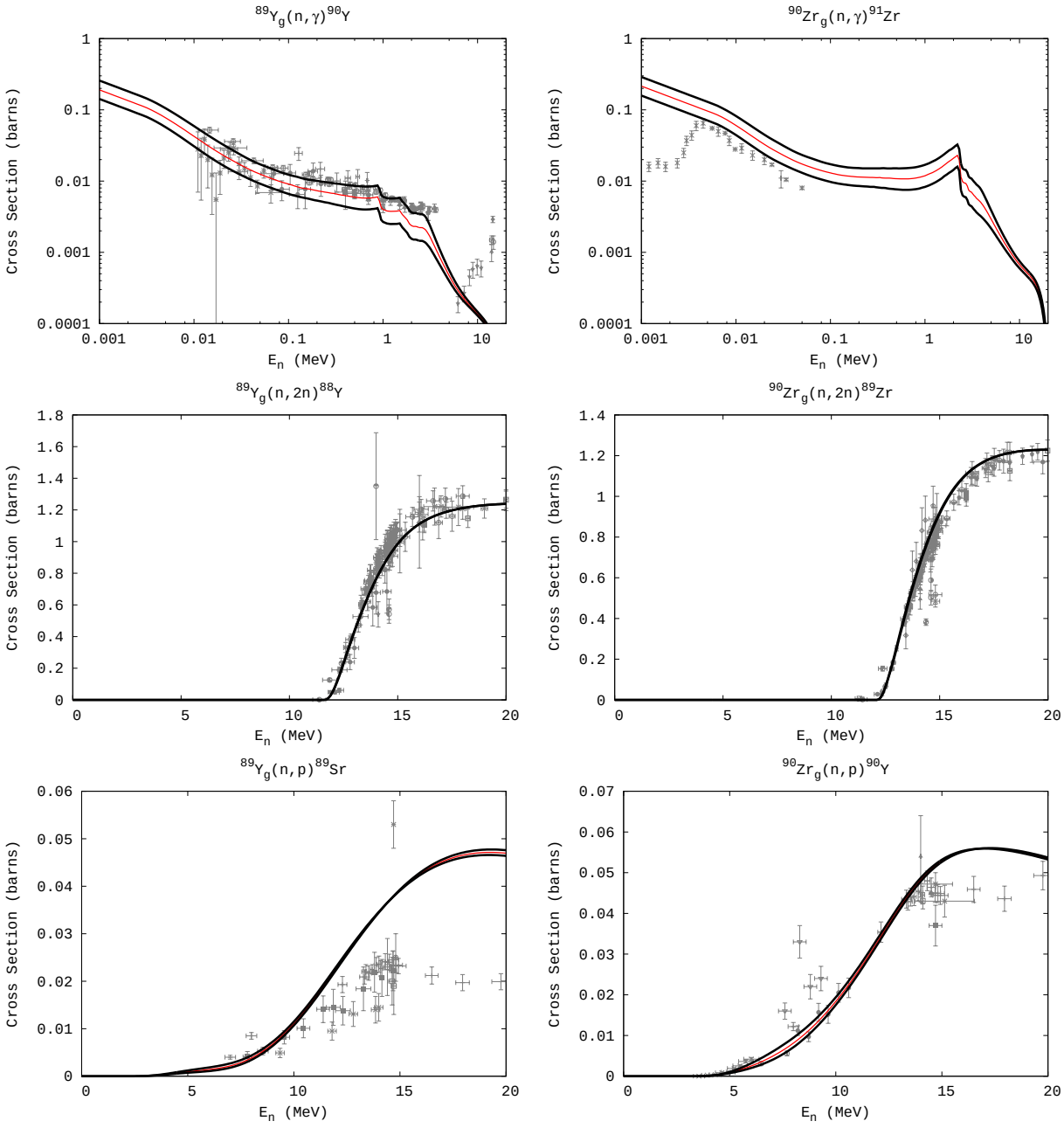

Fig. 21.— Sensitivity to variations in the level density shell correction δW.

little sensitivity. At high incident energies, the effects of these variations are expected to be minimal, since the shell correction is damped and the level density parameter approaches its asymptotic value.

We note further that *all* of the shell corrections (including those for the compound nucleus and each possible exit channel) have been enhanced or reduced in these calculations. The effect of varying an individual shell correction has not been investigated.

4.2.4. Sensitivity to the Normalization of the γ-ray Transmission Coefficient

Figure 22 shows the sensitivity of select capture cross sections to a ±30% change to the value of the average s-wave photon width used to normalize the gamma-ray transmission coefficients (§3.2.3., Figure 7). The solid red line represents the cross section modeled with our adopted value for the radia-

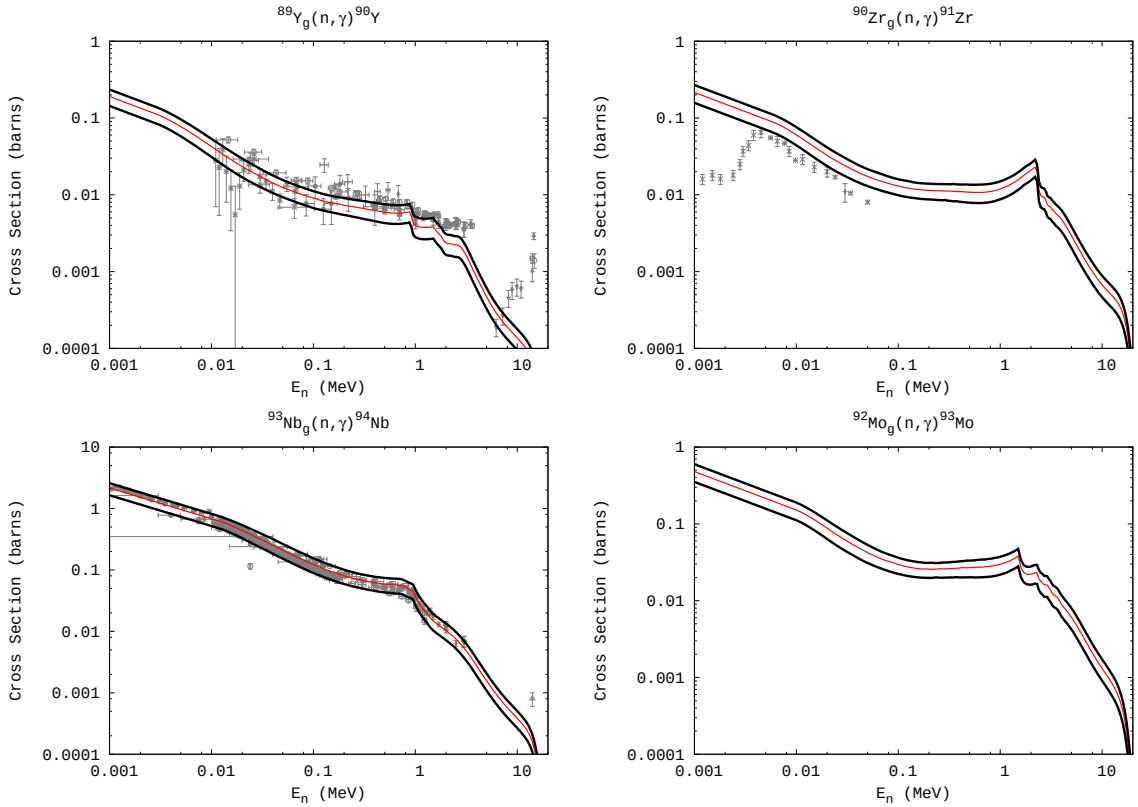

Fig. 22.— Sensitivity to a ±30% adjustment of the experimental s-wave average photon width Γ_γ.

tion width, and the black lines represent cross sections modeled with a 30% variation in the adopted values. The 30% variation translates into a nearly identical change (∼26%) in the cross section from 10 keV to 1 MeV. Other neutron induced cross sections do not exhibit any sensitivity to this parameter since T_γ only enters into Eq. [1] in the denominator. In general, for capture reactions, the smaller of the two transmission coefficients in the HF numerator will be the one that determines the cross section, especially if it is much smaller. This is always the case with photon vs. particle widths. The mean error associated with the experimental values of the gamma ray strength function for isotopes with charge $34 \leq Z \leq 46$ is 21.0% with a standard deviation of 9.8%. Hence, the uncertainties related to the gamma ray strength function in the capture cross sections is likely less than that shown in Figure 22.

4.2.5. Sensitivity to the Inclusion of Width Fluctuation Corrections

We adopt the Moldauer model of the width fluctuation correction (WFC) as embodied in the STAPRE code. Figure 23 shows the affect for the activation neutron capture and inelastic scattering cross sections for select targets both with (solid red line) and without (solid blue line) WFC. As expected a decrease in both channels is noticeable. For capture reactions the decrease is less than 20% below 100 keV. When the projectile energy increases, the capture cross section declines rapidly and the elastic enhancement vanishes. For the inelastic scattering, the correction is most significant between 1-4 MeV incident energy. Other channels that are open below a few MeV of incident energy may also exhibit sensitivity to width fluctuation corrections.

4.3. Calculated Channels by Target

In Appendix D we show all of the calculated neutron and charged particle induced channels leading out of the ground state for select targets of yttrium, zirconium, niobium, and molybdenum. The plots are grouped by common neutron numbers, with the neutron induced reactions on the left panes and the charged particle induced reactions on the right panes. In general, variations in a given cross section from target to target are small, although odd-even effects are apparent.

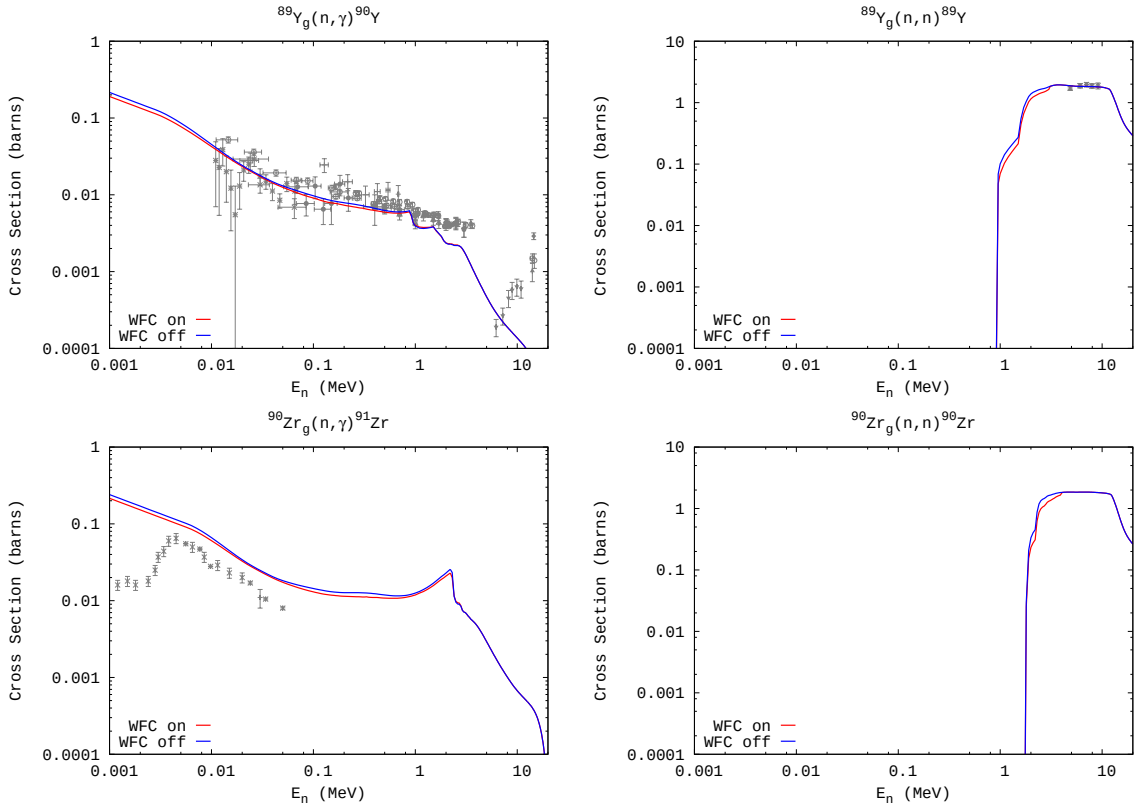

Fig. 23.— Sensitivity to inclusion or exclusion of width fluctuation corrections W.

These plots aid the evaluation of which reaction channels are the most important. For neutrons with low incident energies, the capture reaction is usually dominant, though the (n,p) cross section may be larger for proton rich targets. At energies around 14 MeV the (n,2n) reaction is usually dominant. Occasionally (and again for proton rich species) the (n,np) reaction may also be relatively large. For the charged particle reactions, each of the calculated channels are relatively important, though which channel dominates varies with the incident energy.

Of course the particle fluences play a dominant role in determining the most important cross sections for RADCHEM. More specific details will be disclosed in a classified analysis presented in a subsequent paper.

5. Conclusions

We have developed new neutron and charged particle induced cross section detector sets for radiochemical diagnostics of isotopes in the region $38 \leq Z \leq 45$. The theory and implementation of the Hauser-Feshbach model were described (§2), along with the details of the local systematics used to create a set of input parameters that reflect the latest available experimental data in the local region of interest (§3). Modeled cross sections were compared to available experimental cross sections for the loaded detector elements, as well as other stable targets in the region. Sensitivity to reasonable variations in the input models and parameters was explored (§4.2).

Overall we consider the modeling effort to be quite successful, as our calculated cross sections agree favorably with experimentally measured ones in this region of interest. In particular, we have demonstrated an ability to calculate (n,2n) cross sections to about 7% accuracy (Section 4.1.3), and (n,γ) cross sections to within roughly 30% accuracy (Sections 4.1.1 and 4.1.2). We also provide suggested normalizations to our (n,2n) and (n,γ) capture cross sections on stable targets to bring them into agreement (in an average sense) with the body of experimental data that exists. For charged-particle reactions we achieved an accuracy typically within 15-25%.

In our attempts to model cross sections it should be kept in mind that we are consider-

ing compound nuclear systems for which the important input parameters to our reaction model (e.g. those that affect level densities and photon-transmission coefficients) are often determined by normalization to experimental data (e.g. from resonance analysis), and so one would expect comparisons to measured capture cross sections to be good. Since these compound nuclei often bracket the systems of most interest to us, namely those which account for the dominant destruction reactions, our systematics should reasonably provide for similar agreement.

This work was performed under the auspices of the U.S. Department of Energy by the University of California Lawrence Livermore National Laboratory under contract W-7405-ENG-48.

REFERENCES

Arthur, E.D., "Calculation of neutron cross sections on isotopes of yttrium and zirconium", LA-7789-MS, LANL (1980).

Audi, G., Wapstra, A.H., and Thibault, C., "The AME2003 atomic mass evaluation (II). Tables, graphs, and references", Nuc. Phys. A **729**, 337 (2003).

Avrigeanu, V., Hodgson, P.E., and Avrigeanu, M., "Global optical potentials for emitted alpha particles", Phys. Rev. C **49**, 2136 (1994).

Avrigeanu, M. and Avrigeanu, V., "Recent improvements of the STAPRE-H95 preequilibrium and statistical model code", Report NP-86-1995, IPNE-Bucharest (1995). http://www.nea.fr/abs/html/iaea0971.html

Bao, Z. Y., Beer, H., Kappeler, F., Voss, F., & Wisshak, K., "Neutron cross sections for nucleosynthesis studies", Atomic Data & Nuclear Data Tables, **76**, 70 (2000).

Bauer, R., private communication (2003).

Beer, H., Voss, F., & Winters, R. R., "On the calculation of Maxwellian-averaged capture cross sections", ApJS, **80**, 403 (1992).

Belgya, T., Bersillon, O., Copote Noy, R., Fukahori, T., Zhigang, G., Goriely, S., Herman, M., Ignatyuk, A.V., Kailas, S., Koning, A.J., Oblozinsky, P., Plujko, V, and Young, P.G., "Handbook for calculations of nuclear reaction data, RIPL-2", IAEA, Vienna (2005).

Bohr, A., & Mottelson, B. *Nuclear Structure* Vol. 1, Single-Particle Motion, World Scientific, 1998

Chadwick, M., "The GNASH statistical model code", 1998. http://www.nea.fr/abs/html/psr-0125.html

Cline, C. K., "The Pauli exclusion principle in pre-equilibrium decay", Nucl. Phys. **A195**, 353 (1972).

Cline, C.K., and Blann, M., "The pre-equilibrium statistical model: description of the nuclear equilibration process and parameterization of the model", Nuc. Phys. A **172**, 225 (1971).

Experimental Nuclear Reaction Data File, Brookhaven National Laboratory, US Dept. of Energy (2006). http://www.nndc.bnl.gov/exfor3/

Gardner, D.G., "Model calculations as one means of satisfying the neutron cross section requirements of the ctr program", Invited paper presented at the Conference on Nuclear Cross Sections and Technology, Washington, D.C., March 3-7, 1975.

Gilbert, A. and Cameron, A.G.W., "A composite nuclear-level density formula with shell corrections", Can. J. Phys., **43**, 1446 (1965).

Hauser, W. and Feshbach, H., "The inelastic scattering of neutrons", Phys. Rev. **87**, 366 (1952).

Hilaire, S., Lagrange, Ch., and Koning, A. J., "Comparisons between various width fluctuation correction factors for compound nucleus reactions" Ann. of Phys. **306**, 209 (2003).

Hoffman, R. D., Rauscher, T., Woosley, S. E. & Thielemann, F.-K., "The reaction rate sensitivity of nucleosynthesis in Type II supernovae", ApJ, **521**, 735 (1999).

Hoffman, R.D., Dietrich, F.S., Bauer, R., Kelley, K., and Mustafa, M.G., "Neutron and charged-particle induced cross sections for radiochemistry in the region of bromine and krypton", UCRL-TR-205563, LLNL (2004a).

Hoffman, R.D., Dietrich, F.S., Bauer, R., Kelley, K., and Mustafa, M.G., "Neutron and charged-particle induced cross sections for radiochemistry in the region of iodine and xenon", UCRL-TR-206721, LLNL (2004b).

Hoffman, R.D., Kelley, K., Dietrich, F.S., Bauer, R., and Mustafa, M.G., "Neutron and charged-particle induced cross sections for radiochemistry in the region of samarium, europium and gadolinium", UCRL-TR-211558, LLNL (2004c).

Hofmann, H.M., Richert, J., Tepel, J. W., and Weidenmu̇ller, H.A., "Direct reactions and Hauser-Feshbach theory" Ann. of Phys. **90**, 403 (1975).

Iljinov, A.S., Mebel, M.V., Bianchi, N., De Sanctis, E., Guaraldo, C., Lucherini, V., Muccifora, V., Polli, E., Reolon, A.R., and Rossi, P., "Phenomenological statistical analysis of level densities, decay widths and lifetimes of excited nuclei", Nucl. Phys. A **543**, 517 (1992).

Keisch, B., "Yield ratios of isomers produced by neutron activation", Phys. Rev. **129**, 769 (1963).

Kelley, K., Hoffman, R.D., Dietrich, F.S., Bauer, R., and Mustafa, M.G., "'Neutron and charged-particle induced cross sections for radiochemistry for isotopes of scandium, titanium, vanadium, chromium, manganese, and iron", UCRL-TR-211668, LLNL (2005).

Kelley, K., Hoffman, R.D., Dietrich, F.S., and Mustafa, M.G., "Neutron induced cross sections for radiochemistry for isotopes of arsenic", UCRL-TR-218181, LLNL (2006).

Kelley, K., Hoffman, R.D., Dietrich, F.S., and Mustafa, M.G., "Neutron induced cross sections for radiochemistry for isotopes of nickel, copper, and zinc", UCRL-TR-221759, LLNL (2006).

Koning, A.J., & Delaroche, J.P., "Local and global nucleon optical models from 1 keV to 200 MeV", Nucl. Phys. **A713**, 231 (2003).

Kopecky, J. and Uhl, M., "Test of gamma-ray strength functions in nuclear reaction model calculations", Phys. Rev. C **41**, 1941 (1990).

Lohr, J.M. and Haeberli, W., "Elastic scattering of 9-13 MeV vector polarized deuterons", Nuc. Phys. A **232**, 381 (1974).

Mahaux, C. and Weidenmüller, H.A., "Recent developments in compound-nucleus theory", Ann. Rev. Part. Nucl. Sci. **29**, 1 (1979).

Milazzo-Colli, L., and Braga-Marcazzan, G.M., "α-emission by pre-equilibrium processes in (n,α) reactions", Nuc. Phys. A **210**, 297 (1973).

Moldauer, P. A., "Evaluation of the fluctuation enhancement factor" Phys. Rev. C **14**, 764 (1976).

Möller, P., Nix, J.R., Myers, W.D., and Swiatecki, W.J., "Nuclear ground-state masses and deformations" At. Data & Nuc. Data Tables **59**, 185 (1995).

Mughabghab, S.F., Divadeenam, M., and Holden, N.E., *Neutron Cross Sections*, Vols. 1 and 2, Academic Press (1981).

Mustafa, M.G., West, H.I., O'Brien H., Lanier, R.G., Benhamou, M., and Tamura, T., "Measurement and a direct-reaction plus Hauser-Feshbach analysis of ^{89}Y(p,n)^{89}Zr, ^{89}Y(p,2n)^{88}Zr, and ^{89}Y(p,pn)^{88}Y reactions up to 40 MeV", Phys. Rev. C **38**, 1624 (1998).

Nethaway, D.R., "The cross-section sets used with the Watusi program", A-Division memo, LLNL (5 Nov. 1998).

Prestwood, R.J., Thomas, K.W., Nethaway, D.R., and Smith, N.L., "Measurement of 14-MeV neutron cross sections for ^{88}Zr and ^{88}Y", Phys. Rev. C 29, 805 (1984).

Rauscher, T., Thielemann, F.-K., and Kratz, K.-L., "Nuclear level density and the determination of thermonuclear rates for astrophysics", Phys. Rev. C **56**, 1613 (1997).

Raynal, J. "ECIS96", Proceedings of the Specialists' Meeting on the Nucleon Nucleus Optical Model up to 200 MeV, 13-15 November 1996, Bruyeres-le-Chatel, France. http://www.nea.fr/html/science/om200/raynal.pdf

Reffo, G., ICTP Lecture Series, 17 Jan. - 10 Mar., 1978, Trieste.

Tuli, J.K., "Nuclear wallet cards", 6th Ed., Brookhaven National Laboratory, U.S. Dept. of Energy (2000).

Udagawa, T., & Tamura, T., "Derivation of breakup-fusion cross sections from the optical theorem", Phys. Rev. C 24, 1348 (1981).

Uhl, M., and Strohmaier, B., "STAPRE: A computer code for particle induced activation cross sections and related quantities", IRK-Vienna Report IRK-76/01 (1976, Upd. 1978).

Vonach, H., "User's manual for the code STAPRE as implemented at Lawrence Livermore National Laboratory", UCID-19549, LLNL (1982).

Wapstra, A.H., Audi, G., and Thibault, C., "The AME2003 atomic mass evaluation (I). Evaluation of input data, adjustment procedures", Nuc. Phys. A **729**, 129 (2003).

West, H.I., Lanier, R.G., Mustafa, M.G., Nuckolls, R.M., Nagle, R.J., O'Brien, H., Frehaut, J., Adam, A., and Philis, C., "Some light-ion excitation-function measurements on titanium, yttrium, and europium, and associated results", UCRL-ID-115738, LLNL (1993).

Williams, F.C. Jr., "Intermediate state transition rates in the Griffin model", Phys. Lett. **31B**, 184 (1970).

Woosley, S.E., Fowler, W.A., Holmes, J.A., and Zimmerman, B.A., "Tables of thermonuclear reaction rate data for intermediate mass nuclei", Orange aid preprint series in nuclear, atomic and relativistic astrophysics (1975).

This 2-column preprint was prepared with the AAS LaTeX macros v5.0.

A. Cross Sections Included in the Detector Sets

A.1. Cross Sections in the Existing RADCHEM Detector Sets

Cross sections for the following reactions are provided in the existing RADCHEM data sets YT0585, YT0488, Zr0982, Nb0179, and Mo1278. The majority of these reactions were calculated between 1972 and 1988. A few have been scaled to match measured cross sections at or around 14.1 MeV of incident energy. Seven of the charged-particle reaction in set YT0488 are measured. See (Nethaway 1998) for more details.

Table 5: Cross sections available in existing RADCHEM detector sets

^{86}Y:	^{86}Y(n,γ)^{87g}Y [a]	^{86}Y(n,γ)^{87m}Y [a]	^{86}Y(n,2n)^{85}Y [a]	^{86}Y(n,X) [a]
^{87g}Y:	^{87g}Y(n,γ)^{88g}Y [b]	^{87g}Y(n,γ)^{88m}Y [b]	^{87g}Y(n,n')^{87m}Y [b]	^{87g}Y(n,2n)^{86}Y [b]
	^{87g}Y(n,X) [b]			
^{87m}Y:	^{87m}Y(n,γ)^{88g}Y [b]	^{87m}Y(n,γ)^{88m1}Y [b]	^{87m}Y(n,γ)^{88m2}Y [b]	^{87m}Y(n,n')^{87g}Y [b]
	^{87m}Y(n,2n)^{86}Y [b]	^{87m}Y(n,X) [b]		
^{88g}Y:	^{88g}Y(n,γ)^{89g}Y [b]	^{88g}Y(n,γ)^{89m}Y [b]	^{88g}Y(n,n')^{88m1}Y [b]	^{88g}Y(n,n')^{88m2}Y [b]
	^{88g}Y(n,2n)^{87g}Y [b,g]	^{88g}Y(n,2n)^{87m}Y [b,g]	^{88g}Y(n,X) [b]	^{88g}Y(p,n)^{88}Zr [c]
	^{88g}Y(p,2n)^{87}Zr [c]	^{88g}Y(d,2n)^{88}Zr [c]	^{88g}Y(d,3n)^{87}Zr [c]	
^{88m1}Y:	^{88m1}Y(n,γ)^{89g}Y [b]	^{88m1}Y(n,γ)^{89m}Y [b]	^{88m1}Y(n,n')^{88g}Y [b]	^{88m1}Y(n,n')^{88m2}Y [b]
	^{88m1}Y(n,2n)^{87g}Y [b,g]	^{88m1}Y(n,2n)^{87m}Y [b,g]	^{88m1}Y(n,X) [b]	^{88m1}Y(p,n)^{88}Zr [c]
	^{88m1}Y(p,2n)^{87}Zr [c]	^{88m1}Y(d,2n)^{88}Zr [c]	^{88m1}Y(d,3n)^{87}Zr [c]	
^{88m2}Y:	^{88m2}Y(n,γ)^{89g}Y [b]	^{88m2}Y(n,γ)^{89m}Y [b]	^{88m2}Y(n,n')^{88g}Y [b]	^{88m2}Y(n,n')^{88m1}Y [b]
	^{88m2}Y(n,2n)^{87g}Y [b,g]	^{88m2}Y(n,2n)^{87m}Y [b,g]	^{88m2}Y(n,X) [b]	^{88m2}Y(p,n)^{88}Zr [c]
	^{88m2}Y(p,2n)^{87}Zr [c]	^{88m2}Y(d,2n)^{88}Zr [c]	^{88m2}Y(d,3n)^{87}Zr [c]	
^{89g}Y:	^{89g}Y(n,γ)^{90}Y [a]	^{89g}Y(n,n')^{89m}Y [a]	^{89g}Y(n,2n)^{88g}Y [a,g]	^{89g}Y(n,2n)^{88m1}Y [a,g]
	^{89g}Y(n,2n)^{88m2}Y [a,g]	^{89g}Y(n,X) [a]	^{89g}Y(p,n)^{89g}Zr [e]	^{89g}Y(p,n)^{89m}Zr [e]
	^{89g}Y(p,2n)^{88}Zr [e]	^{89g}Y(p,np)^{88g}Y [e]	^{89g}Y(d,2n)^{89g}Zr [f]	^{89g}Y(d,2n)^{89m}Zr [f]
	^{89g}Y(d,3n)^{88}Zr [f]			
^{89m}Y:	^{89m}Y(n,γ)^{90}Y [a]	^{89m}Y(n,n')^{89g}Y [a]	^{89m}Y(n,2n)^{88g}Y [a]	^{89m}Y(n,2n)^{88m1}Y [a]
	^{89m}Y(n,2n)^{88m2}Y [a]	^{89m}Y(n,X) [a]	^{89m}Y(p,n)^{89g}Zr [c]	^{89m}Y(p,n)^{89m}Zr [c]
	^{89m}Y(p,2n)^{88}Zr [c]	^{89m}Y(d,2n)^{89g}Zr [c]	^{89m}Y(d,2n)^{89m}Zr [c]	
^{90}Y:	^{90}Y(n,γ)^{91}Y [a]	^{90}Y(n,2n)^{89g}Y [a]	^{90}Y(n,2n)^{89m}Y [a]	^{90}Y(n,X) [a]
^{91}Y:	^{91}Y(n,γ)^{92}Y [a]	^{91}Y(n,2n)^{90}Y [a]	^{91}Y(n,3n)^{89g}Y [a]	^{91}Y(n,X) [a]
^{92}Y:	^{92}Y(n,γ)^{93}Y [a]	^{92}Y(n,2n)^{91}Y [a]	^{92}Y(n,3n)^{90}Y [a]	^{92}Y(n,X) [a]
^{87}Zr:	^{87}Zr(n,γ)^{88}Zr [b]	^{87}Zr(n,2n)^{86}Zr [b]	^{87}Zr(n,p)^{87g}Y [b]	
^{88}Zr:	^{88}Zr(n,γ)^{89g}Zr [b]	^{88}Zr(n,γ)^{89m}Zr [b]	^{88}Zr(n,2n)^{87}Zr [b,g]	^{88}Zr(n,p)^{88g}Y [b]
	^{88}Zr(n,np)^{87g}Y [b,g]			
^{89g}Zr:	^{89g}Zr(n,γ)^{90g}Zr [b]	^{89g}Zr(n,γ)^{90m2}Zr [b]	^{89g}Zr(n,γ)^{90m3}Zr [b]	^{89g}Zr(n,n')^{89m}Zr [b]
	^{89g}Zr(n,2n)^{88}Zr [b]	^{89g}Zr(n,p)^{89g}Y [b]	^{89g}Zr(n,np)^{88g}Y [b]	
^{89m}Zr:	^{89m}Zr(n,γ)^{90g}Zr [b]	^{89m}Zr(n,γ)^{90m1}Zr [b]	^{89m}Zr(n,γ)^{90m2}Zr [b]	^{89m}Zr(n,n')^{89g}Zr [b]

Continued on next page...

[a] Calculation from (Arthur 1980).
[b] Calculated by M. Gardner and D. Gardner between 1972 and 1985 at LLNL.
[c] Calculated by M. Mustafa in 1988 at LLNL.
[d] Calculated by M. Gardner in 1978 at LLNL.
[e] Measurement from (Mustafa *et al.* 1988).
[f] Measurement from (West *et al.* 1993).
[g] Scaled to match measured cross section data near 14 MeV incident energy.

Table 5: (continued)

	^{89m}Zr(n,2n)^{88}Zr [b]	^{89m}Zr(n,p)^{89g}Y [b]	^{89m}Zr(n,np)^{88g}Y [b]	
^{90g}Zr:	^{90g}Zr(n,γ)^{91}Zr [b]	^{90g}Zr(n,n')^{90m1}Zr [b]	^{90g}Zr(n,n')^{90m2}Zr [b]	^{90g}Zr(n,n')^{90m3}Zr [b]
	^{90g}Zr(n,2n)^{89g}Zr [b]	^{90g}Zr(n,2n)^{89m}Zr [b]	^{90g}Zr(n,p)^{90}Y [b]	^{90g}Zr(n,np)^{89g}Y [b]
	^{90g}Zr(n,np)^{89m}Y [b]	^{90g}Zr(n,X) [b]		
^{90m1}Zr:	^{90m1}Zr(n,γ)^{91}Zr [b]	^{90m1}Zr(n,n')^{90g}Zr [b]	^{90m1}Zr(n,n')^{90m2}Zr [b]	^{90m1}Zr(n,n')^{90m3}Zr [b]
	^{90m1}Zr(n,2n)^{89g}Zr [b]	^{90m1}Zr(n,2n)^{89m}Zr [b]	^{90m1}Zr(n,p)^{90}Y [b]	^{90m1}Zr(n,np)^{89g}Y [b]
	^{90m1}Zr(n,np)^{89m}Y [b]	^{90m1}Zr(n,X) [b]		
^{90m2}Zr:	^{90m2}Zr(n,γ)^{91}Zr [b]	^{90m2}Zr(n,n')^{90g}Zr [b]	^{90m2}Zr(n,n')^{90m1}Zr [b]	^{90m2}Zr(n,n')^{90m3}Zr [b]
	^{90m2}Zr(n,2n)^{89g}Zr [b]	^{90m2}Zr(n,2n)^{89m}Zr [b]	^{90m2}Zr(n,p)^{90}Y [b]	^{90m2}Zr(n,np)^{89g}Y [b]
	^{90m2}Zr(n,np)^{89m}Y [b]	^{90m2}Zr(n,X) [b]		
^{90m3}Zr:	^{90m3}Zr(n,γ)^{91}Zr [b]	^{90m3}Zr(n,n')^{90g}Zr [b]	^{90m3}Zr(n,n')^{90m1}Zr [b]	^{90m3}Zr(n,n')^{90m2}Zr [b]
	^{90m3}Zr(n,2n)^{89g}Zr [b]	^{90m3}Zr(n,2n)^{89m}Zr [b]	^{90m3}Zr(n,p)^{90}Y [b]	^{90m3}Zr(n,np)^{89g}Y [b]
	^{90m3}Zr(n,np)^{89m}Y [b]	^{90m3}Zr(n,X) [b]		
^{91}Zr:	^{91}Zr(n,2n)^{90g}Zr [b]	^{91}Zr(n,2n)^{90m1}Zr [b]	^{91}Zr(n,2n)^{90m2}Zr [b]	^{91}Zr(n,2n)^{90m3}Zr [b]
	^{91}Zr(n,p)^{91}Y [b]			
^{92}Zr:	^{92}Zr(n,2n)^{91}Zr [b]			
^{92g}Nb:	^{92g}Nb(n,n')^{92m1}Nb [d]	^{92g}Nb(n,n')^{92m2}Nb [d]	^{92g}Nb(n,X) [d]	
^{92m1}Nb:	^{92m1}Nb(n,n')^{92g}Nb [d]	^{92m1}Nb(n,n')^{92m2}Nb[d]	^{92m1}Nb(n,X) [d]	
^{92m2}Nb:	^{92m2}Nb(n,n')^{92g}Nb [d]	^{92m2}Nb(n,n')^{92m1}Nb[d]	^{92m2}Nb(n,X) [d]	
^{93g}Nb:	^{93g}Nb(n,n')^{93m}Nb [d]	^{93g}Nb(n,2n)^{92g}Nb [d,g]	^{93g}Nb(n,2n)^{92m1}Nb[d,g]	^{93g}Nb(n,2n)^{92m2}Nb[d,g]
	^{93g}Nb(n,X) [d]			
^{93m}Nb:	^{93m}Nb(n,n')^{93g}Nb [d]	^{93m}Nb(n,2n)^{92g}Nb [d]	^{93m}Nb(n,2n)^{92m1}Nb[d]	^{93m}Nb(n,2n)^{92m2}Nb[d]
	^{93m}Nb(n,X) [d]			
^{91g}Mo:	^{91g}Mo(n,n')^{91m}Mo [d]	^{91g}Mo(n,α)^{88}Zr [d]	^{91g}Mo(n,X) [d]	
^{91m}Mo:	^{91m}Mo(n,n')^{91g}Mo [d]	^{91m}Mo(n,α)^{88}Zr [d]	^{91m}Mo(n,X) [d]	
^{92}Mo:	^{92}Mo(n,2n)^{91g}Mo [d]	^{92}Mo(n,2n)^{91m}Mo [d]	^{92}Mo(n,p)^{91g}Nb [d]	^{92}Mo(n,p)^{91m1}Nb [d]
	^{92}Mo(n,p)^{91m2}Nb [d]	^{92}Mo(n,α)^{89g}Zr [d]	^{92}Mo(n,α)^{89m}Zr [d]	^{92}Mo(n,nα)^{88}Zr [d]
	^{92}Mo(n,X) [d]			

[a] Calculation from (Arthur 1980).
[b] Calculated by M. Gardner and D. Gardner between 1972 and 1985 at LLNL.
[c] Calculated by M. Mustafa in 1988 at LLNL.
[d] Calculated by M. Gardner in 1978 at LLNL.
[e] Measurement from (Mustafa *et al.* 1988).
[f] Measurement from (West *et al.* 1993).
[g] Scaled to match measured cross section data near 14 MeV incident energy.

A.2. Proposed New Detector Set

Table 6 (beginning on the next page) lists the reaction channels considered in the present work.

The first column indicates the target nucleus, in its ground or isomeric state (if the state is not explicitly listed, then only a ground state exists for the target). Column two indicates the spin and parity of the target. Column four lists the half-life for radioactive targets and the natural abundance (in bold face) for stable targets. Column four lists the excitation energy for isomer targets in keV.

For each of the targets listed, we model the reaction channels indicated in the remaining columns. Closed dots indicate that the reaction channel was also included in the existing RADCHEM data sets. Open dots indicate that the reaction channel is included only in the new set. Reaction channels have only been excluded in the event that the reaction threshold was greater than 20 MeV. The notable exception is ^{100m}Rh, for which the discrete level scheme obtained from (Belgya *et al.* 2005) is not complete up to the isomer energy. In cases where the residual nucleus has a long-lived isomer ($t_{1/2} > 1$ μs), we model not only the activation cross section but also the cross sections leading to the ground and isomeric states. To be consistent with the RADCHEM set zr0982, we treat the first two excited states of ^{90}Zr as isomers. All reaction channels with more than one possible ordering of the outgoing particles include the sum of the cross section for all orderings, i.e. (n,np) represents (n,np)+(n,pn).

The destruction cross sections (n,X), (p,X), and (d,X) have been determined by summing the other included reaction channels and subtracting the total from the reaction cross section, as described in Section 2.7.

Table 6: Proposed New Detector Set

Target	J^π	$t_{1/2}$	Energy	(n,γ)	(n,n')	(n,2n)	(n,3n)	(n,p)	(n,np)	(n,α)	(n,nα)	(n,d)	(n,X)	(p,n)	(p,2n)	(p,p')	(p,pn)	(p,γ)	(p,X)	(d,n)	(d,2n)	(d,3n)	(d,p)	(d,d')	(d,X)
^{83g}Sr	7/2+	32.41 h		○	○	○		○	○	○	○	○	○	○	○	○	○	○	○	○	○	○	○	○	○
^{83m}Sr	1/2-	4.95 s	259.15	○	○	○		○	○	○	○	○	○	○	○	○	○	○	○	○	○	○	○	○	○
^{84}Sr	0+	**0.56%**		○	○	○		○	○	○	○	○	○	○	○	○	○	○	○	○	○	○	○	○	○
^{85g}Sr	9/2+	64.84 d		○	○	○		○	○	○	○	○	○	○	○	○	○	○	○	○	○	○	○	○	○
^{85m}Sr	1/2-	67.63 m	238.66	○	○	○		○	○	○	○	○	○	○	○	○	○	○	○	○	○	○	○	○	○
^{86}Sr	0+	**9.86%**		○	○	○		○	○	○	○	○	○	○	○	○	○	○	○	○	○	○	○	○	○
^{87g}Sr	9/2+	**7.00%**		○	○	○	○	○	○	○	○	○	○	○	○	○	○	○	○	○	○	○	○	○	○
^{87m}Sr	1/2-	2.81 h	388.53	○	○	○	○	○	○	○	○	○	○	○	○	○	○	○	○	○	○	○	○	○	○
^{88}Sr	0+	**82.58%**		○	○	○	○	○	○	○	○	○	○	○	○	○	○	○	○	○	○	○	○	○	○
^{89}Sr	5/2+	50.53 d		○	○	○	○	○	○	○	○	○	○	○	○	○	○	○	○	○	○	○	○	○	○
^{90}Sr	0+	28.79 y		○	○	○	○	○	○	○	○	○	○	○	○	○	○	○	○	○	○	○	○	○	○
^{91}Sr	5/2+	9.63 h		○	○	○	○	○	○	○	○	○	○	○	○	○	○	○	○	○	○	○	○	○	○
^{92}Sr	0+	2.71 h		○	○	○	○	○	○	○	○	○	○	○	○	○	○	○	○	○	○	○	○	○	○
^{84g}Y	1+	4.6 s		○	○	○		○	○	○	○	○	○	○	○	○	○	○	○	○	○	○	○	○	○
^{84m}Y	5-	39.5 m	0.0+	○	○	○		○	○	○	○	○	○	○	○	○	○	○	○	○	○	○	○	○	○
^{85g}Y	1/2-	2.68 h		○	○	○		○	○	○	○	○	○	○	○	○	○	○	○	○	○	○	○	○	○
^{85m}Y	9/2+	4.86 h	29.80	○	○	○		○	○	○	○	○	○	○	○	○	○	○	○	○	○	○	○	○	○
^{86g}Y	4-	14.74 h		●	○	●		○	○	○	○	○	●	○	○	○	○	○	○	○	○	○	○	○	○
^{86m}Y	8+	48 m	218.30	○	○	○		○	○	○	○	○	○	○	○	○	○	○	○	○	○	○	○	○	○
^{87g}Y	1/2-	79.8 h		●	●	●		○	○	○	○	○	●	○	○	○	○	○	○	○	○	○	○	○	○
^{87m}Y	9/2+	13.37 h	380.79	●	●	●		○	○	○	○	○	●	○	○	○	○	○	○	○	○	○	○	○	○
^{88g}Y	4-	106.65 d		●	●	●		○	○	○	○	○	●	●	●	○	○	○	○	○	●	●	○	○	○
^{88m1}Y	1+	300 μs	392.86	●	●	●		○	○	○	○	○	●	●	●	○	○	○	○	○	●	●	○	○	○
^{88m2}Y	8+	13.9 ms	674.55	●	●	●		○	○	○	○	○	●	●	●	○	○	○	○	○	●	●	○	○	○
^{89g}Y	1/2-	**100%**		●	●	●		○	○	○	○	○	●	●	●	○	●	○	○	○	●	●	○	○	○
^{89m}Y	9/2+	15.28 s	908.96	●	●	●	○	○	○	○	○	○	●	●	●	○	○	○	○	○	●	○	○	○	○
^{90g}Y	2-	64.00 h		●	○	●	○	○	○	○	○	○	●	○	○	○	○	○	○	○	○	○	○	○	○
^{90m}Y	7+	3.19 h	682.03	○	○	○	○	○	○	○	○	○	○	○	○	○	○	○	○	○	○	○	○	○	○
^{91g}Y	1/2-	58.51 d		●	○	●	●	○	○	○	○	○	●	○	○	○	○	○	○	○	○	○	○	○	○

Continued on next page...

Table 6: (continued)

Target	J^π	$t_{1/2}$	Energy	(n,γ)	(n,n')	(n,2n)	(n,3n)	(n,p)	(n,np)	(n,α)	(n,nα)	(n,d)	(n,X)	(p,n)	(p,2n)	(p,p')	(p,pn)	(p,γ)	(p,X)	(d,n)	(d,2n)	(d,3n)	(d,p)	(d,d')	(d,X)
^{91m}Y	9/2+	49.71 m	555.58	○	○	○	○	○	○	○	○	○	○	○	○	○	○	○	○	○	○	○	○	○	○
^{92}Y	2-	3.54 h		●	○	●	●	○	○	○	○	○	●	○	○	○	○	○	○	○	○	○	○	○	○
^{93g}Y	1/2-	10.18 h		○	○	○	○	○	○	○	○	○	○	○	○	○	○	○	○	○	○	○	○	○	○
^{93m}Y	7/2+	0.82 s	758.72	○	○	○	○	○	○	○	○	○	○	○	○	○	○	○	○	○	○	○	○	○	○
^{86}Zr	0+	16.5 h		○	○	○		○	○	○	○	○	○	○	○	○	○	○	○	○	○		○	○	○
^{87g}Zr	9/2+	1.68 h		●	○	●		●	○	○	○	○	○	○	○	○	○	○	○	○	○		○	○	○
^{87m}Zr	1/2-	14 s	335.73	○	○	○		○	○	○	○	○	○	○	○	○	○	○	○	○	○		○	○	○
^{88}Zr	0+	83.4 d		●	○	●		●	●	○	○	○	○	○	○	○	○	○	○	○	○		○	○	○
^{89g}Zr	9/2+	78.41 h		●	●	●		●	●	○	○	○	○	○	○	○	○	○	○	○	○	○	○	○	○
^{89m}Zr	1/2-	4.161 m	587.84	●	●	●		●	●	○	○	○	○	○	○	○	○	○	○	○	○	○	○	○	○
^{90g}Zr	0+	**51.45%**		●	●	●		●	●	○	○	○	●	○	○	○	○	○	○	○	○	○	○	○	○
^{90m1}Zr	0+	61.3 ns	1760.71	●	●	●	○	●	●	○	○	○	●	○	○	○	○	○	○	○	○	○	○	○	○
^{90m2}Zr	2+	88.4 fs	2186.27	●	●	●	○	●	●	○	○	○	●	○	○	○	○	○	○	○	○	○	○	○	○
^{90m3}Zr	5-	809.2 ms	2319.00	●	●	●	○	●	●	○	○	○	●	○	○	○	○	○	○	○	○	○	○	○	○
^{91g}Zr	5/2+	**11.22%**		○	○	●	○	●	○	○	○	○	○	○	○	○	○	○	○	○	○	○	○	○	○
^{91m}Zr	21/2+	4.35 μs	3167.30	○	○	○	○	○	○	○	○	○	○	○	○	○	○	○	○	○	○	○	○	○	○
^{92}Zr	0+	**17.15%**		○	○	●	○	○	○	○	○	○	○	○	○	○	○	○	○	○	○	○	○	○	○
^{93}Zr	5/2+	1.53 My		○	○	○	○	○	○	○	○	○	○	○	○	○	○	○	○	○	○	○	○	○	○
^{94}Zr	0+	**17.38%**		○	○	○	○	○	○	○	○	○	○	○	○	○	○	○	○	○	○	○	○	○	○
^{95}Zr	5/2+	64.02 d		○	○	○	○	○	○	○	○	○	○	○	○	○	○	○	○	○	○	○	○	○	○
^{96}Zr	0+	**2.80%**		○	○	○	○	○	○	○	○	○	○	○	○	○	○	○	○	○	○	○	○	○	○
^{87g}Nb	9/2+	2.6 m		○	○	○		○	○	○	○	○	○	○	○	○	○	○	○	○	○		○	○	○
^{87m}Nb	1/2-	3.7 m	0.0+	○	○	○		○	○	○	○	○	○	○	○	○	○	○	○	○	○		○	○	○
^{88g}Nb	8+	14.5 m		○	○	○		○	○	○	○	○	○	○	○	○	○	○	○	○	○	○	○	○	○
^{88m}Nb	4-	7.8 m	0.0+	○	○	○		○	○	○	○	○	○	○	○	○	○	○	○	○	○	○	○	○	○
^{89g}Nb	9/2+	2.03 h		○	○	○		○	○	○	○	○	○	○	○	○	○	○	○	○	○	○	○	○	○
^{89m}Nb	1/2-	66 m	0.0+	○	○	○		○	○	○	○	○	○	○	○	○	○	○	○	○	○	○	○	○	○

Continued on next page...

Table 6: (continued)

Target	J^π	$t_{1/2}$	Energy	(n,γ)	(n,n')	(n,2n)	(n,3n)	(n,p)	(n,np)	(n,α)	(n,nα)	(n,d)	(n,X)	(p,n)	(p,2n)	(p,p')	(p,pn)	(p,γ)	(p,X)	(d,n)	(d,2n)	(d,3n)	(d,p)	(d,d')	(d,X)
^{90g}Nb	8+	14.60 h		○	○	○		○	○	○	○	○	○	○	○	○	○	○	○	○	○	○	○	○	○
^{90m1}Nb	6+	63 μs	122.37	○	○	○		○	○	○	○	○	○	○	○	○	○	○	○	○	○	○	○	○	○
^{90m2}Nb	4-	18.81 s	124.67	○	○	○		○	○	○	○	○	○	○	○	○	○	○	○	○	○	○	○	○	○
^{90m3}Nb	1+	6.19 ms	382.01	○	○	○		○	○	○	○	○	○	○	○	○	○	○	○	○	○	○	○	○	○
^{91g}Nb	9/2+	680 y		○	○	○		○	○	○	○	○	○	○	○	○	○	○	○	○	○	○	○	○	○
^{91m1}Nb	1/2-	60.86 d	104.49	○	○	○		○	○	○	○	○	○	○	○	○	○	○	○	○	○	○	○	○	○
^{91m2}Nb	17/2-	3.76 μs	2034.36	○	○	○		○	○	○	○	○	○	○	○	○	○	○	○	○	○	○	○	○	○
^{92g}Nb	7+	34.7 My		○	●	○	○	○	○	○	○	○	●	○	○	○	○	○	○	○	○	○	○	○	○
^{92m1}Nb	2+	10.15 d	135.50	○	●	○	○	○	○	○	○	○	●	○	○	○	○	○	○	○	○	○	○	○	○
^{92m2}Nb	2-	5.9 μs	225.70	○	●	○	○	○	○	○	○	○	●	○	○	○	○	○	○	○	○	○	○	○	○
^{93g}Nb	9/2+	**100%**		○	●	●	○	○	○	○	○	○	●	○	○	○	○	○	○	○	○	○	○	○	○
^{93m}Nb	1/2-	16.13 y	30.82	○	●	●	○	○	○	○	○	○	●	○	○	○	○	○	○	○	○	○	○	○	○
^{94g}Nb	6+	2030 y		○	○	○	○	○	○	○	○	○	○	○	○	○	○	○	○	○	○	○	○	○	○
^{94m}Nb	3+	6.263 m	40.90	○	○	○	○	○	○	○	○	○	○	○	○	○	○	○	○	○	○	○	○	○	○
^{95g}Nb	9/2+	34.997 d		○	○	○	○	○	○	○	○	○	○	○	○	○	○	○	○	○	○	○	○	○	○
^{95m}Nb	1/2-	86.6 h	235.68	○	○	○	○	○	○	○	○	○	○	○	○	○	○	○	○	○	○	○	○	○	○
^{96}Nb	6+	23.35 h		○	○	○	○	○	○	○	○	○	○	○	○	○	○	○	○	○	○	○	○	○	○
^{97g}Nb	9/2+	72.1 m		○	○	○	○	○	○	○	○	○	○	○	○	○	○	○	○	○	○	○	○	○	○
^{97m}Nb	1/2-	58.7 s	743.35	○	○	○	○	○	○	○	○	○	○	○	○	○	○	○	○	○	○	○	○	○	○
^{98g}Nb	1+	2.86 s		○	○	○	○	○	○	○	○	○	○	○	○	○	○	○	○	○	○	○	○	○	○
^{98m}Nb	5+	51.3 m	84.00	○	○	○	○	○	○	○	○	○	○	○	○	○	○	○	○	○	○	○	○	○	○
^{99g}Nb	9/2+	15.0 s		○	○	○	○	○	○	○	○	○	○	○	○	○	○	○	○	○	○	○	○	○	○
^{99m}Nb	1/2-	2.6 m	365.29	○	○	○	○	○	○	○	○	○	○	○	○	○	○	○	○	○	○	○	○	○	○
^{100}Nb	1+	1.5 s		○	○	○	○	○	○	○	○	○	○	○	○	○	○	○	○	○	○	○	○	○	○
^{90g}Mo	0+	5.56 h		○	○	○		○	○	○	○	○	○	○		○	○	○	○	○	○		○	○	○
^{90m}Mo	8+	1.12 μs	2874.73	○	○	○		○	○	○	○	○	○	○	○	○	○	○	○	○	○		○	○	○
^{91g}Mo	9/2+	15.49 m		○	●	○		○	○	●	○	○	●	○	○	○	○	○	○	○	○		○	○	○
^{91m}Mo	1/2-	64.6 s	653.01	○	●	○		○	○	●	○	○	●	○	○	○	○	○	○	○	○		○	○	○
^{92}Mo	0+	**14.84%**		○	○	●		●	○	●	●	○	●	○	○	○	○	○	○	○	○		○	○	○

Continued on next page...

Table 6: (continued)

Target	J^π	$t_{1/2}$	Energy	(n,γ)	(n,n')	(n,2n)	(n,3n)	(n,p)	(n,np)	(n,α)	(n,nα)	(n,d)	(n,X)	(p,n)	(p,2n)	(p,p')	(p,pn)	(p,γ)	(p,X)	(d,n)	(d,2n)	(d,3n)	(d,p)	(d,d')	(d,X)
^{93g}Mo	5/2+	4000 y		o	o	o		o	o	o	o	o	o	o	o	o	o	o	o	o	o	o	o	o	o
^{93m}Mo	21/2+	6.85 h	2424.89	o	o	o	o	o	o	o	o	o	o	o	o	o	o	o	o	o	o	o	o	o	o
^{94}Mo	0+	**9.25%**		o	o	o	o	o	o	o	o	o	o	o	o	o	o	o	o	o	o	o	o	o	o
^{95}Mo	5/2+	**15.92%**		o	o	o	o	o	o	o	o	o	o	o	o	o	o	o	o	o	o	o	o	o	o
^{96}Mo	0+	**16.68%**		o	o	o	o	o	o	o	o	o	o	o	o	o	o	o	o	o	o	o	o	o	o
^{97}Mo	5/2+	**9.55%**		o	o	o	o	o	o	o	o	o	o	o	o	o	o	o	o	o	o	o	o	o	o
^{98}Mo	0+	**24.13%**		o	o	o	o	o	o	o	o	o	o	o	o	o	o	o	o	o	o	o	o	o	o
^{99g}Mo	1/2+	65.94 h		o	o	o	o	o	o	o	o	o	o	o	o	o	o	o	o	o	o	o	o	o	o
^{99m}Mo	5/2+	15.5 μs	97.79	o	o	o	o	o	o	o	o	o	o	o	o	o	o	o	o	o	o	o	o	o	o
^{100}Mo	0+	**9.63%**		o	o	o	o	o	o	o	o	o	o	o	o	o	o	o	o	o	o	o	o	o	o
^{101}Mo	1/2+	14.61 m		o	o	o	o	o	o	o	o	o	o	o	o	o	o	o	o	o	o	o	o	o	o
^{91g}Tc	9/2+	3.14 m		o	o	o		o	o	o	o	o	o	o	o	o	o	o	o	o	o		o	o	o
^{91m}Tc	1/2-	3.3 m	350.00	o	o	o		o	o	o	o	o	o	o	o	o	o	o	o	o	o		o	o	o
^{92g}Tc	8+	4.23 m		o	o	o		o	o	o	o	o	o	o	o	o	o	o	o	o	o		o	o	o
^{92m}Tc	4+	1.03 μs	270.15	o	o	o		o	o	o	o	o	o	o	o	o	o	o	o	o	o		o	o	o
^{93g}Tc	9/2+	2.75 h		o	o	o		o	o	o	o	o	o	o	o	o	o	o	o	o	o		o	o	o
^{93m1}Tc	1/2-	43.5 m	391.84	o	o	o		o	o	o	o	o	o	o	o	o	o	o	o	o	o	o	o	o	o
^{93m2}Tc	17/2-	10.2 μs	2185.16	o	o	o		o	o	o	o	o	o	o	o	o	o	o	o	o	o	o	o	o	o
^{94g}Tc	7+	293 m		o	o	o		o	o	o	o	o	o	o	o	o	o	o	o	o	o	o	o	o	o
^{94m}Tc	2+	52.0 m	75.70	o	o	o		o	o	o	o	o	o	o	o	o	o	o	o	o	o	o	o	o	o
^{95g}Tc	9/2+	20.0 h		o	o	o	o	o	o	o	o	o	o	o	o	o	o	o	o	o	o	o	o	o	o
^{95m}Tc	1/2-	61 d	38.89	o	o	o	o	o	o	o	o	o	o	o	o	o	o	o	o	o	o	o	o	o	o
^{96g}Tc	7+	4.28 d		o	o	o	o	o	o	o	o	o	o	o	o	o	o	o	o	o	o	o	o	o	o
^{96m}Tc	4+	51.5 m	34.28	o	o	o	o	o	o	o	o	o	o	o	o	o	o	o	o	o	o	o	o	o	o
^{97g}Tc	9/2+	4.21 My		o	o	o	o	o	o	o	o	o	o	o	o	o	o	o	o	o	o	o	o	o	o
^{97m}Tc	1/2-	91.4 d	96.56	o	o	o	o	o	o	o	o	o	o	o	o	o	o	o	o	o	o	o	o	o	o
^{98g}Tc	6+	4.2 My		o	o	o	o	o	o	o	o	o	o	o	o	o	o	o	o	o	o	o	o	o	o
^{98m}Tc	2-	14.7 μs	90.76	o	o	o	o	o	o	o	o	o	o	o	o	o	o	o	o	o	o	o	o	o	o
^{99g}Tc	9/2+	0.2111 My		o	o	o	o	o	o	o	o	o	o	o	o	o	o	o	o	o	o	o	o	o	o

Continued on next page...

Table 6: (continued)

Target	J^π	$t_{1/2}$	Energy	(n,γ)	(n,n')	(n,2n)	(n,3n)	(n,p)	(n,np)	(n,α)	(n,nα)	(n,d)	(n,X)	(p,n)	(p,2n)	(p,p')	(p,pn)	(p,γ)	(p,X)	(d,n)	(d,2n)	(d,3n)	(d,p)	(d,d')	(d,X)
^{99m}Tc	1/2-	6.01 h	142.68	o	o	o	o	o	o	o	o	o	o	o	o	o	o	o	o	o	o	o	o	o	o
^{100g}Tc	1+	15.8 s		o	o	o	o	o	o	o	o	o	o	o	o	o	o	o	o	o	o	o	o	o	o
^{100m1}Tc	4+	8.32 μs	200.67	o	o	o	o	o	o	o	o	o	o	o	o	o	o	o	o	o	o	o	o	o	o
^{100m2}Tc	6+	3.2 μs	243.96	o	o	o	o	o	o	o	o	o	o	o	o	o	o	o	o	o	o	o	o	o	o
^{101g}Tc	9/2+	14.22 m		o	o	o	o	o	o	o	o	o	o	o	o	o	o	o	o	o	o	o	o	o	o
^{101m}Tc	1/2-	636 μs	207.53	o	o	o	o	o	o	o	o	o	o	o	o	o	o	o	o	o	o	o	o	o	o
^{102g}Tc	1+	5.28 s		o	o	o	o	o	o	o	o	o	o	o	o	o	o	o	o	o	o	o	o	o	o
^{102m}Tc	5+	4.35 m	0.0+	o	o	o	o	o	o	o	o	o	o	o	o	o	o	o	o	o	o	o	o	o	o
^{103}Tc	5/2+	54.2 s		o	o	o	o	o	o	o	o	o	o	o	o	o	o	o	o	o	o	o	o	o	o
^{104g}Tc	3+	18.3 m		o	o	o	o	o	o	o	o	o	o	o	o	o	o	o	o	o	o	o	o	o	o
^{104m}Tc	5+	3.5 μs	69.70	o	o	o	o	o	o	o	o	o	o	o	o	o	o	o	o	o	o	o	o	o	o
^{95}Ru	5/2+	1.643 h		o	o	o		o	o	o	o	o	o	o	o	o	o	o	o	o	o		o	o	o
^{96}Ru	0+	**5.54%**		o	o	o	o	o	o	o	o	o	o	o	o	o	o	o	o	o	o	o	o	o	o
^{97}Ru	5/2+	2.791 d		o	o	o	o	o	o	o	o	o	o	o	o	o	o	o	o	o	o	o	o	o	o
^{98}Ru	0+	**1.87%**		o	o	o	o	o	o	o	o	o	o	o	o	o	o	o	o	o	o	o	o	o	o
^{99}Ru	5/2+	**12.76%**		o	o	o	o	o	o	o	o	o	o	o	o	o	o	o	o	o	o	o	o	o	o
^{100}Ru	0+	**12.60%**		o	o	o	o	o	o	o	o	o	o	o	o	o	o	o	o	o	o	o	o	o	o
^{101g}Ru	5/2+	**17.06%**		o	o	o	o	o	o	o	o	o	o	o	o	o	o	o	o	o	o	o	o	o	o
^{101m}Ru	11/2-	17.5 μs	527.50	o	o	o	o	o	o	o	o	o	o	o	o	o	o	o	o	o	o	o	o	o	o
^{102}Ru	0+	**31.55%**		o	o	o	o	o	o	o	o	o	o	o	o	o	o	o	o	o	o	o	o	o	o
^{103g}Ru	3/2+	39.26 d		o	o	o	o	o	o	o	o	o	o	o	o	o	o	o	o	o	o	o	o	o	o
^{103m}Ru	11/2-	1.69 ms	238.20	o	o	o	o	o	o	o	o	o	o	o	o	o	o	o	o	o	o	o	o	o	o
^{104}Ru	0+	**18.62%**		o	o	o	o	o	o	o	o	o	o	o	o	o	o	o	o	o	o	o	o	o	o
^{105}Ru	3/2+	4.44 h		o	o	o	o	o	o	o	o	o	o	o	o	o	o	o	o	o	o	o	o	o	o
^{96g}Rh	6+	9.90 m		o	o	o		o	o	o	o	o	o	o	o	o	o	o	o	o	o		o	o	o
^{96m}Rh	3+	1.51 m	52.00	o	o	o		o	o	o	o	o	o	o	o	o	o	o	o	o	o		o	o	o
^{97g}Rh	9/2+	30.7 m		o	o	o		o	o	o	o	o	o	o	o	o	o	o	o	o	o	o	o	o	o

Continued on next page...

Table 6: (continued)

Target	J^π	$t_{1/2}$	Energy	(n,γ)	(n,n')	(n,2n)	(n,3n)	(n,p)	(n,np)	(n,α)	(n,nα)	(n,d)	(n,X)	(p,n)	(p,2n)	(p,p')	(p,pn)	(p,γ)	(p,X)	(d,n)	(d,2n)	(d,3n)	(d,p)	(d,d')	(d,X)
^{97m}Rh	1/2-	46.2 m	258.85	o	o	o		o	o	o	o	o	o	o	o	o	o	o	o	o	o	o	o	o	o
^{98g}Rh	2+	8.7 m		o	o	o	o	o	o	o	o	o	o	o	o	o	o	o	o	o	o	o	o	o	o
^{98m}Rh	5+	3.5 m	0.0+	o	o	o	o	o	o	o	o	o	o	o	o	o	o	o	o	o	o	o	o	o	o
^{99g}Rh	1/2-	16.1 d		o	o	o	o	o	o	o	o	o	o	o	o	o	o	o	o	o	o	o	o	o	o
^{99m}Rh	9/2+	4.7 h	64.30	o	o	o	o	o	o	o	o	o	o	o	o	o	o	o	o	o	o	o	o	o	o
^{100g}Rh	1-	20.8 h		o	o	o	o	o	o	o	o	o	o	o	o	o	o	o	o	o	o	o	o	o	o
^{100m}Rh	5+	4.6 m	265.00																						
^{101g}Rh	1/2-	3.3 y		o	o	o	o	o	o	o	o	o	o	o	o	o	o	o	o	o	o	o	o	o	o
^{101m}Rh	9/2+	4.34 d	157.32	o	o	o	o	o	o	o	o	o	o	o	o	o	o	o	o	o	o	o	o	o	o
^{102g}Rh	2-	207 d		o	o	o	o	o	o	o	o	o	o	o	o	o	o	o	o	o	o	o	o	o	o
^{102m}Rh	6+	2.9 y	140.75	o	o	o	o	o	o	o	o	o	o	o	o	o	o	o	o	o	o	o	o	o	o
^{103g}Rh	1/2-	**100%**		o	o	o	o	o	o	o	o	o	o	o	o	o	o	o	o	o	o	o	o	o	o
^{103m}Rh	7/2+	56.114 m	39.76	o	o	o	o	o	o	o	o	o	o	o	o	o	o	o	o	o	o	o	o	o	o
^{104g}Rh	1+	42.3 s		o	o	o	o	o	o	o	o	o	o	o	o	o	o	o	o	o	o	o	o	o	o
^{104m}Rh	5+	4.34 m	128.97	o	o	o	o	o	o	o	o	o	o	o	o	o	o	o	o	o	o	o	o	o	o
^{105g}Rh	7/2+	35.36 h		o	o	o	o	o	o	o	o	o	o	o	o	o	o	o	o	o	o	o	o	o	o
^{105m}Rh	1/2-	43.0 s	129.78	o	o	o	o	o	o	o	o	o	o	o	o	o	o	o	o	o	o	o	o	o	o
^{106g}Rh	1+	29.80 s		o	o	o	o	o	o	o	o	o	o	o	o	o	o	o	o	o	o	o	o	o	o
^{106m}Rh	6+	131 m	137.00	o	o	o	o	o	o	o	o	o	o	o	o	o	o	o	o	o	o	o	o	o	o

B. Model Input Parameters

B.1. Binding and Separation Energies

Here we present the binding energies for each of the compound nuclei included in this study. We also provide separation energies for neutrons, protons, α-particles, and deuterons. These quantities were calculated from our adopted mass excesses, as described in section 3.1.1. All quantities are given in MeV. For isomeric states, each of these quantities should be reduced by the isomer energy.

Table 7: Binding and Separation Energies

^{A}Z	Binding Energy	S_n	S_p	S_α	S_d
^{75}Se	650.91803	8.02771	8.59808	4.68622	14.34802
^{76}Se	662.07239	11.15436	9.50854	5.09100	17.52783
^{77}Se	669.49121	7.41882	9.59900	5.72693	14.70276
^{78}Se	679.98895	10.49774	10.39838	6.02856	17.87213
^{79}Se	686.95190	6.96295	10.38928	6.48615	15.13672
^{80}Se	696.86548	9.91357	11.41235	6.97174	18.07825
^{81}Se	703.56635	6.70087	11.51917	7.60028	15.88861
^{82}Se	712.84216	9.27582	12.34955	8.15668	18.57037
^{83}Se	718.66016	5.81799	12.30554	8.27698	15.94293
^{84}Se	727.34271	8.68256	13.36029	8.86163	18.76349
^{85}Se	731.89038	4.54767	13.63519	8.54980	15.68335
^{86}Se	738.07410	6.18372	14.50659	7.34155	17.59430
^{87}Se	742.18665	4.11255	14.72083	8.10583	16.39453
^{76}Br	656.32709	9.22137	5.40906	4.48425	11.21216
^{77}Br	667.34418	11.01709	5.27179	4.70312	14.20154
^{78}Br	675.63281	8.28864	6.14160	5.01721	11.33582
^{79}Br	686.32037	10.68756	6.33142	5.46088	14.60455
^{80}Br	694.21271	7.89233	7.26080	6.02484	11.99915
^{81}Br	704.36938	10.15668	7.50391	6.48315	15.19287
^{82}Br	711.96222	7.59283	8.39587	7.10394	12.87213
^{83}Br	721.54608	9.58386	8.70392	7.79730	15.75513
^{84}Br	728.40778	6.86169	9.74762	8.06494	13.34100
^{85}Br	737.29010	8.88232	9.94739	8.50183	16.40533
^{86}Br	742.39069	5.10059	10.50031	7.74042	12.82336
^{87}Br	748.67932	6.28864	10.60522	6.40125	14.56433
^{88}Br	753.62592	4.94659	11.43927	7.07507	13.32721
^{89}Br	759.53668	5.91077	11.98236	7.67352	15.12543
^{90}Br	763.65631	4.11963	12.71289	7.89484	13.87738
^{77}Kr	663.49640	9.22650	7.16931	4.37677	14.16608
^{78}Kr	675.57800	12.08160	8.23383	4.39203	17.02631
^{79}Kr	683.91229	8.33429	8.27948	4.69861	14.34351
^{80}Kr	695.43341	11.52112	9.11304	5.06537	17.57599
^{81}Kr	703.30621	7.87280	9.09351	5.51935	14.76123
^{82}Kr	714.27301	10.96680	9.90363	5.98840	17.83569
^{83}Kr	721.73657	7.46356	9.77435	6.48901	15.14258
^{84}Kr	732.25720	10.52063	10.71112	7.09607	18.07037

Continued on next page...

Table 7: (continued)

^{A}Z	Binding Energy	S_n	S_p	S_α	S_d
^{85}Kr	739.37769	7.12048	10.96991	7.51569	15.60699
^{86}Kr	749.23438	9.85669	11.94427	8.09656	18.60199
^{87}Kr	754.74951	5.51514	12.35883	7.79370	15.23480
^{88}Kr	761.80359	7.05408	13.12427	6.16522	17.18829
^{89}Kr	766.90942	5.10583	13.28351	6.72339	16.00549
^{90}Kr	773.22388	6.31445	13.68719	6.85413	17.37335
^{91}Kr	777.63568	4.41180	13.97937	7.15338	15.87439
^{77}Rb	657.36908	12.41595	3.09918	3.62042	13.63660
^{78}Rb	667.55212	10.18304	4.05573	4.05511	11.05762
^{79}Rb	679.49060	11.93848	3.91260	4.08923	13.76959
^{80}Rb	688.93140	9.44080	5.01910	4.30865	11.12878
^{81}Rb	700.28473	11.35333	4.85132	4.64490	14.14783
^{82}Rb	709.08942	8.80469	5.78320	5.16095	11.43140
^{83}Rb	720.04730	10.95789	5.77429	5.43127	14.51648
^{84}Rb	728.79382	8.74652	7.05725	6.28546	12.29620
^{85}Rb	739.28247	10.48865	7.02527	6.61743	15.32129
^{86}Rb	747.93347	8.65100	8.55579	7.67560	13.45166
^{87}Rb	757.85559	9.92212	8.62122	8.01385	16.25330
^{88}Rb	763.93811	6.08252	9.18860	7.23468	12.47913
^{89}Rb	771.11292	7.17480	9.30933	5.52716	14.13879
^{90}Rb	776.83337	5.72046	9.92395	6.14703	12.80518
^{91}Rb	783.28839	6.45502	10.06451	6.31342	14.15436
^{92}Rb	788.38641	5.09802	10.75073	6.46484	12.93793
^{93}Rb	794.30322	5.91681	11.12152	6.47089	14.44293
^{94}Rb	798.31030	4.00708	11.82483	6.35834	12.90399
^{95}Rb	803.68219	5.37189	11.99988	6.77057	14.97211
^{78}Sr	663.00751	13.44122	5.63843	3.26733	15.82977
^{79}Sr	673.38147	10.37396	5.82935	3.57794	13.78778
^{80}Sr	686.28442	12.90295	6.79382	3.71887	16.50769
^{81}Sr	695.57520	9.29077	6.64380	3.78314	13.85999
^{82}Sr	708.12720	12.55200	7.84247	4.25354	16.97119
^{83}Sr	716.98560	8.85840	7.89618	4.77765	14.47626
^{84}Sr	728.90527	11.91968	8.85797	5.17621	17.59125
^{85}Sr	737.43542	8.53015	8.64160	5.83356	15.16351
^{86}Sr	748.92767	11.49225	9.64520	6.35901	17.90924
^{87}Sr	757.35577	8.42810	9.42230	7.32355	15.84869
^{88}Sr	768.46851	11.11273	10.61292	7.91565	18.31042
^{89}Sr	774.82721	6.35870	10.88910	7.15387	14.74701
^{90}Sr	782.63098	7.80377	11.51807	5.10095	16.46826
^{91}Sr	788.40601	5.77502	11.57263	5.36084	15.06848
^{92}Sr	795.69971	7.29370	12.41132	5.60046	16.64172
^{93}Sr	800.98792	5.28821	12.60150	5.78284	15.47491
^{94}Sr	807.81512	6.82721	13.51190	6.29559	17.20410

Continued on next page...

Table 7: (continued)

^{A}Z	Binding Energy	S_n	S_p	S_α	S_d
^{95}Sr	812.16272	4.34760	13.85242	6.23138	15.63489
^{96}Sr	818.05621	5.89349	14.37402	6.57886	17.52130
^{97}Sr	821.97668	3.92047	14.85236	7.19556	16.06989
^{98}Sr	827.90558	5.92889	15.57837	7.92761	18.55664
^{80}Y	676.41162	10.93250	3.03015	3.16284	11.17950
^{81}Y	689.28247	12.87085	2.99805	3.61774	13.67639
^{82}Y	699.52887	10.24640	3.95367	3.68109	11.01984
^{83}Y	711.73438	12.20551	3.60718	3.94812	13.93457
^{84}Y	721.63702	9.90265	4.65143	4.40997	11.28522
^{85}Y	733.39258	11.75555	4.48730	4.81219	14.18237
^{86}Y	742.90527	9.51270	5.46985	5.52020	11.77539
^{87}Y	754.71179	11.80652	5.78412	6.36884	15.05176
^{88}Y	764.06348	9.35168	6.70770	6.97400	12.91119
^{89}Y	775.53748	11.47400	7.06897	7.95935	15.95709
^{90}Y	782.39447	6.85699	7.56726	6.16534	11.70135
^{91}Y	790.32343	7.92896	7.69244	4.17218	13.27161
^{92}Y	796.86298	6.53955	8.45697	4.62921	12.00739
^{93}Y	804.34412	7.48114	8.64441	4.93555	13.71350
^{94}Y	810.54077	6.19666	9.55286	5.41174	12.61646
^{95}Y	817.47070	6.92993	9.65558	5.88666	14.25818
^{96}Y	822.68158	5.21088	10.51886	5.99951	12.64185
^{97}Y	828.66388	5.98230	10.60767	6.06500	14.27655
^{98}Y	832.94501	4.28113	10.96832	6.33905	12.66418
^{99}Y	838.74982	5.80481	10.84424	6.77197	14.54852
^{100}Y	843.91449	5.16467	12.39752	8.49451	13.78430
^{101}Y	849.60370	5.68921	11.98187	8.98083	15.86212
^{81}Zr	680.97131	11.04272	4.55969	3.10938	13.26758
^{82}Zr	694.74615	13.77484	5.46368	3.44299	16.10992
^{83}Zr	705.08398	10.33783	5.55511	3.40686	13.57690
^{84}Zr	718.18884	13.10486	6.45447	3.60876	16.43536
^{85}Zr	727.91718	9.72833	6.28015	4.04633	13.95819
^{86}Zr	740.64380	12.72662	7.25122	4.22095	16.78217
^{87}Zr	750.25891	9.61511	7.35364	4.97766	14.64172
^{88}Zr	762.60510	12.34619	7.89331	5.40417	17.47522
^{89}Zr	771.92218	9.31708	7.85870	6.19110	14.98578
^{90}Zr	783.89197	11.96979	8.35449	6.66864	17.60388
^{91}Zr	791.08643	7.19446	8.69196	5.43500	13.32434
^{92}Zr	799.72119	8.63477	9.39777	2.95703	15.10211
^{93}Zr	806.45569	6.73450	9.59271	3.33282	13.90765
^{94}Zr	814.67682	8.22113	10.33270	3.75018	15.58923
^{95}Zr	821.13898	6.46216	10.59821	4.43732	14.57025
^{96}Zr	828.99542	7.85645	11.52472	5.00006	16.23004
^{97}Zr	834.57050	5.57507	11.88892	5.28693	14.87518

Continued on next page...

Table 7: (continued)

^{A}Z	Binding Energy	S_n	S_p	S_α	S_d
^{98}Zr	840.98212	6.41162	12.31824	4.87134	16.07593
^{99}Zr	845.53497	4.55286	12.58997	5.07660	14.64648
^{100}Zr	852.44220	6.90723	13.69238	6.09033	17.27258
^{101}Zr	857.36639	4.92419	13.45190	7.09406	16.39197
^{102}Zr	863.72290	6.35651	14.11920	7.52167	17.58380
^{103}Zr	868.42383	4.70093	13.76855	8.61121	16.59552
^{104}Zr	874.46411	6.04028	14.69403	8.54663	17.58423
^{83}Nb	696.80170	14.05591	2.05554	3.02692	13.60577
^{84}Nb	707.79340	10.99170	2.70941	3.08612	10.82263
^{85}Nb	721.13489	13.34149	2.94604	3.55676	13.82629
^{86}Nb	731.88342	10.74854	3.96625	4.05890	11.46997
^{87}Nb	744.31152	12.42810	3.66772	4.28149	14.16974
^{88}Nb	754.27283	9.96130	4.01392	4.34015	11.40442
^{89}Nb	766.92139	12.64856	4.31628	5.23315	14.43787
^{90}Nb	776.99860	10.07721	5.07642	5.79767	12.16888
^{91}Nb	789.04608	12.04749	5.15411	6.03864	14.89929
^{92}Nb	796.93329	7.88721	5.84686	4.57416	10.81671
^{93}Nb	805.76459	8.83130	6.04340	1.93146	12.45355
^{94}Nb	812.99213	7.22754	6.53644	2.30200	11.04633
^{95}Nb	821.48077	8.48865	6.80396	2.86169	12.80048
^{96}Nb	828.37390	6.89313	7.23492	3.21527	11.47247
^{97}Nb	836.44720	8.07330	7.45178	3.80743	13.08362
^{98}Nb	842.44135	5.99414	7.87085	3.60492	11.22131
^{99}Nb	849.31110	6.86975	8.32898	3.54474	12.51599
^{100}Nb	854.99481	5.68372	9.45984	4.01758	11.78809
^{101}Nb	862.06897	7.07416	9.62677	5.10944	14.30939
^{102}Nb	867.54553	5.47656	10.17914	6.30487	12.87872
^{103}Nb	874.58649	7.04095	10.86359	7.54102	14.99548
^{104}Nb	879.56439	4.97791	11.14056	7.35425	13.61688
^{105}Nb	886.26471	6.70032	11.80060	8.36536	15.61627
^{84}Mo	700.93811	16.12933	4.13641	2.71387	15.96771
^{85}Mo	712.30640	11.36829	4.51300	3.03943	13.28009
^{86}Mo	725.83112	13.52472	4.69623	2.78931	15.81311
^{87}Mo	737.04102	11.20990	5.15759	3.66138	13.68152
^{88}Mo	750.11737	13.07635	5.80585	3.63287	16.00934
^{89}Mo	760.49261	10.37524	6.21979	4.27979	13.95648
^{90}Mo	773.72729	13.23468	6.80591	4.78784	17.22986
^{91}Mo	783.83551	10.10822	6.83691	5.28094	14.68951
^{92}Mo	796.50763	12.67212	7.46155	5.60687	17.28442
^{93}Mo	804.57739	8.06976	7.64410	4.35956	13.30670
^{94}Mo	814.25500	9.67761	8.49042	2.06738	15.09711
^{95}Mo	821.62408	7.36908	8.63196	2.24200	13.63489
^{96}Mo	830.77838	9.15430	9.29761	2.76154	15.56165

Continued on next page...

Table 7: (continued)

^{A}Z	Binding Energy	S_n	S_p	S_α	S_d
^{97}Mo	837.59961	6.82123	9.22571	2.84827	13.89423
^{98}Mo	846.24219	8.64258	9.79498	3.26971	15.64368
^{99}Mo	852.16772	5.92554	9.72638	2.73309	13.49591
^{100}Mo	860.45752	8.28979	11.14642	3.16644	15.79156
^{101}Mo	865.85571	5.39819	10.86090	2.98956	14.32001
^{102}Mo	873.97333	8.11761	11.90436	4.69556	16.75391
^{103}Mo	879.33411	5.36078	11.78857	5.50348	15.04053
^{104}Mo	886.88708	7.55298	12.30060	6.14923	17.11694
^{105}Mo	891.96741	5.08032	12.40302	6.30536	15.15631
^{106}Mo	898.95612	6.98871	12.69141	6.93756	17.16711
^{107}Mo	903.71521	4.75909	13.13574	6.99573	15.22589
^{87}Tc	727.68573	13.98633	1.85461	2.58838	13.15472
^{88}Tc	739.34497	11.65924	2.30396	3.25592	11.28925
^{89}Tc	752.55029	13.20532	2.43292	3.11975	13.28467
^{90}Tc	763.98419	11.43390	3.49158	3.80511	11.64221
^{91}Tc	776.83313	12.84894	3.10583	4.22595	14.11591
^{92}Tc	787.85492	11.02179	4.01941	5.28644	11.90302
^{93}Tc	800.59412	12.73920	4.08649	5.37708	14.53400
^{94}Tc	809.21692	8.62280	4.63953	3.92267	10.48468
^{95}Tc	819.15112	9.93420	4.89612	1.80939	12.34912
^{96}Tc	827.02283	7.87170	5.39874	1.79388	10.54321
^{97}Tc	836.49701	9.47418	5.71863	2.43677	12.64832
^{98}Tc	843.77588	7.27887	6.17627	2.48810	10.77289
^{99}Tc	852.74261	8.96674	6.50043	2.96619	12.91840
^{100}Tc	859.50702	6.76440	7.33929	2.83746	11.04022
^{101}Tc	867.89801	8.39099	7.44049	3.15515	13.50568
^{102}Tc	874.19910	6.30109	8.34338	3.46210	11.51697
^{103}Tc	882.30182	8.10272	8.32849	4.69507	14.22150
^{104}Tc	888.26221	5.96039	8.92810	4.97174	12.06427
^{105}Tc	896.13501	7.87280	9.24792	5.77039	14.57629
^{106}Tc	901.69379	5.55878	9.72638	5.85260	12.58209
^{107}Tc	909.09290	7.39911	10.13678	6.21075	14.90088
^{108}Tc	914.01422	4.92133	10.29901	6.15417	12.83350
^{88}Ru	731.49969	16.37939	3.81396	2.26593	15.57568
^{89}Ru	743.43701	11.93732	4.09204	2.83496	13.52667
^{90}Ru	757.30231	13.86530	4.75201	3.17554	15.73273
^{91}Ru	768.72461	11.42230	4.74042	3.38794	13.94971
^{92}Ru	782.54590	13.82129	5.71277	4.13287	16.33710
^{93}Ru	793.47479	10.92889	5.61987	4.68652	14.41705
^{94}Ru	806.84851	13.37372	6.25439	4.82556	16.76898
^{95}Ru	815.80170	8.95319	6.58478	3.67053	12.98297
^{96}Ru	826.49530	10.69360	7.34418	1.69202	15.05377
^{97}Ru	834.60681	8.11151	7.58398	1.73376	13.23108

Continued on next page...

Table 7: (continued)

^{A}Z	Binding Energy	S_n	S_p	S_α	S_d
^{98}Ru	844.79028	10.18347	8.29327	2.23962	15.54285
^{99}Ru	852.25409	7.46381	8.47821	2.33435	13.53247
^{100}Ru	861.92743	9.67334	9.18481	2.85339	15.92694
^{101}Ru	868.72949	6.80206	9.22247	2.83423	13.76227
^{102}Ru	877.94910	9.21960	10.05109	3.41125	16.21747
^{103}Ru	884.18121	6.23212	9.98212	3.71783	14.05859
^{104}Ru	893.08258	8.90137	10.78076	4.32941	16.65887
^{105}Ru	898.99268	5.91010	10.73047	4.84131	14.46625
^{106}Ru	907.45837	8.46570	11.32336	5.18939	16.97156
^{107}Ru	913.13049	5.67212	11.43671	5.50073	14.77087
^{108}Ru	920.95190	7.82141	11.85901	5.76917	17.03351
^{109}Ru	926.20099	5.24908	12.18677	5.93793	14.88348
^{91}Rh	758.38733	13.95844	1.08502	2.40594	12.72571
^{92}Rh	770.71558	12.32825	1.99097	3.07495	11.18866
^{93}Rh	784.59991	13.88434	2.05402	3.75397	13.65070
^{94}Rh	796.43616	11.83624	2.96136	4.15631	11.66565
^{95}Rh	809.90942	13.47327	3.06091	4.78064	14.21002
^{96}Rh	819.32031	9.41089	3.51862	3.16974	10.24719
^{97}Rh	830.30139	10.98108	3.80609	1.41162	12.27509
^{98}Rh	838.95831	8.65692	4.35150	1.44574	10.23840
^{99}Rh	849.42920	10.47089	4.63892	1.98242	12.59778
^{100}Rh	857.51031	8.08112	5.25623	2.19183	10.49542
^{101}Rh	867.40552	9.89520	5.47809	2.61285	12.92682
^{102}Rh	874.84381	7.43829	6.11432	2.77228	10.69177
^{103}Rh	884.16229	9.31848	6.21320	3.12402	13.20819
^{104}Rh	891.16119	6.99890	6.97998	3.35852	10.98749
^{105}Rh	900.12830	8.96710	7.04572	3.93463	13.72247
^{106}Rh	906.71552	6.58722	7.72284	4.22076	11.40833
^{107}Rh	915.28857	8.57306	7.83020	4.69110	14.07129
^{108}Rh	921.51599	6.22742	8.38550	4.95813	11.83301
^{109}Rh	929.57861	8.06262	8.62671	5.14795	14.22351
^{110}Rh	935.41522	5.83661	9.21423	5.42578	12.23871
^{94}Pd	789.06592	14.72229	4.46600	3.46796	16.12573
^{95}Pd	800.93817	11.87225	4.50201	3.91791	14.11365
^{96}Pd	815.08789	14.14972	5.17847	4.24634	16.42712
^{97}Pd	824.72913	9.64124	5.40881	2.95868	12.59509
^{98}Pd	836.30109	11.57196	5.99969	1.15692	14.75616
^{99}Pd	845.26019	8.95911	6.30188	1.16284	12.73419
^{100}Pd	856.37000	11.10980	6.94080	1.57904	15.18707
^{101}Pd	864.64313	8.27313	7.13281	1.74066	12.98932
^{102}Pd	875.21149	10.56836	7.80597	2.12555	15.47656
^{103}Pd	882.83679	7.62531	7.99298	2.28705	13.20667
^{104}Pd	892.81909	9.98230	8.65680	2.59601	15.75067

Continued on next page...

Table 7: (continued)

^{A}Z	Binding Energy	S_n	S_p	S_α	S_d
^{105}Pd	899.91321	7.09412	8.75201	2.88806	13.52631
^{106}Pd	909.47412	9.56091	9.34583	3.22937	16.08832
^{107}Pd	916.01062	6.53650	9.29510	3.53375	13.65771
^{108}Pd	925.23859	9.22797	9.95001	3.86035	16.29846
^{109}Pd	931.39221	6.15363	9.87622	4.10388	13.87903
^{97}Ag	816.96667	14.31946	1.87878	4.07111	13.80389
^{98}Ag	827.27942	10.31274	2.55029	2.54761	9.96692
^{99}Ag	839.04779	11.76837	2.74670	0.84271	12.09406
^{100}Ag	848.50983	9.46204	3.24963	0.89386	9.98413
^{101}Ag	859.65692	11.14709	3.28693	1.05988	12.17212
^{102}Ag	868.76898	9.11206	4.12585	1.51501	10.17438
^{103}Ag	879.36670	10.59772	4.15521	1.64185	12.49896
^{104}Ag	887.75812	8.39142	4.92133	1.95215	10.32202
^{105}Ag	897.78601	10.02789	4.96692	2.08484	12.72461
^{106}Ag	905.72668	7.94067	5.81348	2.58722	10.68298
^{107}Ag	915.26239	9.53571	5.78827	2.80444	13.12457
^{108}Ag	922.53381	7.27142	6.52319	3.07697	10.83508
^{109}Ag	931.72589	9.19208	6.48730	3.30194	13.49066
^{110}Ag	938.53510	6.80920	7.14288	3.52393	11.07190

B.2. Q-Values for Reactions Studied

Here we present the Q-values (in MeV) for each of the reactions included in this study. The values provided in this table are for reactions proceeding from the ground state of the target to the ground state of the residual. The Q-value for reactions proceeding from/to other states can be obtained by adding the energy of the target state to the given Q-value and subtracting the energy of the residual state. The values are calculated from our adopted mass excesses, as described in section 3.1.1. Separate tables are provided for neutron-induced (Table 8) and charged-particle (Table 9) reactions. Inelastic scattering reactions such as (n,n') have thresholds equal to the energy of the first excited state and are not listed in the tables.

Table 8: Neutron-induced reaction Q-values

Target	$Q_{(n,\gamma)}$	$Q_{(n,2n)}$	$Q_{(n,3n)}$	$Q_{(n,p)}$	$Q_{(n,np)}$	$Q_{(n,\alpha)}$	$Q_{(n,n\alpha)}$	$Q_{(n,d)}$
^{83}Sr	11.920	-8.858	-21.410	3.062	-7.896	6.743	-4.778	-5.672
^{84}Sr	8.530	-11.920	-20.778	-0.111	-8.858	2.697	-5.176	-6.633
^{85}Sr	11.492	-8.530	-20.450	1.847	-8.642	5.133	-5.834	-6.417
^{86}Sr	8.428	-11.492	-20.022	-0.994	-9.645	1.105	-6.359	-7.421
^{87}Sr	11.113	-8.428	-19.920	0.500	-9.422	3.197	-7.324	-7.198
^{88}Sr	6.359	-11.113	-19.541	-4.530	-10.613	-0.795	-7.916	-8.388
^{89}Sr	7.804	-6.359	-17.471	-3.714	-10.889	2.703	-7.154	-8.664
^{90}Sr	5.775	-7.804	-14.162	-5.798	-11.518	0.414	-5.101	-9.293
^{91}Sr	7.294	-5.775	-13.579	-5.118	-11.573	1.693	-5.361	-9.348
^{92}Sr	5.288	-7.294	-13.069	-7.313	-12.411	-0.495	-5.600	-10.187
^{84}Y	11.756	-9.903	-22.108	7.268	-4.651	6.943	-4.410	-2.427
^{85}Y	9.513	-11.756	-21.658	4.043	-4.487	3.992	-4.812	-2.263
^{86}Y	11.807	-9.513	-21.268	6.022	-5.470	5.438	-5.520	-3.245
^{87}Y	9.352	-11.807	-21.319	2.644	-5.784	2.378	-6.369	-3.560
^{88}Y	11.474	-9.352	-21.158	4.405	-6.708	3.515	-6.974	-4.483
^{89}Y	6.857	-11.474	-20.826	-0.710	-7.069	0.692	-7.959	-4.844
^{90}Y	7.929	-6.857	-18.331	0.237	-7.567	3.757	-6.165	-5.343
^{91}Y	6.540	-7.929	-14.786	-1.917	-7.692	1.910	-4.172	-5.468
^{92}Y	7.481	-6.540	-14.469	-1.163	-8.457	2.546	-4.629	-6.232
^{93}Y	6.197	-7.481	-14.021	-3.356	-8.644	0.785	-4.936	-6.420
^{86}Zr	9.615	-12.727	-22.455	2.261	-7.251	4.637	-4.221	-5.027
^{87}Zr	12.346	-9.615	-22.342	4.453	-7.354	6.942	-4.978	-5.129
^{88}Zr	9.317	-12.346	-21.961	1.458	-7.893	3.126	-5.404	-5.669
^{89}Zr	11.970	-9.317	-21.663	3.615	-7.859	5.301	-6.191	-5.634
^{90}Zr	7.194	-11.970	-21.287	-1.497	-8.354	1.759	-6.669	-6.130
^{91}Zr	8.635	-7.194	-19.164	-0.763	-8.692	5.678	-5.435	-6.467
^{92}Zr	6.734	-8.635	-15.829	-2.858	-9.398	3.402	-2.957	-7.173
^{93}Zr	8.221	-6.734	-15.369	-2.112	-9.593	4.471	-3.333	-7.368
^{94}Zr	6.462	-8.221	-14.956	-4.136	-10.333	2.025	-3.750	-8.108
^{95}Zr	7.856	-6.462	-14.683	-3.668	-10.598	2.856	-4.437	-8.374
^{96}Zr	5.575	-7.856	-14.319	-6.314	-11.525	0.288	-5.000	-9.300
^{87}Nb	9.961	-12.428	-23.177	5.947	-3.668	5.621	-4.281	-1.443

Continued on next page...

Table 8: (continued)

Target	$Q_{(n,\gamma)}$	$Q_{(n,2n)}$	$Q_{(n,3n)}$	$Q_{(n,p)}$	$Q_{(n,np)}$	$Q_{(n,\alpha)}$	$Q_{(n,n\alpha)}$	$Q_{(n,d)}$
^{88}Nb	12.649	-9.961	-22.389	8.332	-4.014	7.415	-4.340	-1.789
^{89}Nb	10.077	-12.649	-22.610	5.001	-4.316	4.280	-5.233	-2.092
^{90}Nb	12.047	-10.077	-22.726	6.893	-5.076	6.009	-5.798	-2.852
^{91}Nb	7.887	-12.047	-22.125	2.040	-5.154	3.313	-6.039	-2.930
^{92}Nb	8.831	-7.887	-19.935	2.788	-5.847	6.900	-4.574	-3.622
^{93}Nb	7.228	-8.831	-16.719	0.691	-6.043	4.926	-1.931	-3.819
^{94}Nb	8.489	-7.228	-16.059	1.685	-6.536	5.627	-2.302	-4.312
^{95}Nb	6.893	-8.489	-15.716	-0.342	-6.804	3.678	-2.862	-4.579
^{96}Nb	8.073	-6.893	-15.382	0.622	-7.235	4.266	-3.215	-5.010
^{97}Nb	5.994	-8.073	-14.966	-1.877	-7.452	2.389	-3.807	-5.227
^{98}Nb	6.870	-5.994	-14.067	-1.459	-7.871	3.325	-3.605	-5.646
^{99}Nb	5.684	-6.870	-12.864	-3.776	-8.329	1.666	-3.545	-6.104
^{100}Nb	7.074	-5.684	-12.553	-2.553	-9.460	1.965	-4.018	-7.235
^{90}Mo	10.108	-13.235	-23.610	3.271	-6.806	4.827	-4.788	-4.581
^{91}Mo	12.672	-10.108	-23.343	5.211	-6.837	7.065	-5.281	-4.612
^{92}Mo	8.070	-12.672	-22.780	0.426	-7.462	3.710	-5.607	-5.237
^{93}Mo	9.678	-8.070	-20.742	1.187	-7.644	7.610	-4.360	-5.419
^{94}Mo	7.369	-9.678	-17.747	-1.263	-8.490	5.127	-2.067	-6.266
^{95}Mo	9.154	-7.369	-17.047	-0.143	-8.632	6.393	-2.242	-6.407
^{96}Mo	6.821	-9.154	-16.523	-2.404	-9.298	3.973	-2.762	-7.073
^{97}Mo	8.643	-6.821	-15.976	-1.152	-9.226	5.373	-2.848	-7.001
^{98}Mo	5.926	-8.643	-15.464	-3.801	-9.795	3.192	-3.270	-7.570
^{99}Mo	8.290	-5.926	-14.568	-2.857	-9.726	5.123	-2.733	-7.502
^{100}Mo	5.398	-8.290	-14.215	-5.463	-11.146	2.409	-3.166	-8.922
^{101}Mo	8.118	-5.398	-13.688	-3.787	-10.861	3.422	-2.990	-8.636
^{91}Tc	11.022	-12.849	-24.283	7.002	-3.106	5.735	-4.226	-0.881
^{92}Tc	12.739	-11.022	-23.871	8.653	-4.019	7.362	-5.286	-1.795
^{93}Tc	8.623	-12.739	-23.761	3.983	-4.086	4.700	-5.377	-1.862
^{94}Tc	9.934	-8.623	-21.362	5.038	-4.640	8.125	-3.923	-2.415
^{95}Tc	7.872	-9.934	-18.557	2.473	-4.896	6.078	-1.809	-2.672
^{96}Tc	9.474	-7.872	-17.806	3.756	-5.399	7.037	-1.794	-3.174
^{97}Tc	7.279	-9.474	-17.346	1.103	-5.719	4.791	-2.437	-3.494
^{98}Tc	8.967	-7.279	-16.753	2.466	-6.176	6.001	-2.488	-3.952
^{99}Tc	6.764	-8.967	-16.246	-0.575	-6.500	3.927	-2.966	-4.276
^{100}Tc	8.391	-6.764	-15.731	0.951	-7.339	5.236	-2.837	-5.115
^{101}Tc	6.301	-8.391	-15.155	-2.042	-7.440	2.839	-3.155	-5.216
^{102}Tc	8.103	-6.301	-14.692	-0.226	-8.343	3.408	-3.462	-6.119
^{103}Tc	5.960	-8.103	-14.404	-2.968	-8.328	0.989	-4.695	-6.104
^{104}Tc	7.873	-5.960	-14.063	-1.375	-8.928	2.102	-4.972	-6.703
^{95}Ru	10.694	-8.953	-22.327	3.349	-6.585	9.002	-3.671	-4.360
^{96}Ru	8.112	-10.694	-19.647	0.528	-7.344	6.378	-1.692	-5.120

Continued on next page...

Table 8: (continued)

Target	$Q_{(n,\gamma)}$	$Q_{(n,2n)}$	$Q_{(n,3n)}$	$Q_{(n,p)}$	$Q_{(n,np)}$	$Q_{(n,\alpha)}$	$Q_{(n,n\alpha)}$	$Q_{(n,d)}$
^{97}Ru	10.183	-8.112	-18.805	1.890	-7.584	7.944	-1.734	-5.359
^{98}Ru	7.464	-10.183	-18.295	-1.014	-8.293	5.129	-2.240	-6.069
^{99}Ru	9.673	-7.464	-17.647	0.489	-8.478	6.820	-2.334	-6.254
^{100}Ru	6.802	-9.673	-17.137	-2.420	-9.185	3.968	-2.853	-6.960
^{101}Ru	9.220	-6.802	-16.475	-0.831	-9.222	5.808	-2.834	-6.998
^{102}Ru	6.232	-9.220	-16.022	-3.750	-10.051	2.514	-3.411	-7.826
^{103}Ru	8.901	-6.232	-15.452	-1.879	-9.982	4.572	-3.718	-7.758
^{104}Ru	5.910	-8.901	-15.133	-4.820	-10.781	1.069	-4.329	-8.556
^{105}Ru	8.466	-5.910	-14.811	-2.858	-10.730	3.276	-4.841	-8.506
^{96}Rh	10.981	-9.411	-22.884	7.175	-3.519	9.569	-3.170	-1.294
^{97}Rh	8.657	-10.981	-20.392	4.305	-3.806	7.211	-1.412	-1.581
^{98}Rh	10.471	-8.657	-19.638	5.832	-4.352	8.488	-1.446	-2.127
^{99}Rh	8.081	-10.471	-19.128	2.825	-4.639	5.889	-1.982	-2.414
^{100}Rh	9.895	-8.081	-18.552	4.417	-5.256	7.282	-2.192	-3.032
^{101}Rh	7.438	-9.895	-17.976	1.324	-5.478	4.666	-2.613	-3.253
^{102}Rh	9.318	-7.438	-17.333	3.105	-6.114	6.194	-2.772	-3.890
^{103}Rh	6.999	-9.318	-16.757	0.019	-6.213	3.640	-3.124	-3.989
^{104}Rh	8.967	-6.999	-16.317	1.921	-6.980	5.032	-3.359	-4.755
^{105}Rh	6.587	-8.967	-15.966	-1.136	-7.046	2.366	-3.935	-4.821
^{106}Rh	8.573	-6.587	-15.554	0.743	-7.723	3.882	-4.221	-5.498

Table 9: Charged-particle reaction Q-values

Target	$Q_{(p,\gamma)}$	$Q_{(p,n)}$	$Q_{(p,2n)}$	$Q_{(p,np)}$	$Q_{(d,n)}$	$Q_{(d,2n)}$	$Q_{(d,3n)}$	$Q_{(d,p)}$
^{83}Sr	4.651	-5.251	-17.457	-8.858	2.427	-7.476	-19.681	9.695
^{84}Sr	4.487	-7.268	-17.171	-11.920	2.263	-9.493	-19.395	6.306
^{85}Sr	5.470	-4.043	-15.798	-8.530	3.245	-6.267	-18.023	9.268
^{86}Sr	5.784	-6.022	-15.535	-11.492	3.560	-8.247	-17.760	6.204
^{87}Sr	6.708	-2.644	-14.451	-8.428	4.483	-4.869	-16.675	8.888
^{88}Sr	7.069	-4.405	-13.757	-11.113	4.844	-6.630	-15.981	4.134
^{89}Sr	7.567	0.710	-10.764	-6.359	5.343	-1.514	-12.988	5.579
^{90}Sr	7.692	-0.237	-7.094	-7.804	5.468	-2.461	-9.318	3.550
^{91}Sr	8.457	1.917	-6.012	-5.775	6.232	-0.307	-8.236	5.069
^{92}Sr	8.644	1.163	-5.376	-7.294	6.420	-1.061	-7.601	3.064
^{84}Y	6.280	-3.448	-16.553	-9.903	4.056	-5.673	-18.778	9.531
^{85}Y	7.251	-5.475	-15.204	-11.756	5.027	-7.700	-17.428	7.288
^{86}Y	7.354	-2.261	-14.988	-9.513	5.129	-4.486	-17.213	9.582
^{87}Y	7.893	-4.453	-14.068	-11.807	5.669	-6.677	-16.293	7.127
^{88}Y	7.859	-1.458	-13.805	-9.352	5.634	-3.683	-16.029	9.249
^{89}Y	8.354	-3.615	-12.932	-11.474	6.130	-5.840	-15.157	4.632
^{90}Y	8.692	1.497	-10.472	-6.857	6.467	-0.727	-12.697	5.704
^{91}Y	9.398	0.763	-6.431	-7.929	7.173	-1.462	-8.656	4.315
^{92}Y	9.593	2.858	-5.777	-6.540	7.368	0.634	-8.001	5.257
^{93}Y	10.333	2.112	-4.623	-7.481	8.108	-0.113	-6.848	3.972
^{86}Zr	3.668	-8.760	-19.509	-12.727	1.443	-10.985	-21.734	7.391
^{87}Zr	4.014	-5.947	-18.375	-9.615	1.789	-8.172	-20.600	10.122
^{88}Zr	4.316	-8.332	-18.294	-12.346	2.092	-10.557	-20.518	7.092
^{89}Zr	5.076	-5.001	-17.649	-9.317	2.852	-7.225	-19.874	9.745
^{90}Zr	5.154	-6.893	-16.971	-11.970	2.930	-9.118	-19.195	4.970
^{91}Zr	5.847	-2.040	-14.088	-7.194	3.622	-4.265	-16.312	6.410
^{92}Zr	6.043	-2.788	-10.675	-8.635	3.819	-5.013	-12.900	4.510
^{93}Zr	6.536	-0.691	-9.522	-6.734	4.312	-2.916	-11.747	5.997
^{94}Zr	6.804	-1.685	-8.912	-8.221	4.579	-3.909	-11.137	4.238
^{95}Zr	7.235	0.342	-8.147	-6.462	5.010	-1.883	-10.371	5.632
^{96}Zr	7.452	-0.622	-7.515	-7.856	5.227	-2.846	-9.739	3.350
^{87}Nb	5.806	-7.271	-18.480	-12.428	3.581	-9.495	-20.705	7.737
^{88}Nb	6.220	-4.155	-17.232	-9.961	3.995	-6.380	-19.456	10.424
^{89}Nb	6.806	-6.429	-16.804	-12.649	4.581	-8.653	-19.029	7.853
^{90}Nb	6.837	-3.271	-16.506	-10.077	4.612	-5.496	-18.731	9.823
^{91}Nb	7.462	-5.211	-15.319	-12.047	5.237	-7.435	-17.543	5.663
^{92}Nb	7.644	-0.426	-13.098	-7.887	5.420	-2.650	-15.322	6.607
^{93}Nb	8.490	-1.187	-9.257	-8.831	6.266	-3.412	-11.482	5.003
^{94}Nb	8.632	1.263	-8.415	-7.228	6.407	-0.962	-10.639	6.264
^{95}Nb	9.298	0.143	-7.226	-8.489	7.073	-2.081	-9.450	4.669
^{96}Nb	9.226	2.404	-6.750	-6.893	7.001	0.180	-8.974	5.849

Continued on next page...

Table 9: (continued)

Target	$Q_{(p,\gamma)}$	$Q_{(p,n)}$	$Q_{(p,2n)}$	$Q_{(p,np)}$	$Q_{(d,n)}$	$Q_{(d,2n)}$	$Q_{(d,3n)}$	$Q_{(d,p)}$
^{97}Nb	9.795	1.152	-5.669	-8.073	7.570	-1.072	-7.893	3.770
^{98}Nb	9.726	3.801	-4.842	-5.994	7.502	1.576	-7.066	4.645
^{99}Nb	11.146	2.857	-3.069	-6.870	8.922	0.632	-5.294	3.459
^{100}Nb	10.861	5.463	-2.827	-5.684	8.636	3.238	-5.052	4.850
^{90}Mo	3.106	-9.743	-21.177	-13.235	0.881	-11.968	-23.402	7.884
^{91}Mo	4.019	-7.002	-19.851	-10.108	1.795	-9.227	-22.076	10.448
^{92}Mo	4.086	-8.653	-19.674	-12.672	1.862	-10.877	-21.899	5.845
^{93}Mo	4.640	-3.983	-16.722	-8.070	2.415	-6.208	-18.947	7.453
^{94}Mo	4.896	-5.038	-13.661	-9.678	2.672	-7.263	-15.885	5.144
^{95}Mo	5.399	-2.473	-12.407	-7.369	3.174	-4.698	-14.632	6.930
^{96}Mo	5.719	-3.756	-11.627	-9.154	3.494	-5.980	-13.852	4.597
^{97}Mo	6.176	-1.103	-10.577	-6.821	3.952	-3.327	-12.801	6.418
^{98}Mo	6.500	-2.466	-9.745	-8.643	4.276	-4.691	-11.970	3.701
^{99}Mo	7.339	0.575	-8.392	-5.926	5.115	-1.650	-10.616	6.065
^{100}Mo	7.440	-0.951	-7.715	-8.290	5.216	-3.175	-9.940	3.174
^{101}Mo	8.343	2.042	-6.349	-5.398	6.119	-0.182	-8.573	5.893
^{91}Tc	5.713	-8.109	-19.531	-12.849	3.488	-10.333	-21.755	8.797
^{92}Tc	5.620	-5.309	-19.130	-11.022	3.395	-7.534	-21.355	10.515
^{93}Tc	6.254	-7.119	-18.048	-12.739	4.030	-9.344	-20.273	6.398
^{94}Tc	6.585	-2.368	-15.742	-8.623	4.360	-4.593	-17.967	7.710
^{95}Tc	7.344	-3.349	-12.303	-9.934	5.120	-5.574	-14.527	5.647
^{96}Tc	7.584	-0.528	-11.221	-7.872	5.359	-2.752	-13.446	7.250
^{97}Tc	8.293	-1.890	-10.002	-9.474	6.069	-4.115	-12.226	5.054
^{98}Tc	8.478	1.014	-9.169	-7.279	6.254	-1.210	-11.394	6.742
^{99}Tc	9.185	-0.489	-7.952	-8.967	6.960	-2.713	-10.177	4.540
^{100}Tc	9.222	2.420	-7.253	-6.764	6.998	0.196	-9.478	6.166
^{101}Tc	10.051	0.831	-5.971	-8.391	7.826	-1.393	-8.195	4.076
^{102}Tc	9.982	3.750	-5.470	-6.301	7.758	1.525	-7.694	5.878
^{103}Tc	10.781	1.879	-4.353	-8.103	8.556	-0.345	-6.577	3.736
^{104}Tc	10.730	4.820	-4.081	-5.960	8.506	2.596	-6.306	5.648
^{95}Ru	3.519	-5.892	-19.366	-8.953	1.294	-8.117	-21.590	8.469
^{96}Ru	3.806	-7.175	-16.586	-10.694	1.581	-9.400	-18.810	5.887
^{97}Ru	4.352	-4.305	-15.286	-8.112	2.127	-6.530	-17.511	7.959
^{98}Ru	4.639	-5.832	-14.489	-10.183	2.414	-8.057	-16.713	5.239
^{99}Ru	5.256	-2.825	-13.296	-7.464	3.032	-5.049	-15.520	7.449
^{100}Ru	5.478	-4.417	-12.498	-9.673	3.253	-6.642	-14.723	4.577
^{101}Ru	6.114	-1.324	-11.219	-6.802	3.890	-3.549	-13.444	6.995
^{102}Ru	6.213	-3.105	-10.544	-9.220	3.989	-5.330	-12.768	4.008
^{103}Ru	6.980	-0.019	-9.337	-6.232	4.755	-2.244	-11.562	6.677
^{104}Ru	7.046	-1.921	-8.920	-8.901	4.821	-4.146	-11.145	3.685
^{105}Ru	7.723	1.136	-7.831	-5.910	5.498	-1.089	-10.056	6.241

Continued on next page...

Table 9: (continued)

Target	$Q_{(p,\gamma)}$	$Q_{(p,n)}$	$Q_{(p,2n)}$	$Q_{(p,np)}$	$Q_{(d,n)}$	$Q_{(d,2n)}$	$Q_{(d,3n)}$	$Q_{(d,p)}$
^{96}Rh	5.409	-4.232	-18.382	-9.411	3.184	-6.457	-20.607	8.756
^{97}Rh	6.000	-5.572	-15.214	-10.981	3.775	-7.797	-17.438	6.432
^{98}Rh	6.302	-2.657	-14.229	-8.657	4.077	-4.882	-16.454	8.246
^{99}Rh	6.941	-4.169	-13.128	-10.471	4.716	-6.394	-15.353	5.857
^{100}Rh	7.133	-1.140	-12.250	-8.081	4.908	-3.365	-14.475	7.671
^{101}Rh	7.806	-2.762	-11.036	-9.895	5.581	-4.987	-13.260	5.214
^{102}Rh	7.993	0.368	-10.201	-7.438	5.768	-1.857	-12.425	7.094
^{103}Rh	8.657	-1.326	-8.951	-9.318	6.432	-3.550	-11.175	4.774
^{104}Rh	8.752	1.658	-8.324	-6.999	6.527	-0.567	-10.549	6.743
^{105}Rh	9.346	-0.215	-7.309	-8.967	7.121	-2.440	-9.534	4.363
^{106}Rh	9.295	2.759	-6.802	-6.587	7.071	0.534	-9.027	6.348

B.3. Modified Discrete Level Schemes

As stated in section 3.1.2, most of our discrete level schemes are taken directly from (Belgya *et al.* 2005). For a few of the isotopes we have made significant modifications, such as changes in the spin and parity assignments, adjustments to the branching ratios, and the addition or removal of levels. The following figures present our modified level schemes, up to 25 levels. The modified level data for bromine, krypton, and rubidium isotopes may be found in (Hoffman *et al.* 2004a).

In these plots, the level energy is listed on the right hand side, and the spin and parity of the level on the left. The γ-ray transitions are indicated by arrows. Each arrow is labeled with the transition energy, followed by the branching ratio (as a percent) in parenthesis. Isomeric states are indicated by thick black lines.

We have made minor changes to a few additional nuclei not included in this appendix. See section 3.1.2 for details.

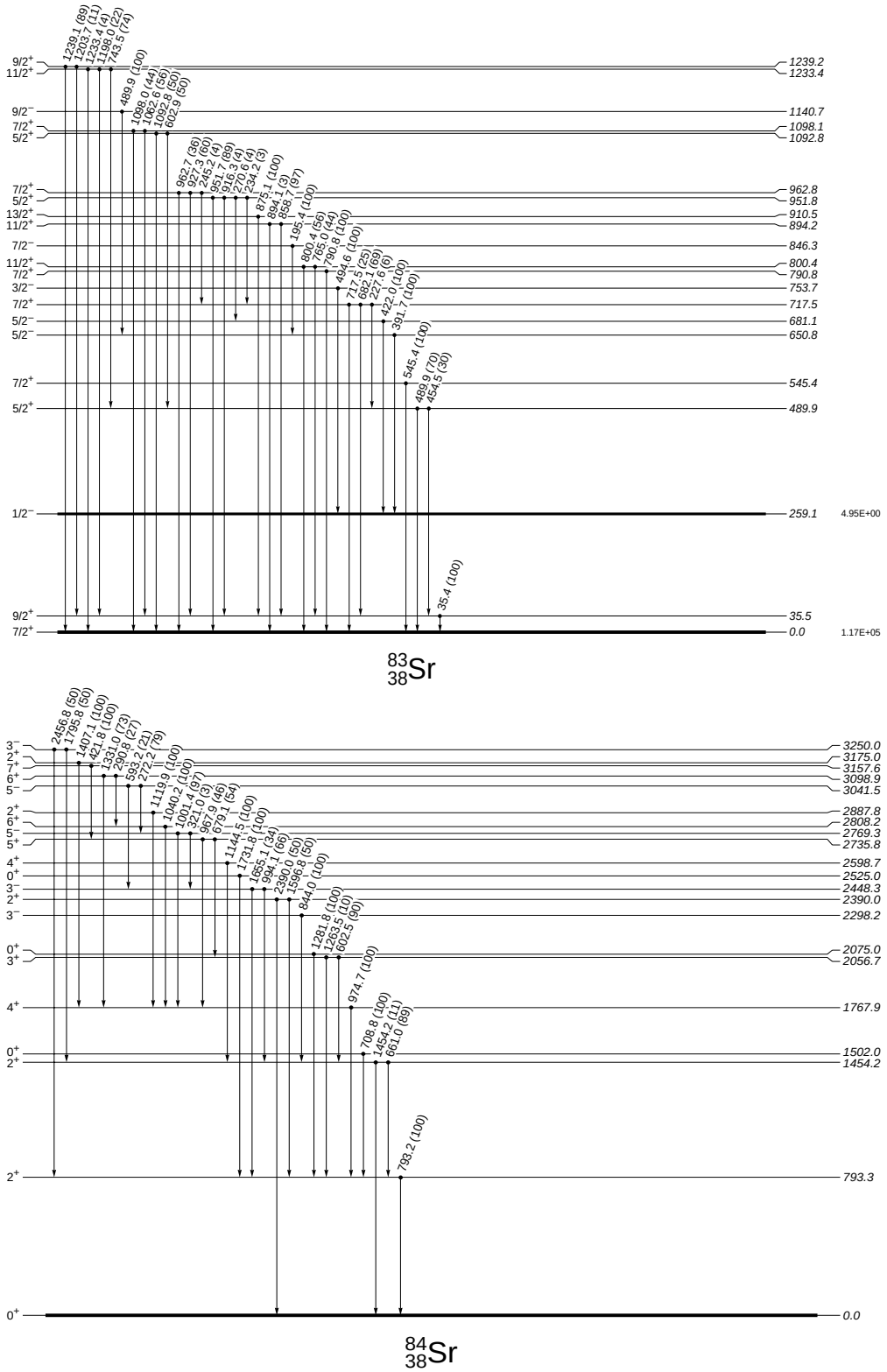

Fig. 24.— Adopted level schemes for select nuclei.

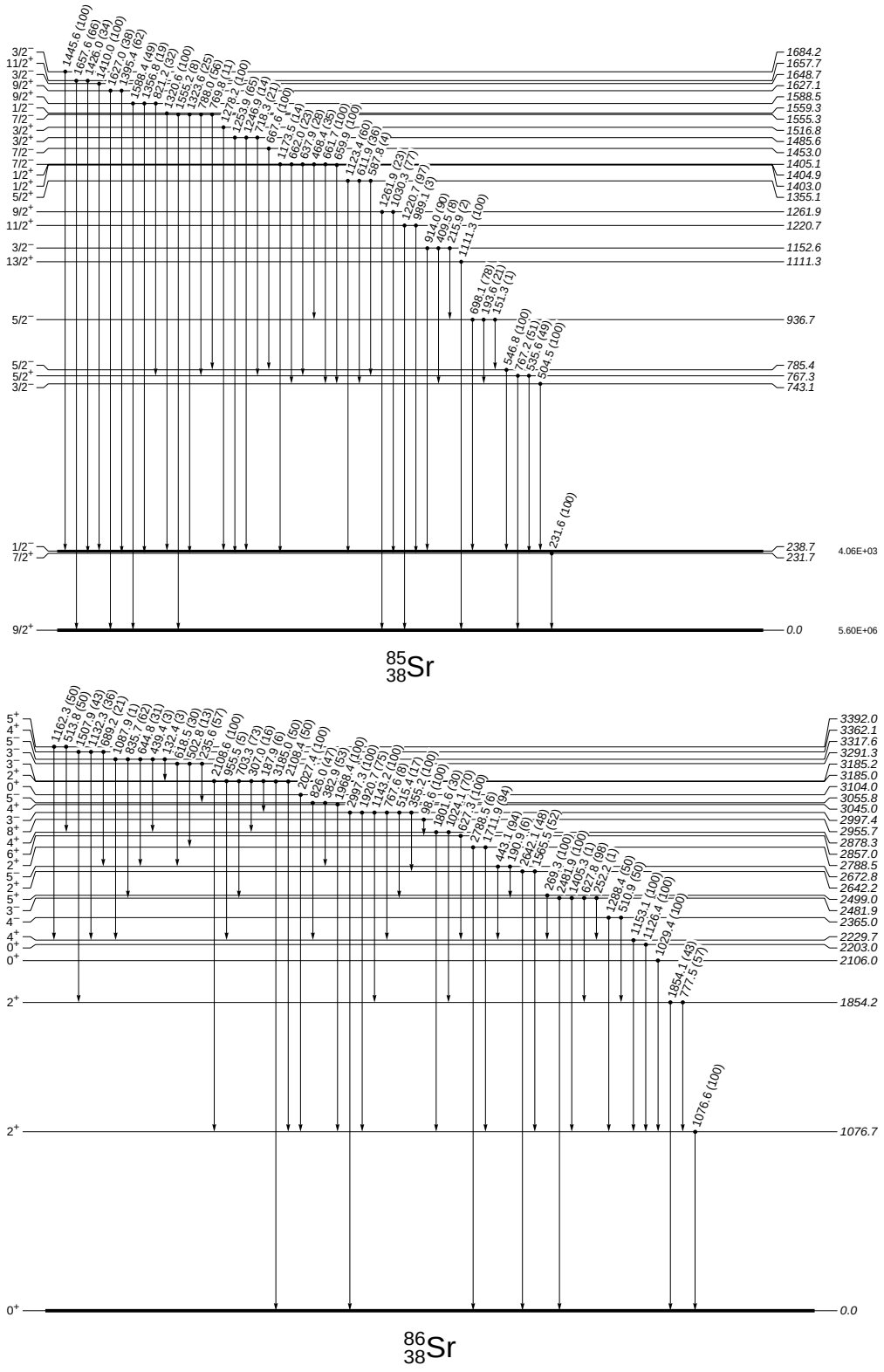

Fig. 24.— (continued)

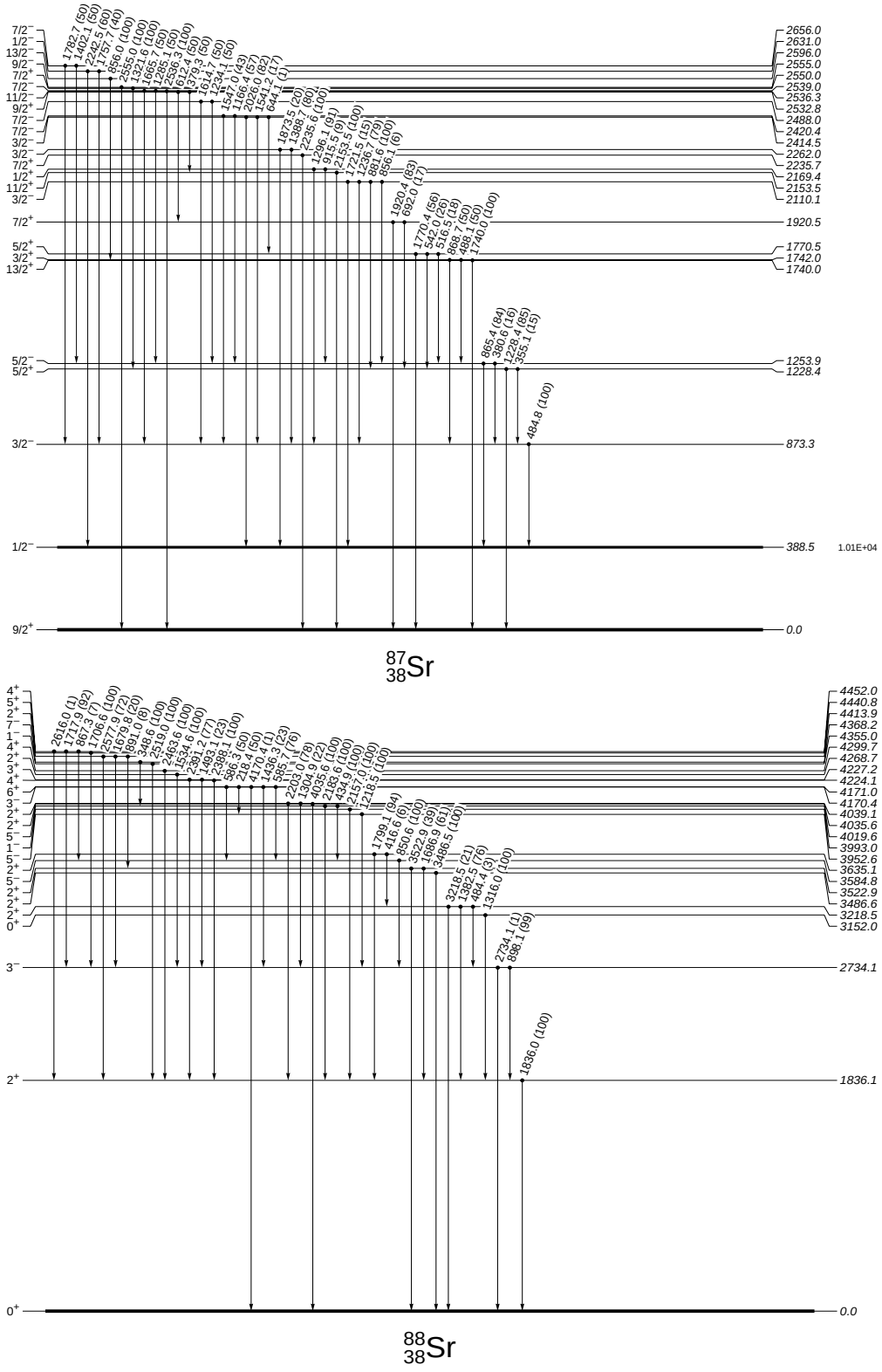

Fig. 24.— (continued)

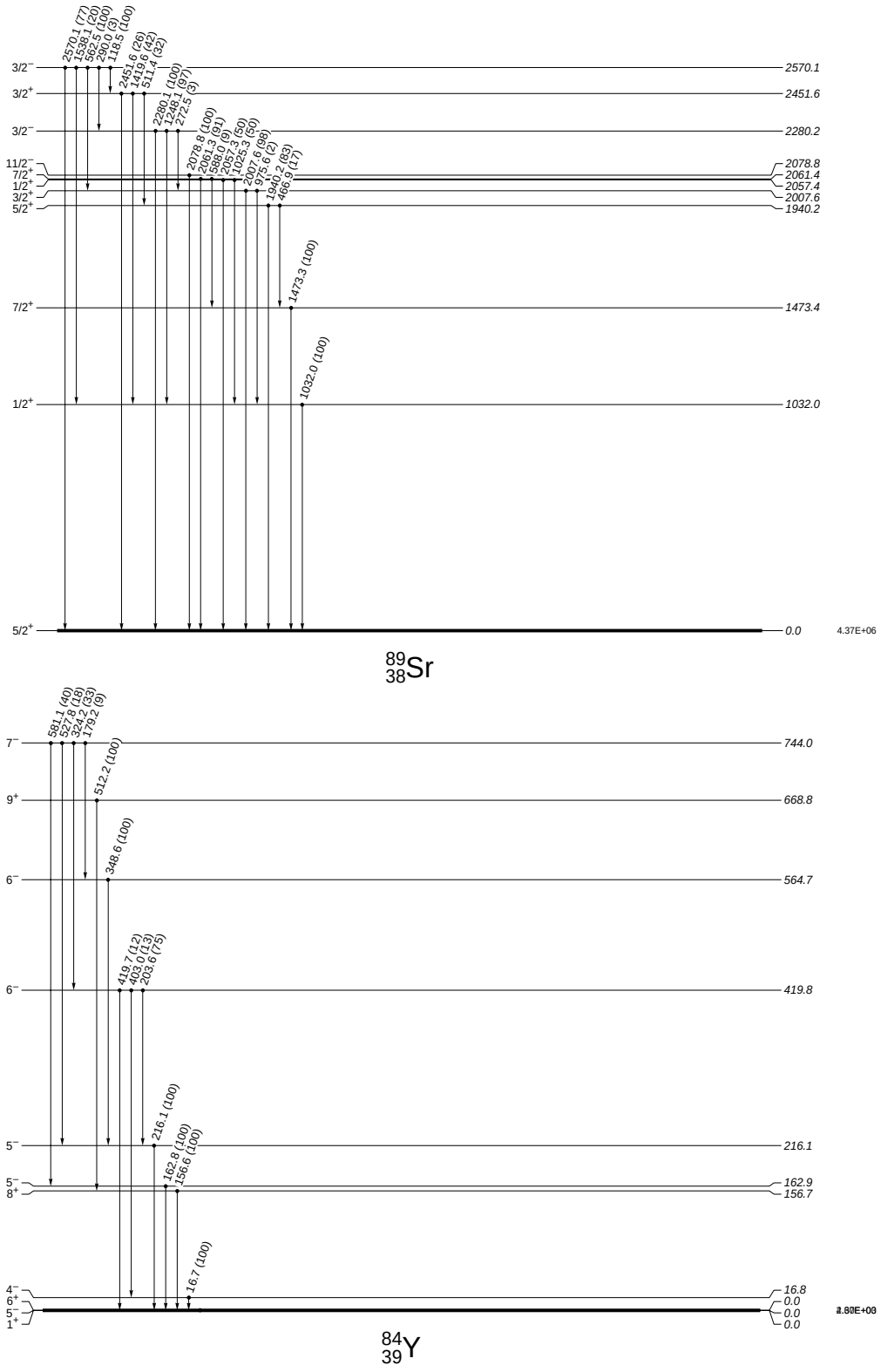

Fig. 24.— (continued)

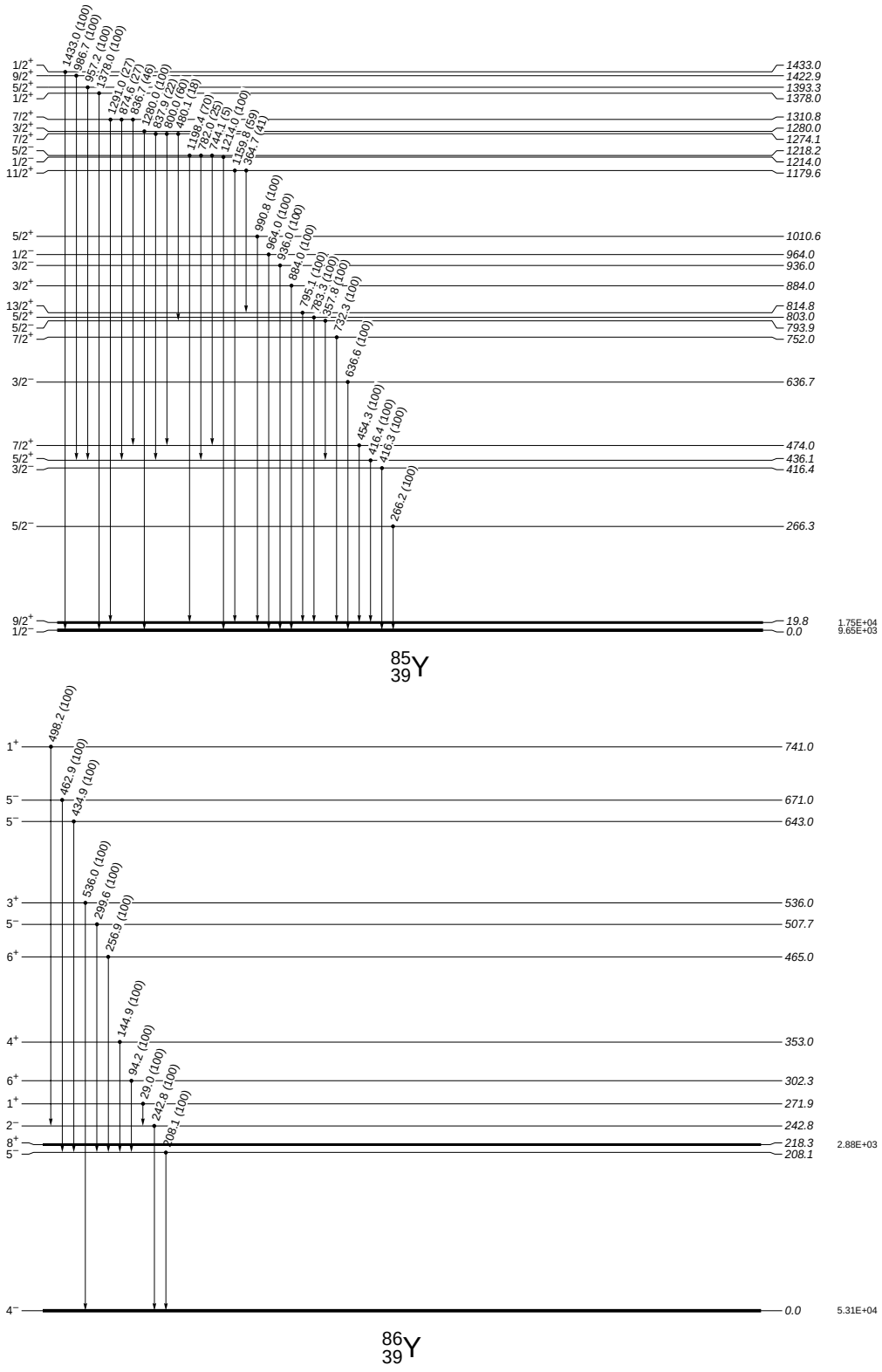

Fig. 24.— (continued)

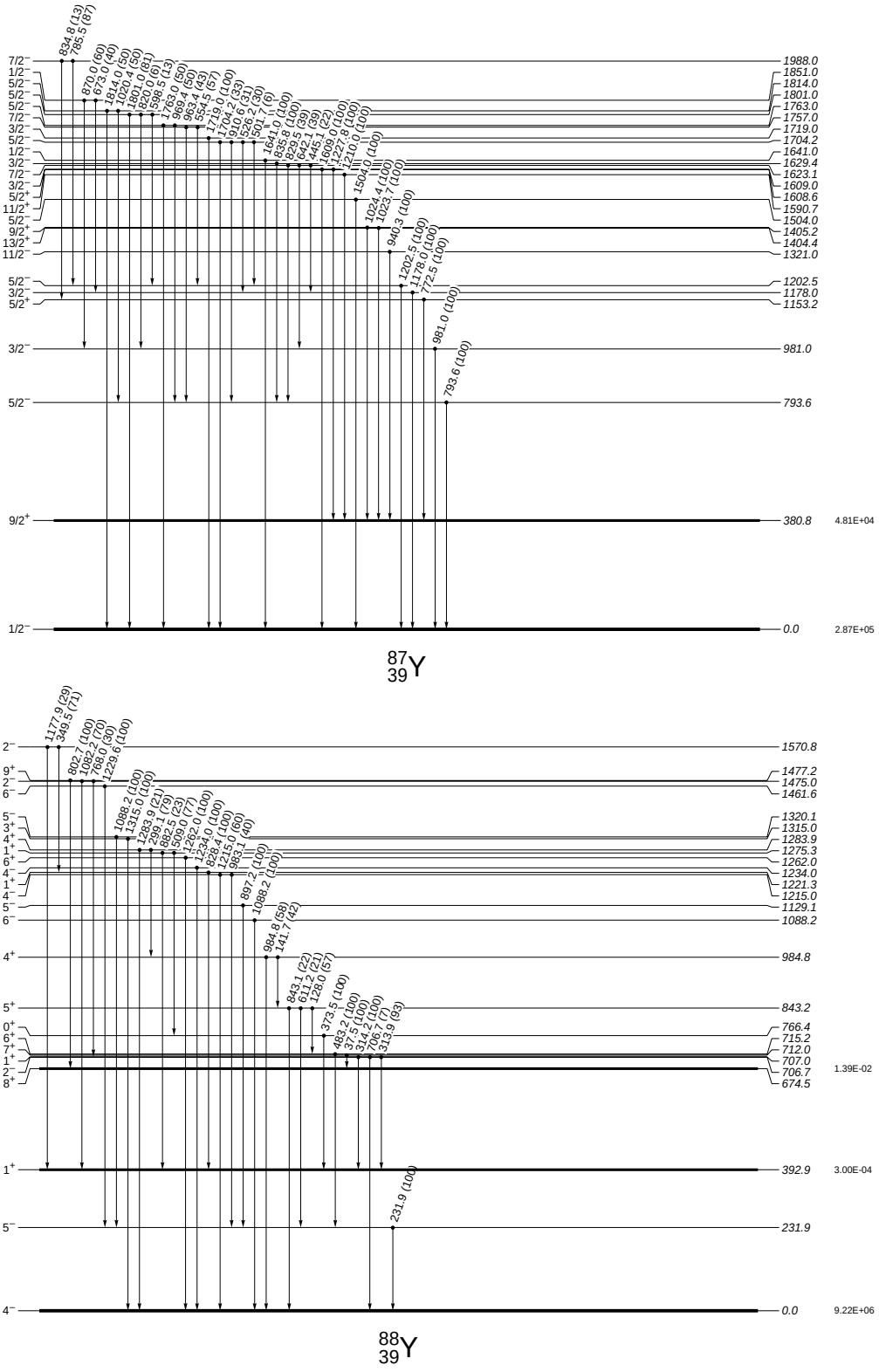

Fig. 24.— (continued)

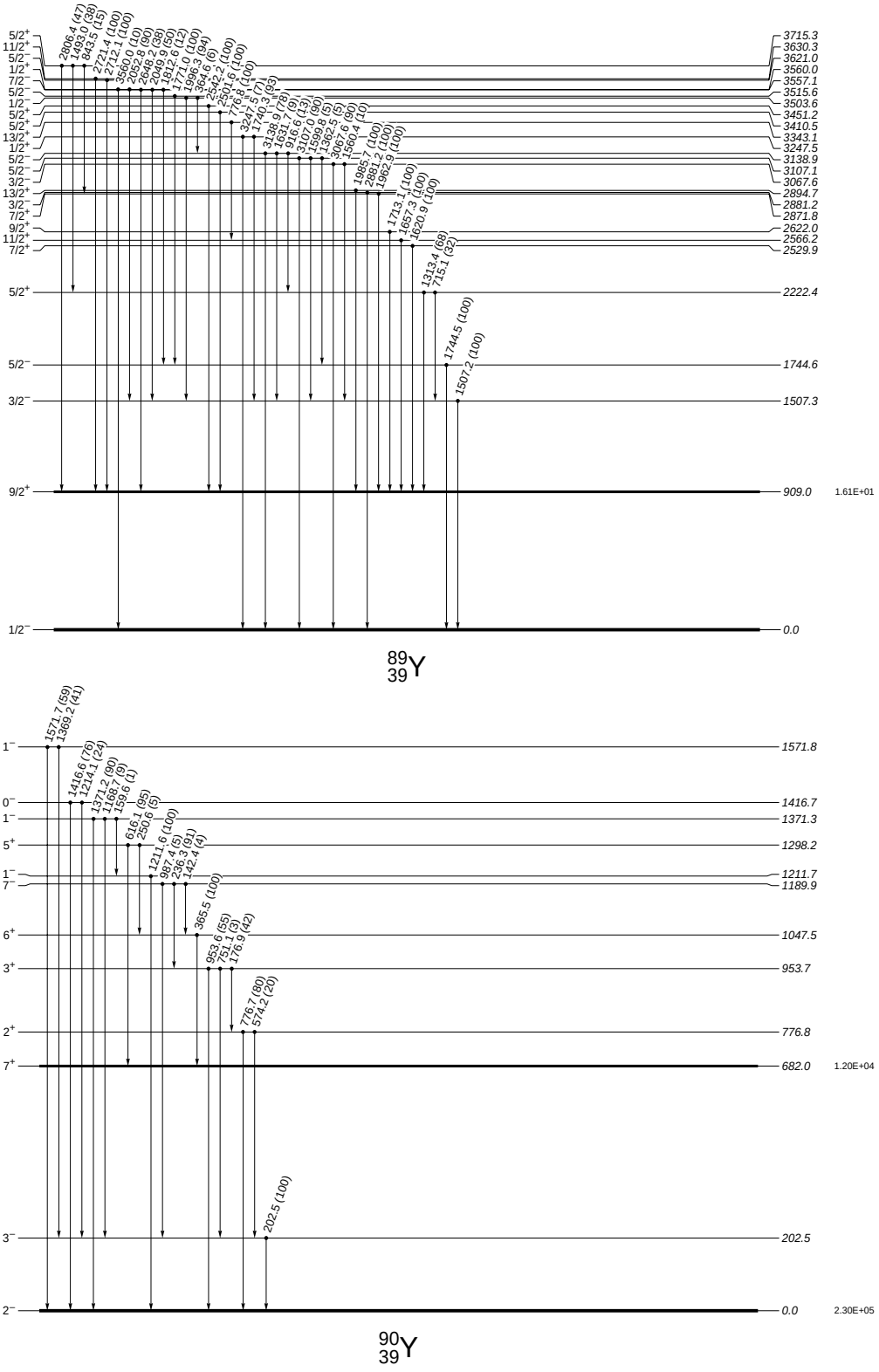

Fig. 24.— (continued)

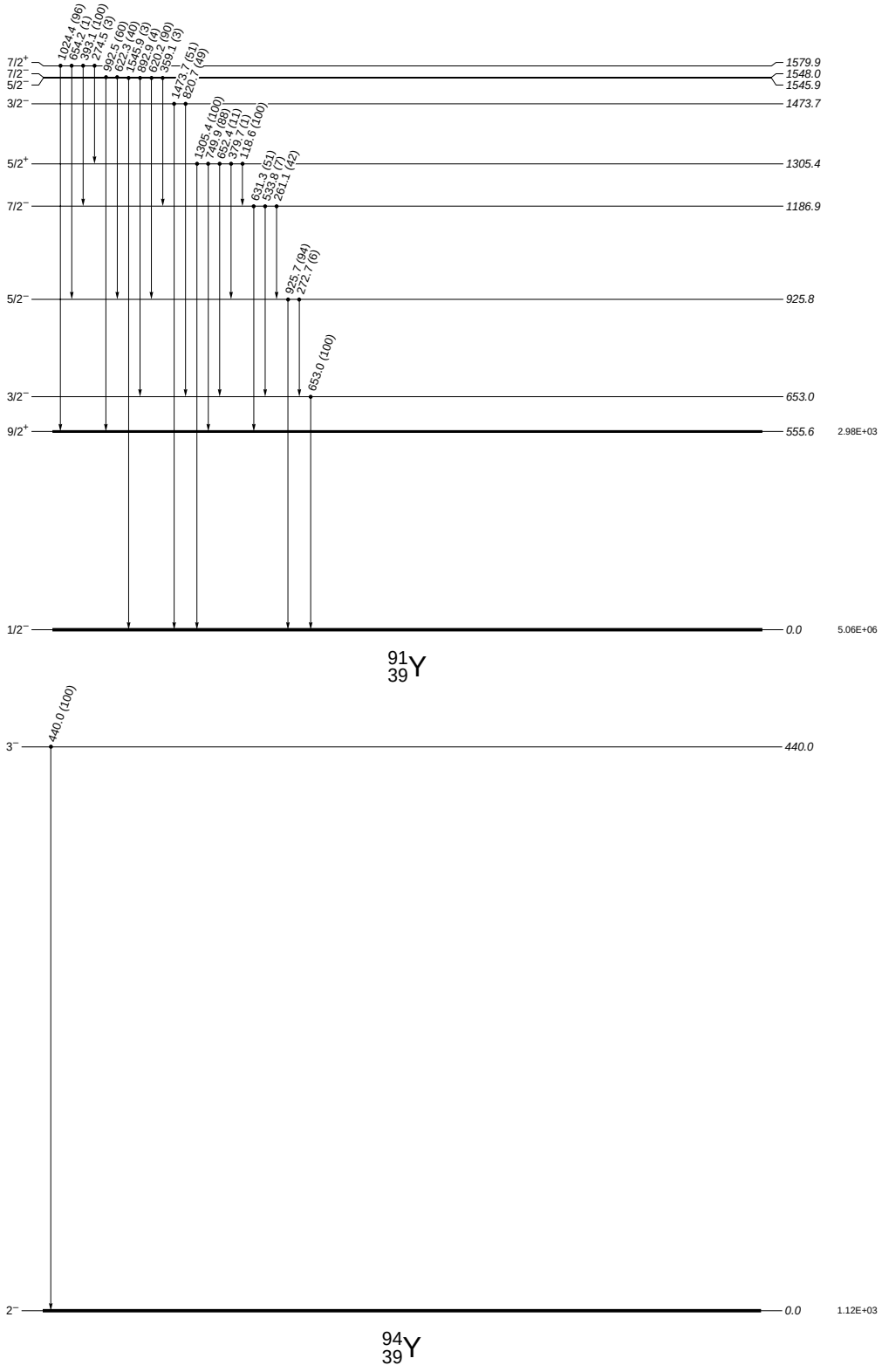

Fig. 24.— (continued)

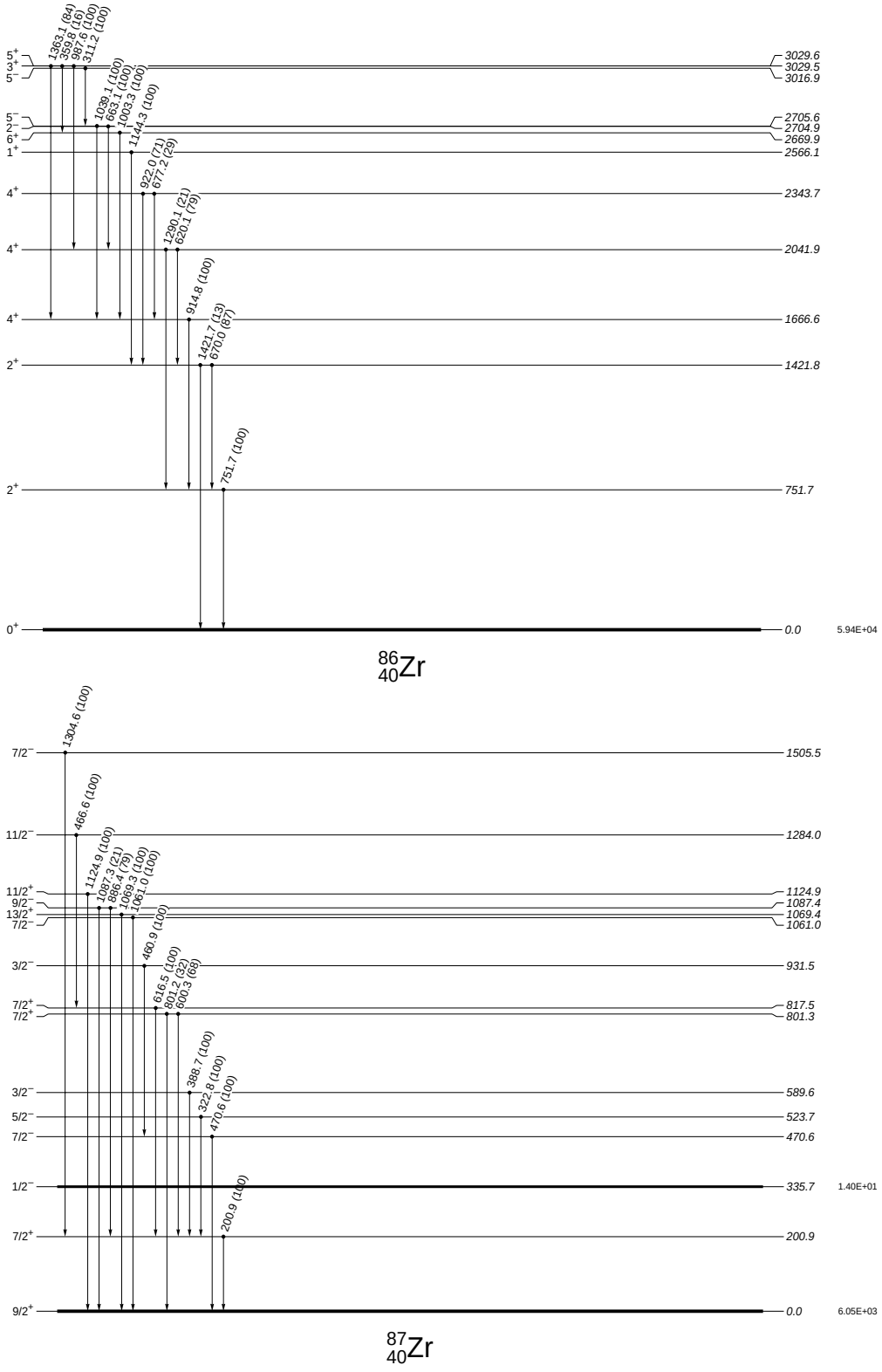

Fig. 24.— (continued)

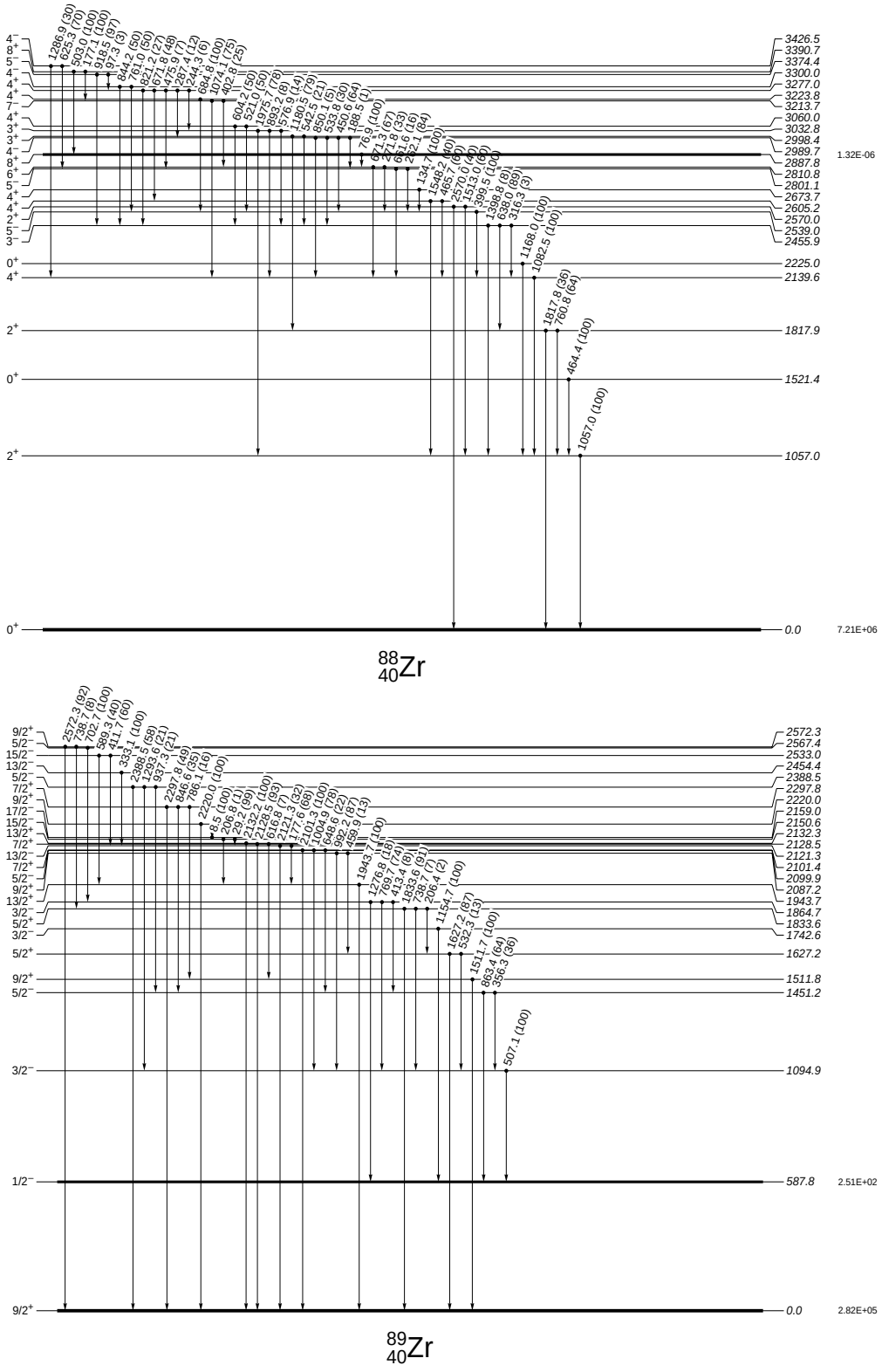

Fig. 24.— (continued)

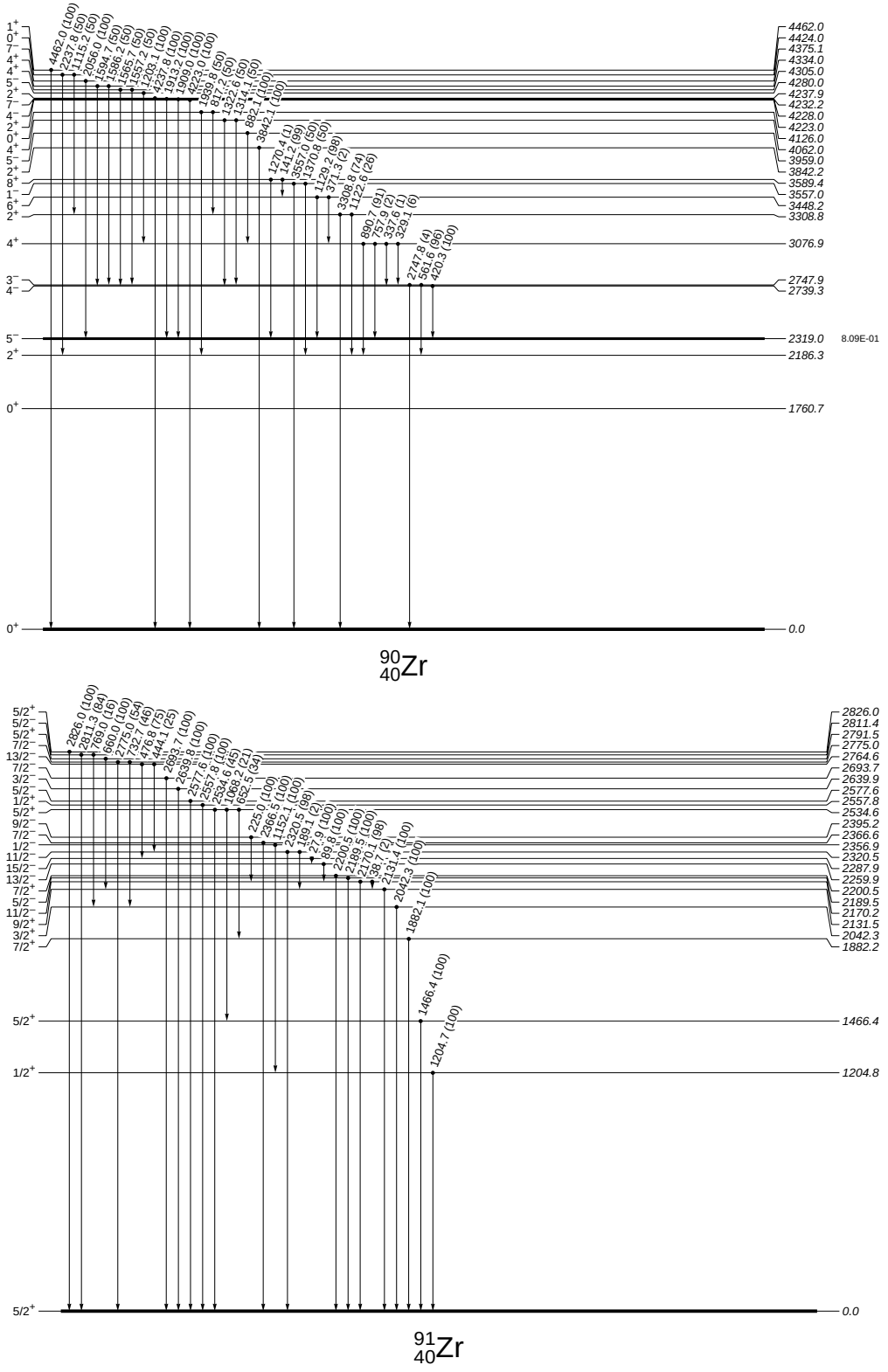

Fig. 24.— (continued)

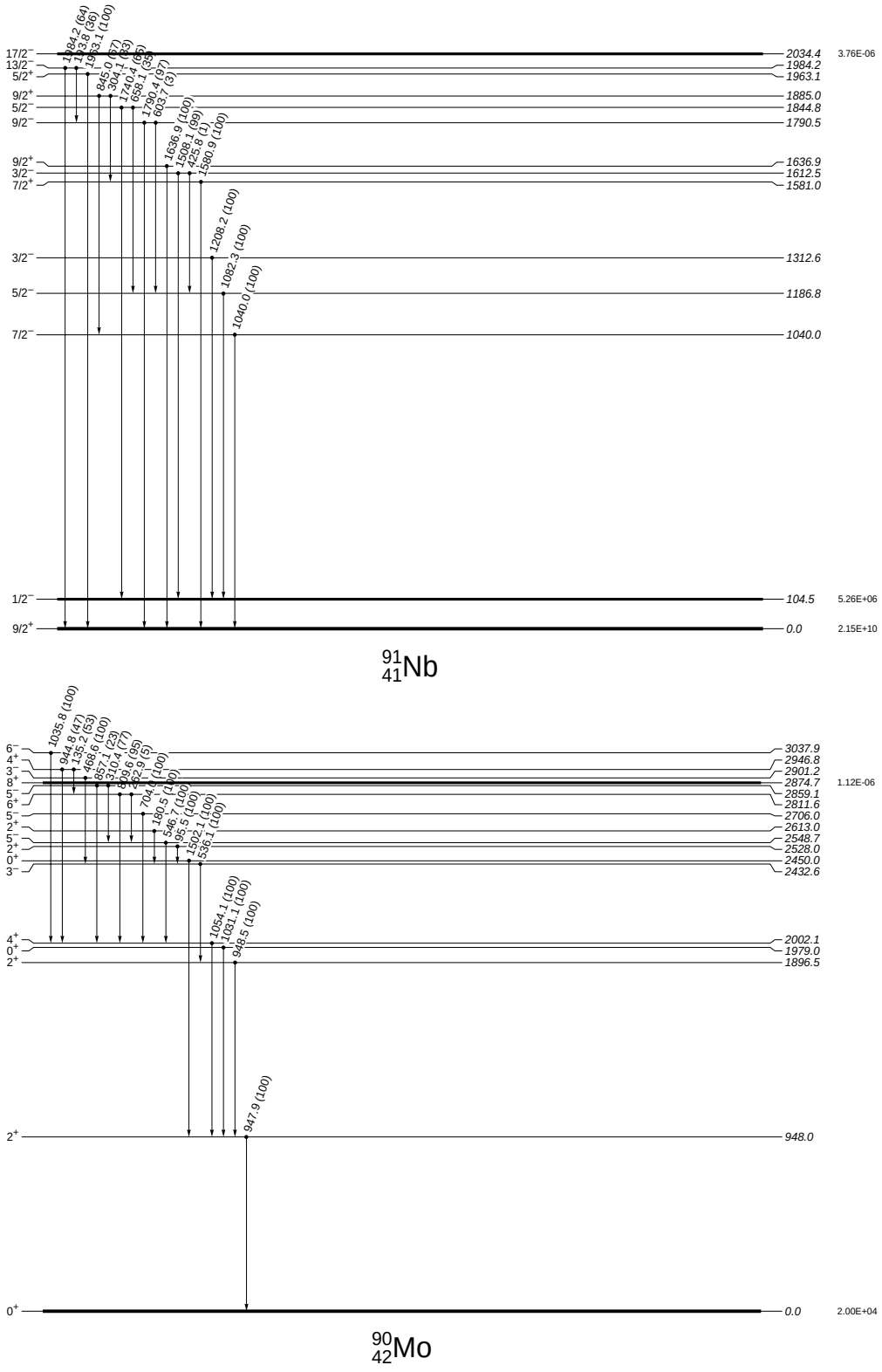

Fig. 24.— (continued)

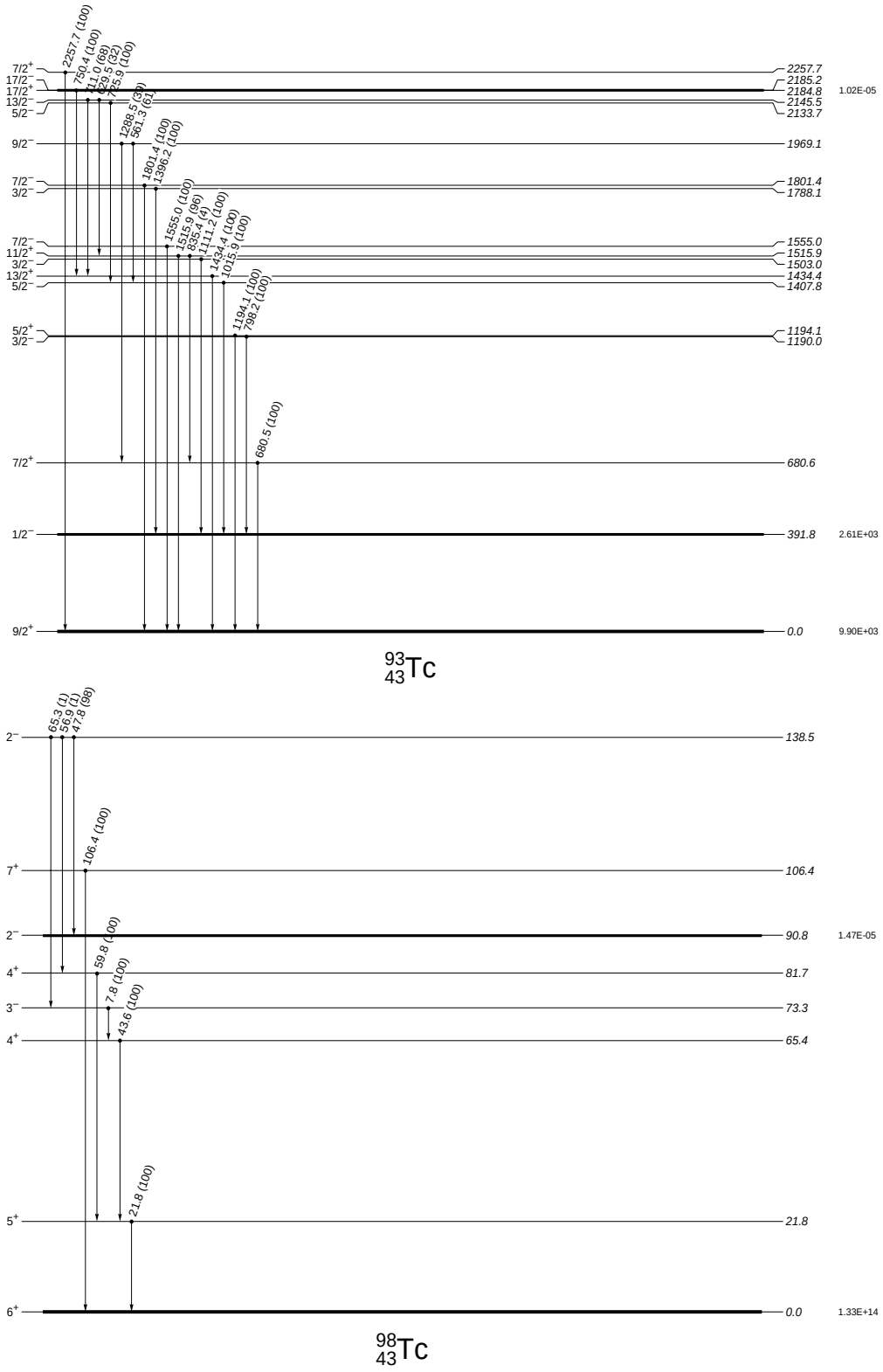

Fig. 24.— (continued)

B.4. Level Density Parameters

Here we present the level density parameters, as described in section 3.3, for each nucleus considered as a target, compound nucleus, or possible exit channel in this study. The first column lists the nuclei included. The second column is the asymptotic level density parameter in MeV^{-1}. Column three is the backshift in MeV. Columns four and five are the shell correction in MeV and a flag that indicates whether the shell correction is based on an experimentally measured resonance spacing (x) or is taken from systematics (s). Column six gives the matching energy. Columns seven, eight, and nine are the constant temperature parameters. The last column indicates the number of excited states to which the level density was fit, which is also the number of excited states included in our Hauser-Feshbach calculations.

Table 10: Level Density Parameters

Target	$\tilde{a}$	Δ	δW	x/s	E_x	T	$\sigma(E_x)$	E_0	N
^{75}Se	8.859	0.016	6.663	x	4.765	0.836	3.585	-3.664	17
^{76}Se	8.982	1.993	6.238	s	6.887	0.845	3.654	-1.795	17
^{77}Se	9.106	0.095	5.947	x	4.758	0.826	3.645	-3.488	17
^{78}Se	9.229	1.900	5.504	x	6.560	0.825	3.686	-1.663	17
^{79}Se	9.352	0.044	3.062	x	6.000	0.944	4.041	-4.459	1
^{80}Se	9.476	1.780	3.765	s	5.778	0.790	3.654	-1.189	20
^{81}Se	9.600	0.137	3.552	x	4.490	0.813	3.768	-3.104	4
^{82}Se	9.723	1.776	1.156	s	3.925	0.676	3.256	0.180	8
^{83}Se	9.847	-0.077	2.267	x	3.000	0.726	3.545	-2.315	1
^{84}Se	9.970	1.887	-2.368	s	7.500	0.985	4.366	-1.912	1
^{85}Se	10.094	0.375	-2.500	s	4.000	0.850	3.953	-2.097	0
^{86}Se	10.218	1.493	-1.379	s	5.737	0.862	4.082	-1.444	0
^{87}Se	10.342	0.507	-0.343	s	4.731	0.833	4.056	-2.471	0
^{76}Br	8.982	-0.889	6.284	s	3.393	0.800	3.530	-4.166	24
^{77}Br	9.106	-0.058	6.238	s	4.774	0.833	3.669	-3.796	25
^{78}Br	9.229	-1.134	5.963	s	3.465	0.814	3.659	-4.665	24
^{79}Br	9.352	0.003	5.459	s	4.586	0.813	3.698	-3.496	26
^{80}Br	9.476	-1.024	4.753	x	1.958	0.695	3.361	-3.238	7
^{81}Br	9.600	0.041	3.765	s	4.413	0.811	3.765	-3.223	25
^{82}Br	9.723	-0.842	3.085	x	2.014	0.700	3.427	-2.937	24
^{83}Br	9.847	0.179	1.156	s	1.000	0.579	2.577	-0.763	25
^{84}Br	9.970	-0.811	-0.492	s	0.500	0.632	2.973	-1.942	2
^{85}Br	10.094	0.446	-2.368	s	3.716	0.822	3.847	-1.804	9
^{86}Br	10.218	-0.762	-2.500	s	5.000	0.982	4.461	-4.654	0
^{87}Br	10.342	-0.294	-1.379	s	3.300	0.810	3.943	-2.789	0
^{88}Br	10.466	-0.702	-0.343	s	3.502	0.826	4.078	-3.666	0
^{89}Br	10.589	0.022	0.609	s	4.207	0.800	4.057	-2.974	0
^{90}Br	10.713	-0.527	1.476	s	3.640	0.778	4.041	-3.547	0
^{77}Kr	9.106	0.065	6.284	s	4.803	0.826	3.649	-3.595	24
^{78}Kr	9.229	2.017	6.238	s	6.737	0.818	3.674	-1.626	26
^{79}Kr	9.352	0.018	5.397	x	5.431	0.872	3.861	-4.177	26
^{80}Kr	9.476	1.978	5.459	s	3.000	0.517	2.549	1.050	23
^{81}Kr	9.600	0.054	5.893	x	3.837	0.735	3.559	-2.806	24

Continued on next page...

Table 10: (continued)

Target	$\tilde{a}$	Δ	δW	x/s	E_x	T	$\sigma(E_x)$	E_0	N
^{82}Kr	9.723	1.908	3.765	s	5.801	0.769	3.681	-0.981	24
^{83}Kr	9.847	-0.085	2.575	s	1.000	0.556	2.720	-1.068	23
^{84}Kr	9.970	1.771	-1.076	x	6.629	0.911	4.150	-1.610	25
^{85}Kr	10.094	-0.081	2.781	x	0.500	0.541	2.352	-0.959	16
^{86}Kr	10.218	1.916	-2.368	s	5.534	0.840	3.971	-0.556	3
^{87}Kr	10.342	0.408	-2.500	s	3.131	0.770	3.732	-1.497	11
^{88}Kr	10.466	1.441	-1.379	s	5.401	0.829	4.066	-1.303	16
^{89}Kr	10.589	0.538	-0.343	s	3.257	0.710	3.681	-1.399	19
^{90}Kr	10.713	1.381	0.609	s	4.245	0.698	3.713	-0.669	20
^{91}Kr	10.837	0.524	1.476	s	4.000	0.723	3.886	-1.983	0
^{77}Rb	9.106	-0.077	6.101	s	1.700	0.589	2.849	-1.448	13
^{78}Rb	9.229	-0.882	6.284	s	1.000	0.590	2.908	-2.320	1
^{79}Rb	9.352	-0.096	6.238	s	4.607	0.810	3.698	-3.726	13
^{80}Rb	9.476	-0.884	5.963	s	2.000	0.669	3.296	-3.041	0
^{81}Rb	9.600	-0.111	5.459	s	4.409	0.795	3.739	-3.561	7
^{82}Rb	9.723	-1.067	4.726	s	2.186	0.705	3.486	-3.483	7
^{83}Rb	9.847	-0.218	3.765	s	3.824	0.774	3.743	-3.224	5
^{84}Rb	9.970	-0.832	2.575	s	0.500	0.568	2.883	-1.929	2
^{85}Rb	10.094	-0.196	1.156	s	3.298	0.765	3.754	-2.706	9
^{86}Rb	10.218	-0.534	-1.622	x	2.520	0.782	3.773	-2.667	10
^{87}Rb	10.342	0.462	-2.368	s	4.131	0.837	4.011	-2.043	8
^{88}Rb	10.466	-0.698	-1.938	x	4.577	0.927	4.394	-4.313	5
^{89}Rb	10.589	-0.189	-1.379	s	2.000	0.689	3.531	-1.777	12
^{90}Rb	10.713	-0.596	-0.343	s	3.483	0.805	4.099	-3.472	11
^{91}Rb	10.837	-0.247	0.609	s	2.900	0.714	3.826	-2.494	6
^{92}Rb	10.961	-0.667	1.476	s	0.500	0.532	2.974	-1.655	8
^{93}Rb	11.085	-0.120	2.260	s	1.400	0.542	3.170	-1.291	5
^{94}Rb	11.209	-0.848	2.959	s	1.000	0.555	3.326	-2.223	0
^{95}Rb	11.333	-0.111	3.574	s	3.968	0.713	4.060	-3.150	0
^{78}Sr	9.229	1.559	6.101	s	2.000	0.558	2.023	0.605	4
^{79}Sr	9.352	0.068	6.284	s	1.862	0.576	2.894	-1.308	9
^{80}Sr	9.476	1.852	6.238	s	6.315	0.787	3.675	-1.577	2
^{81}Sr	9.600	-0.143	5.963	s	5.385	0.857	3.919	-4.472	10
^{82}Sr	9.723	1.982	5.459	s	6.464	0.786	3.757	-1.438	5
^{83}Sr	9.847	0.046	4.726	s	3.780	0.736	3.635	-2.746	20
^{84}Sr	9.970	1.940	3.765	s	5.104	0.702	3.542	-0.391	20
^{85}Sr	10.094	0.052	2.678	x	2.099	0.621	3.230	-1.473	39
^{86}Sr	10.218	1.731	1.156	s	3.535	0.622	3.202	0.362	41
^{87}Sr	10.342	0.007	-2.979	x	1.000	0.671	2.923	-1.071	7
^{88}Sr	10.466	2.074	-3.517	x	3.000	0.685	2.913	0.986	35
^{89}Sr	10.589	0.469	-3.309	x	1.000	0.782	2.545	-0.903	7
^{90}Sr	10.713	1.464	-1.379	s	4.329	0.737	3.800	-0.547	7
^{91}Sr	10.837	0.399	-0.343	s	1.000	0.583	2.557	-0.546	7

Continued on next page...

Table 10: (continued)

Target	$\tilde{a}$	Δ	δW	x/s	E_x	T	$\sigma(E_x)$	E_0	N
^{92}Sr	10.961	1.443	0.609	s	2.000	0.554	2.496	0.541	10
^{93}Sr	11.085	0.377	1.476	s	3.000	0.648	3.666	-1.516	0
^{94}Sr	11.209	1.584	2.260	s	3.977	0.612	3.575	-0.158	22
^{95}Sr	11.333	0.447	2.959	s	3.317	0.634	3.738	-1.646	9
^{96}Sr	11.458	1.435	3.574	s	4.770	0.656	3.882	-1.021	16
^{97}Sr	11.582	0.469	4.105	s	4.901	0.720	4.176	-2.877	16
^{98}Sr	11.706	1.763	4.552	s	5.847	0.686	4.097	-1.317	11
^{80}Y	9.476	-0.867	6.284	s	3.508	0.780	3.655	-4.225	0
^{81}Y	9.600	0.040	6.238	s	3.814	0.730	3.546	-2.822	7
^{82}Y	9.723	-0.890	5.963	s	0.500	0.528	2.780	-1.999	10
^{83}Y	9.847	-0.136	5.459	s	4.398	0.784	3.794	-3.601	11
^{84}Y	9.970	-0.870	4.726	s	1.000	0.579	3.073	-2.284	7
^{85}Y	10.094	-0.130	3.765	s	2.759	0.674	3.485	-2.256	24
^{86}Y	10.218	-1.044	2.575	s	1.000	0.617	3.254	-2.566	6
^{87}Y	10.342	0.086	1.156	s	3.035	0.711	3.646	-2.036	43
^{88}Y	10.466	-0.818	-0.492	s	1.000	0.646	3.313	-2.193	9
^{89}Y	10.589	0.833	-2.368	s	1.200	1.027	2.291	-1.386	7
^{90}Y	10.713	-0.549	-3.925	x	1.000	0.701	3.374	-1.805	10
^{91}Y	10.837	-0.079	-1.379	s	1.000	0.596	2.998	-1.089	9
^{92}Y	10.961	-0.519	-0.343	s	2.000	0.678	3.681	-2.319	0
^{93}Y	11.085	-0.101	0.609	s	1.000	0.539	2.978	-1.065	3
^{94}Y	11.209	-0.445	1.476	s	1.000	0.545	3.176	-1.572	1
^{95}Y	11.333	-0.038	2.260	s	0.500	0.491	2.473	-0.833	3
^{96}Y	11.458	-0.535	2.959	s	0.500	0.478	2.910	-1.420	1
^{97}Y	11.582	-0.002	3.574	s	0.500	0.454	2.427	-0.738	2
^{98}Y	11.706	-0.786	4.105	s	0.200	0.448	2.876	-1.625	12
^{99}Y	11.830	-0.552	4.552	s	0.300	0.428	2.776	-1.318	2
^{100}Y	11.954	-0.395	4.914	s	2.971	0.622	3.933	-2.907	9
^{101}Y	12.079	-0.375	5.193	s	0.000	0.428	2.271	-1.090	8
^{81}Zr	9.600	0.013	6.284	s	4.365	0.772	3.676	-3.326	0
^{82}Zr	9.723	1.711	6.238	s	5.666	0.737	3.614	-1.299	2
^{83}Zr	9.847	0.020	5.963	s	6.140	0.882	4.079	-4.835	4
^{84}Zr	9.970	1.721	5.459	s	6.007	0.760	3.766	-1.539	1
^{85}Zr	10.094	-0.171	4.726	s	4.094	0.763	3.812	-3.389	0
^{86}Zr	10.218	1.674	3.765	s	3.000	0.536	2.884	0.601	12
^{87}Zr	10.342	0.152	2.575	s	2.675	0.652	3.454	-1.693	14
^{88}Zr	10.466	1.652	1.156	s	4.308	0.682	3.575	-0.267	25
^{89}Zr	10.589	0.032	-0.492	s	1.000	0.581	2.849	-0.934	1
^{90}Zr	10.713	1.994	-2.368	s	4.300	0.716	3.645	0.346	10
^{91}Zr	10.837	0.351	-2.398	x	1.000	0.649	2.676	-0.701	40
^{92}Zr	10.961	1.314	-1.743	x	4.658	0.769	4.016	-0.999	5
^{93}Zr	11.085	0.392	-0.126	x	2.054	0.598	3.329	-0.872	2
^{94}Zr	11.209	1.322	2.169	x	3.058	0.558	3.301	0.020	8

Continued on next page...

Table 10: (continued)

Target	$\tilde{a}$	Δ	δW	x/s	E_x	T	$\sigma(E_x)$	E_0	N
^{95}Zr	11.333	0.492	0.771	x	2.000	0.558	3.255	-0.673	0
^{96}Zr	11.458	1.589	2.260	s	2.000	0.524	2.327	0.694	7
^{97}Zr	11.582	0.795	0.130	x	2.000	0.536	3.138	-0.205	9
^{98}Zr	11.706	1.462	3.574	s	4.487	0.624	3.832	-0.757	9
^{99}Zr	11.830	0.194	4.105	s	3.976	0.666	4.058	-2.629	20
^{100}Zr	11.954	1.512	4.552	s	6.154	0.713	4.282	-2.032	7
^{101}Zr	12.079	0.460	4.914	s	4.623	0.673	4.175	-2.701	8
^{102}Zr	12.203	1.228	5.193	s	5.484	0.671	4.212	-2.022	2
^{103}Zr	12.327	0.322	5.387	s	2.456	0.511	3.549	-1.251	6
^{104}Zr	12.452	1.210	5.497	s	3.120	0.488	3.467	-0.201	4
^{83}Nb	9.847	0.246	6.238	s	4.411	0.747	3.688	-2.939	2
^{84}Nb	9.970	-1.038	5.963	s	1.000	0.576	3.105	-2.569	0
^{85}Nb	10.094	0.211	5.459	s	4.475	0.753	3.787	-3.033	0
^{86}Nb	10.218	-0.718	4.726	s	3.526	0.756	3.833	-3.920	0
^{87}Nb	10.342	0.082	3.765	s	1.000	0.500	2.647	-0.785	7
^{88}Nb	10.466	-1.223	2.575	s	1.000	0.622	3.368	-2.860	1
^{89}Nb	10.589	0.020	1.156	s	1.000	0.543	2.803	-0.909	6
^{90}Nb	10.713	-0.933	-0.492	s	1.000	0.644	3.408	-2.367	11
^{91}Nb	10.837	0.463	-2.368	s	3.992	0.801	4.076	-1.949	13
^{92}Nb	10.961	-0.685	-2.500	s	4.631	0.914	4.546	-4.287	7
^{93}Nb	11.085	-0.211	-1.379	s	2.570	0.713	3.843	-2.163	6
^{94}Nb	11.209	-0.839	0.445	x	3.192	0.764	4.154	-3.718	10
^{95}Nb	11.333	-0.225	0.609	s	1.000	0.538	3.096	-1.237	2
^{96}Nb	11.458	-0.793	1.476	s	2.335	0.672	3.902	-3.045	3
^{97}Nb	11.582	-0.066	2.260	s	0.500	0.475	2.535	-0.833	2
^{98}Nb	11.706	-0.683	2.959	s	1.000	0.524	3.327	-1.941	1
^{99}Nb	11.830	-0.408	3.574	s	1.000	0.487	3.180	-1.488	4
^{100}Nb	11.954	-0.698	4.105	s	3.302	0.677	4.140	-3.697	1
^{101}Nb	12.079	-0.170	4.552	s	2.689	0.586	3.808	-2.280	21
^{102}Nb	12.203	-0.793	4.914	s	3.177	0.656	4.148	-3.797	0
^{103}Nb	12.327	0.157	5.193	s	3.941	0.636	4.111	-2.704	16
^{104}Nb	12.452	-0.746	5.387	s	3.196	0.640	4.169	-3.743	0
^{105}Nb	12.576	0.374	5.497	s	1.483	0.415	3.040	-0.501	5
^{84}Mo	9.970	2.437	6.238	s	6.723	0.749	3.740	-0.849	1
^{85}Mo	10.094	0.241	5.963	s	4.506	0.746	3.770	-3.020	0
^{86}Mo	10.218	1.289	5.459	s	3.535	0.591	3.240	-0.383	2
^{87}Mo	10.342	0.247	4.726	s	4.471	0.749	3.853	-2.941	0
^{88}Mo	10.466	1.519	3.765	s	3.621	0.593	3.281	-0.042	2
^{89}Mo	10.589	-0.033	2.575	s	2.776	0.665	3.595	-2.079	2
^{90}Mo	10.713	1.707	1.156	s	4.786	0.705	3.758	-0.505	16
^{91}Mo	10.837	0.063	-0.492	s	1.000	0.568	2.862	-0.879	1
^{92}Mo	10.961	1.994	-2.368	s	5.348	0.783	4.051	-0.303	16
^{93}Mo	11.085	0.349	-2.758	x	1.000	0.646	2.725	-0.695	18

Continued on next page...

Table 10: (continued)

Target	$\tilde{a}$	Δ	δW	x/s	E_x	T	$\sigma(E_x)$	E_0	N
^{94}Mo	11.209	1.476	-1.379	s	5.056	0.767	4.118	-1.009	5
^{95}Mo	11.333	0.362	0.300	x	4.394	0.761	4.186	-2.512	8
^{96}Mo	11.458	1.478	0.755	x	5.274	0.732	4.128	-1.241	2
^{97}Mo	11.582	0.307	1.833	x	3.944	0.698	4.062	-2.332	5
^{98}Mo	11.706	1.503	2.627	x	4.679	0.648	3.917	-0.811	5
^{99}Mo	11.830	0.006	3.376	x	3.545	0.660	4.019	-2.605	12
^{100}Mo	11.954	1.649	3.574	s	5.822	0.696	4.206	-1.470	14
^{101}Mo	12.079	-0.050	5.249	x	4.066	0.666	4.150	-3.184	5
^{102}Mo	12.203	1.583	4.552	s	5.965	0.688	4.268	-1.747	7
^{103}Mo	12.327	0.167	4.914	s	3.555	0.612	4.007	-2.365	16
^{104}Mo	12.452	1.381	5.193	s	5.332	0.643	4.179	-1.617	16
^{105}Mo	12.576	0.192	5.387	s	3.313	0.579	3.951	-2.138	2
^{106}Mo	12.700	1.196	5.497	s	4.955	0.619	4.160	-1.654	6
^{107}Mo	12.825	0.291	5.522	s	4.193	0.624	4.222	-2.680	0
^{87}Tc	10.342	0.092	5.459	s	1.000	0.472	2.596	-0.743	0
^{88}Tc	10.466	-0.834	4.726	s	3.371	0.742	3.874	-4.006	0
^{89}Tc	10.589	-0.137	3.765	s	4.048	0.749	3.930	-3.261	0
^{90}Tc	10.713	-0.666	2.575	s	3.501	0.760	3.996	-3.731	0
^{91}Tc	10.837	-0.195	1.156	s	2.350	0.657	3.606	-2.033	2
^{92}Tc	10.961	-0.829	-0.492	s	0.500	0.584	3.143	-1.923	8
^{93}Tc	11.085	0.487	-2.368	s	3.752	0.770	4.049	-1.752	17
^{94}Tc	11.209	-0.814	-2.500	s	3.282	0.825	4.316	-3.593	1
^{95}Tc	11.333	-0.096	-1.379	s	3.781	0.782	4.225	-2.785	8
^{96}Tc	11.458	-0.947	-0.343	s	5.000	0.886	4.674	-5.209	1
^{97}Tc	11.582	-0.095	0.609	s	3.789	0.736	4.183	-2.874	10
^{98}Tc	11.706	-0.997	1.476	s	4.226	0.803	4.492	-4.847	7
^{99}Tc	11.830	-0.121	2.260	s	2.895	0.638	3.903	-2.307	5
^{100}Tc	11.954	-0.877	5.180	x	1.877	0.574	3.729	-2.916	24
^{101}Tc	12.079	-0.130	3.574	s	3.448	0.651	4.068	-2.778	23
^{102}Tc	12.203	-0.860	4.105	s	2.000	0.588	3.846	-2.964	1
^{103}Tc	12.327	-0.077	4.552	s	3.906	0.657	4.189	-3.081	5
^{104}Tc	12.452	-0.929	4.914	s	1.000	0.496	3.494	-2.350	1
^{105}Tc	12.576	0.060	5.193	s	4.307	0.658	4.280	-3.187	18
^{106}Tc	12.700	-0.888	5.387	s	2.000	0.559	3.895	-3.034	0
^{107}Tc	12.825	0.189	5.497	s	4.091	0.624	4.223	-2.781	0
^{108}Tc	12.949	-0.905	5.522	s	2.984	0.620	4.241	-3.867	0
^{88}Ru	10.466	2.239	5.459	s	6.444	0.732	3.849	-0.958	0
^{89}Ru	10.589	0.293	4.726	s	4.478	0.735	3.895	-2.865	0
^{90}Ru	10.713	1.527	3.765	s	5.694	0.742	3.951	-1.583	0
^{91}Ru	10.837	0.088	2.575	s	0.600	0.515	2.376	-0.755	4
^{92}Ru	10.961	1.638	1.156	s	4.000	0.637	3.561	-0.075	2
^{93}Ru	11.085	0.053	-0.492	s	0.500	0.639	2.408	-1.064	4
^{94}Ru	11.209	1.904	-2.368	s	4.557	0.719	3.869	0.054	3

Continued on next page...

Table 10: (continued)

Target	$\tilde{a}$	Δ	δW	x/s	E_x	T	$\sigma(E_x)$	E_0	N
^{95}Ru	11.333	0.331	-2.500	s	3.000	0.718	3.905	-1.524	1
^{96}Ru	11.458	1.530	-1.379	s	5.998	0.815	4.403	-1.572	27
^{97}Ru	11.582	0.290	-0.343	s	4.000	0.740	4.179	-2.325	12
^{98}Ru	11.706	1.594	0.609	s	5.939	0.761	4.328	-1.530	13
^{99}Ru	11.830	0.253	1.476	s	4.250	0.719	4.224	-2.647	23
^{100}Ru	11.954	1.645	2.625	x	5.666	0.699	4.205	-1.320	12
^{101}Ru	12.079	0.173	2.959	s	4.374	0.702	4.262	-2.947	7
^{102}Ru	12.203	1.706	4.441	x	5.572	0.655	4.138	-1.197	13
^{103}Ru	12.327	0.083	3.471	x	4.990	0.730	4.461	-3.636	5
^{104}Ru	12.452	1.682	4.552	s	4.293	0.555	3.785	-0.239	26
^{105}Ru	12.576	0.113	5.983	x	4.560	0.662	4.300	-3.331	4
^{106}Ru	12.700	1.572	5.193	s	5.499	0.634	4.218	-1.410	7
^{107}Ru	12.825	0.225	5.387	s	5.000	0.681	4.450	-3.479	0
^{108}Ru	12.949	1.451	5.497	s	5.673	0.641	4.331	-1.789	9
^{109}Ru	13.074	0.255	5.522	s	4.784	0.657	4.432	-3.249	2
^{91}Rh	10.837	-0.242	3.765	s	3.906	0.735	3.971	-3.339	0
^{92}Rh	10.961	-0.798	2.575	s	3.332	0.747	4.038	-3.837	0
^{93}Rh	11.085	-0.091	1.156	s	1.000	0.528	2.953	-1.042	0
^{94}Rh	11.209	-0.794	-0.492	s	0.500	0.571	3.161	-1.861	1
^{95}Rh	11.333	0.486	-2.368	s	1.000	0.663	2.587	-0.641	2
^{96}Rh	11.458	-0.865	-2.500	s	4.600	0.897	4.690	-4.577	3
^{97}Rh	11.582	0.033	-1.379	s	3.514	0.743	4.163	-2.384	19
^{98}Rh	11.706	-0.941	-0.343	s	3.090	0.757	4.292	-3.787	1
^{99}Rh	11.830	0.022	0.609	s	2.957	0.658	3.946	-2.072	29
^{100}Rh	11.954	-0.923	1.476	s	2.852	0.699	4.187	-3.655	2
^{101}Rh	12.079	0.032	2.260	s	3.293	0.647	4.026	-2.337	13
^{102}Rh	12.203	-0.940	2.959	s	3.182	0.692	4.266	-3.998	22
^{103}Rh	12.327	-0.031	3.574	s	2.180	0.540	3.644	-1.647	37
^{104}Rh	12.452	-0.935	3.746	x	2.404	0.619	4.059	-3.402	22
^{105}Rh	12.576	0.020	4.552	s	2.844	0.568	3.882	-2.063	5
^{106}Rh	12.700	-0.890	4.914	s	3.026	0.636	4.226	-3.852	1
^{107}Rh	12.825	0.056	5.193	s	3.388	0.589	4.068	-2.439	10
^{108}Rh	12.949	-0.831	5.387	s	3.057	0.621	4.246	-3.789	0
^{109}Rh	13.074	0.056	5.497	s	2.420	0.508	3.758	-1.687	26
^{110}Rh	13.198	-0.780	5.522	s	1.000	0.458	3.516	-2.092	0
^{94}Pd	11.209	1.569	1.156	s	5.665	0.756	4.139	-1.388	0
^{95}Pd	11.333	0.129	-0.492	s	4.208	0.779	4.236	-2.743	0
^{96}Pd	11.458	1.952	-2.368	s	5.262	0.757	4.137	-0.315	4
^{97}Pd	11.582	0.232	-2.500	s	1.000	0.588	2.899	-0.708	2
^{98}Pd	11.706	1.466	-1.379	s	3.446	0.624	3.639	0.028	3
^{99}Pd	11.830	0.225	-0.343	s	4.576	0.773	4.400	-2.854	3
^{100}Pd	11.954	1.623	0.609	s	5.155	0.697	4.157	-0.901	10
^{101}Pd	12.079	0.178	1.476	s	2.000	0.546	3.508	-1.164	18

Continued on next page...

Table 10: (continued)

Target	$\tilde{a}$	Δ	δW	x/s	E_x	T	$\sigma(E_x)$	E_0	N
^{102}Pd	12.203	1.648	2.260	s	4.912	0.643	4.050	-0.723	3
^{103}Pd	12.327	0.179	2.959	s	3.983	0.666	4.204	-2.629	6
^{104}Pd	12.452	1.645	3.574	s	5.099	0.630	4.101	-0.908	7
^{105}Pd	12.576	0.118	2.765	x	3.851	0.656	4.238	-2.630	5
^{106}Pd	12.700	1.645	3.824	x	5.307	0.633	4.197	-1.079	26
^{107}Pd	12.825	0.020	3.413	x	4.288	0.674	4.404	-3.180	8
^{108}Pd	12.949	1.634	4.142	x	5.436	0.631	4.270	-1.215	10
^{109}Pd	13.074	0.018	5.329	x	2.912	0.550	3.962	-2.132	2
^{102}Ag	12.203	-0.758	1.476	s	1.400	0.570	3.681	-2.322	13
^{103}Ag	12.327	-0.028	2.260	s	1.000	0.459	3.047	-0.890	9
^{104}Ag	12.452	-0.806	2.959	s	2.230	0.608	3.993	-3.022	6
^{105}Ag	12.576	-0.075	3.574	s	1.981	0.520	3.617	-1.579	6
^{106}Ag	12.700	-0.779	4.105	s	0.200	0.418	3.003	-1.588	4
^{107}Ag	12.825	-0.022	4.552	s	0.752	0.394	2.833	-0.721	10
^{97}Ag	11.582	0.446	-2.368	s	0.700	2.226	2.195	-6.523	4
^{98}Ag	11.706	-0.747	-2.500	s	3.284	0.798	4.403	-3.485	0
^{99}Ag	11.830	0.068	-1.379	s	1.641	0.586	3.456	-1.132	3
^{100}Ag	11.954	-0.831	-0.343	s	4.443	0.825	4.643	-4.596	2
^{101}Ag	12.079	-0.105	0.609	s	1.000	0.502	3.125	-1.034	14
^{108}Ag	12.949	-0.898	3.188	x	1.804	0.565	3.954	-2.868	19
^{109}Ag	13.074	-0.012	5.193	s	2.321	0.509	3.757	-1.730	4
^{110}Ag	13.198	-0.991	4.695	x	1.000	0.484	3.645	-2.452	0

C. Modeled Cross Sections Compared to Measurements

C.1. (n,γ)

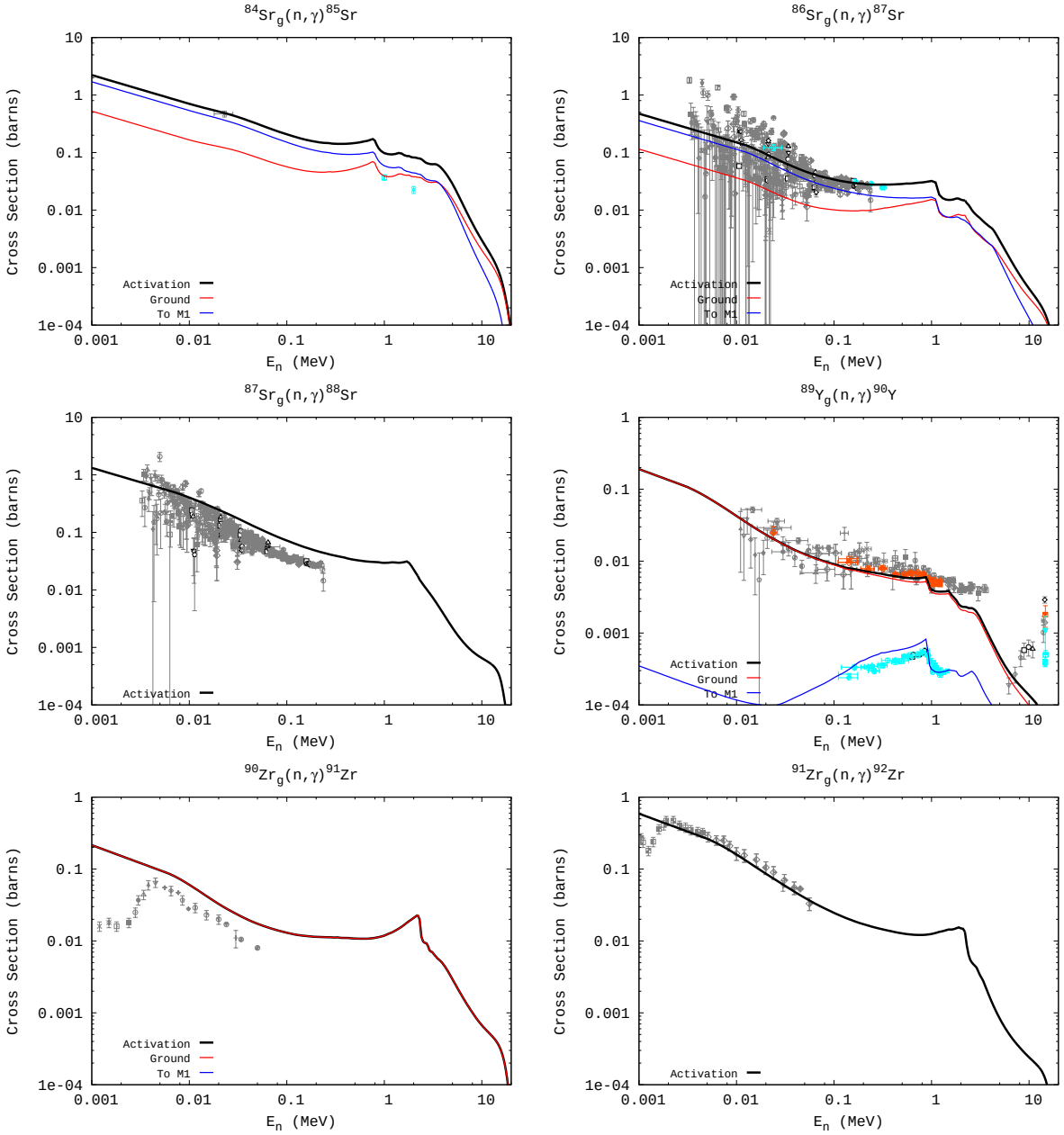

Fig. 25.— Modeled neutron capture cross sections compared to measurement. The data is taken from (EXFOR 2006). The black, red, and blue solid lines represent our modeled cross sections (total, leading to the ground state, and leading to the first isomer, respectively). The gray, orange, and light blue data points are measured cross section data (total, ground state, and first isomer).

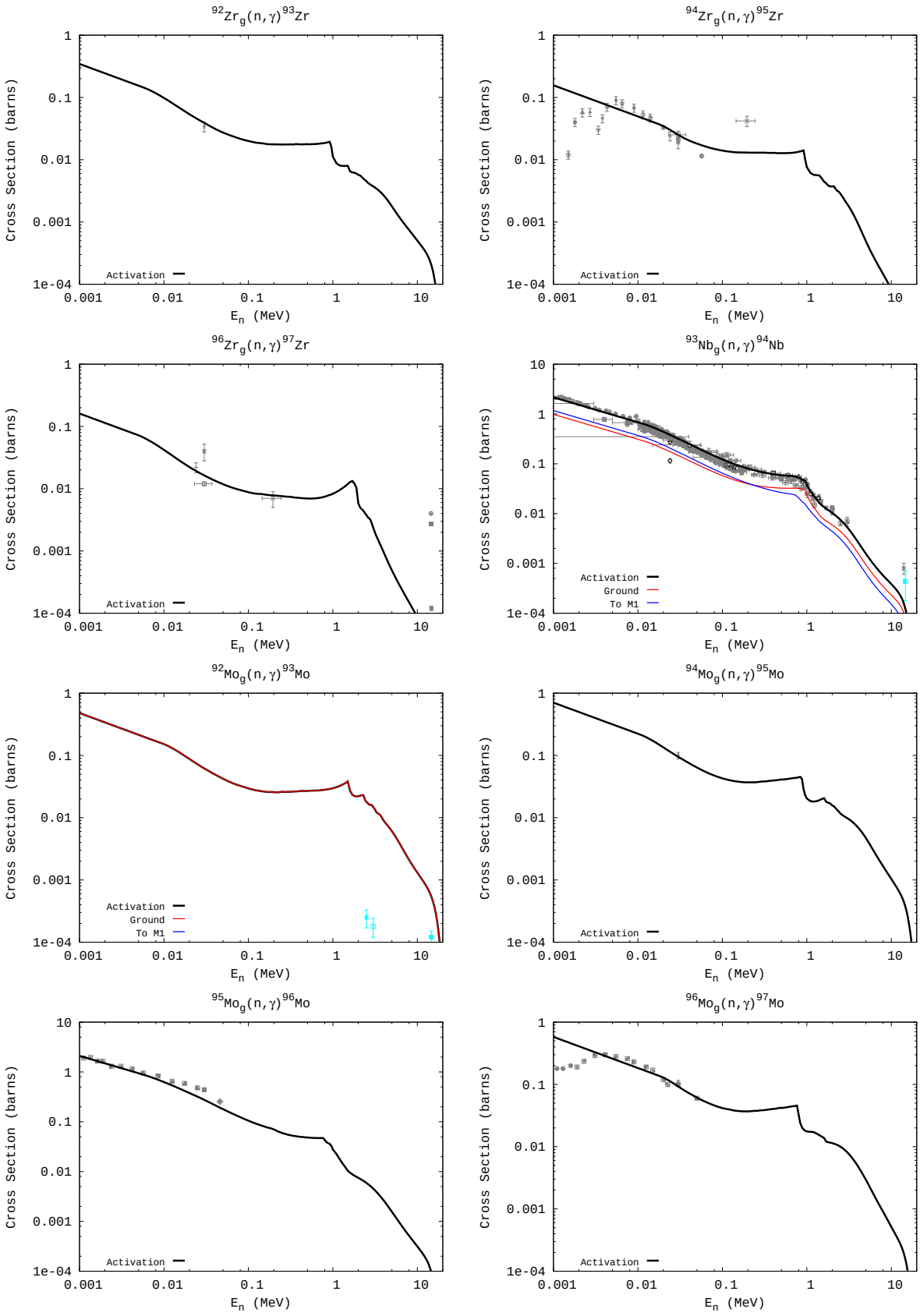

Fig. 25.— (continued)

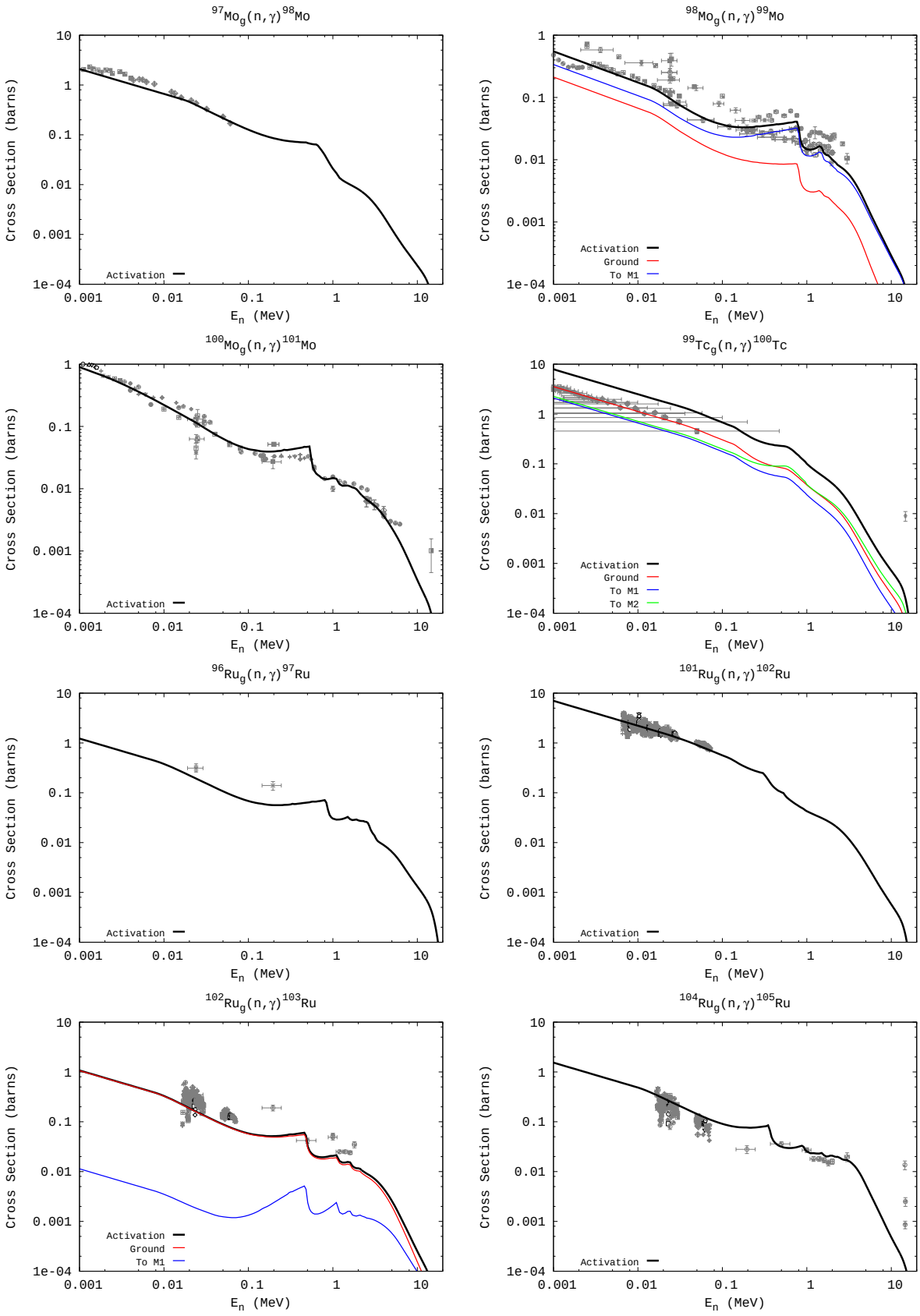

Fig. 25.— (continued)

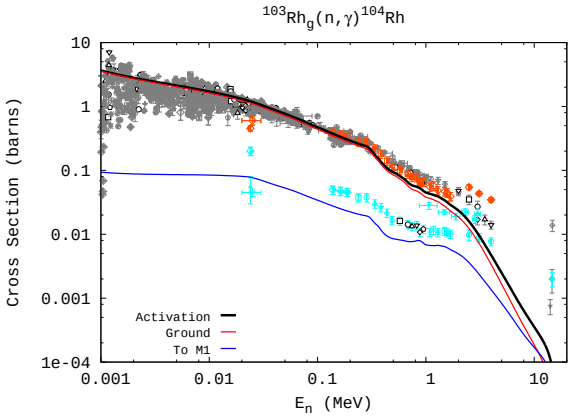

Fig. 25.— (continued)

C.2. Maxwellian-averaged (n,γ)

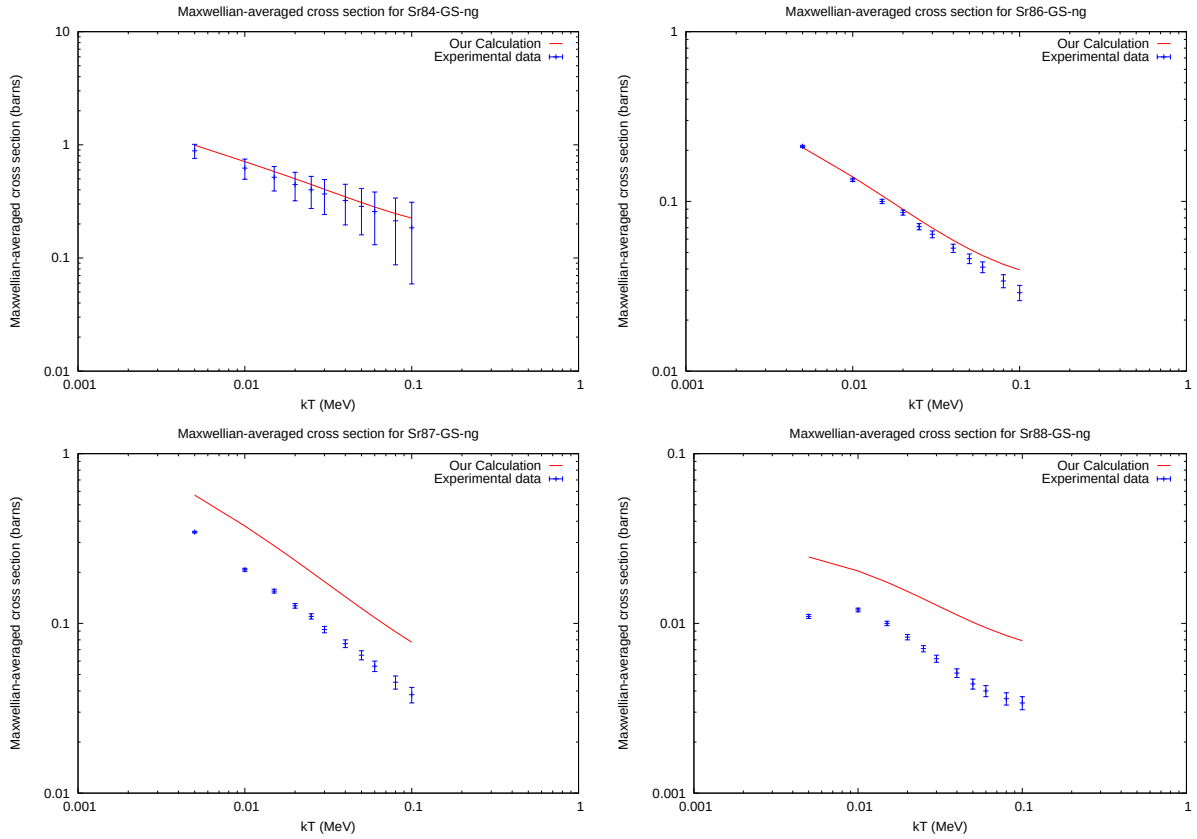

Fig. 26.— Modeled Maxwellian-averaged neutron capture cross sections compared to measurement. The data is taken from (Bao *et al.* 2000). The solid lines represent our modeled cross sections. The errors on the recommended value for each energy are identical to the stated error at 30 keV.

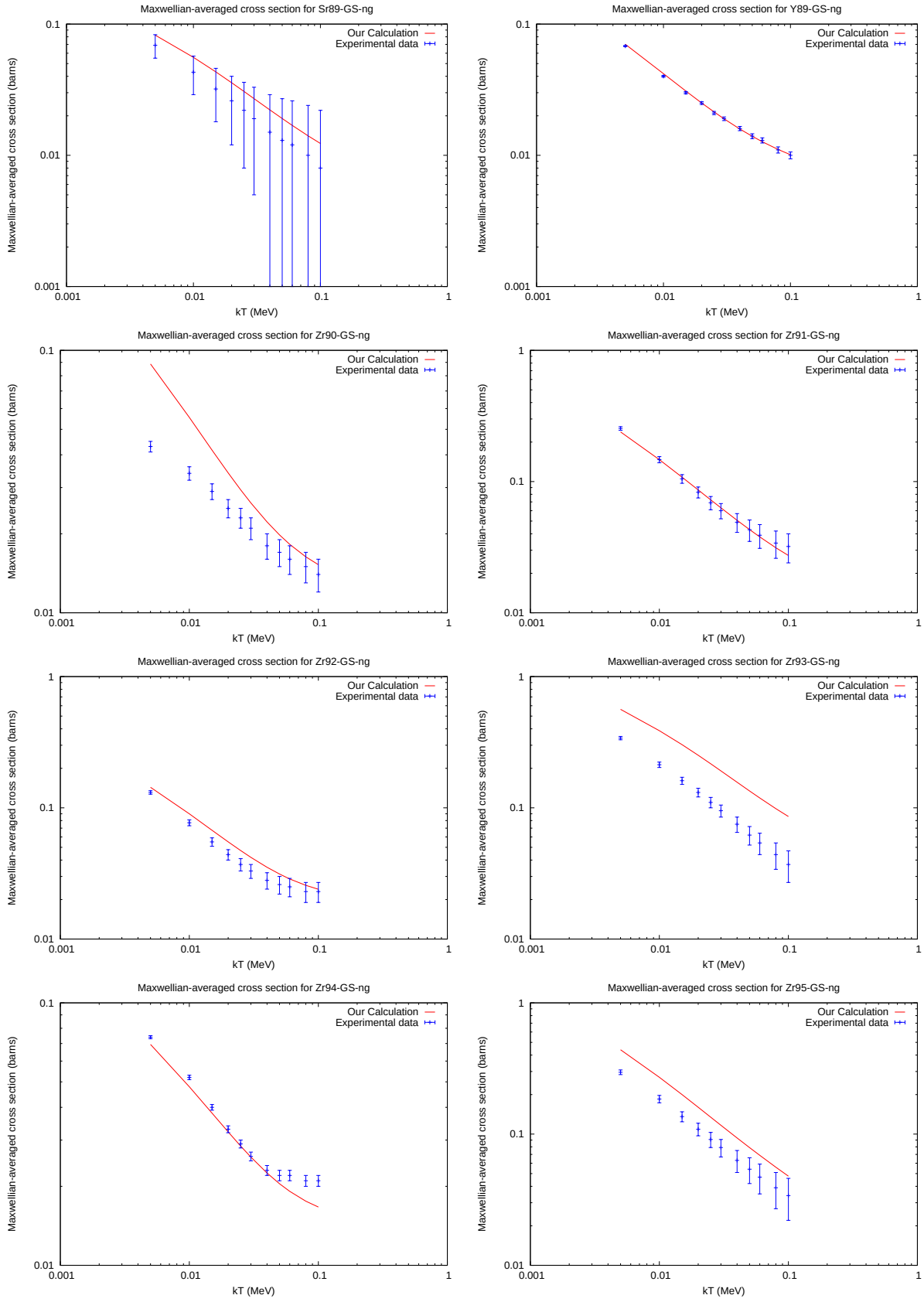

Fig. 26.— (continued)

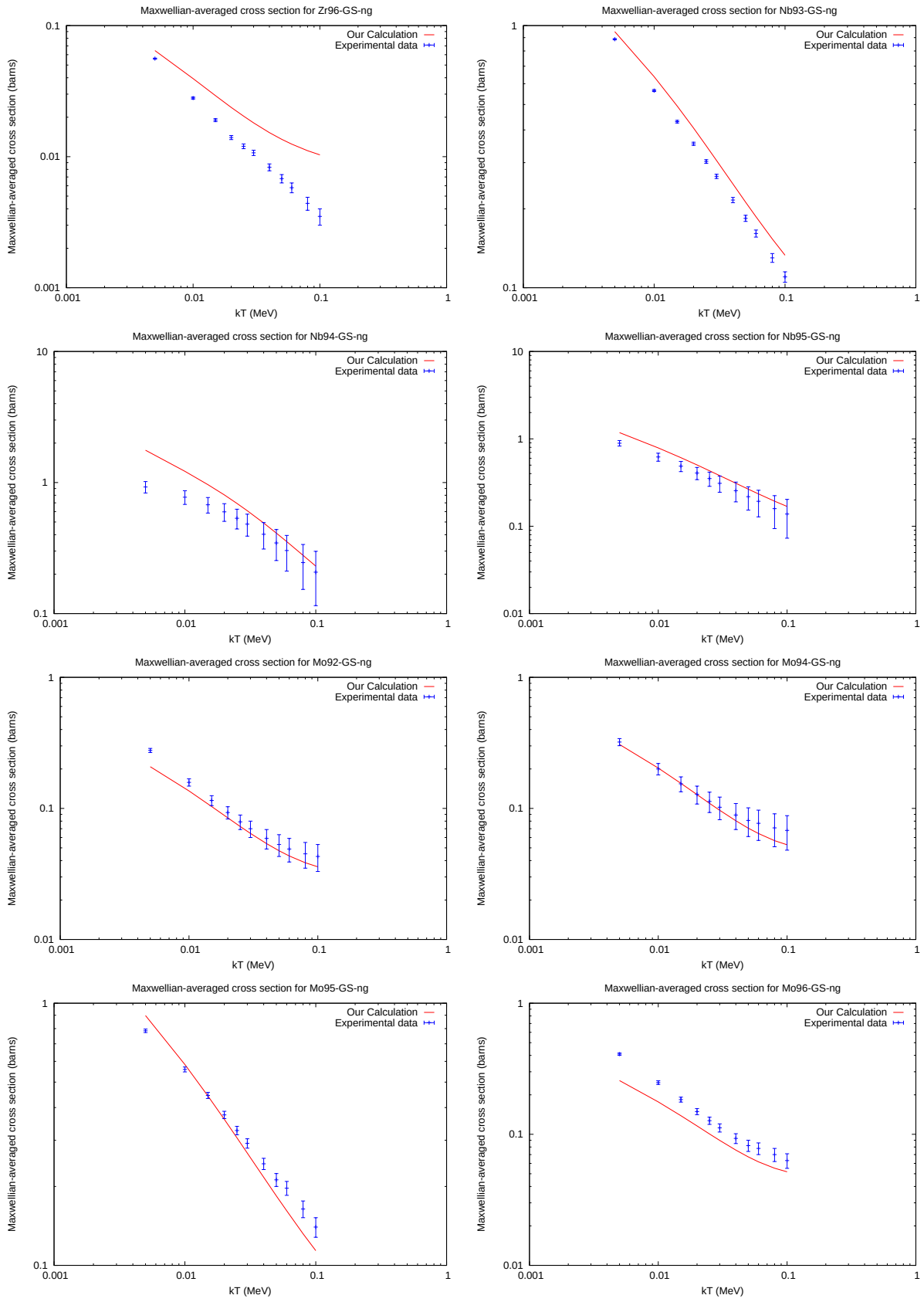

Fig. 26.— (continued)

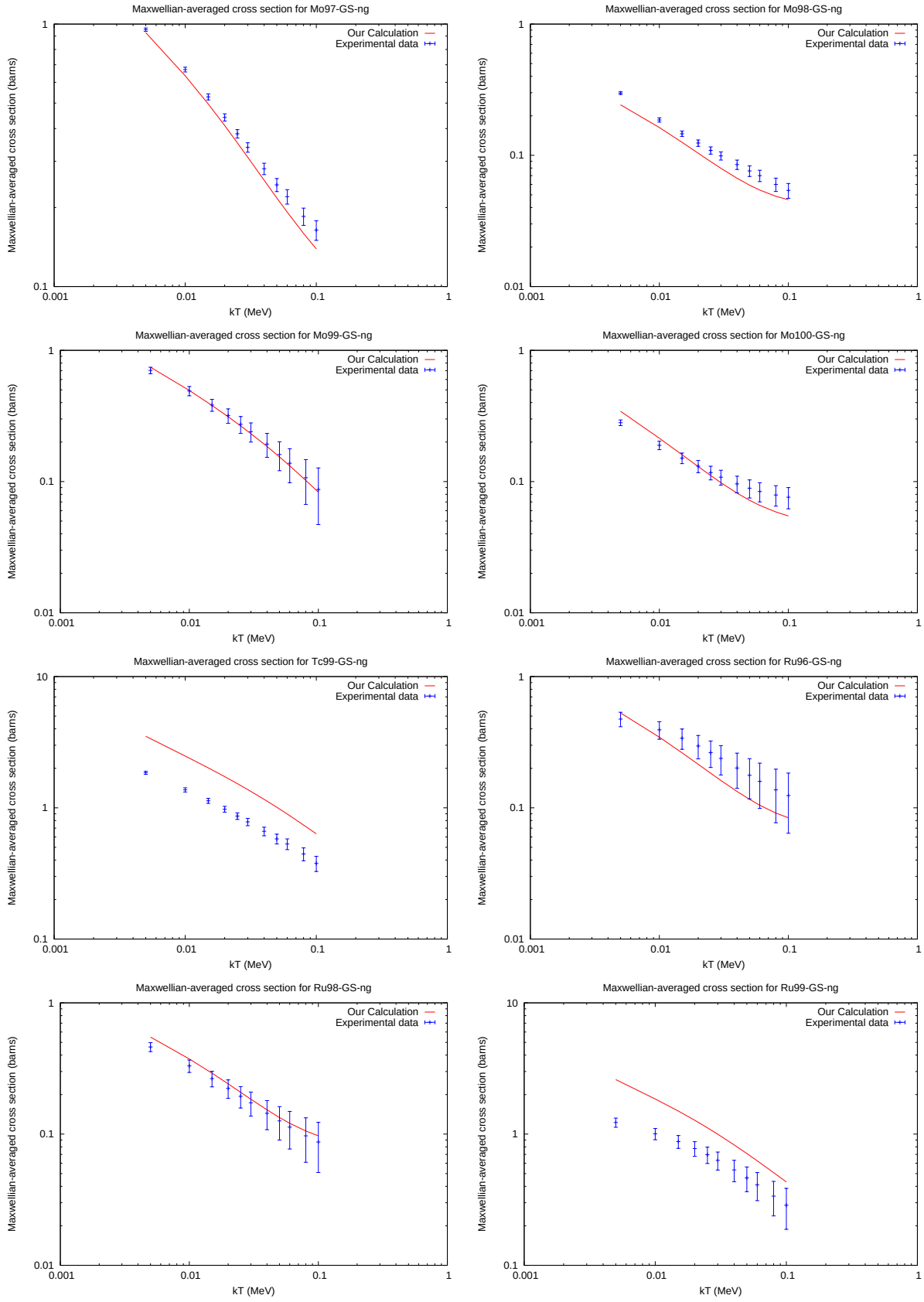

Fig. 26.— (continued)

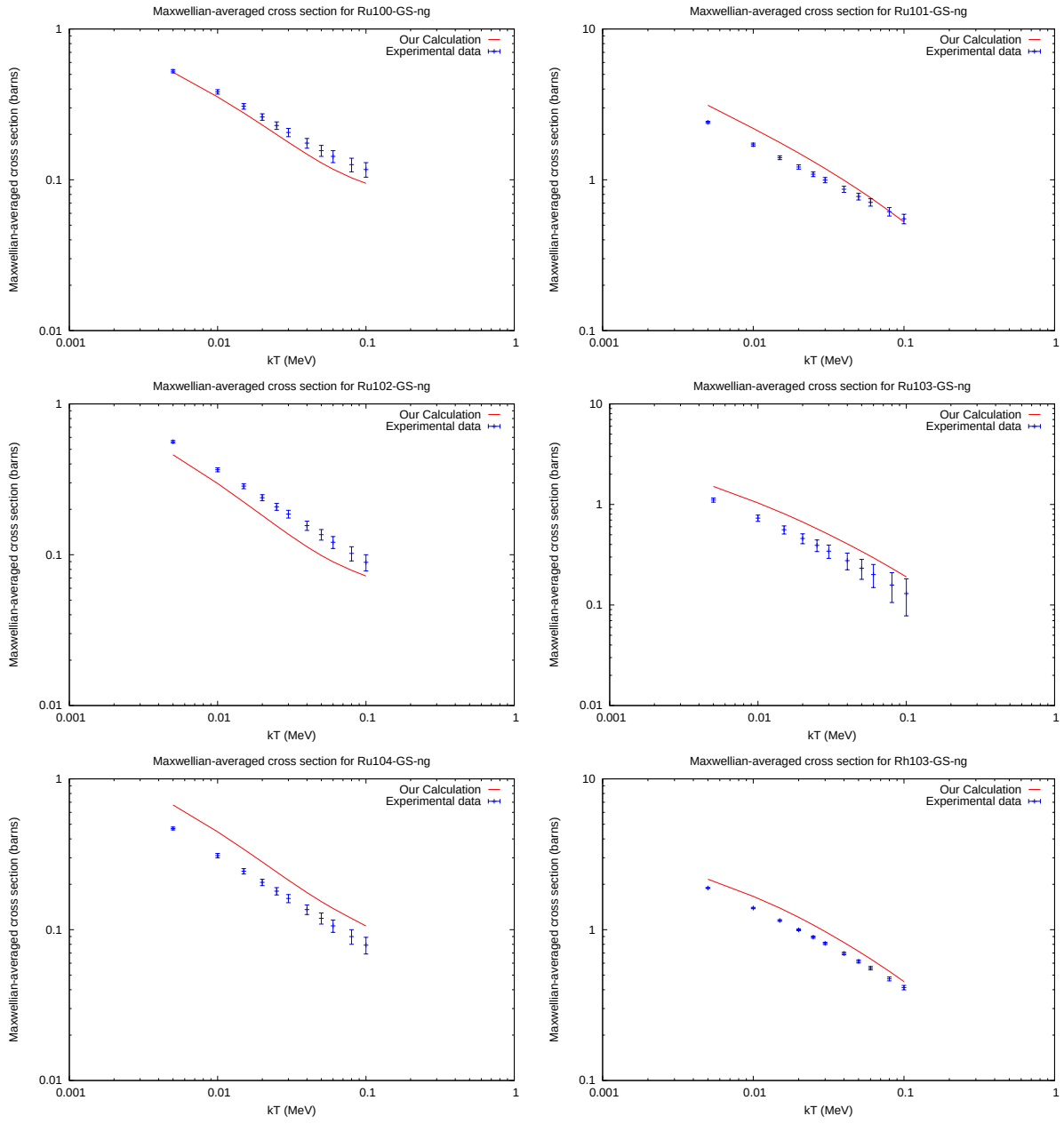

Fig. 26.— (continued)

C.3. (n,2n)

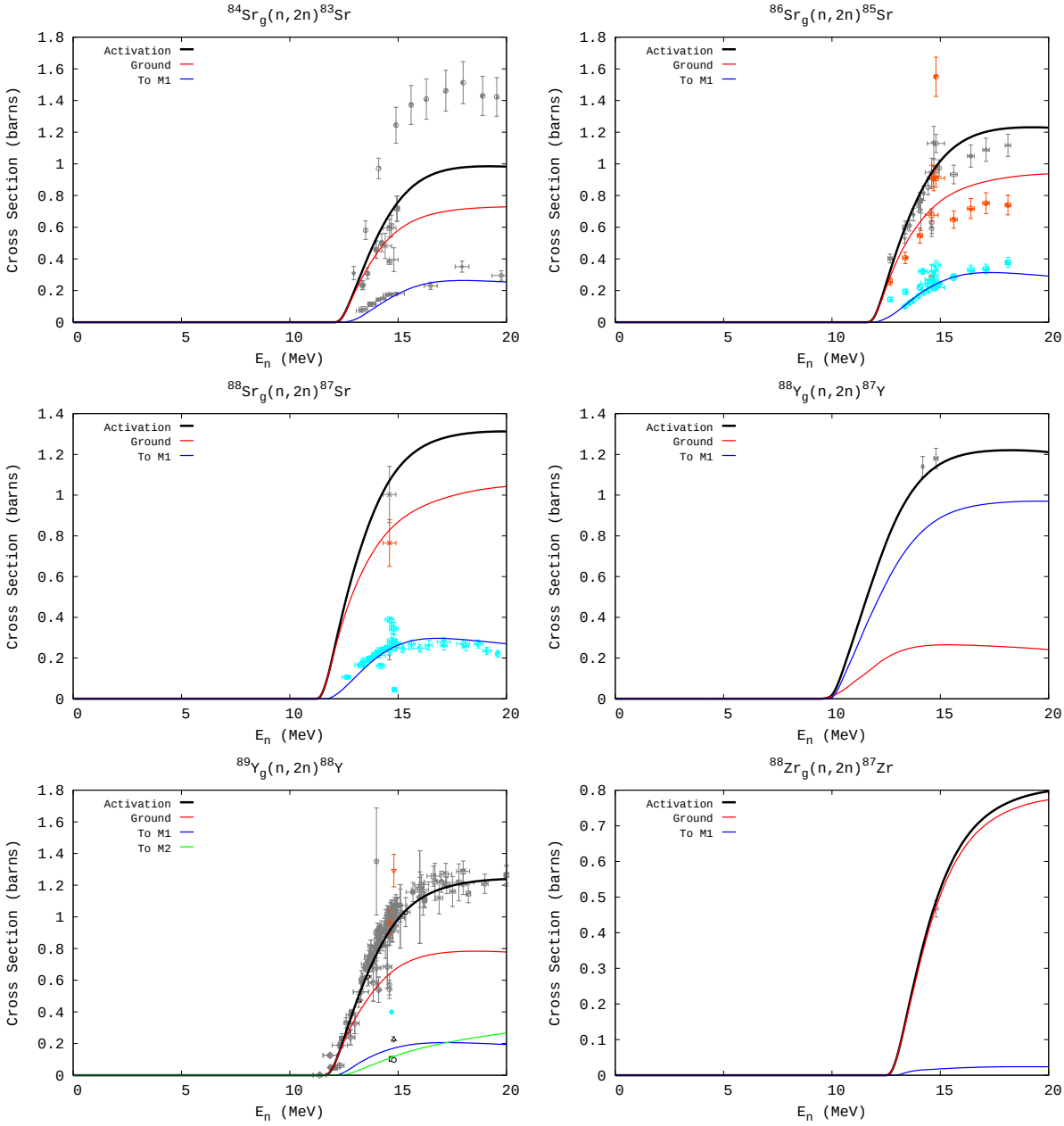

Fig. 27.— Modeled (n,2n) cross sections compared to measurement. The data is taken from (EXFOR 2006). The black, red, and blue solid lines represent our modeled cross sections (total, leading to the ground state, and leading to the first isomer, respectively). The Gery, orange, and light blue data points are measured cross section data (total, ground state, and first isomer).

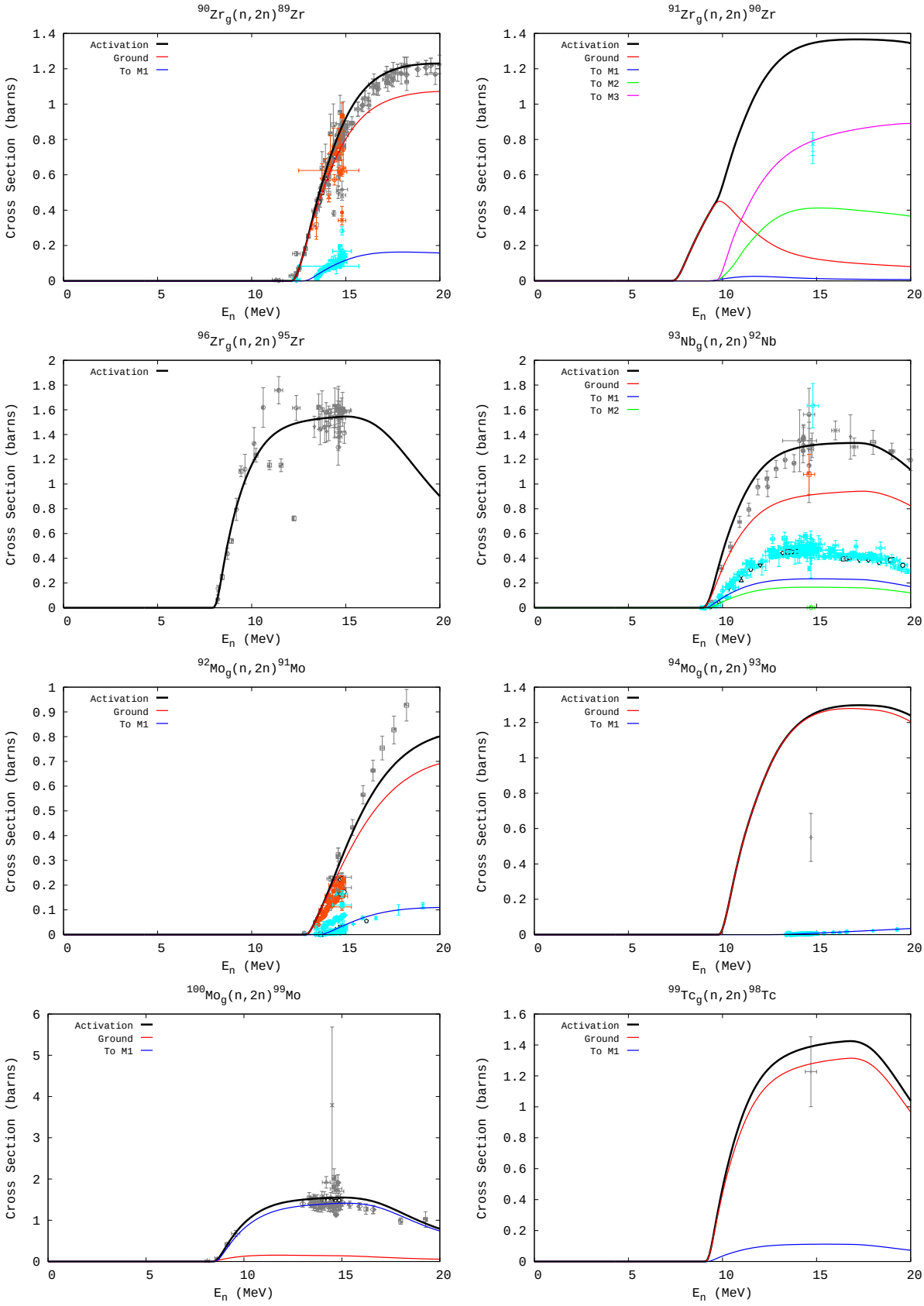

Fig. 27.— (continued)

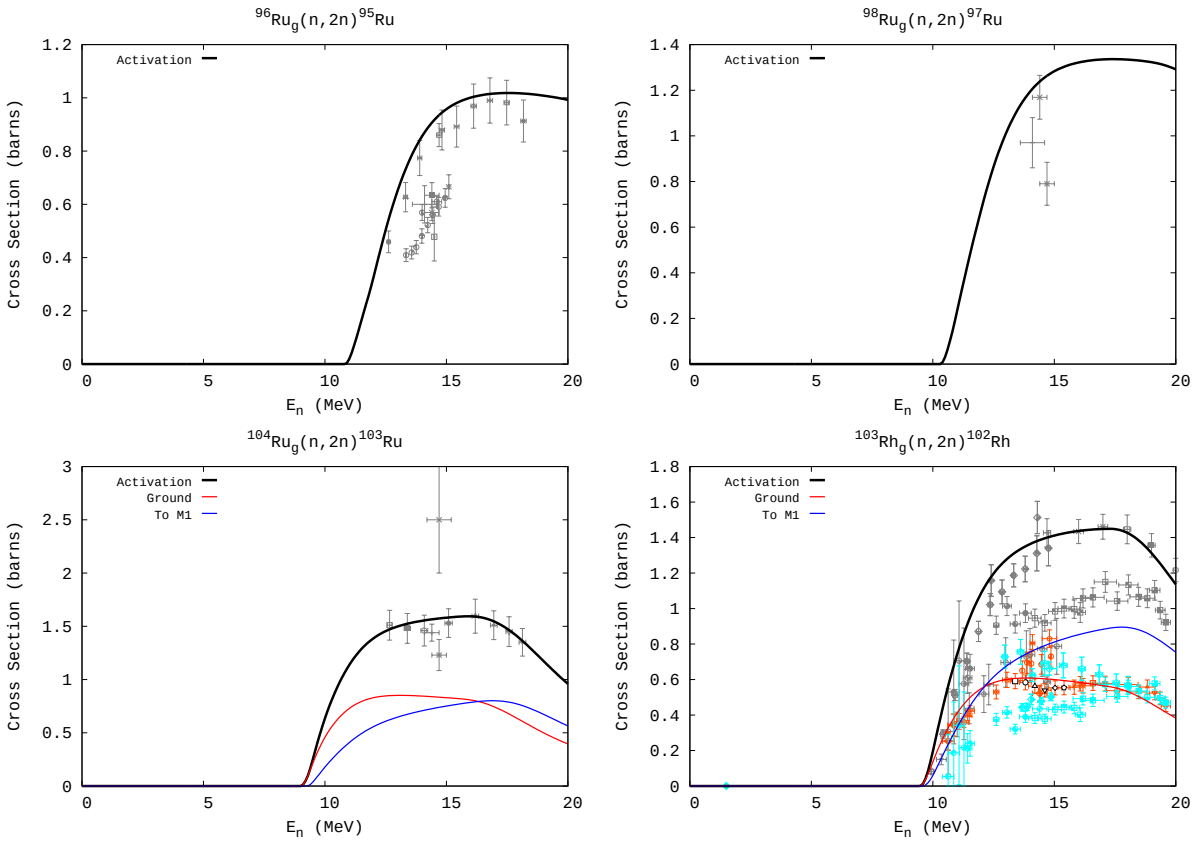

Fig. 27.— (continued)

C.4. (n,3n)

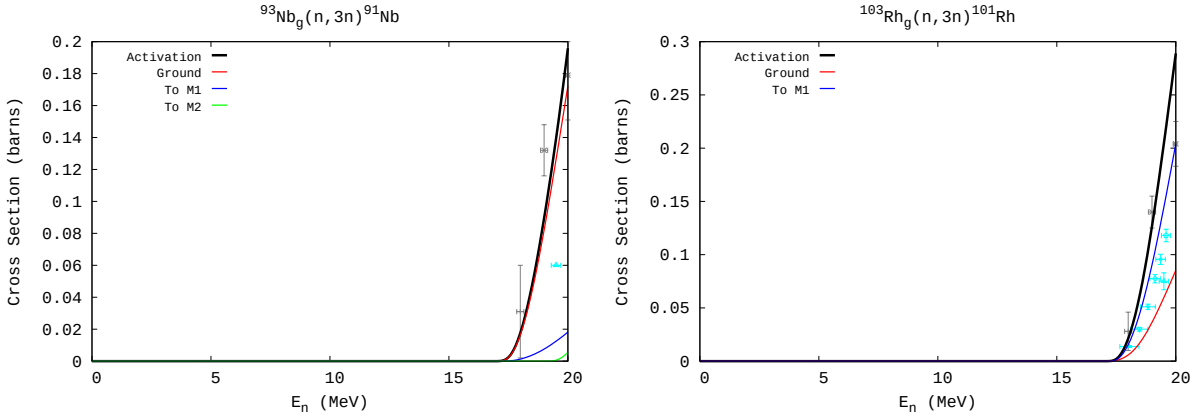

Fig. 28.— Modeled (n,3n) cross sections compared to measurement. The data is taken from (EXFOR 2006). The black, red, and blue solid lines represent our modeled cross sections (total, leading to the ground state, and leading to the first isomer, respectively). The Gery, orange, and light blue data points are measured cross section data (total, ground state, and first isomer).

C.5. (n,n')

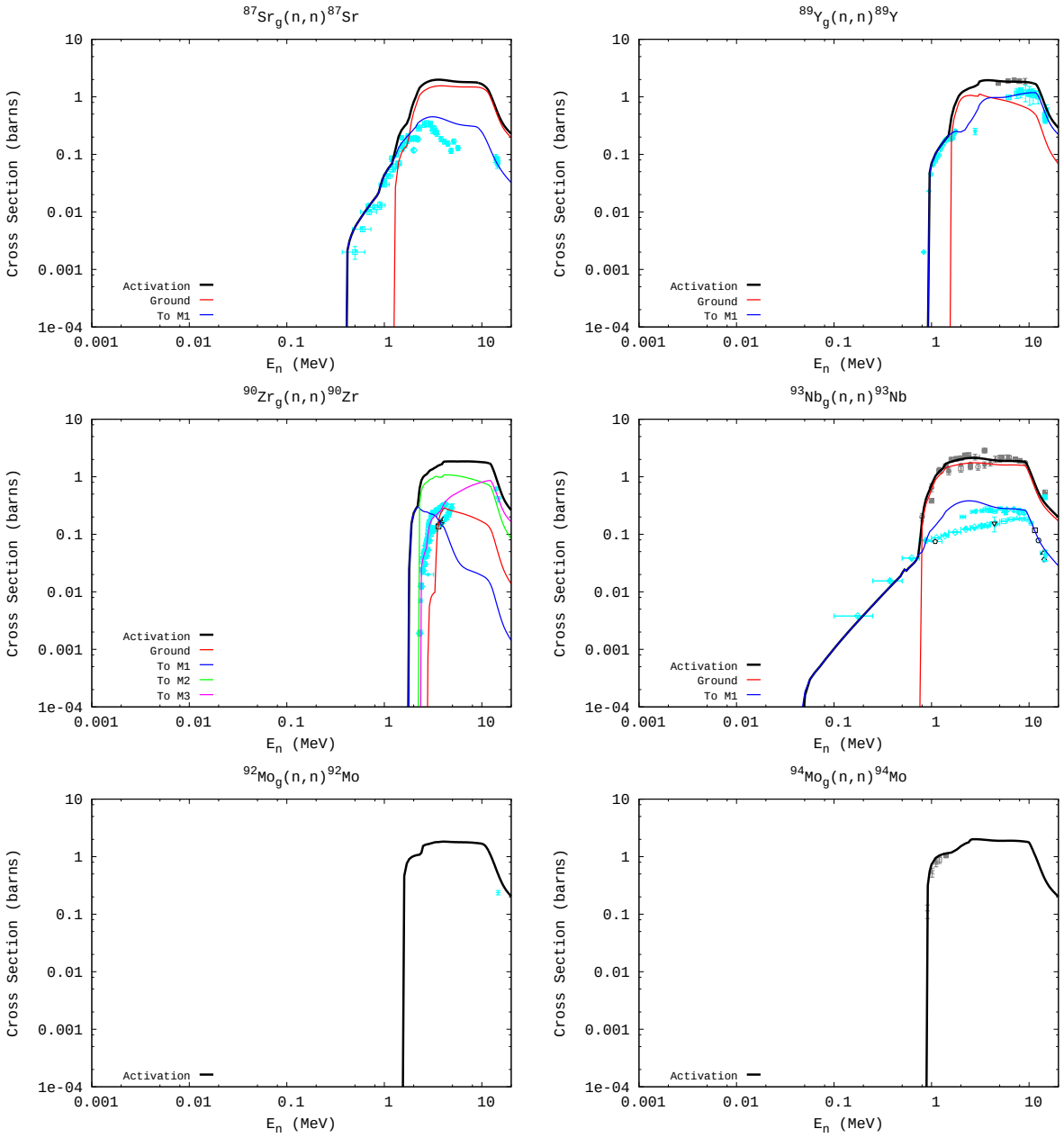

Fig. 29.— Modeled (n,n') cross sections compared to measurement. The data is taken from (EXFOR 2006). The black, red, and blue solid lines represent our modeled cross sections (total, leading to the ground state, and leading to the first isomer, respectively). The Gery, orange, and light blue data points are measured cross section data (total, ground state, and first isomer).

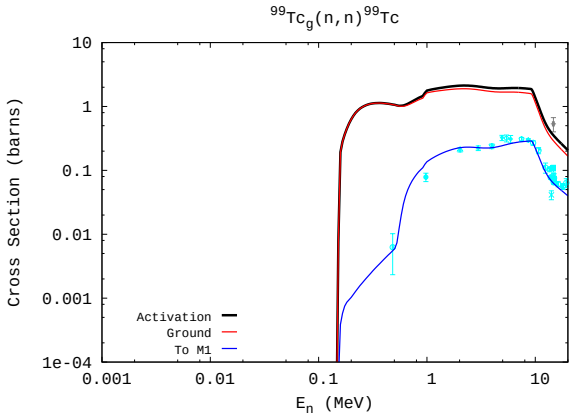

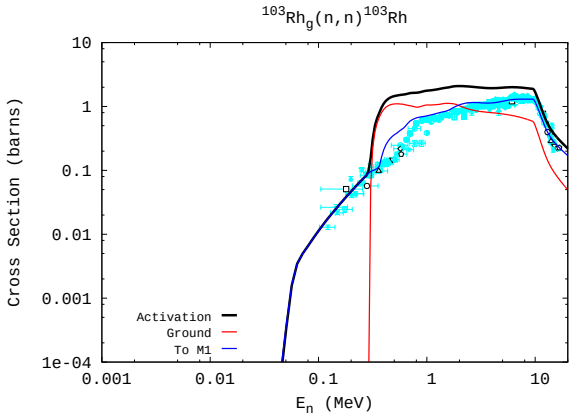

Fig. 29.— (continued)

C.6. (n,p)

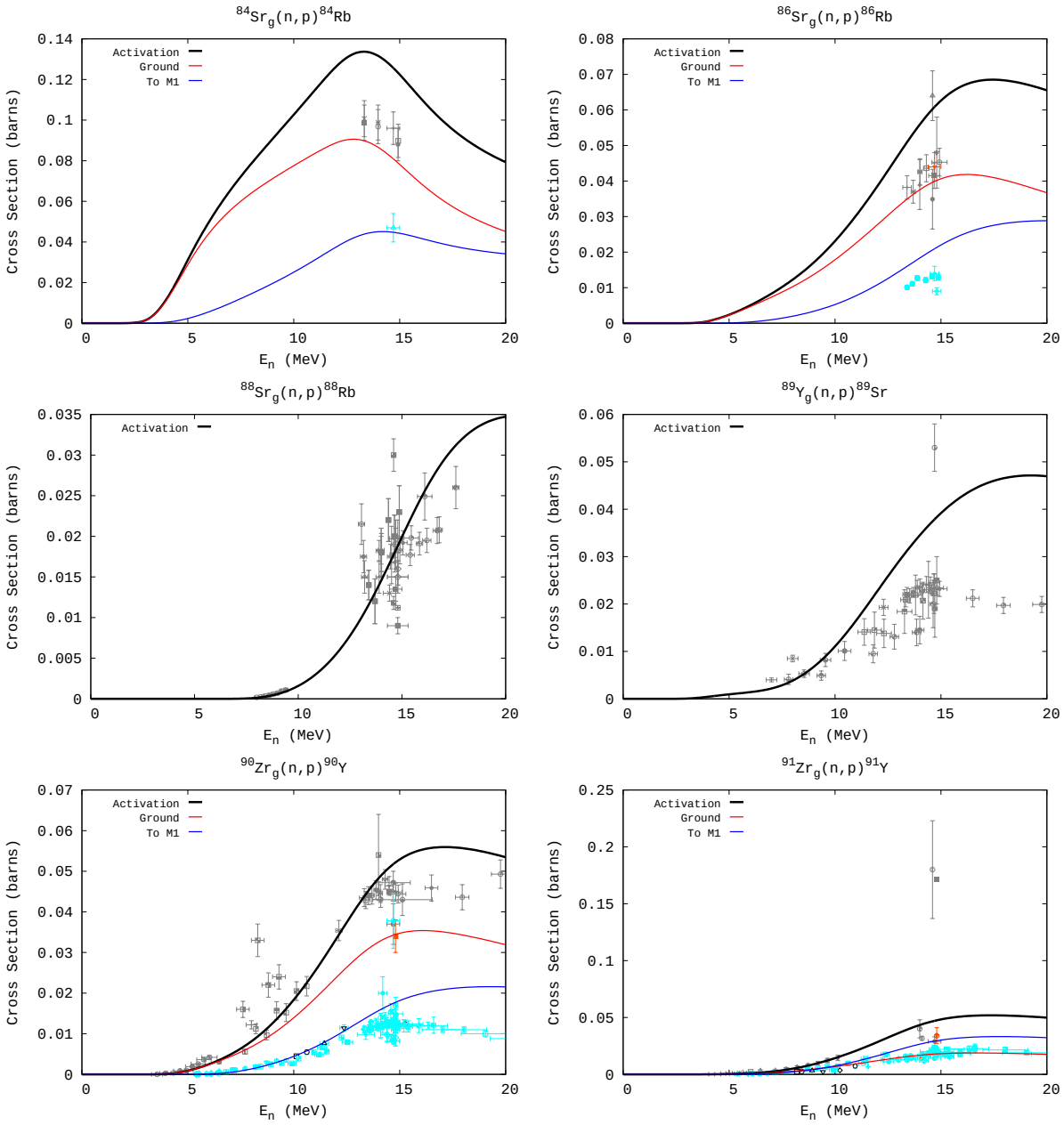

Fig. 30.— Modeled (n,p) cross sections compared to measurement. The data is taken from (EXFOR 2006). The black, red, and blue solid lines represent our modeled cross sections (total, leading to the ground state, and leading to the first isomer, respectively). The Gery, orange, and light blue data points are measured cross section data (total, ground state, and first isomer).

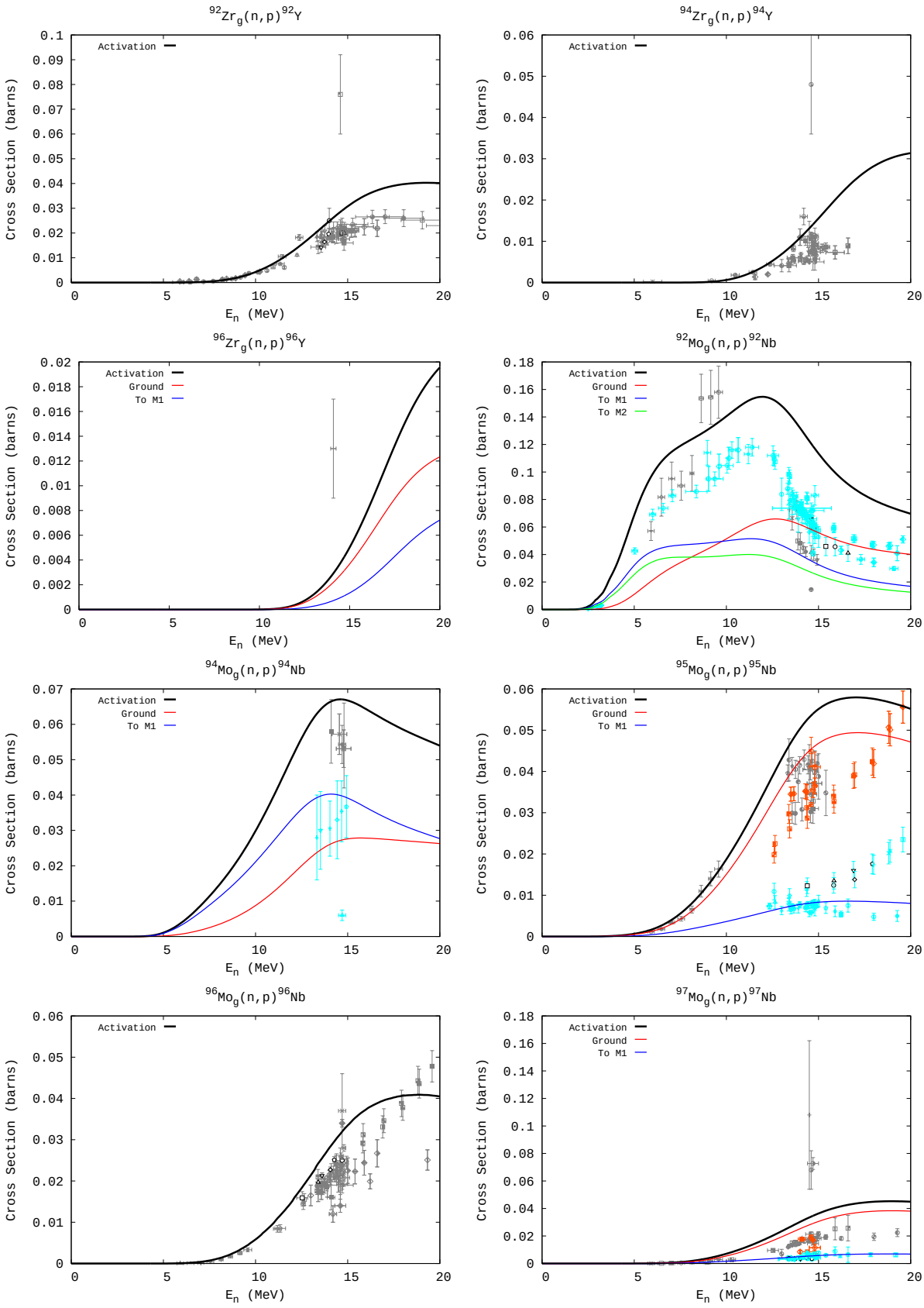

Fig. 30.— (continued)

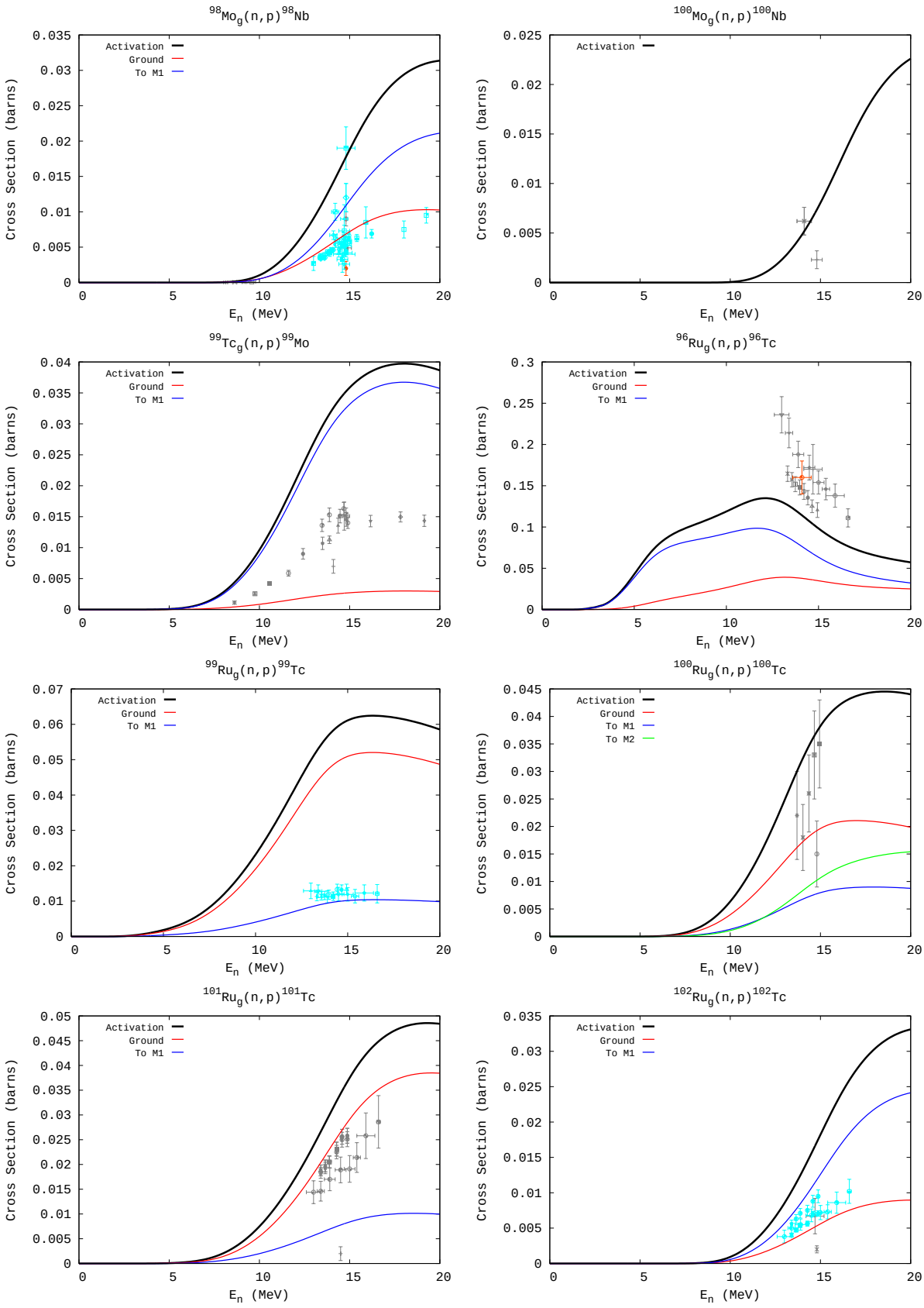

Fig. 30.— (continued)

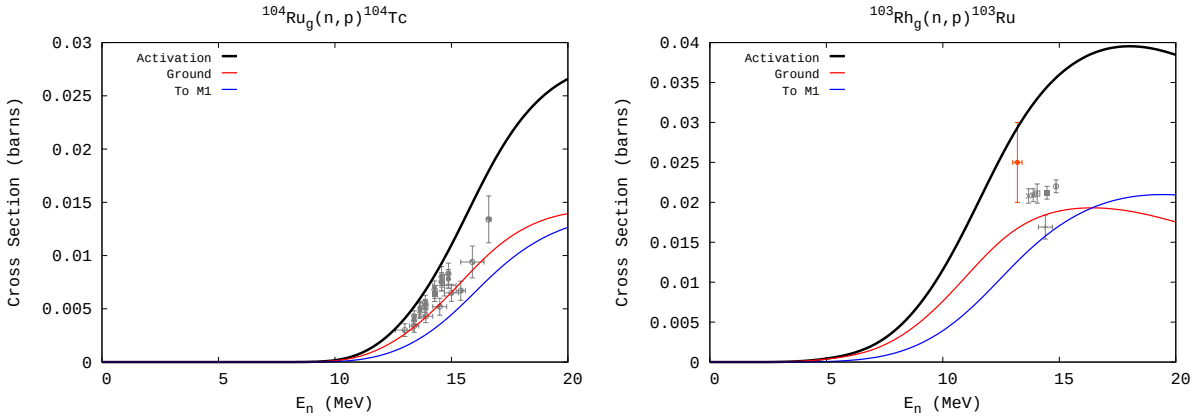

Fig. 30.— (continued)

C.7. (n,np)

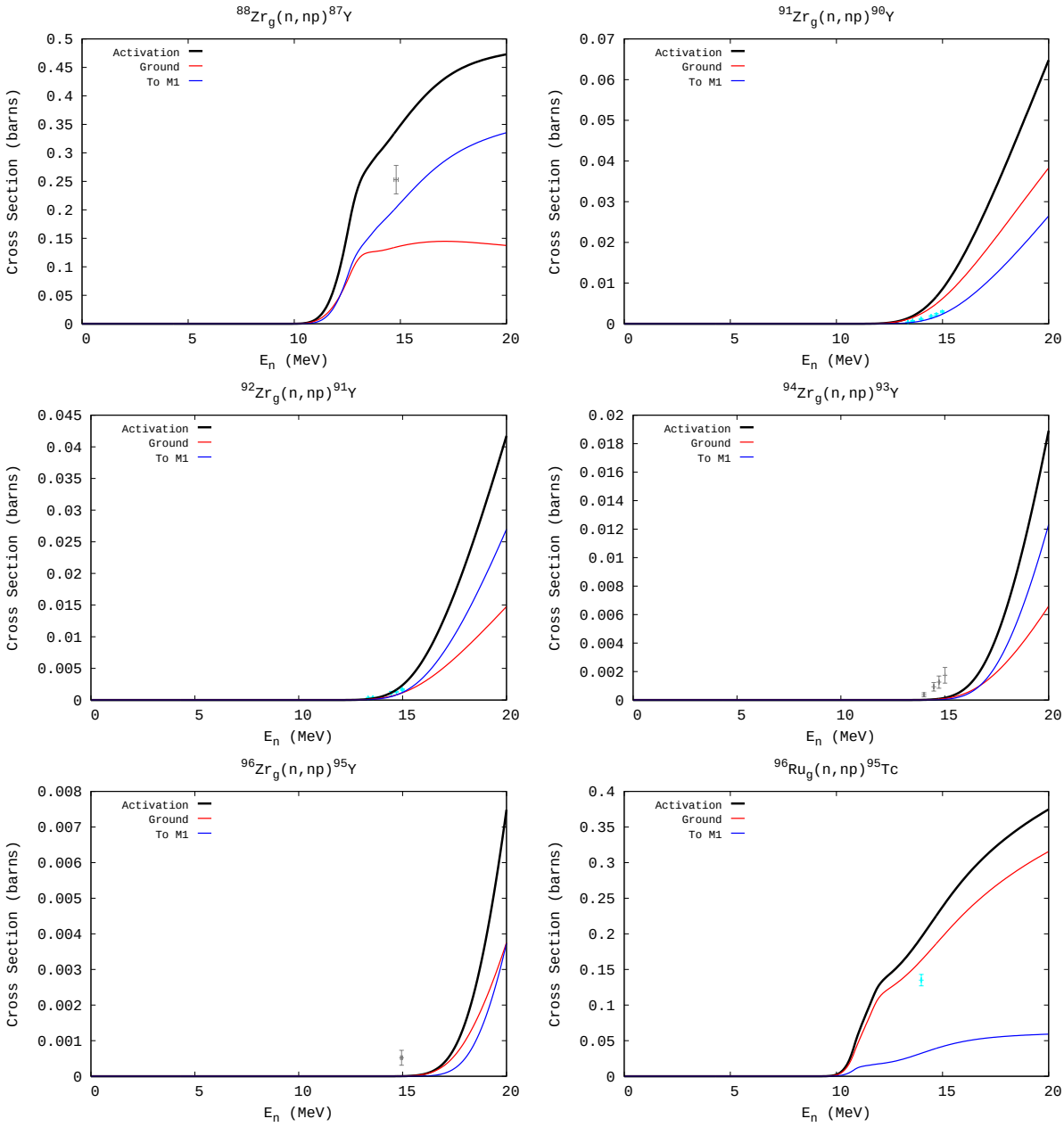

Fig. 31.— Modeled (n,np) cross sections compared to measurement. The data is taken from (EXFOR 2006). The black, red, and blue solid lines represent our modeled cross sections (total, leading to the ground state, and leading to the first isomer, respectively). The Gery, orange, and light blue data points are measured cross section data (total, ground state, and first isomer).

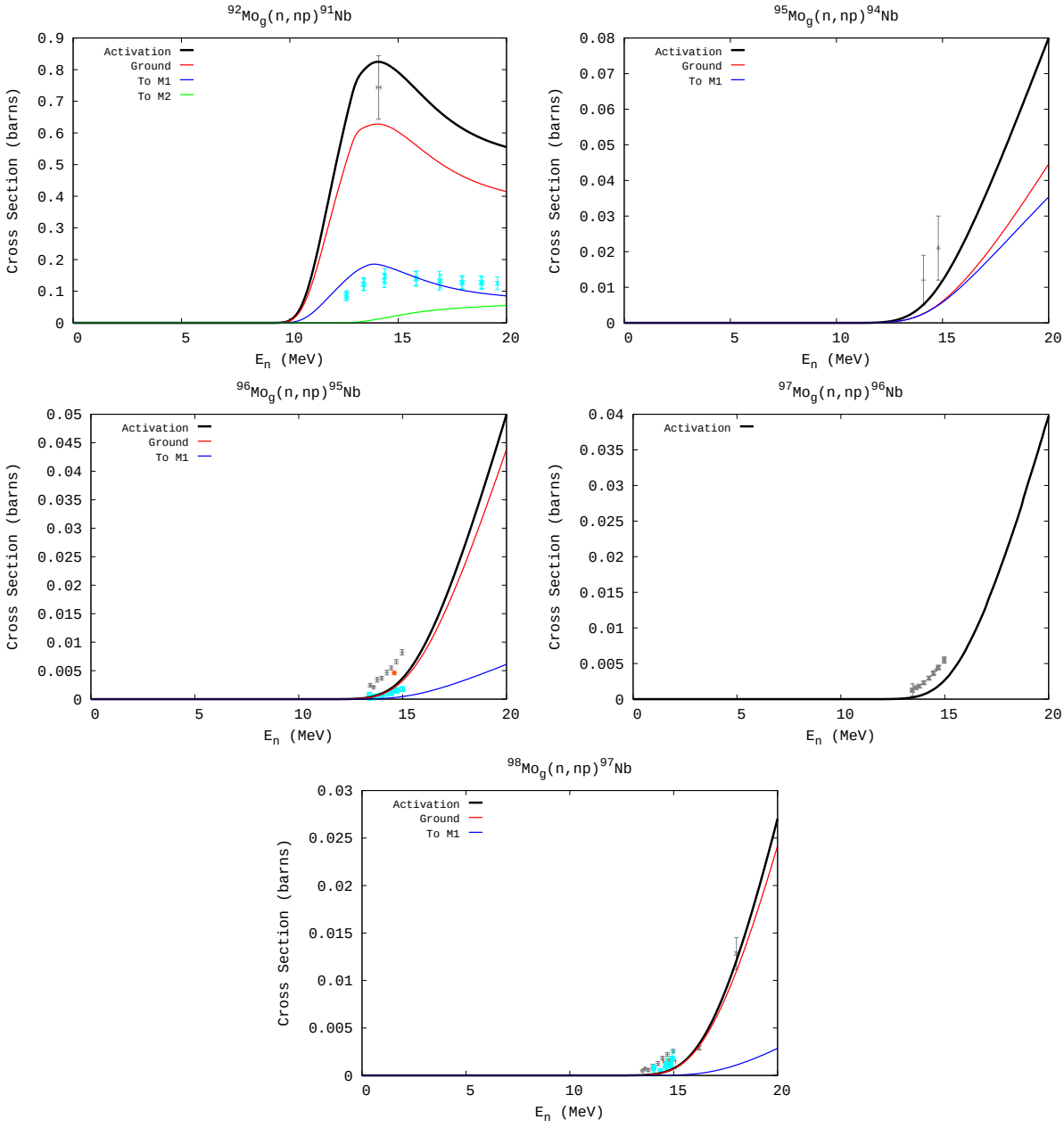

Fig. 31.— (continued)

C.8. (n,α)

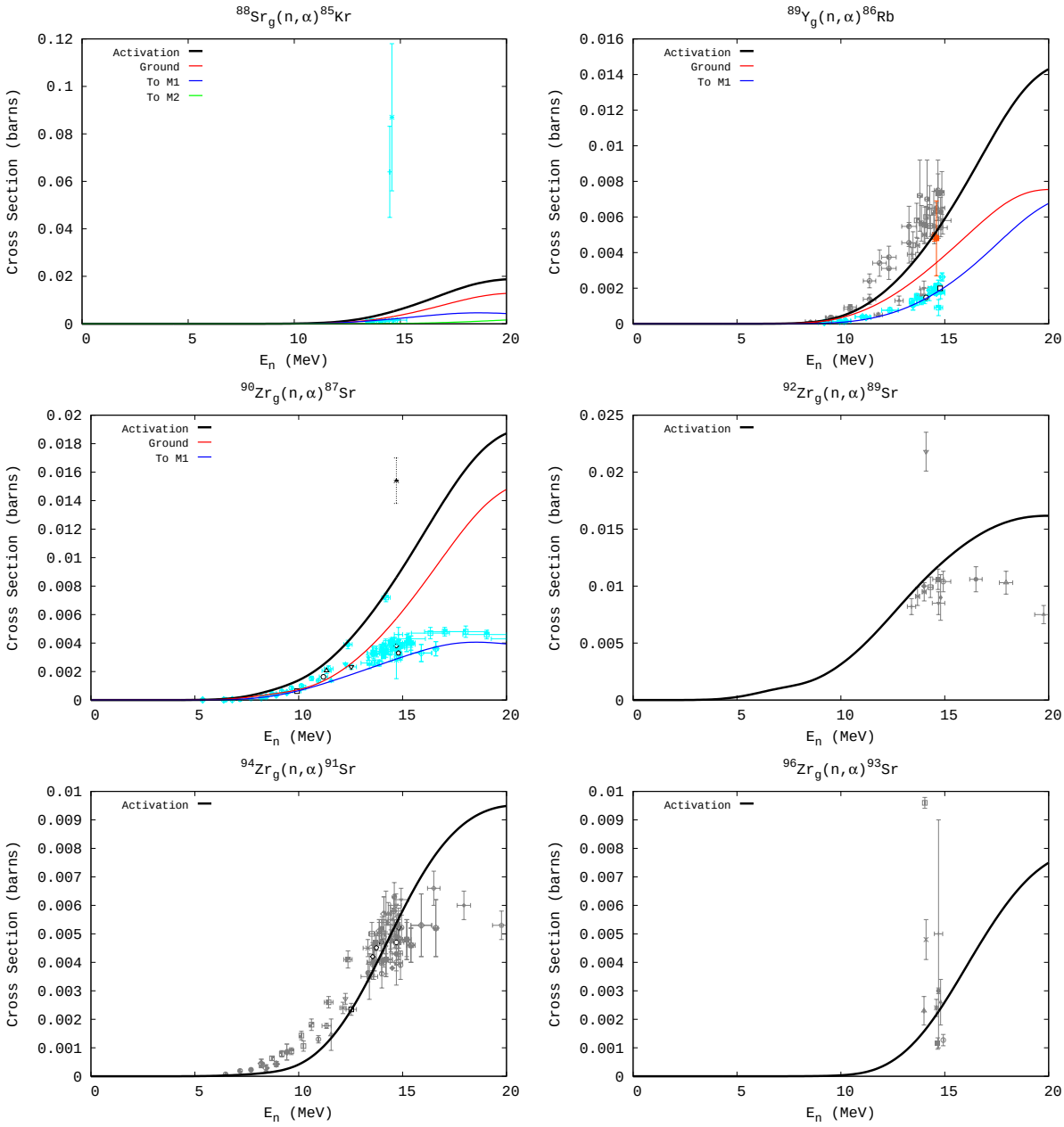

Fig. 32.— Modeled (n,α) cross sections compared to measurement. The data is taken from (EXFOR 2006). The black, red, and blue solid lines represent our modeled cross sections (total, leading to the ground state, and leading to the first isomer, respectively). The Gery, orange, and light blue data points are measured cross section data (total, ground state, and first isomer).

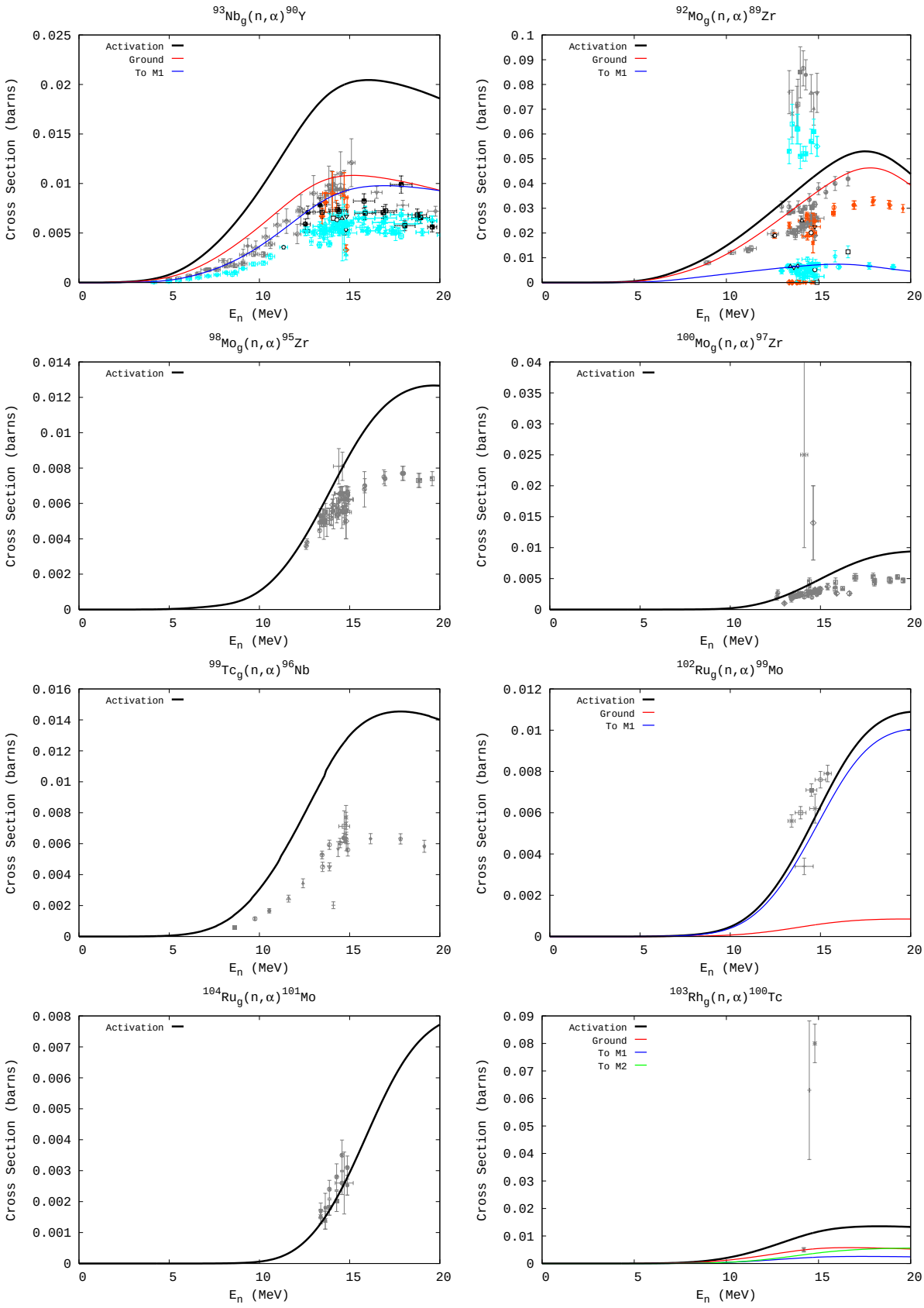

Fig. 32.— (continued)

C.9. (n,nα)

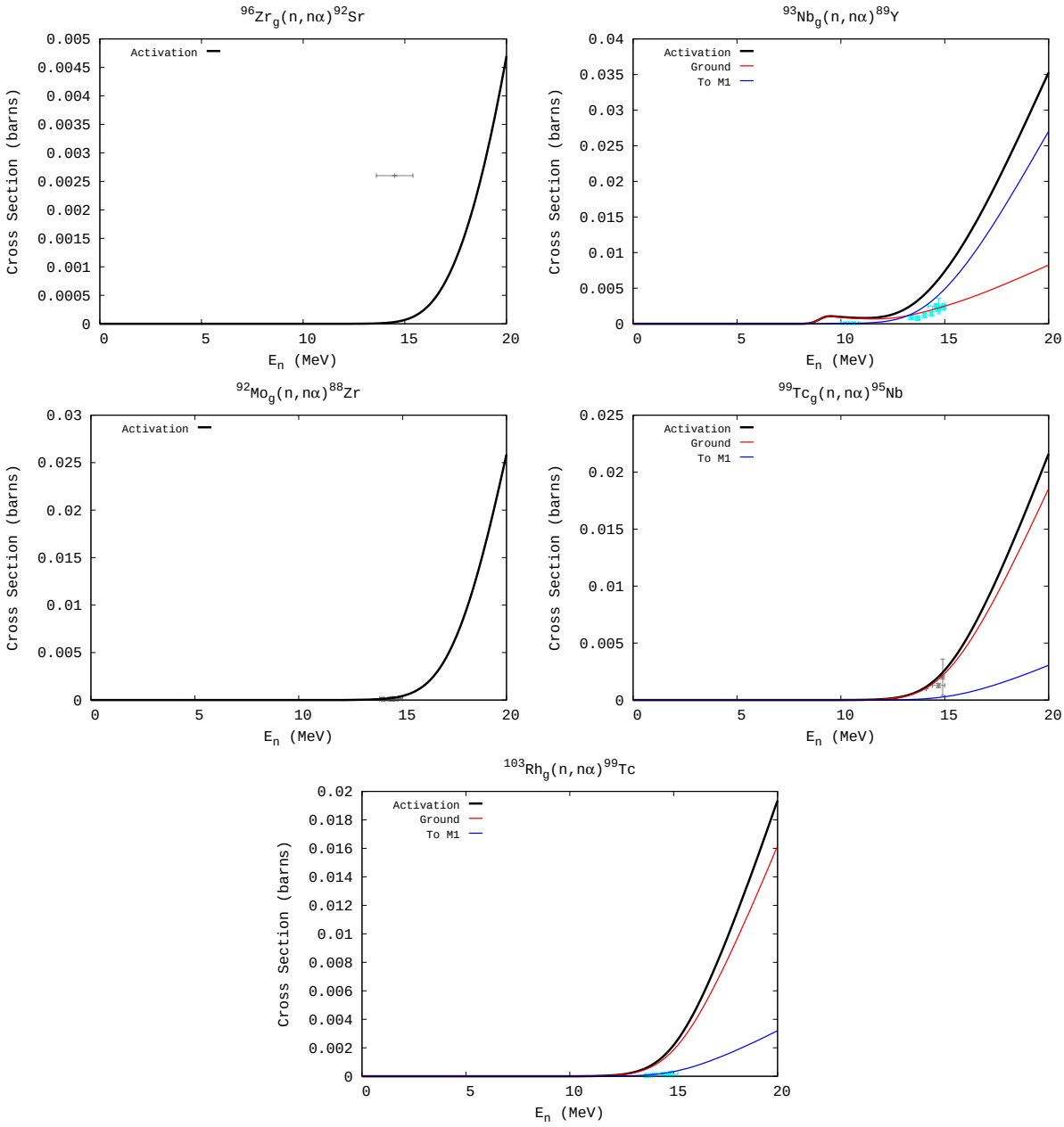

Fig. 33.— Modeled (n,nα) cross sections compared to measurement. The data is taken from (EXFOR 2006). The black, red, and blue solid lines represent our modeled cross sections (total, leading to the ground state, and leading to the first isomer, respectively). The Gery, orange, and light blue data points are measured cross section data (total, ground state, and first isomer).

C.10. (n,d)

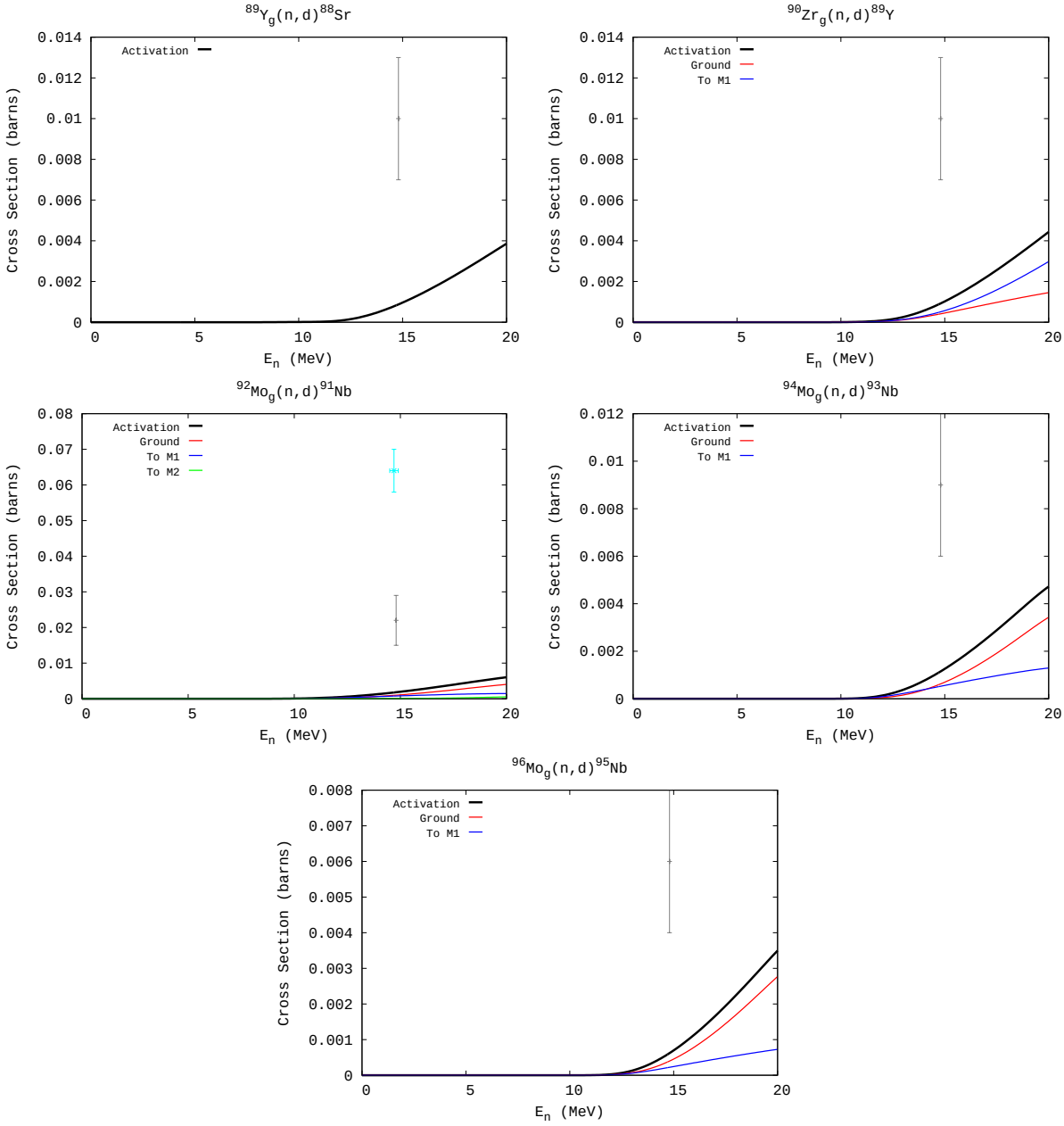

Fig. 34.— Modeled (n,d) cross sections compared to measurement. The data is taken from (EXFOR 2006). The black, red, and blue solid lines represent our modeled cross sections (total, leading to the ground state, and leading to the first isomer, respectively). The Gery, orange, and light blue data points are measured cross section data (total, ground state, and first isomer).

C.11. (p,n)

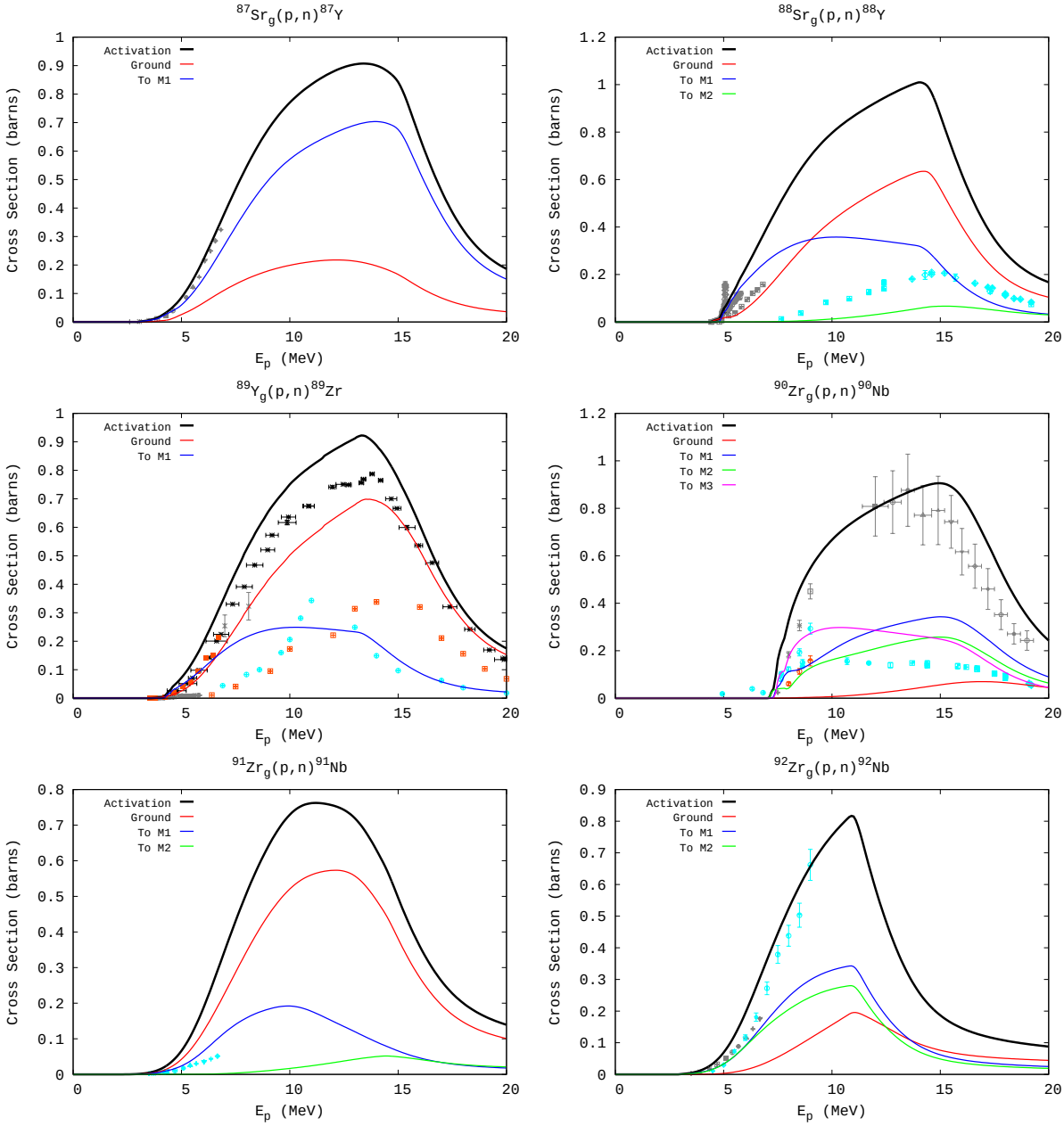

Fig. 35.— Modeled (p,n) cross sections compared to measurement. The data is taken from (EXFOR 2006). The black, red, and blue solid lines represent our modeled cross sections (total, leading to the ground state, and leading to the first isomer, respectively). The Gray, orange, and light blue data points are measured cross section data (total, ground state, and first isomer).

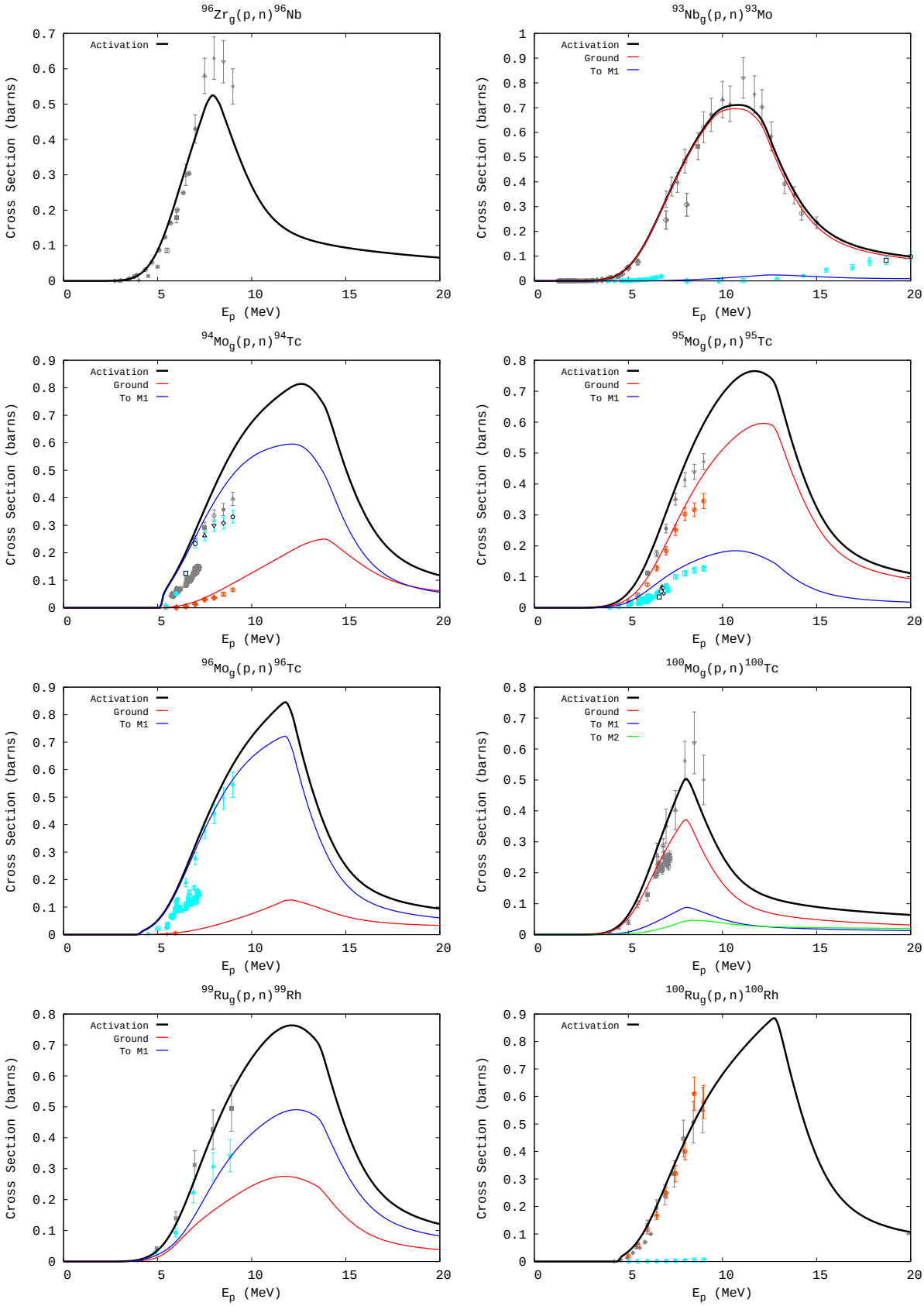

Fig. 35.— (continued)

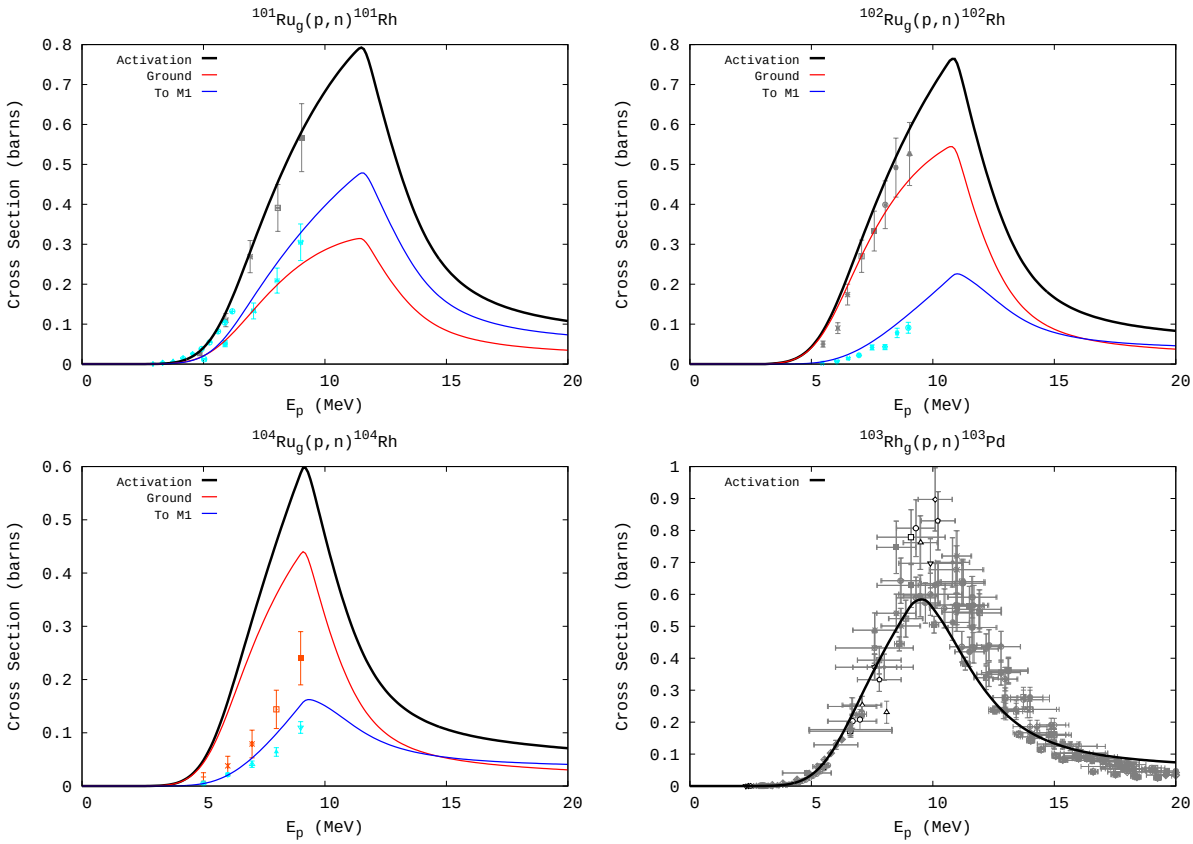

Fig. 35.— (continued)

C.12. (p,2n)

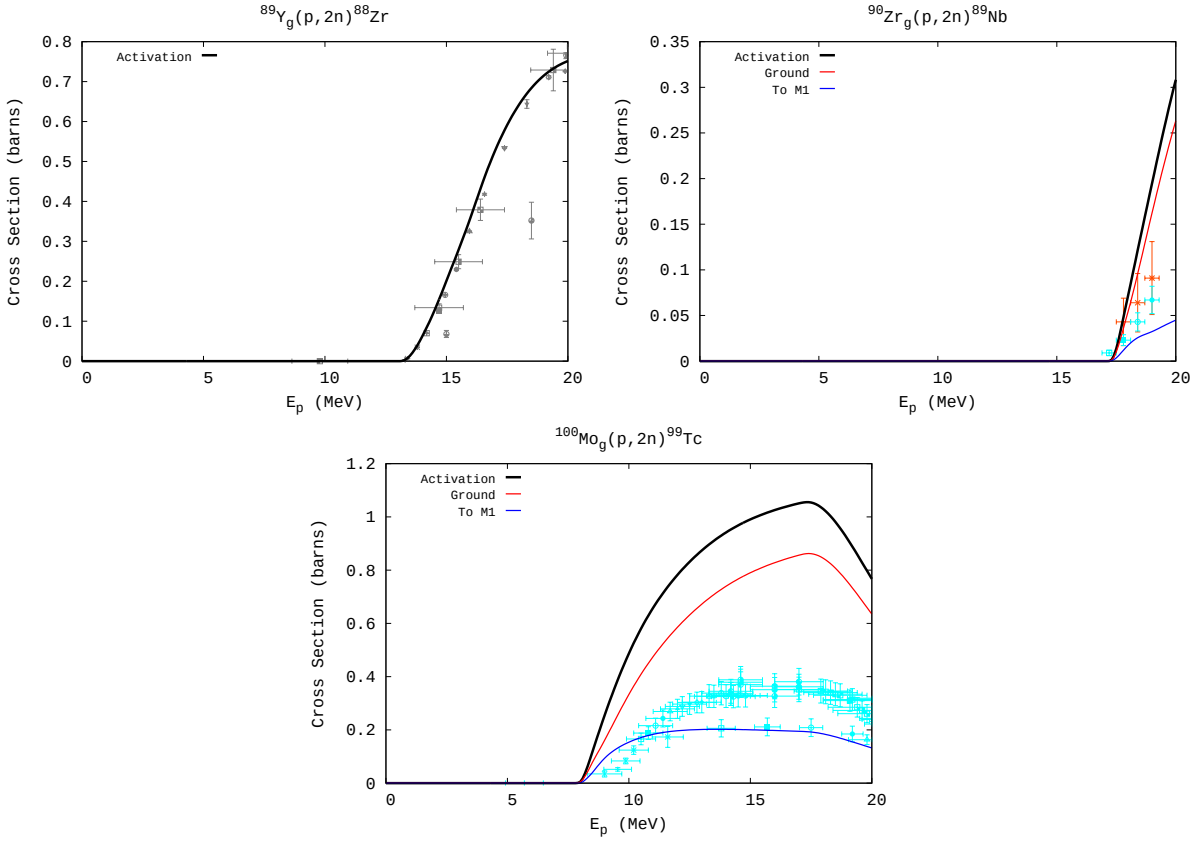

Fig. 36.— Modeled (p,2n) cross sections compared to measurement. The data is taken from (EXFOR 2006). The black, red, and blue solid lines represent our modeled cross sections (total, leading to the ground state, and leading to the first isomer, respectively). The Rey, orange, and light blue data points are measured cross section data (total, ground state, and first isomer).

C.13. (p,np)

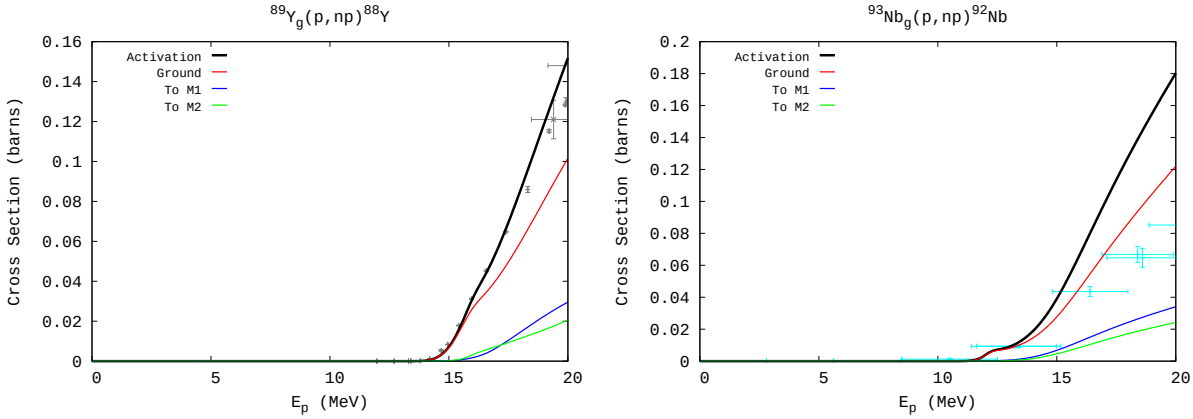

Fig. 37.— Modeled (p,np) cross sections compared to measurement. The data is taken from (EXFOR 2006). The black, red, and blue solid lines represent our modeled cross sections (total, leading to the ground state, and leading to the first isomer, respectively). The Frey, orange, and light blue data points are measured cross section data (total, ground state, and first isomer).

C.14. (p,p')

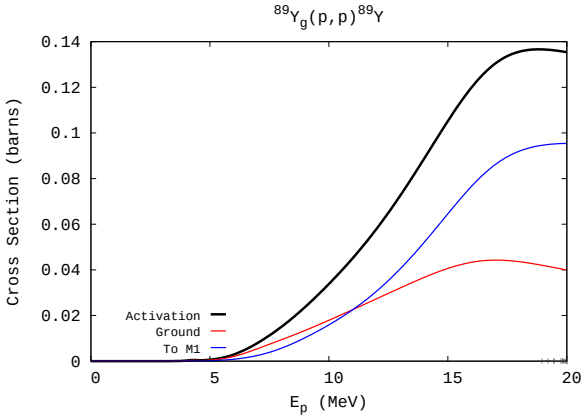

Fig. 38.— Modeled (p,p') cross sections compared to measurement. The data is taken from (EXFOR 2006). The black, red, and blue solid lines represent our modeled cross sections (total, leading to the ground state, and leading to the first isomer, respectively). The Gorey, orange, and light blue data points are measured cross section data (total, ground state, and first isomer).

C.15. (p,γ)

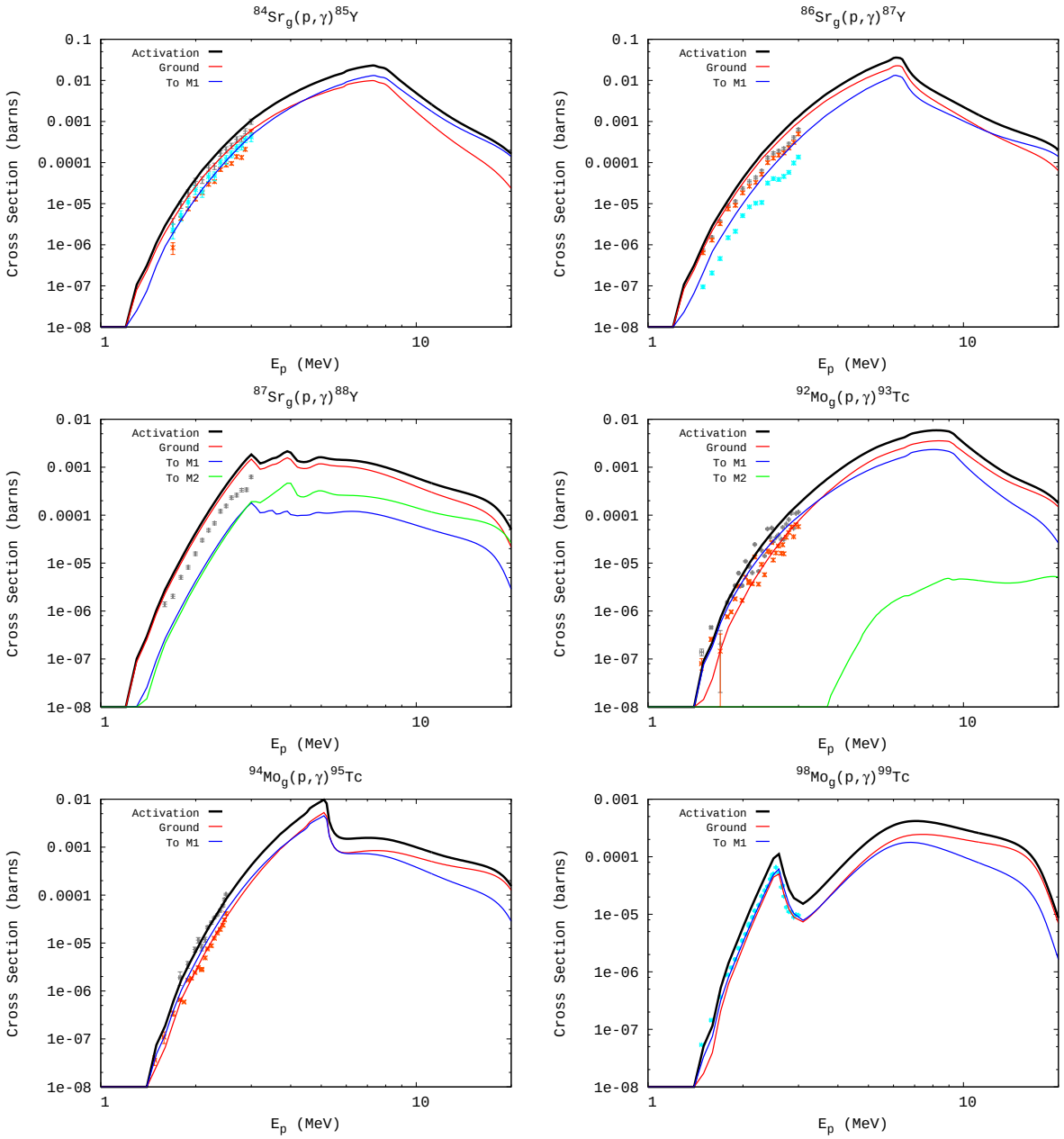

Fig. 39.— Modeled (p,γ) cross sections compared to measurement. The data is taken from (EXFOR 2006). The black, red, and blue solid lines represent our modeled cross sections (total, leading to the ground state, and leading to the first isomer, respectively). The Garey, orange, and light blue data points are measured cross section data (total, ground state, and first isomer).

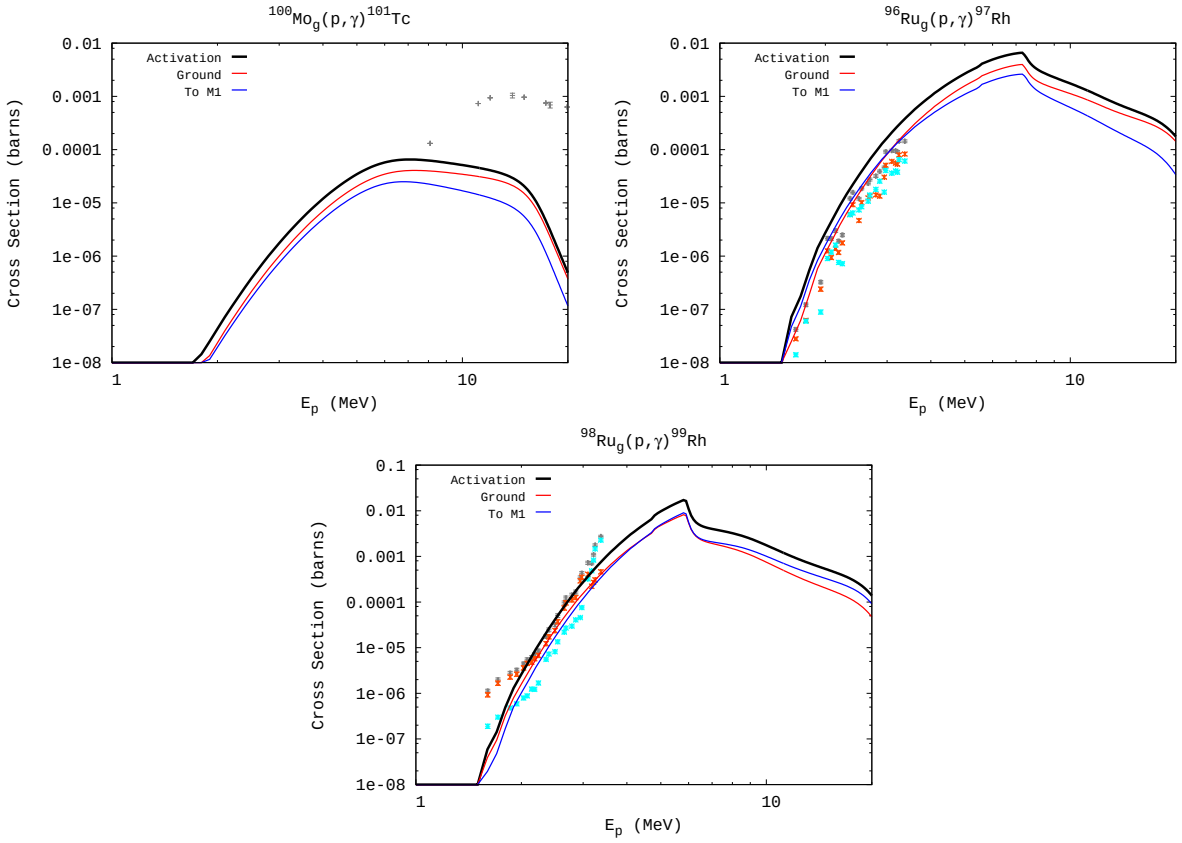

Fig. 39.— (continued)

C.16. (d,n)

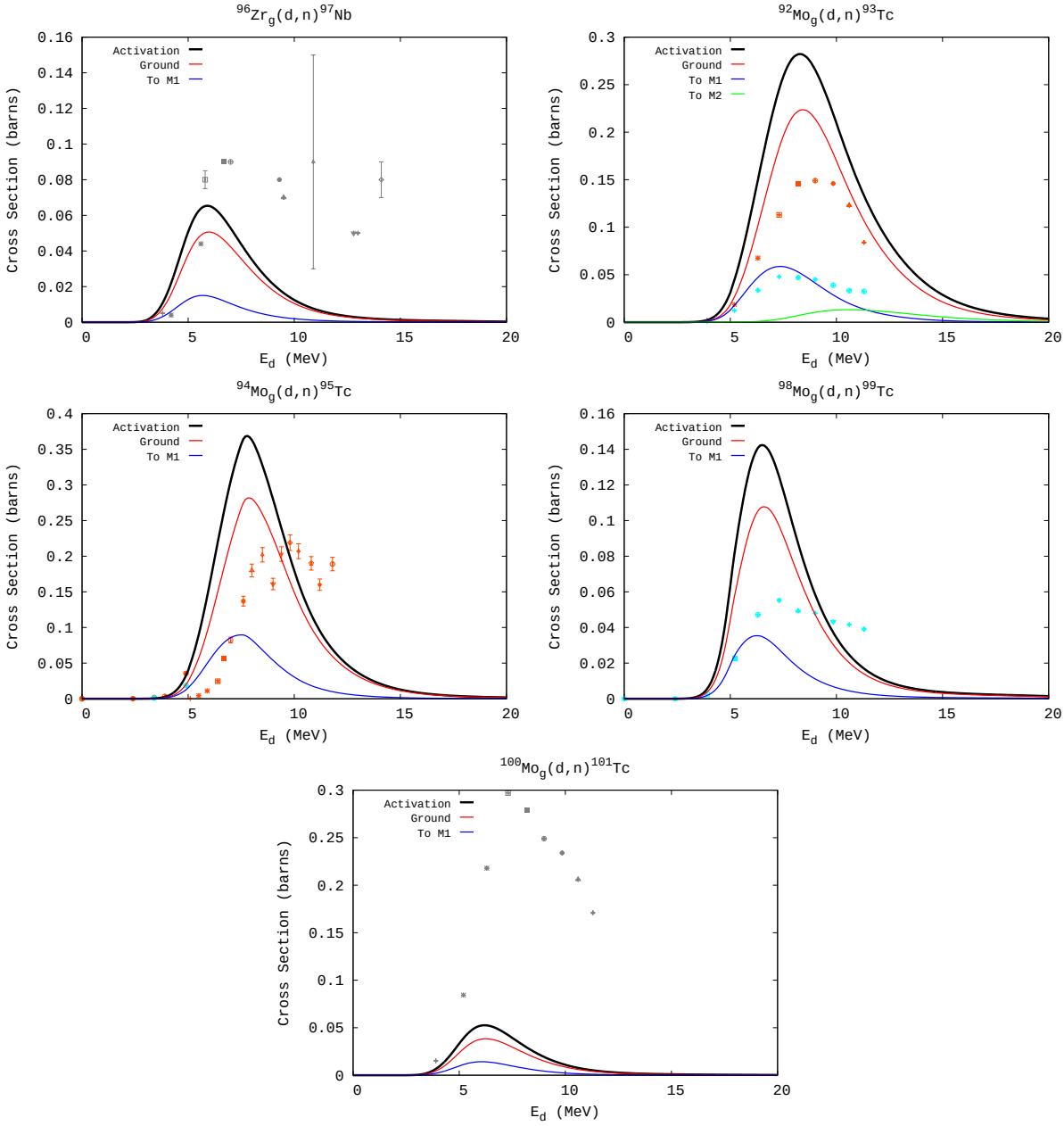

Fig. 40.— Modeled (d,n) cross sections compared to measurement. The data is taken from (EXFOR 2006). The black, red, and blue solid lines represent our modeled cross sections (total, leading to the ground state, and leading to the first isomer, respectively). The Gery, orange, and light blue data points are measured cross section data (total, ground state, and first isomer).

C.17. (d,2n)

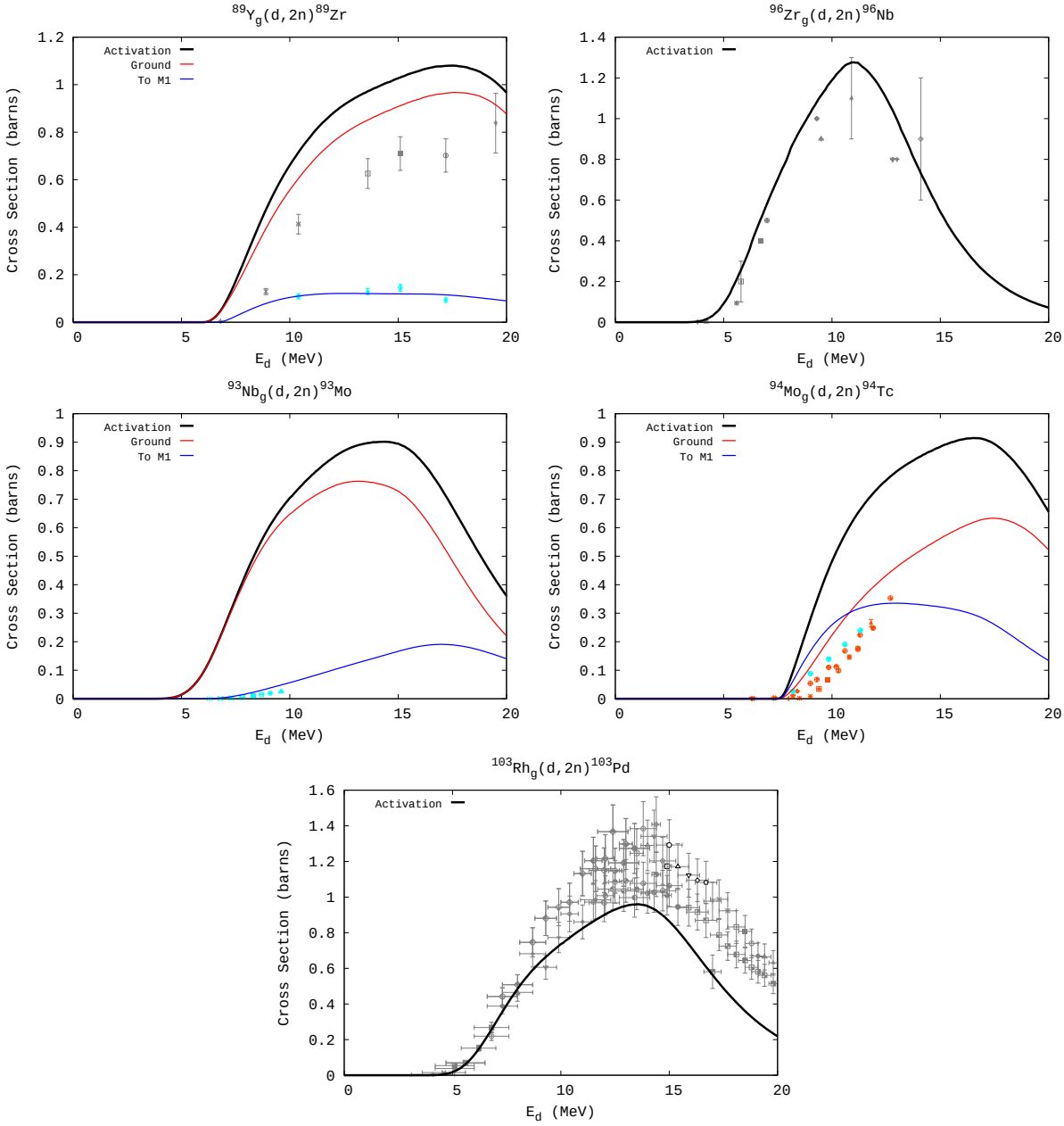

Fig. 41.— Modeled (d,2n) cross sections compared to measurement. The data is taken from (EXFOR 2006). The black, red, and blue solid lines represent our modeled cross sections (total, leading to the ground state, and leading to the first isomer, respectively). The Gery, orange, and light blue data points are measured cross section data (total, ground state, and first isomer).

C.18. (d,3n)

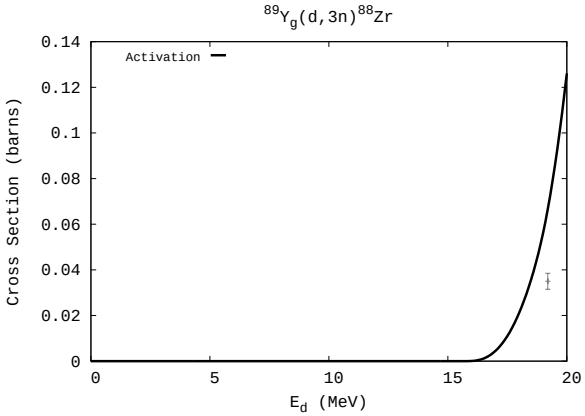

Fig. 42.— Modeled (d,3n) cross sections compared to measurement. The data is taken from (EXFOR 2006). The black, red, and blue solid lines represent our modeled cross sections (total, leading to the ground state, and leading to the first isomer, respectively). The Gery, orange, and light blue data points are measured cross section data (total, ground state, and first isomer).

C.19. (d,p)

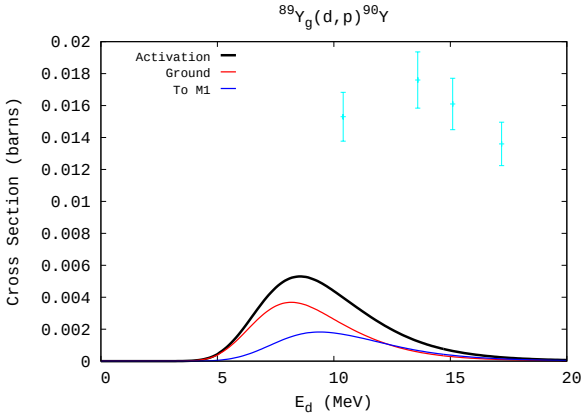

Fig. 43.— Modeled (d,p) cross sections compared to measurement. The data is taken from (EXFOR 2006). The black, red, and blue solid lines represent our modeled cross sections (total, leading to the ground state, and leading to the first isomer, respectively). The Gery, orange, and light blue data points are measured cross section data (total, ground state, and first isomer).

D. Activation Cross Sections by Target

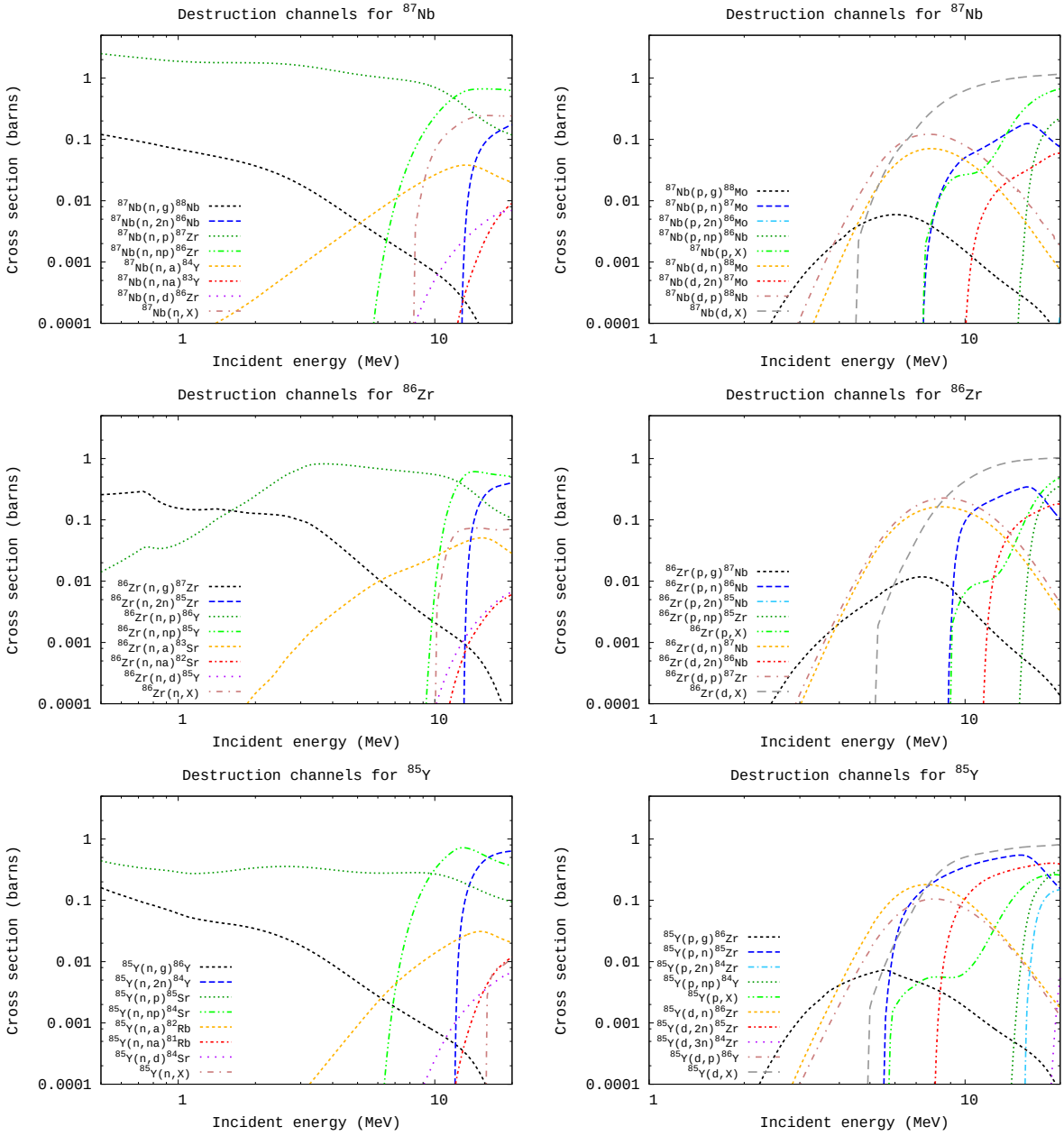

Fig. 44.— Activation cross sections for N=46 ground state targets of Y, Zr, and Nb.

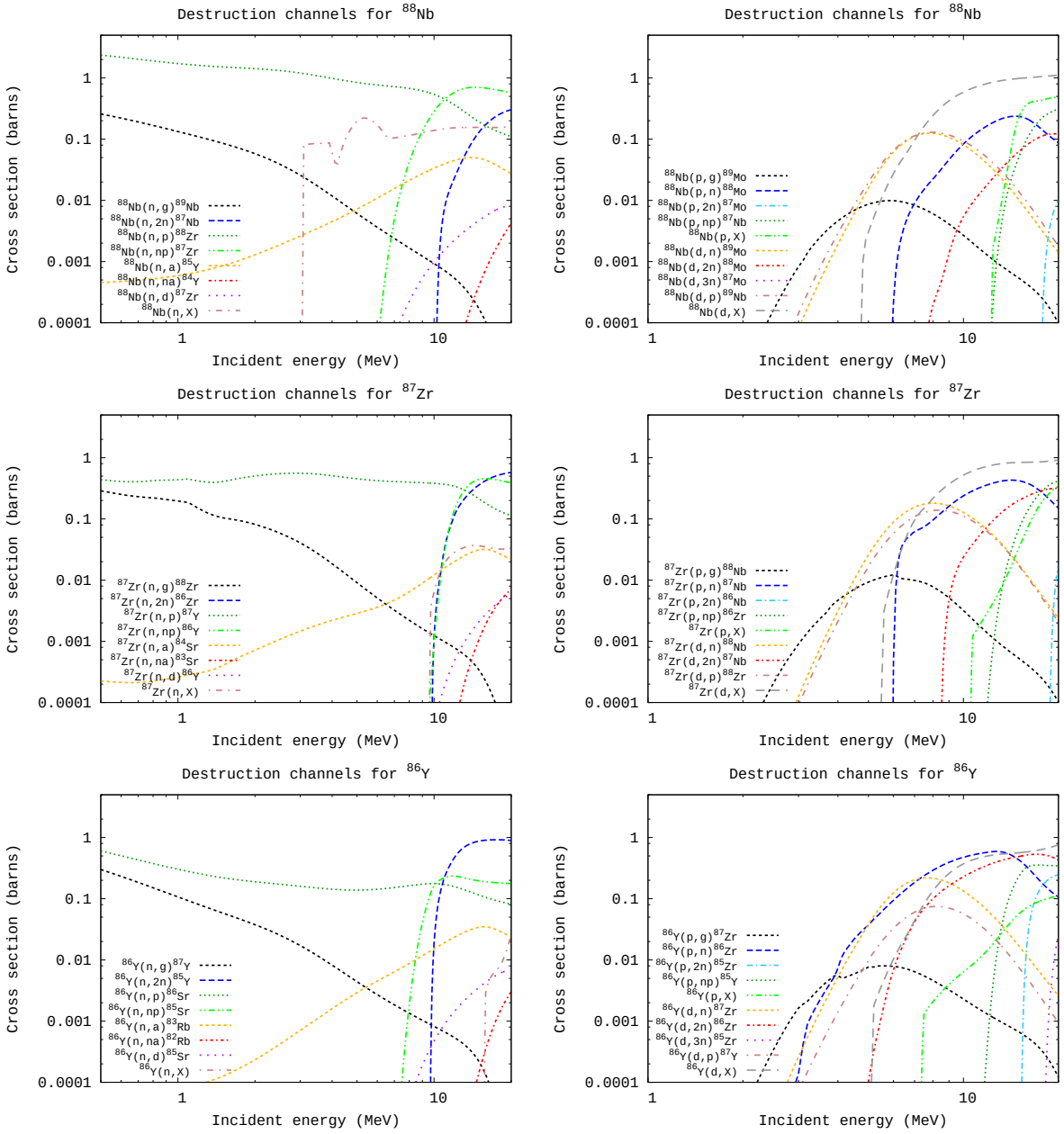

Fig. 45.— Activation cross sections for N=47 ground state targets of Y, Zr, and Nb.

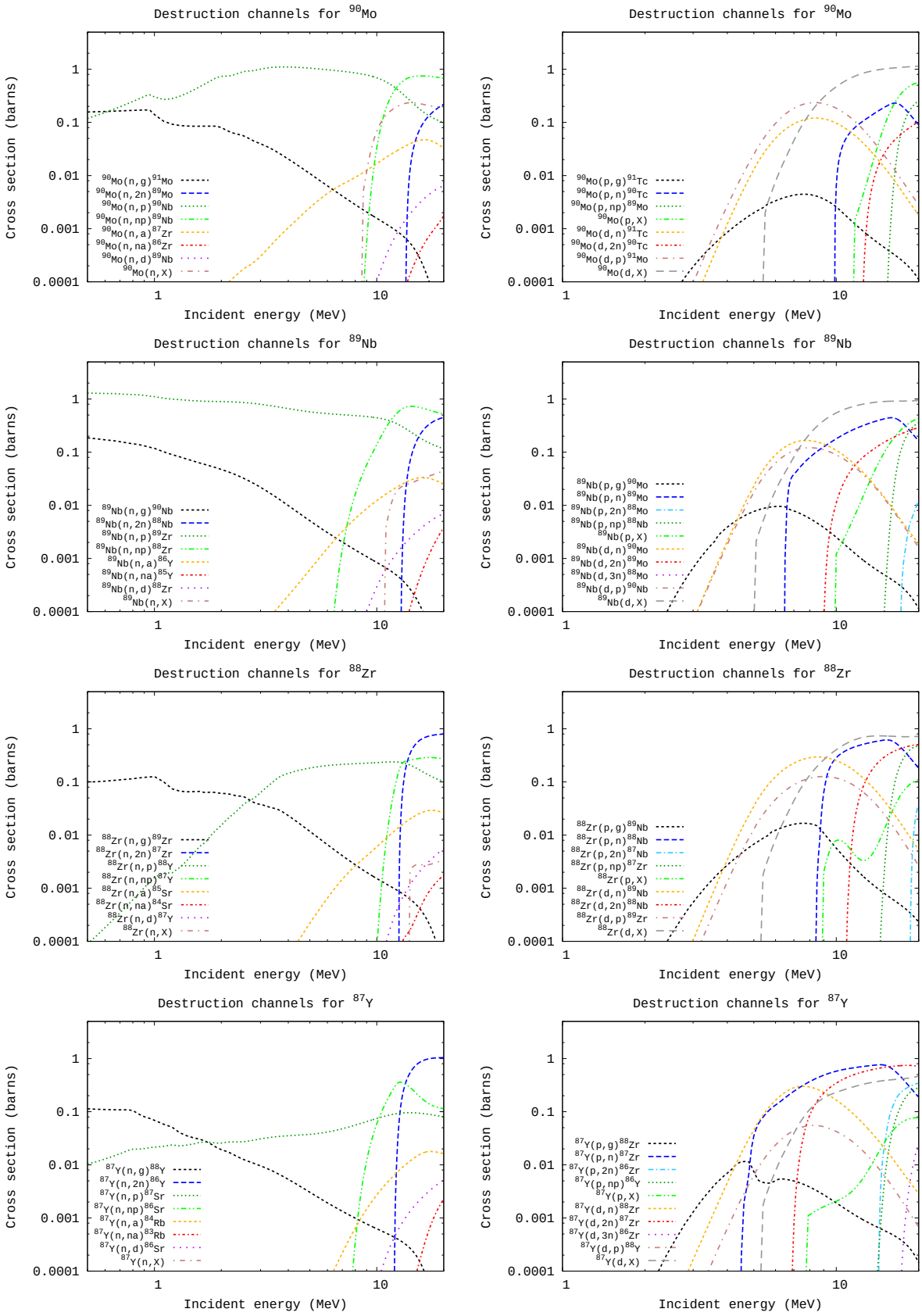

Fig. 46.— Activation cross sections for N=48 ground state targets of Y, Zr, Nb, and Mo.

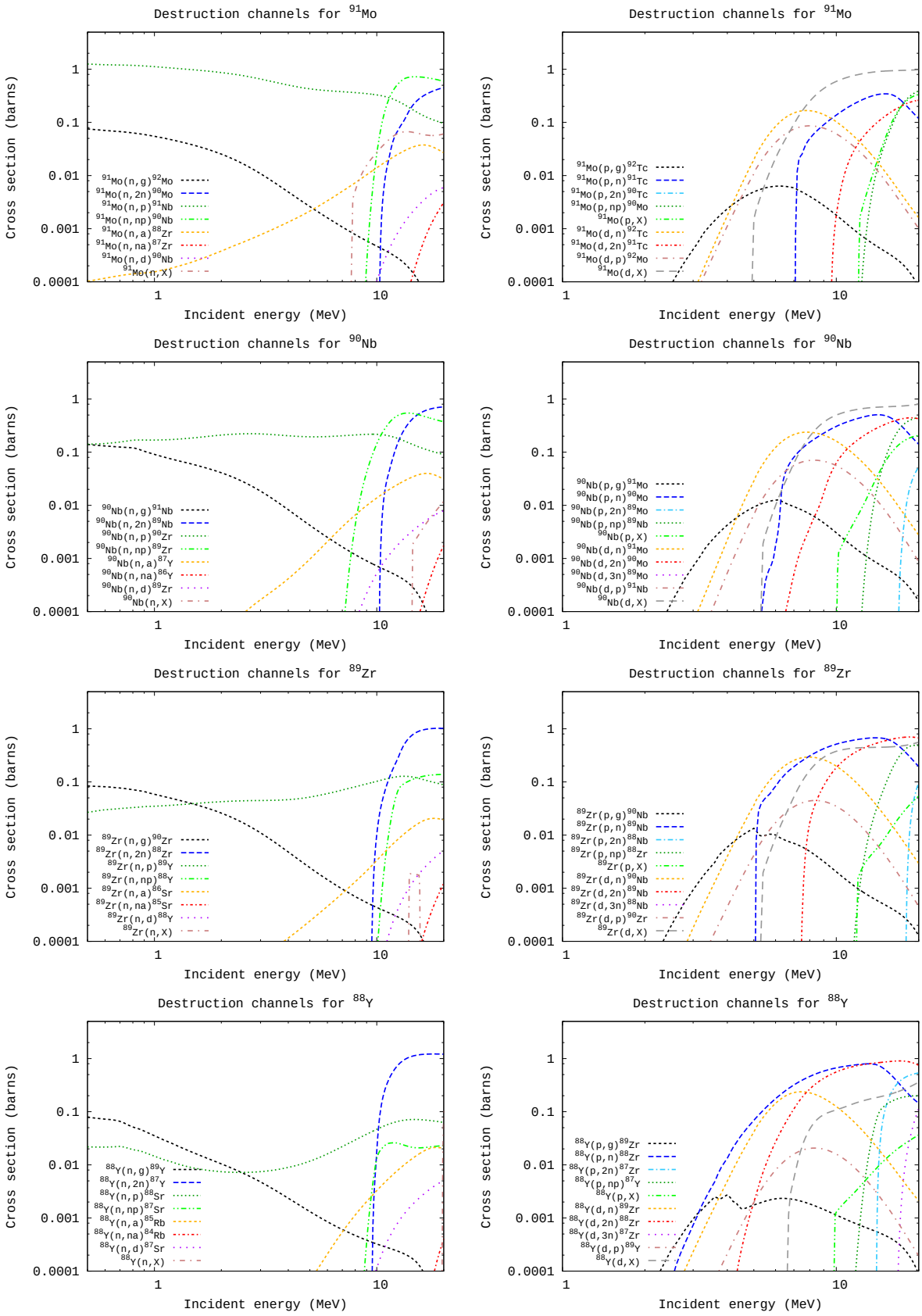

Fig. 47.— Activation cross sections for N=49 ground state targets of Y, Zr, Nb, and Mo.

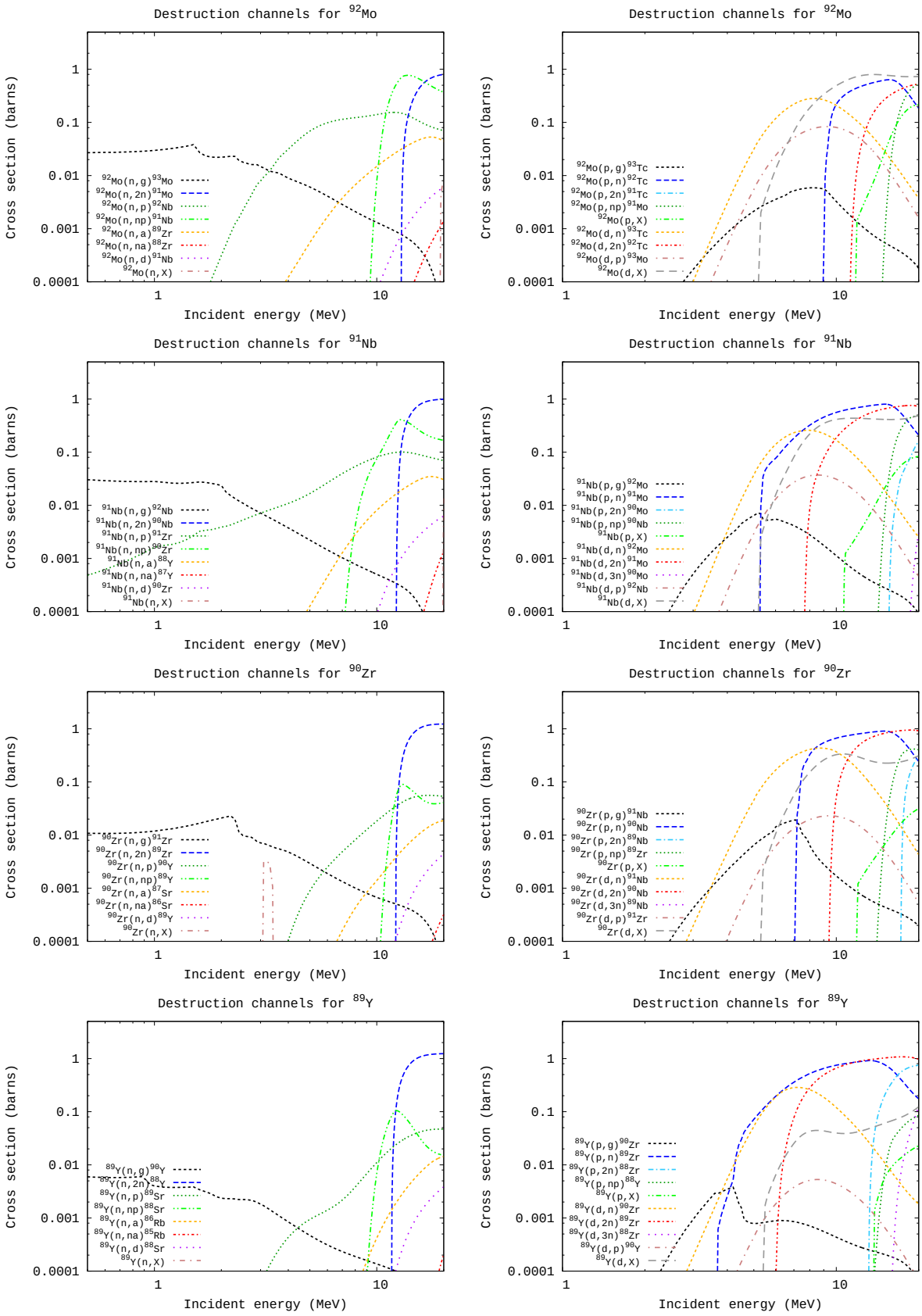

Fig. 48.— Activation cross sections for N=50 ground state targets of Y, Zr, Nb, and Mo.

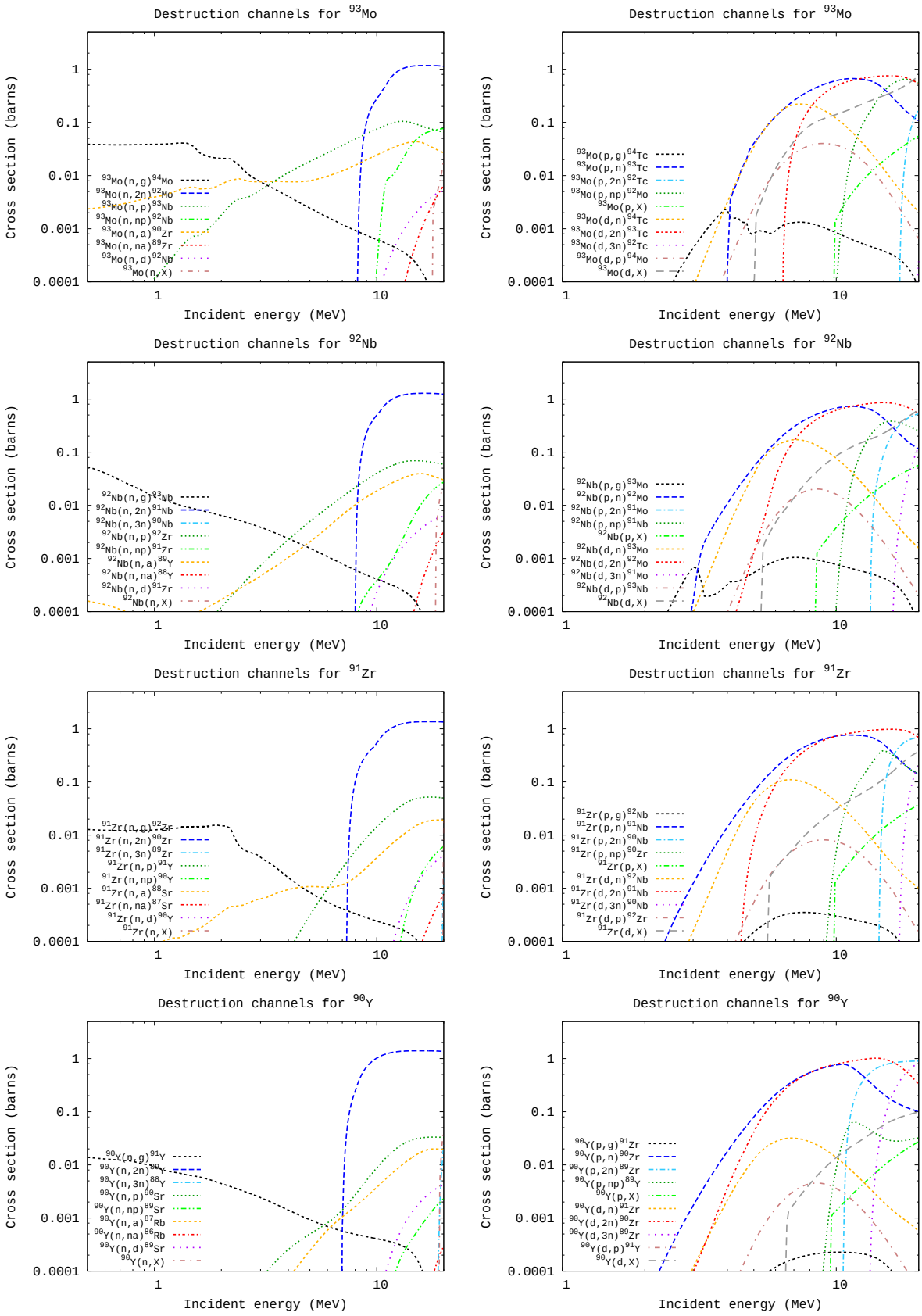

Fig. 49.— Activation cross sections for N=51 ground state targets of Y, Zr, Nb, and Mo.

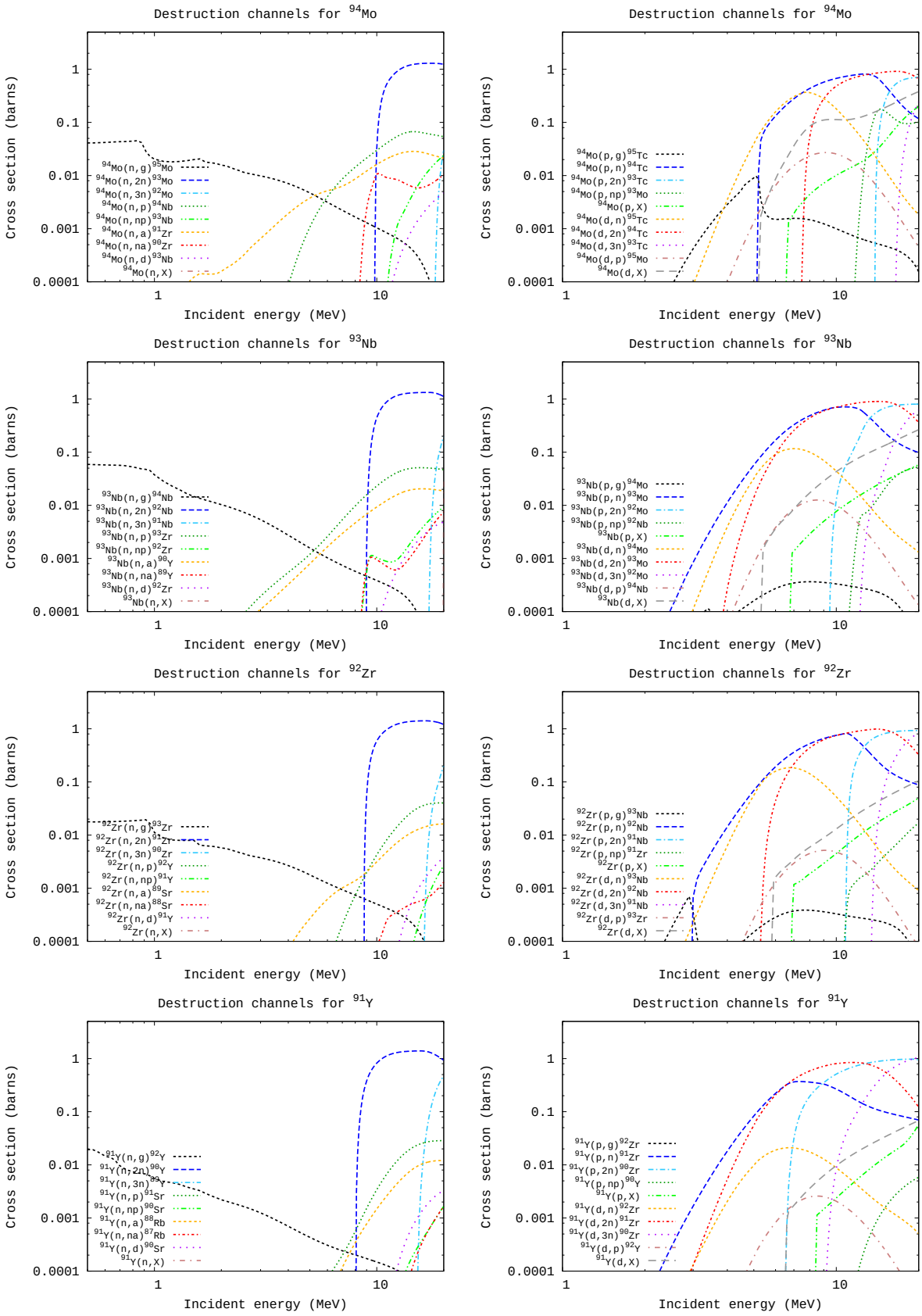

Fig. 50.— Activation cross sections for N=52 ground state targets of Y, Zr, Nb, and Mo.

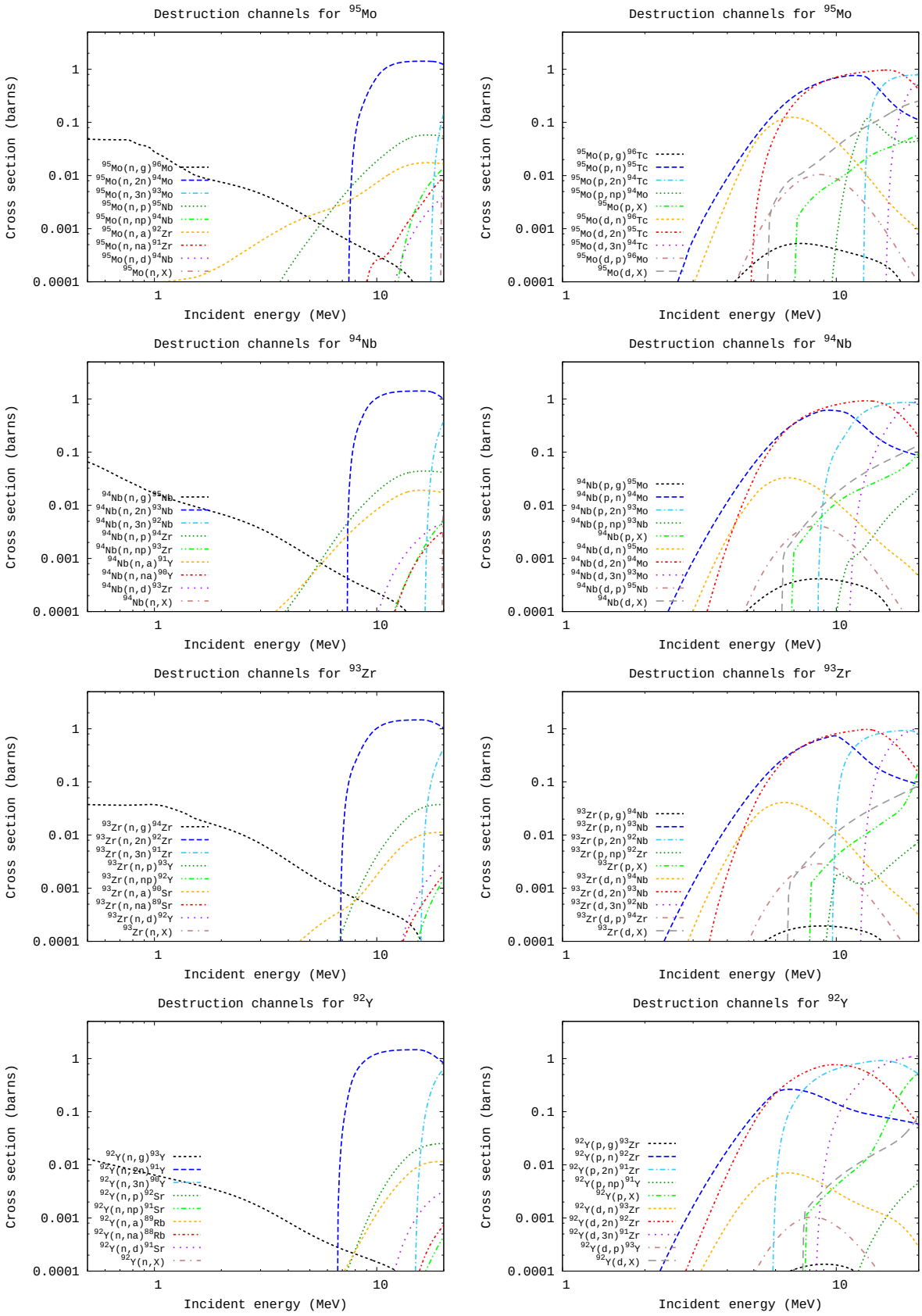

Fig. 51.— Activation cross sections for N=53 ground state targets of Y, Zr, Nb, and Mo.

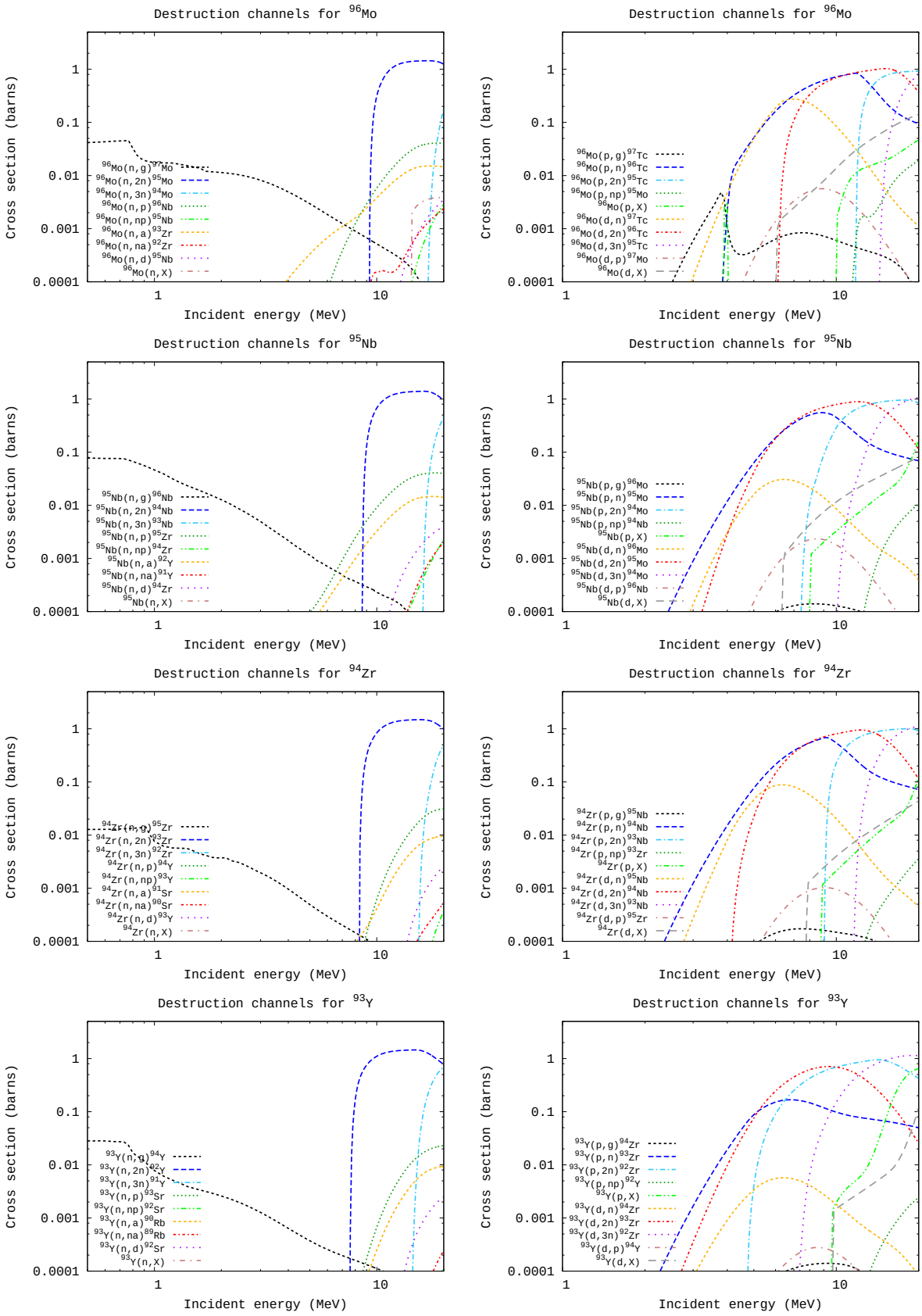

Fig. 52.— Activation cross sections for N=54 ground state targets of Y, Zr, Nb, and Mo.

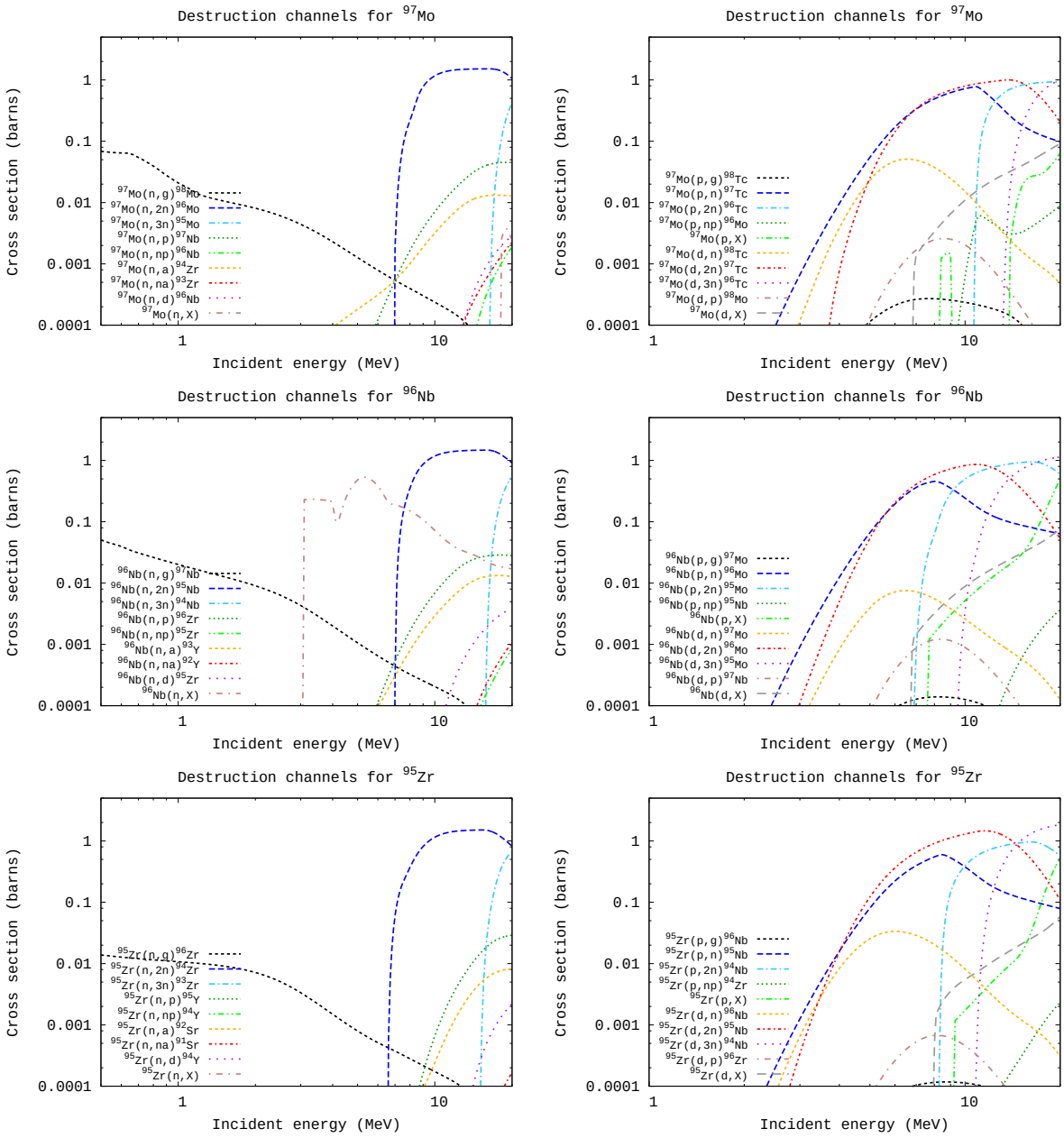

Fig. 53.— Activation cross sections for N=55 ground state targets of Zr, Nb, and Mo.

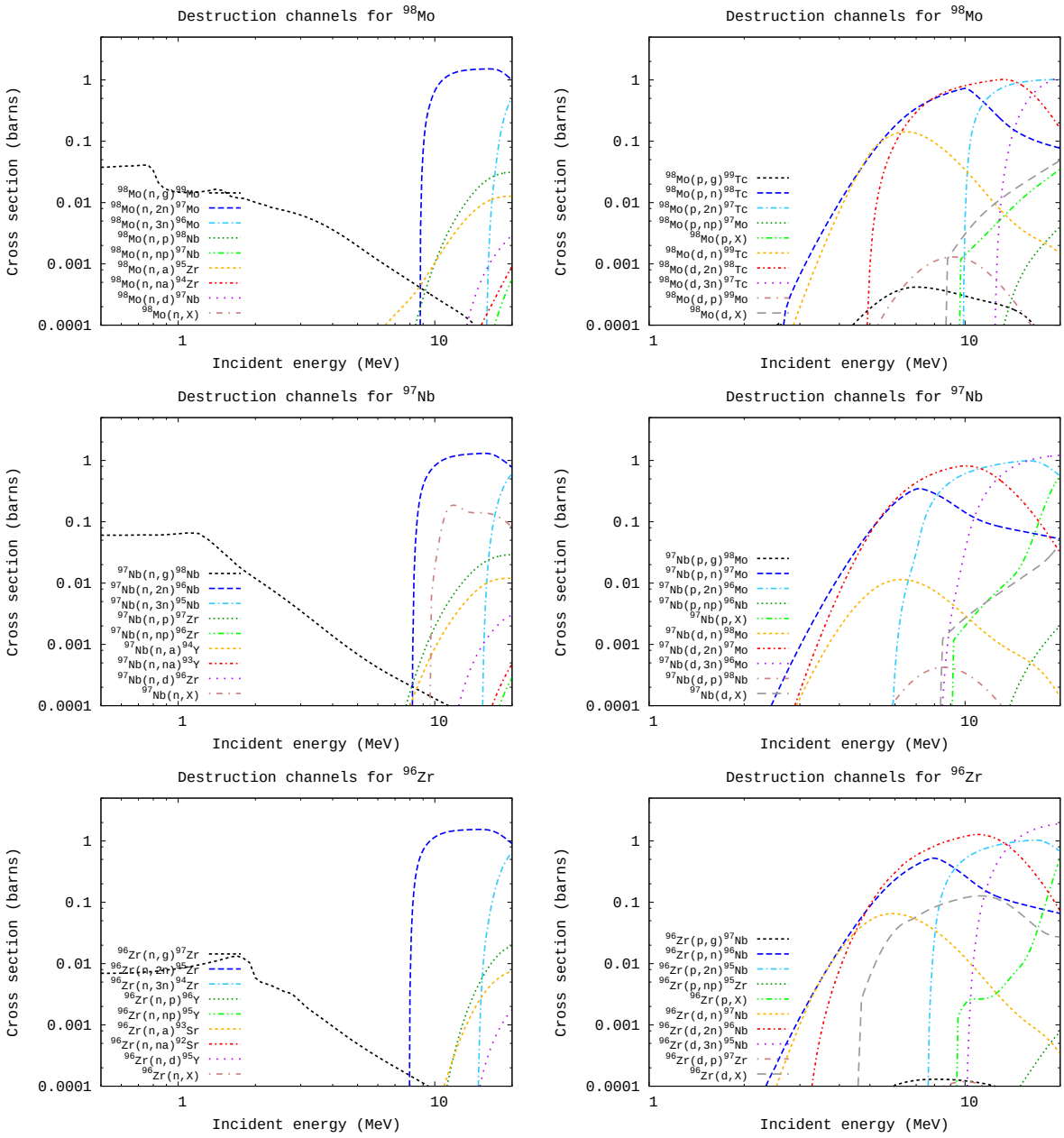

Fig. 54.— Activation cross sections for N=56 ground state targets of Zr, Nb, and Mo.